Interrogating the Insulin Granule

Investigating the Composition and Function of Insulin Secretory Granules

Nicholas Norris

A thesis submitted in fulfilment of the requirements of the degree

Doctor of Philosophy

Faculty of Medicine and Health

University of Sydney

2025

Table of Contents

Declaration

This is to certify, to the best of my knowledge that this thesis is a representation of my individual writing and is less than 80,000 words excluding the appendices. This project was done in collaboration with others and detailed below are the individuals who have contributed to the generation of the results presented.

Associate Professor Mark Larance performed label free quantification proteomics in **Chapters 2** & **3**. Analysis pertaining to this data was done by myself with mentorship and assistance from Dr Alistair Senior on RStudio.

Associate Professor Melkam Kebede & Dr Belinda Yau contributed to supervising this study, designing experiments, interpreting results and editing of this current thesis.

Some of the data points presented in **Figure 27** includes data reproduced from my Honours thesis titled "**Characterization of Insulin Secretory Granules as a Function of Age**" submitted to the University of Sydney, with additional experiments performed during my candidature.

Hayley Webster performed immunofluorescent staining of INS-1 cells and Dr. Belinda Yau acquired the images in **Chapter 2**, **Supplementary Figure 2**. A/Prof. Melkam Kebede generated qPCR data in **Supplementary Figure 2**.

Carlo Famularo assisted in generating data for **Figure 17** and immunofluorescent staining for **Figure 31**.

Glucose uptake assays on 3T3-L1 adipocytes were performed by me and Billy Jiang in **Figure 32**.

All author contributions to publications within this thesis are outlined within their respective sections. Generative AI was not used within this thesis. Those who have contributed to this thesis have been acknowledged.

The research within this thesis is supported by a University Postgraduate Award from the University of Sydney, and the Australian Government Research Training Program offset scholarship.

*

Nicholas Norris

Acknowledgements

This thesis is brought to you by questionable life decisions, copious amounts of caffeine, countless existential crises and the incredible people who kept me from spiralling into an inescapable pit. To all my friends and family who have helped me get to the end of my PhD journey… *why didn't you stop me from starting*?

Jokes aside, I would obviously like to thank everyone throughout my candidature. Melkam, thank you so much for all the opportunities you've given me, your unwavering support, teaching me the bare bones of science and for always making sure I stayed on the right track. Your mentorship has moulded not just my research but my entire academic journey. Bel, of course, I would like to thank you for shaping me into the enthusiastic, big-brained, over-caffeinated (*but also cynical*) scientist I am today. I appreciate the countless hours you've spent teaching me everything I know today, both in and out of the lab, backing me in everything I did, and deterring me from the scarier parts of science. Straight up, without you, this thesis would be non-existent. The two of you together are an unbeatable duo that I will forever be grateful for, both personally and professionally.

To my auxiliary supervisors, Al and Mark L., thank you for taking me on as a student with open arms. Mark L., thank you for running all my proteomics samples and I apologise for the endless pestering with questions about said proteomics samples. Al, your support has meant so much to me – Thank you for making me feel so included and welcomed into your lab, and for always helping me with my data-related questions. I feel like a stats wiz now, thanks to you!

Thank you to all the Kebede Lab members, current and former: Sunny, Mark, Sheyda, Patricia, Hayley, Matt, Carlo and Cara (*I hope I haven't pulled a Melkam and forgotten someone*). As well as those on 5 West who have made the PhD experience so much more enjoyable. Honourable mentions to Jeremy & Jen for keeping me distracted and entertained, and Nikki for keeping me employed... If all of you weren't around to make it all so fun on the day-to-day grinds, you'd be reading my eulogy instead of a thesis.

To my main homies, those who look at me and think "Wow, PhD students aren't actually smart are they?" - this one's for you: *suck it*. I'd name you all, but none of you will ever read my thesis so it might just be a waste of space… Though, Ethan you'd probably read this bit –

Thanks for being the most patient friend I've had. For sticking it through with me with every toss and turn, you're truly the best and I hope our future kids are best friends too…

Now, the most important: Family. To my mum and dad, who again, will also probably never read this thesis… Thank you for always supporting me in life and pushing me to do the best I can. Though I struggle to show it, the two of you have been a pillar in my life that I can always trust and lean on to keep me afloat. Chris, thank you for always being around when I needed someone to rant to, or just needed company when I first moved to Sydney… I hope I've repaid and continue to repay the support you've provided me over the years. Melissa (Jie), thanks for pestering me to keep in touch with the family back home, I'm terrible at it but you've kept me grounded.

To my second (*borderline adoptive*) family… I couldn't have done it without you. Jenny & James, you have been so helpful to maintaining the resilience I needed to get through tougher times. I always look forward to our catch ups that provide a brief respite from life's challenges. The two of you have supported me so immensely and I am forever grateful. Except when you beat me in cards, could you please stop doing that? As James always says, it's all about the journey at the end of the day, and this journey has been made better with you two around.

Last, but certainly not least, Tom. Thank you for being an open ear to all my rants, supporting my silly decisions, and being the reason, I've made it through these years intact. You've doubled my happiness, halved my sorrows, and have made this experience so much more enjoyable. You've been my immovable rock, and I cannot thank you enough for everything you've done to ensure I come out of this PhD journey not only surviving but cherishing every moment. Literally not a single day goes by I am not grateful to have you by my side. Love you lots.

With that, my friends & family, I love and thank you all. Every single one of you are the wind beneath my wings, that lift me up to do my greatest. Best believe I will be insufferably insisting you refer to me as Dr. Nick, whom I share striking similarities with from the Simpsons.

Publications

Chapter 1.8 of this thesis is published in *Metabolites* as Norris et al., 2021. Manuscript was conceptualised, written and edited by me, Associate Professor Melkam Kebede and Dr Belinda Yau. (**DOI: 10.3390/metabo11050288**).

Chapter 2 of this thesis is published in *Diabetes* as Norris et al. 2024. This study was conceptualised by me, Associate Professor Melkam Kebede and Dr Belinda Yau. Data collection was done by me with assistance from co-authors. Contributions to the publications are listed within the manuscript chapter (**DOI: 10.2337/db24-0355**).

In addition to the statements above, where I am not the corresponding author of the published content, permission has been granted to include this published material by the corresponding author.

*

Nicholas Norris

As supervisor for the candidature upon this thesis is based, I can confirm that the author attribution statements are correct.

*

Associate Professor Melkam Kebede

List of Abbreviations

ADP	Adenosine diphosphate
ATP	Adenosine triphosphate
BCA	Bicinchoninic acid
BSA	Bovine serum albumin
cAMP	Cyclic AMP
cDNA	Complementary DNA
Chg/Cg	Chromogranin-
CPE	Carboxypeptidase E
CTRL	Control
DAG	Diacylglycerol
DMEM	Dulbecco's Modified Eagle Medium
DMSO	Dimethyl sulfoxide
ELISA	Enzyme-linked immunosorbent assay
EM	Electron microscopy
ER	Endoplasmic reticulum
EtOH	Ethanol
FA	Fatty acid
FBS	Fetal bovine serum
FFA	Free fatty acid
FFAR	Free fatty acid receptor
G6P	Glucose-6-phosphate
GA	Glutaraldehyde
GLUT2	Glucose transporter 2
GO	Gene ontology
GSIS	Glucose stimulated insulin secretion
GTP	Guanosine triphosphate
HG	High glucose
HRP	Horseradish peroxidase
HTRF	Homogenous time resolved fluorescence
IAPP	Islet amyloid polypeptide

ICA1	Islet cell autoantigen 1
ICC	Intraclass-correlation
IDE	Insulin degrading enzyme
IF	Immunofluorescence
iISG	Immature insulin secretory granules
ISG	Insulin secretory granule
K_{ATP}	ATP-sensitive potassium channel
KD	Knock-down
KRBH	Krebs ringer buffer with HEPES
LC	Liquid chromatography
LC-CoA	Long chain acyl-CoA
LC-MS/MS	Liquid chromatography tandem mass-spectrometry
LDCV	Large dense core vesicle
LFQ	Label free quantitation
LG	Low glucose
MAG	Monoacylglycerol
mISG	Mature insulin secretory granule
MW	Molecular weight
NADPH	Nicotinamide adenine dinucleotide phosphate
NHMRC	National health and medical research council
NTC	non-targeting control
PA	Palmitate
PBS(T)	Phosphate buffered saline (Tween20)
PC1/PCSK1	Prohormone convertase 1 (PC1/3)
PC2/PCSK2	Prohormone convertase 2
PCP	Protein correlation profiling
PDI	Protein disulfide isomerase
PFA	Paraformaldehyde
PICK1	Protein interacting with C alpha kinase 1
PM	Plasma membrane
PVDF	Polyvinylidene (di)fluoride
rER	Rough endoplasmic reticulum

RP	Reserve pool
RPMI	Roswell Park Memorial Institute
RRP	Readily releasable pool
RT	Room temperature
RT-PCR	Reverse transcription polymerase chain reaction
S.E.M.	Standard error of the mean
Scamp3	Secretory associated membrane protein 3
Scg	Secretogranin
SDC	Sodium deoxycholate
SDS	Sodium dodecyl sulphate
SG	Secretory granule
siRNA	Small interfering RNA/silencing RNA
Sorcs1	Sortilin-related VPS10 domain-containing receptor 1
Stx	Syntaxin-
SVM	Supervised machine learning
Syp	Synaptophysin
Syt	Synaptotagmin-
T2D	Type 2 diabetes
TAG	Triacylglycerol
TBS(T)	Tris buffered saline (Tween-20)
TCA	Tricarboxylic acid
TGN	Trans-Golgi network
Vamp	Vesicle-associated membrane protein
VDCC	Voltage dependent calcium channel
VGF	Nerve growth factor inducible
VPS41	Vacuolar protein sorting 41
VSN	Variance stabilisation normalisation
WB	Western Blotting

List of Figures

List of Supplementary Figures

Supplementary Tables

All supplementary tables (**1 - 10**) have been deposited online and is publicly available for download or viewing, accessible through GitHub.

Link: ***https://github.com/NickNorris1/Nicholas_Norris_Thesis_Supplementary***

Table 1: List of antibodies used

Protein Target	**Antibody Source**	**Product Code**	**Host Species**	**Dilution Factor**
Insulin (SDS-PAGE/Western)	Santa Cruz	SC-8033	Mouse	1:200
Insulin (Immunofluorescence)	DAKO	IR002	Guinea pig	1:1
Proinsulin	DSHB	GS-9A8	Mouse	1:100
Pcsk2 (C-Terminus)	Seidah*	-	Rabbit	1:2500
EEA1	CST	48453S	Mouse	1:1000 (WB), 1:100 (IF)
Lamp1	Abcam	Ab24170	Rabbit	1:1000 (WB), 1:100 (IF)
ATP5A	Abcam	Ab14748	Mouse	1:1000 (WB), 1:200 (IF)
GRP	Santa Cruz	Sc-271045	Mouse	1:1000
Beta-actin	Sigma Aldrich	A5441	Mouse	1:3000
KDM1/LSD1	Abcam	Ab224270	Rabbit	1:200 (IF)
LC3A/B	CST	12741S	Rabbit	1:1000 (WB), 1:100 (IF)
Synaptophysin	ProteinTech	17785-1-AP	Rabbit	1:500 (IF), 1:5000 (WB)
Synaptotagmin-13	Abcam	Ab154695	Rabbit	1:250
Syntaxin-7	ProteinTech	12322-1-AP	Rabbit	1:250
Scamp3	ThermoFisher	PA-21428	Rabbit	1:1000 (WB), 1:200 (IF)

Chromogranin-A	Novus Biologicals	NB12-15160	Rabbit	1:100
PDI	ThermoFisher	MA3-019	Mouse	1:100
GM130	BD Biosciences	610823	Mouse	1:500
GAPDH	Santa Cruz	Sc-25778	Rabbit	1:1000
Secondary Antibodies	**Antibody Source**	**Product Code**	**Species Reactivity**	**Dilution Factor**
Goat anti-rabbit IgG-HRP	Santa Cruz	Sc-2004	Rabbit	1:5000 (WB)
Goat anti-mouse IgG-HRP	Santa Cruz	Sc-2005	Mouse	1:5000 (WB)
Mouse IgG_K BP-HRP	Santa Cruz	Sc-516102	Mouse	1:1000 (WB, insulin)
Secondary antibodies for IF: Goat anti-mouse, rabbit and guinea pig conjugated to Alexa fluor 488, 594 or 647	ThermoFisher		Mouse, Rabbit, Guinea pig	1:500

**Anti-PCSK2 antibody provided by Nabil Seidah (Clinical Research Institute of Montreal).*

Abstract

Glucose homeostasis is a tightly regulated process that relies on the pancreatic beta-cells to produce and secrete insulin, a peptide hormone that facilitates glucose uptake into insulin-sensitive tissues. Insulin is stored within specialised vesicles termed insulin secretory granules, which play a critical role in controlling insulin turnover in beta-cells through coordinated processes of exocytosis and degradation. Type 2 diabetes is characterised by chronic hyperglycaemia and insulin resistance which negatively impact insulin production and secretion from pancreatic beta-cells. Recent research has shifted towards understanding how insulin granules are affected during the progression of type 2 diabetes and exploring the heterogeneity of insulin granule populations within beta-cells. Current diabetes therapies primarily target the distal stages of exocytosis to enhance insulin secretion, overlooking the distinct functional properties of discrete granule populations within. This thesis focuses on the insulin secretory granules as a key regulator of beta-cell function, aiming to elucidate its composition and the impact of metabolic stress on granule properties. Furthermore, it investigates the role of insulin granule aging and its response to pharmacological stimuli.

A key outcome of this work is the identification of the murine (MIN6) insulin granule proteome, along with the validation of novel insulin secretory granule proteins involved in regulating beta-cell function (**Chapter 2 & 2A**). This thesis also demonstrates that metabolic stress, induced by elevated fatty acids disrupts the docking machinery of insulin granules (**Chapter 3**). Using a fluorescent protein timer and commonly used anti-diabetic drugs we show that the preferential release of younger, more newly synthesised insulin granules is a glucose-dependent phenomena (**Chapter 4**). Together, these studies provide novel insights into insulin granule biology, highlighting the adaptive role of beta-cells in response to metabolic

stress and underscore the importance of studying the proximal stages of insulin granule regulation to inform future diabetic therapies.

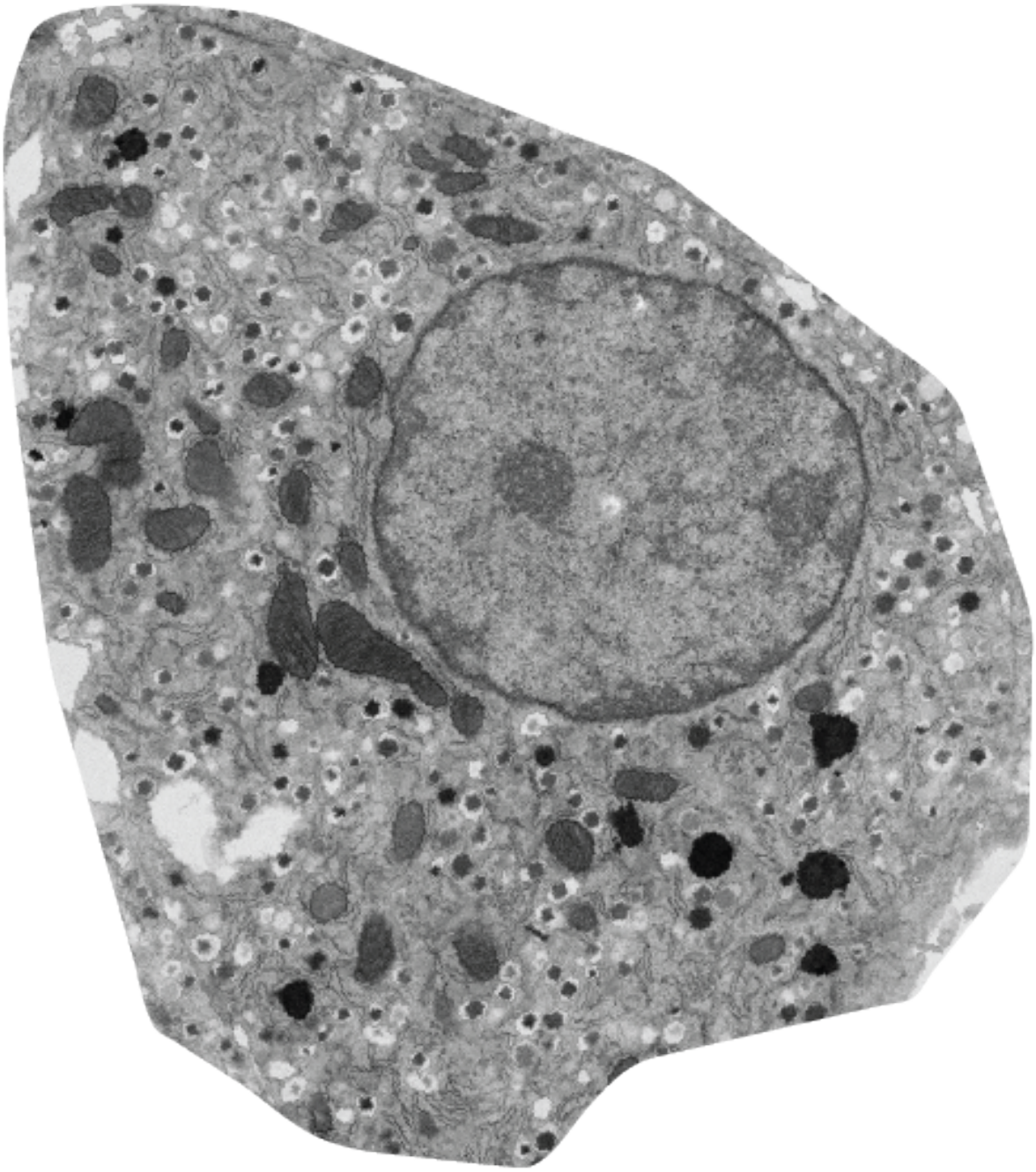

Chapter 1

Literature Review

1.1 Pancreatic Islets of Langerhans

Pancreatic islets of Langerhans are micro-organs made up of a diverse array of endocrine cells embedded within the exocrine pancreatic parenchyma. Each cell type within the islet is responsible for producing and secreting specific peptide hormones in response to distinct nutrient stimuli [1]. The cellular composition of islets differ both inter and intra-species [2]. In humans, islets are predominantly composed of beta-cells (60 %) and glucagon producing alpha-cells (30 %) [3, 4]. The remaining 10 % consists of less abundant cell types, including pancreatic polypeptide producing F-cells, somatostatin producing delta cells and ghrelin producing epsilon cells [1] (**Figure 1**).

In many mammalian species, the islet architecture features a central core of beta-cells, surrounded by a peripheral mantle of non-beta-cell endocrine cells [5]. However, human pancreatic islet morphology is highly variable. While some studies suggest a random arrangement of cells within the islet [6], others propose that the mantle-core organisation is at least partially maintained [7, 8]. The pancreatic islet also contains an extensive network of capillaries contacting beta-cells that enable the rapid detection of nutrient stimuli from the blood and subsequent secretion of peptide hormones into the bloodstream [9].

On average, in healthy fasted individuals, blood glucose levels typically range from 3.9 – 5.6 mmol/L, while postprandial glucose levels can rise to a peak of 7.8 mmol/L. This elevation triggers insulin secretion from beta-cells and promotes glucose uptake by peripheral tissue, facilitating the normalisation of glucose levels within approximately two hours [10].

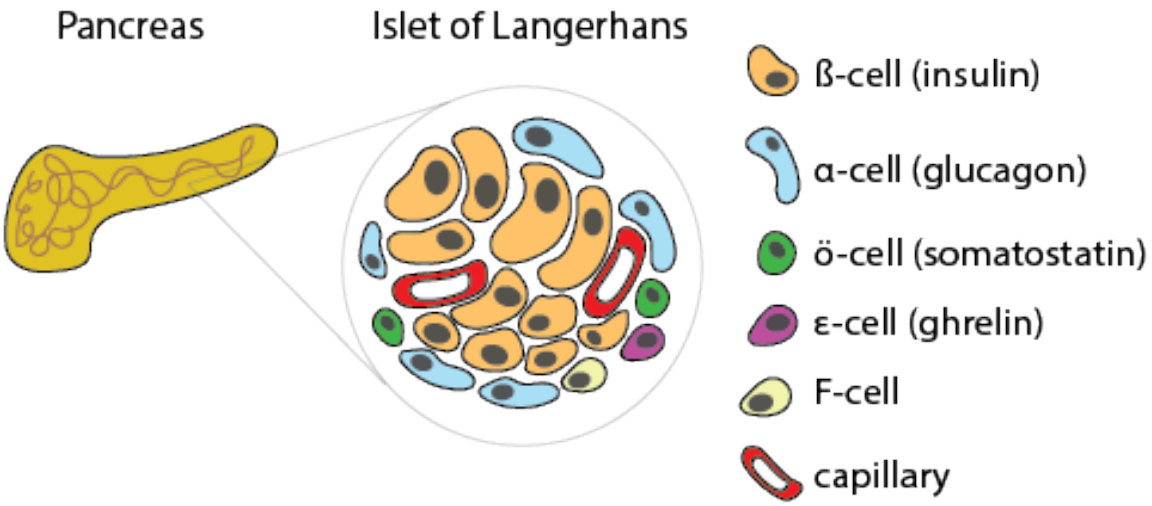

Figure 1: Structure of the Pancreatic Islets of Langerhans. The pancreatic islet of Langerhans is composed of five major endocrine cell types, arranged in a seemingly random distribution within human islets. These cell types include: (i) insulin producing beta-cells, (ii) glucagon producing alpha cells, (iii) somatostatin producing delta cells, (iv) ghrelin producing epsilon cells and (v) pancreatic polypeptide producing F-/gamma cells. Blood capillaries are interspersed throughout the islet, facilitating the exchange of nutrients and enabling rapid detection of blood glucose changes to support hormone secretion.

1.2 Pancreatic beta-cells

Beta-cells are the most abundant cell type within the islets of Langerhans, accounting for 60 % of total cells in human islets [3, 11, 12]. These cells play a critical role in maintaining euglycaemia (~5 mmol/L) within the body [1, 13]. In healthy individuals, beta-cells detect elevated blood glucose levels after food consumption through glucose transporters (GLUT2) and respond by secreting the peptide hormone insulin.

Glucose-stimulated insulin secretion (GSIS) occurs in two distinct phases (**Figure 2**). The first phase involves a rapid and immediate release of insulin, followed by a slower, sustained second phase [14-17]. Once secreted, insulin enters the bloodstream and binds to insulin receptors on insulin-sensitive tissues (primarily skeletal muscle and adipose). This interaction promotes the uptake of glucose from the blood, thereby maintaining euglycaemia [18-20].

In type 2 diabetes (T2D), the progressive disruption of GSIS and insulin signaling contributes to the development of chronic hyperglycaemia. A hallmark of T2D pathophysiology is the loss of first-phase insulin secretion (**Figure 2**, red line), which exacerbates glycaemic dysregulation and highlights the critical role of beta-cell dysfunction in disease progression.

1.3 Pathogenesis of type 2 diabetes

It is well understood that both genetic and environmental factors contribute to the development of T2D [21-23]. The predominant elements that contribute to the etiology of T2D is the interplay between insulin resistance and hyperinsulinemia. Metabolic stress such as lipid accumulation in insulin-sensitive tissues disrupts the body's insulin signaling pathways [24]. This disruption leads to insulin resistance, impairing glucose uptake by peripheral tissues [25]. Perturbation to insulin signaling results in elevated circulating glucose levels. As a result, blood glucose levels remain elevated, promoting pancreatic beta-cells to compensate by increasing

both the synthesis and secretion of insulin through beta-cell hyperplasia and hypertrophy to increase beta-cell mass, promoting hyperinsulinemia [12]. Often, beta-cells successfully compensate in insulin-resistant individuals to maintain euglycaemia. However, exacerbation of insulin resistance, alongside genetic predisposition of beta-cell 'fragility' [26-28] advances the development of disease by initiating beta-cell decompensation, a process marked by a progressive decline in beta-cell function. Key stages of this decline include:

(1) **Loss of acute first-phase GSIS**: The initial phase of GSIS is lost, while second-phase GSIS remains intact (**Figure 2**, orange line). This early dysfunction is a hallmark of pre-diabetes and early-stage T2D.

(2) **Later-stage T2D**: As the disease progresses, chronic hyperglycaemia becomes more severe, accompanied by beta-cell degranulation (loss of insulin stores) and beta-cell dedifferentiation, where beta-cells lose their specialised insulin-producing and secreting phenotype.

(3) **End-stage T2D**: In the final stages, beta-cell apoptosis occurs leading to a reduction in total beta-cell mass. This process is often accompanied by pancreatic fibrosis, where pancreatic tissue becomes scarred. Together, these changes result in a reliance on exogenous insulin therapy to maintain blood glucose control [27, 29].

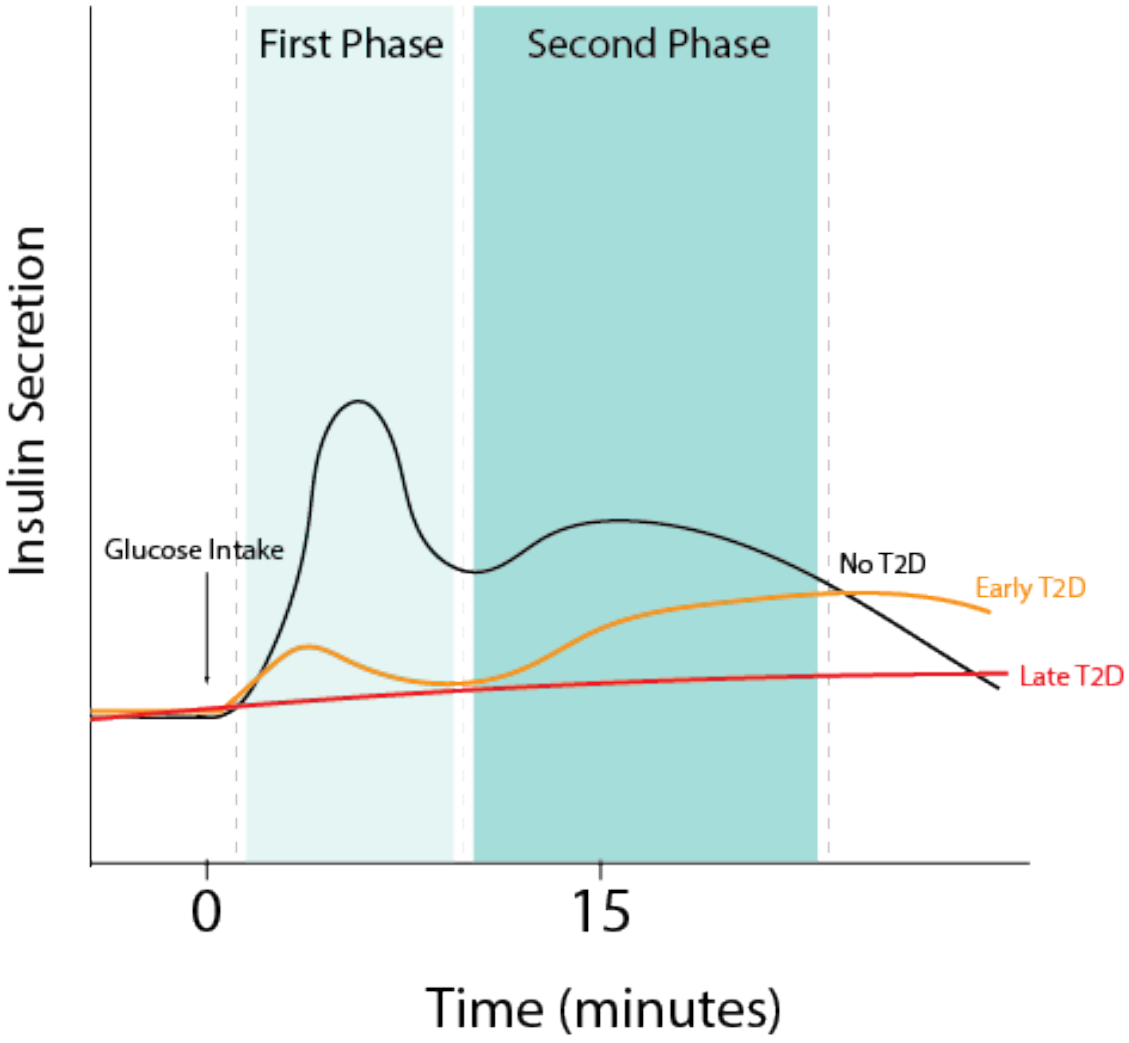

Figure 2: Biphasic insulin secretion from beta-cells. Following glucose intake, beta-cells exhibit a biphasic pattern of insulin secretion. The first phase is rapid and occurs immediately, while the second phase is more prolonged, lasting up to 2 hours before insulin secretion returns to basal levels. The **black** line represents insulin secretion in non-type 2 diabetic individuals, characterised by a robust first-phase response and sustained second-phase secretion. The orange line illustrates early T2D, where the first phase of insulin secretion is diminished but the second phase remains intact. The red line depicts late T2D, marked by a complete loss of first-phase secretion and a severely impaired second-phase response. *This figure is adapted from Westermeier et al., 2019* [30].

1.4 Insulin granule biogenesis, maturation, and trafficking

Insulin biosynthesis begins with the translation of preproinsulin from insulin mRNA (**Figure 3**) [31]. Preproinsulin consists of four key regions: a signal peptide, A- and B- chains and the C-peptide. Upon entry into the rough endoplasmic reticulum (rER), the signal peptide region is rapidly cleaved, converting preproinsulin to proinsulin (**Figure 3**). Proinsulin undergoes folding and disulfide bond formation, a process mediated by protein disulfide isomerase (PDI) [32], which helps establish proinsulin's native conformation (**Figure 3**) [33]. Once properly folded, proinsulin is then trafficked from the ER to the cis-Golgi via small, coated vesicles. As it moves through the Golgi from the cis to trans regions of the Golgi body, proinsulin is sorted along with other insulin granule cargo proteins into the immature insulin secretory granule (iISG) (**Figure 4**) [34]. The iISG then undergoes a series of modifications that ultimately lead to its maturation. Key steps include:

(1) **Lumen acidification**: Proton pumps (ATPases) lower the pH within the granule [35, 36], creating the optimal environment for the action of prohormone convertases.

(2) **Proinsulin cleavage**: Prohormone convertases 1/3 (PC1/3) and 2 (PC2) cleave proinsulin at specific sites, generating mature insulin and C-peptide [37].

(3) **Insulin crystallisation**: Zn^{2+} ions are transported into the granule lumen through the ZnT8 zinc transporter promoting the crystallisation of insulin, which stabilises the hormone within the mature ISG [38].

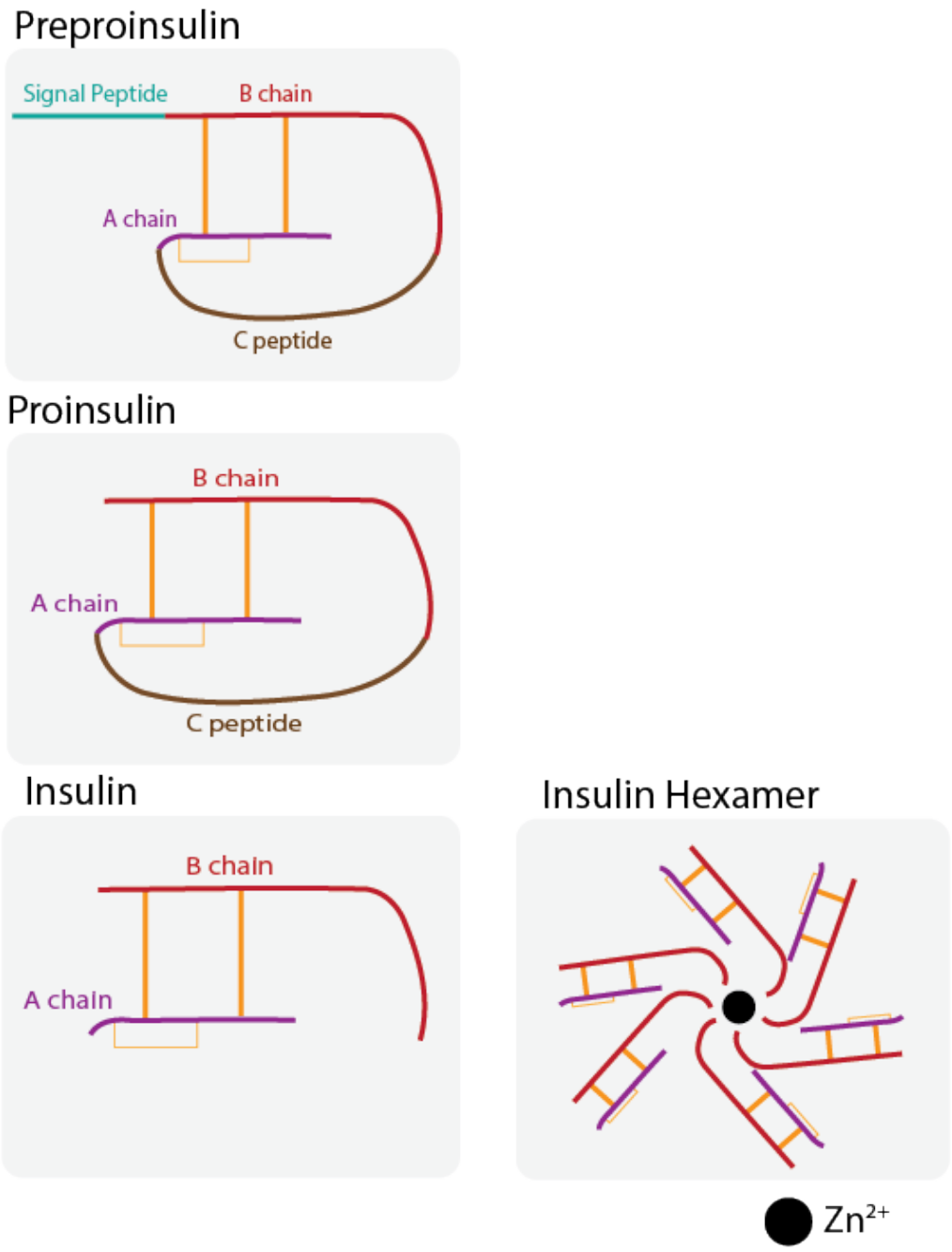

Figure 3: Insulin Biosynthesis. Insulin biosynthesis begins with the synthesis of preproinsulin, a precursor molecule containing a signal peptide, A- and B- chains and a C-peptide. Signal peptide is cleaved from preproinsulin to form proinsulin. Proinsulin is then folded and stabilised by disulfide bonds to achieve native structure. In the immature insulin granule, proinsulin is cleaved to form insulin. The mature insulin molecules then assemble into hexamers around a $\mathbf{Zn^{2+}}$ core which stabilises the hormone for storage and secretion.

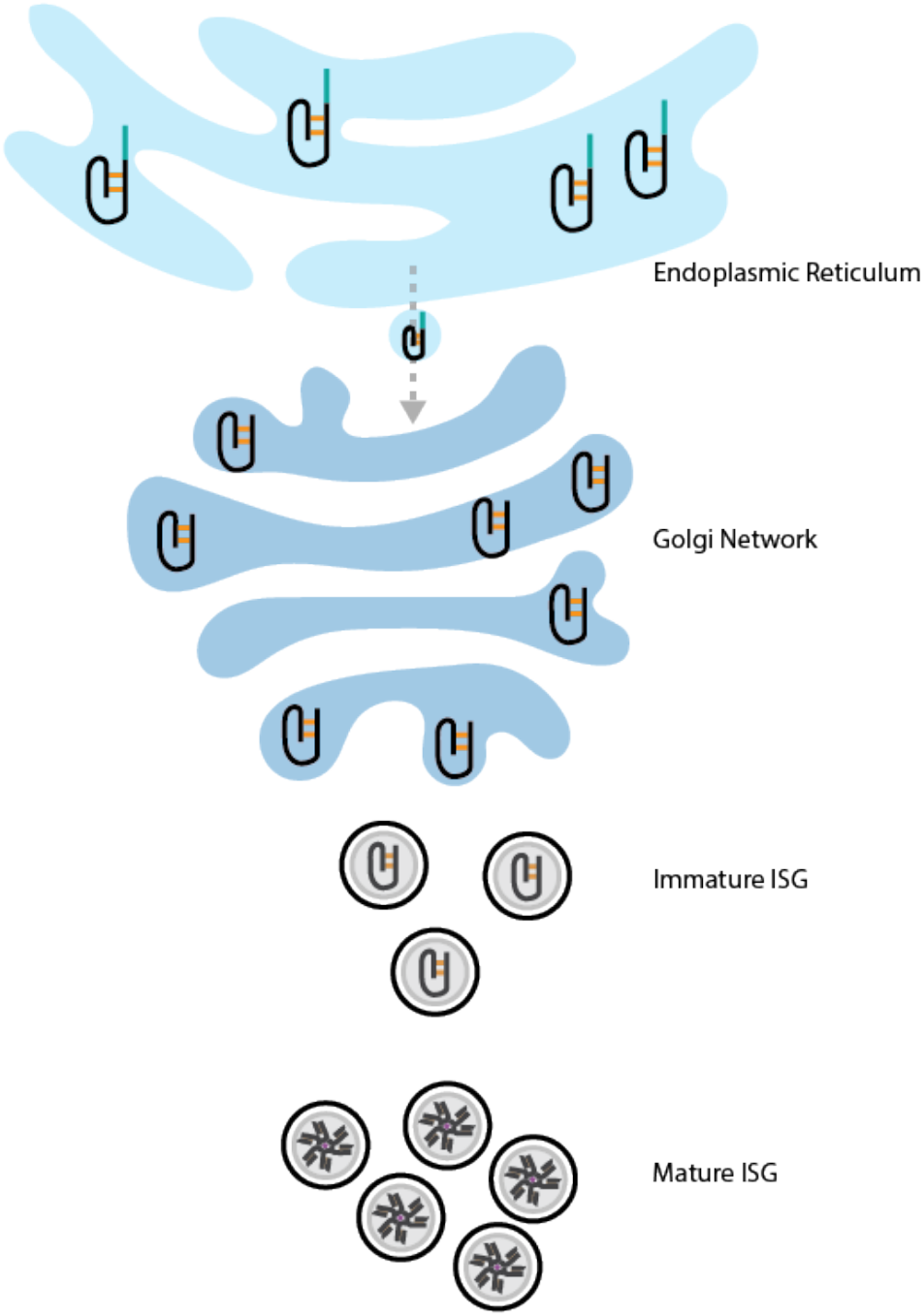

Figure 4: Insulin granule biogenesis. Preproinsulin is synthesised and folded in the endoplasmic reticulum, is then transported to the Golgi, cleaved into proinsulin, and is sorted within immature ISGs that bud from the trans-Golgi network. Immature ISGs then undergo maturation that include the cleavage of proinsulin into mature insulin and C-peptide, crystallisation with Zn^{2+} and acidification of the granule lumen to form the mature ISG.

1.5 Glucose-stimulated insulin granule secretion

Glucose metabolism and insulin granule exocytosis is a tightly regulated process within beta-cells and consists of six main steps that tether glucose sensing and insulin secretion (**Figure 5**). These steps include:

(1) **Glucose detection**: Glucose transporters on the plasma membrane, primarily GLUT2, facilitating the translocation of glucose from the blood into the cytosol of beta-cells [39].

(2) **Glycolysis of glucose**: Cytoplasmic glucose is phosphorylated by glucokinase to glucose-6-phosphate (G6P). Through glycolysis, G6P is then converted into pyruvate [40].

(3) **Krebs cycle**: Pyruvate is translocated into the mitochondria and undergoes further oxidisation through the Krebs/TCA cycle, producing adenosine triphosphate (ATP), increasing intracellular ATP/ADP ratios.

(4) **Closure of ATP-sensitive K^+ channels**: The elevated ATP/ADP ratio acts upon ATP-dependent potassium channels (K_{ATP}) to close, inhibiting the export of potassium from the cytosol. K_{ATP} closure results in a relative depolarisation of the plasma membrane.

(5) **Opening of Ca^{2+} channels**: Membrane depolarisation stimulates voltage-dependent calcium channels (VDCC) to open, causing an influx of Ca^{2+} ions into the cytosol, triggering exocytosis of insulin granules, releasing insulin into the bloodstream (**Figure 5**) [40, 41].

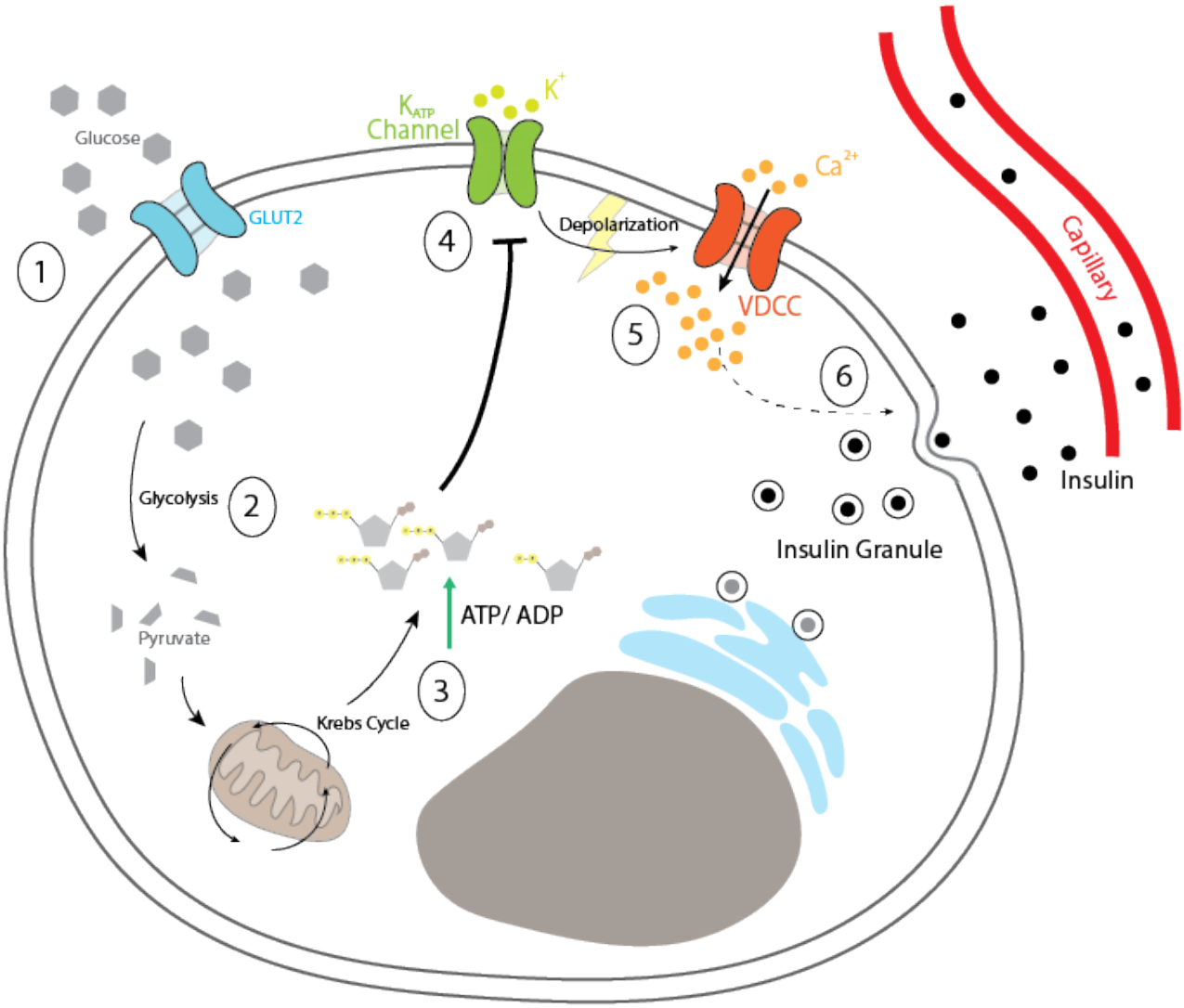

Figure 5: Glucose-stimulated insulin secretion coupling in pancreatic beta-cells. (**1**) Glucose enters the beta-cell primarily through GLUT2 transporters (**2**) Glucose undergoes glycolysis, generating pyruvate, which is transported into the mitochondria. (**3**) Within the mitochondria, pyruvate is metabolised via the Krebs cycle, producing ATP, leading to a rise in cytosolic ATP/ADP ratios. The rise in ATP/ADP ratio causes the closure of ATP-sensitive K^+ (K_{ATP}) channels (**4**), depolarising the membrane. (**5**) Membrane depolarisation causes the opening of voltage-dependent calcium channels (VDCC), allowing the influx of Ca^{2+} into the cytosol. (**6**) Cytosolic Ca^{2+} influx signals the trafficking and exocytosis of insulin secretory granules (ISGs) mediated by calcium-sensitive proteins to release insulin into the circulation.

1.6 Insulin secretion dynamics

While the stages and molecular mechanisms of insulin granule secretion from beta-cells are well-studied, there is still uncertainty surrounding how beta-cells select insulin granules for exocytosis. The discovery of biphasic GSIS suggests that there are functionally distinct pools of ISGs within beta-cells, which are selected for secretion at different times [42].

1.6.1 Pre-docked, readily releasable and reserve pool granules

Initially, through electron microscopy (EM), a generally accepted model speculates a population of ISGs that are pre-docked at the PM with SNARE and calcium-sensitive proteins (synaptotagmins) that "prime" ISGs in proximity to elevations of Ca^{2+} at the PM [43, 44]. In similar secretory cell types (neurons, neuroendocrine cells), secretory vesicles dock at the PM, recruiting SNARE proteins that hold and prime granules near Ca^{2+} channels [45, 46]. This differential localisation was hypothesised to coincide with the beta-cell's natural biphasic insulin release. These granules were subdivided and aptly named the readily releasable pool (RRP), that constituted for the majority of calcium-dependent first phase insulin secretion. Concurrently, a second population of ISGs localise deeper within the cell as a reserve pool (RP) that is recruited to similar sites of exocytosis that accounts for the sustained second phase of GSIS [47, 48]. Characterisation of the electrophysiological properties of ISG exocytosis supports this, identifying two ISG populations with different trafficking kinetics, with ~100 granules constituting the RRP (~2 % of ISGs) that is rapidly released and remaining granules to the RP, with a slower, steady release [49] (**Figure 6**). Beta-cell decompensation in T2D accounts for the loss of first-phase GSIS [50] and is strongly linked to the dysfunction in fusion capacity of the pre-docked ISG population [51].

1.6.2 Newcomer insulin granules

The discovery of 'newcomer' granules identified a population of granules that have been shown to rapidly fuse with the PM, with a short-term or no residence at the PM before fusing [47] (**Figure 6**). This model suggests the newcomers accounting for second-phase GSIS and were responsible for replenishing the RRP [51]. Through the investigation of GSIS enhancement by cAMP signalling pathways [52], which increases ISG fusion through both phases of GSIS, newcomer populations were subclassified. *Old faces*; pre-docked granules that remained on the PM when stimulated with KCl, but absent from the PM when stimulated with glucose [52, 53]. *Restless newcomers*: granules that made up the increase of GSIS by cAMP signalling that rapidly fuse with the PM and *resting newcomers*, which make up the smallest proportion of released granules that transiently remain on the PM before fusion. These granules are incongruent with "dock and prime" granules, instead postulating that pre-docking temporally constrains ISGs at the PM and is not essential for insulin exocytosis [54]. In fact, perturbations to the docking machinery by knocking out granuphilin eliminated docking granules; interestingly improving fusion and secretion of ISGs [55].

1.6.3 Compound exocytosis

Beta-cells have also been shown to present compound exocytosis, a phenomena where exocytotic events involve more than a single ISG [56] (**Figure 6**). This is further subcategorised as sequential and multigranular exocytosis [57, 58]. Sequential exocytosis involves the fusion of vesicles to other vesicles that are already fused with the PM, resembling a strand of beads at the PM. While this mechanism enables beta-cells to increase the efficiency of insulin release, it accounts for less than 10 % of total exocytic events under various stimulation conditions [58]. Secondly, multigranular exocytosis involves multiple ISG vesicles fusing with each other within the cytoplasm to form a large multi-granular body before fusion with the PM. While this

type of exocytosis is observed in other secretory cell types, it is rarely, if ever, observed in pancreatic beta-cells [57, 58].

1.6.4 Kiss-and-run exocytosis

Kiss-and-run exocytosis (cavicapture) has also been observed previously in beta-cells where ISGs contact the PM briefly forming a transient fusion pore (**Figure 6**) to release small transmitters but retain the insulin peptide [59, 60].

In summary, the explanation of biphasic insulin secretion is largely dictated by the release of discrete functional ISG populations released at different stages of GSIS. Moreover, *in vivo* in humans with T2D, this first-phase of postprandial insulin secretion is markedly reduced or even lost [61]. This highlights the functional significance of ISG pool heterogeneity in beta-cell physiology. The clear distinction between these functional ISG pools demonstrates the beta-cell's ability to target specific ISGs to the PM and control granule exocytosis. What we lack is a clear understanding of the molecular underpinnings that drive the formation of these functionally discrete ISG pools or how the beta-cell discriminate between these granule populations.

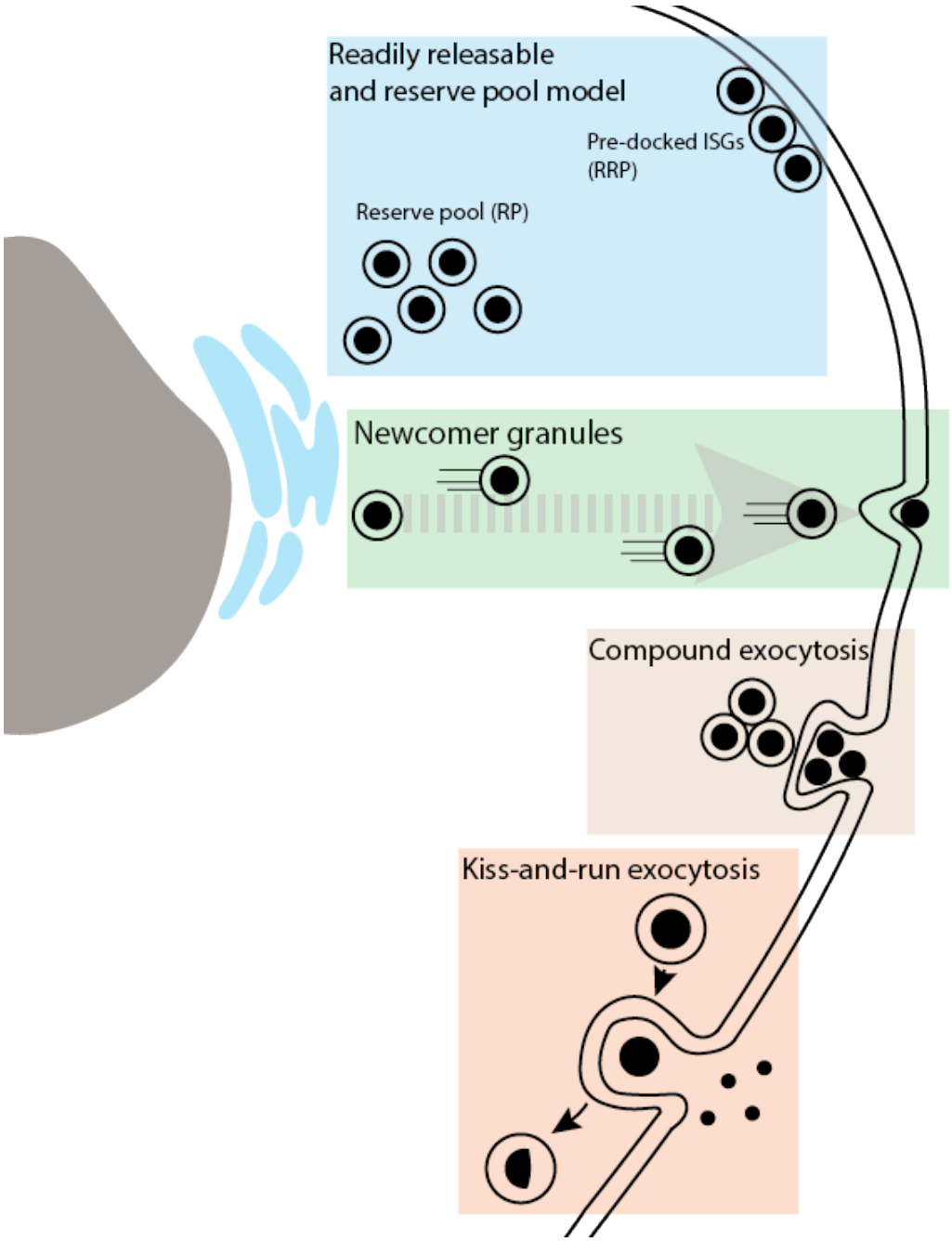

Figure 6: Exocytotic Models of Insulin Secretory Granules. This figure illustrates the various exocytotic models used by pancreatic beta-cells to regulate insulin secretion. *Readily releasable and reserve pool* model, where pre-docked readily releasable pool of insulin granules (RRP) drive first-phase secretion, while a sustained slower release of a reserve pool (RP) of ISGs follows. *Newcomer granules* are a population of granules that rapidly fuse with the PM without pre-docking with the plasma membrane. *Compound exocytosis* whereby multiple ISGs participate in a single exocytotic event, and *kiss-and-run exocytosis*, where ISGs

form a transient fusion pore with the plasma membrane, releasing small transmitters but retaining insulin peptides.

1.7 Insulin granule age

Aspects of ISG exocytosis covered in **Chapter 1.6** focus primarily on the spatial localisation of ISG populations through electron microscopy or electrophysiological characterisation of ISGs [49]. Through live-cell microscopy however, biphasic insulin secretion has been constrained not spatially but by their mechanisms of exocytosis. The inclusion of a temporal variable; granule age, has been a pivotal discovery with the advancement of labelling techniques, implicating insulin granule age having considerable impacts on the beta-cell's selection for ISG exocytosis.

Early observations through radioactive labelling of insulin granules show that stimulation of these cells showed a higher proportion of radio-labelled insulin secreted than what remained within the islet [62]. Moving from radiolabelling, recent studies instead focused on using fluorescent proteins instead to label and visualise age-distinct populations of ISGs. These include the use of SNAP and Halo tagged insulin and fluorescent protein substrates (TMR-star) to successfully discriminate between granules at different time points, effectively demonstrating an age-dependent labelling of ISGs within beta-cells [63, 64]. This labelling technique identified that granule motility was age-dependent, showing that younger ISGs were significantly faster compared to older ISGs. Furthermore, SGs that were located closer to the PM have a reduction in fusion capacity and motility further contrasting the classical dock-and-prime model of secretion [63].

Other approaches to label age-distinct granules are with the use of fluorescent proteins with staggered folding that shift fluorescent spectra over time [65-67]. One such example is DsRed-E5 [67], fused to cargo proteins in bovine chromaffin cells which enabled the

discrimination and imaging of large dense core vesicles (LDCVs) as a function of age, ultimately showing differences in their localisations and secretion dynamics [65]. Another study utilises Kusabira Green Orange (mK-GO) within neuroendocrine cells (PC12) and show preferential release of younger LDCVs when stimulated [66]. These techniques have now been extended to use within beta-cells, by conjugating dsRed-E5 to syncollin which localises to ISGs. This protein does not affect normal ISG behaviour and was used to show that younger ISGs are preferentially secreted when stimulated with elevated glucose levels [68].

There has been a great deal of work understanding complex mechanisms that govern ISG populations, and a growing consensus that ISG populations are spatiotemporally segregated that involve PM proximity and the age of granules. Further, that newly synthesised ISGs are preferentially secreted from pancreatic beta-cells. However, the molecular mechanisms that dictate changes in granule motility, localisation and exocytosis is still poorly understood. This is primarily due to the difficulties in isolating granules from beta-cells and characterising them as a function of age. One recent study has employed a phogrin-CLIP tag and TMR-star to isolate age-distinct ISGs from beta-cells to implicate changes in small GTPases and motor proteins that associate differentially with SGs and changes in lipid composition of aged granules, exhibiting higher membrane fluidity [64].

To build on the current understanding of ISG turnover, exocytosis and the proteins that regulate these systems, we must first build upon the current knowledge surrounding ISG composition before investigating changes that occur which influence the separation of functionally distinct ISG populations.

1.8 Isolation and Proteomics of Insulin Secretory Granules

There grows clear appreciation of ISGs as vesicles with intrinsic regulatory structures that dictate secretion dynamics within beta-cells. However, there lacks thorough understanding, and a full picture of the ISG composition. The following section (**Chapter 1.8**) is a review article published in a special Islet Biology and Metabolism Edition in the journal *Metabolites* (DOI: 10.3390/metabo11050288) [69], with figure and citation numbers updated to reflect this current thesis structure. This article details current knowledge of insulin secretory granule proteins with techniques and challenges to ISG isolation and purification.

Isolation and Proteomics of Insulin Secretory Granules

Authors: Nicholas Norris, Belinda Yau, Melkam Alamerew Kebede.

Abstract: Insulin, a vital hormone for glucose homeostasis is produced by pancreatic beta-cells and when secreted, stimulates the uptake and storage of glucose from the blood. In the pancreas, insulin is stored in vesicles termed insulin secretory granules (ISGs). In Type 2 diabetes (T2D), defects in insulin action results in peripheral insulin resistance and beta-cell compensation, ultimately leading to dysfunctional ISG production and secretion. ISGs are functionally dynamic and many proteins present either on the membrane or in the lumen of the ISG may modulate and affect different stages of ISG trafficking and secretion. Previously, studies have identified few ISG proteins and more recently, proteomics analyses of purified ISGs have uncovered potential novel ISG proteins. This review summarizes the proteins identified in the current ISG proteomes from rat insulinoma INS-1 and INS-1E cell lines. Here, we also discuss techniques of ISG isolation and purification, its challenges and potential future directions.

1. Insulin Granule Biogenesis and Function

The insulin secretory granule (ISG) is the storage vesicle for insulin in pancreatic beta-cells. It was long treated as an inert carrier for insulin but is now appreciated as a regulatory structure all on its own. There is a continuous turnover of insulin granules in the beta-cell, which is highly specialised in its capacity for ISG biogenesis, and insulin represents the most abundant protein within the beta-cell at 5 – 10% of total cell protein mass [70]. Production of insulin first begins in the rough endoplasmic reticulum with the synthesis of preproinsulin [71]. The signal peptide of preproinsulin is cleaved to form proinsulin, which is folded and trafficked to the Golgi complex [72]. Here, proinsulin is packaged with other proteins destined for

secretion into a budding immature ISG at the *trans*-Golgi network via a mechanism termed '*sorting by entry*' [73]. Following the release of these granules from the *trans*-Golgi network, maturation of the immature ISG includes acidification of the granule lumen by ATP-dependent proton pumps and promotion of endoprotease convertases (PC1/3 and PC2) activity that cleave proinsulin to form free C-peptide and mature insulin, comprised of the A and B chains bound together by two inter-chain disulfide bonds [35, 74, 75]. Through a secondary mechanism called '*sorting by retention*', proinsulin and other proteins are retained in the immature ISG [35], while in parallel, proteins such as clathrin are removed from the immature ISG via '*sorting by exit*' [37, 76]. Finally, insulin crystallises with zinc cations (Zn^{2+}), assembling an ~ 300 nm dense-core mature ISG [77]. From its point of synthesis, proinsulin enters an ISG within 4 hours [35] and is processed into insulin in a mature ISG within 40 minutes [37].

The ISG has a half-life of 3 – 5 days within the beta-cell cytoplasm [78] (**Figure 7**), and are ultimately destined for secretion or degradation. Upon glucose stimulation, ISG are motivated to undergo exocytosis, which requires the coordination of cellular machinery present both on ISGs and at the plasma membrane. It is therefore likely that ISG composition contributes to exocytosis, though the variables that determine whether an ISG eventually undergoes secretion are still unclear. Only 1-2% of total ISG content is released upon a single glucose stimulation [79]. Plasma membrane proximity [79, 80] and docking [44, 81] have long been suggested to contribute to an ISG's secretory capacity. More recently, ISG motility [82] and age [63, 82, 83] have also been shown to significantly contribute to an ISG's propensity for translocation to the plasma membrane and its necessity for docking [82, 83]. Finally, an ISG's fusion capacity – whether the ISG collapses or is recycled – may also be intrinsically regulated [59].

ISGs that are not secreted are targeted to the lysosome for degradation, either through autophagosome-dependent or independent pathways [84]. As insulin accounts for a large

proportion of protein synthesis in pancreatic beta-cells [85], ISG homeostasis is essential to maintaining beta-cell function [86]. In autophagosome-dependent degradation, ISGs are engulfed by autophagosomes and subsequently fuse with the lysosomes, degrading ISG contents [86, 87]. Autophagosome-independent degradation involves the fusion of ISGs with the lysosomes directly (crinophagy) [88]. Apart from whole ISG degradation, many proteases involved may also directly influence insulin turnover. For example, insulin has been shown to be degraded by insulin-degrading enzyme (IDE) in beta-cells and deletion or inhibition of this enzyme perturbs insulin secretion in beta-cells [89, 90].

It is now appreciated that all these processes are not only externally regulated by the ISG environment, and proteins both in and on ISG can modulate both the processing and trafficking of ISGs, ultimately controlling granule mobility, secretion capacity, and degradation. Our current review focuses on the continuing pursuit to characterise ISG-localised proteins from pancreatic beta-cells.

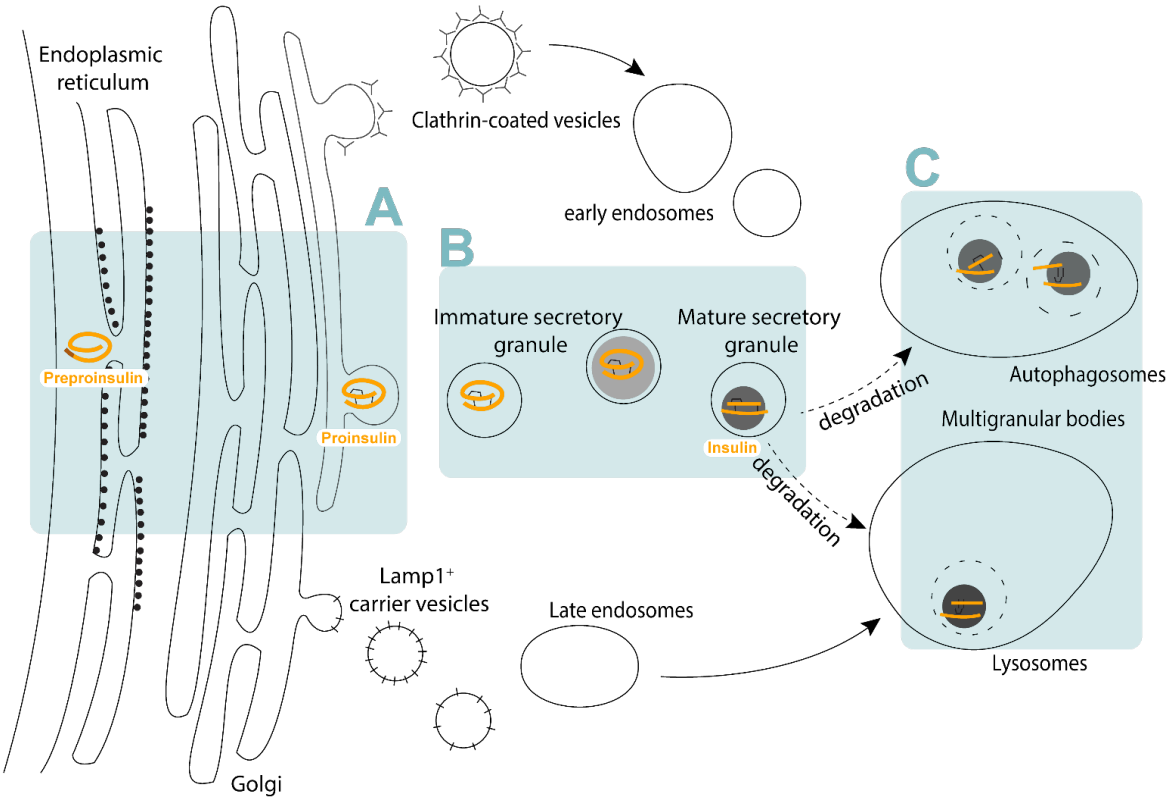

Figure 7: The insulin secretory pathway. A) Proinsulin is synthesised and folded at the endoplasmic reticulum, trafficked to the trans-golgi network, and sorted into budding immature insulin secretory granules. B) Immature insulin secretory granules undergo maturation where proinsulin is cleaved into mature insulin and condenses with zinc to form the dense core within the mature insulin secretory granule. C) Aged mature insulin secretory granules that do not undergo secretion are trafficked for degradation within lysosomes or autophagosomes

The ISG is key to beta-cell identity. Pathological dysfunction related to insulin occurs at all stages, from synthesis to secretion and primarily results in diabetes. Loss of ISG in beta-cells, termed degranulation, is particularly characteristic of Type 2 diabetes (T2D) and recognised as a marker of beta-cell failure. It is most commonly visualised as a loss of insulin content [91] and seen as a precursor to beta-cell dedifferentiation [92]. Degranulation may occur at the point of SG biogenesis, such as in instances of chromogranin B (CgB) deficiency [93] or the loss of vacuolar sorting protein 41 [94], which regulate ISG budding and ISG coat formation respectively. Alternatively, degranulation may also be the result of chronic overnutrition leading to beta-cell exhaustion, where persistent hyperglycaemia driving increased insulin secretion is unable to be matched by proinsulin biosynthesis in the beta-cell [95, 96]. Degranulation can also be a result of increased ISGs degradation as in the case of Sorcs1 deficiency [97]. Many genes relevant to the ISG secretory pathway have recently been reviewed extensively by Liu and colleagues in the context of pathology [98]. These include the hydrolases that function both as an endopeptidase for prohormone maturation and as lysosomal proteases [99, 100], vacuolar-type H^+-transporting ATPases which regulate granule pH [101], and ZnT8 (SLC30A8), the key membrane transporter for zinc translocation into the maturing ISG [102]. Additionally, SNARE proteins and Rabs such as Vamp8 and Rab37 mediate ISG fusion at the site of insulin secretion [103]. Particularly interesting are the roles of cargo proteins within the ISG, which appear to have interdependent relationships. These include the well described soluble proteins carboxypeptidase E [104], VGF [105], the prohormone convertases PC1/3 and PC2, and the granin proteins chromogranin A [106], CgB and secretogranin II [107, 108]. **Figure 8** collates these ISG proteins and their localizations to immature and mature ISG. Mutations in these proteins can affect ISG formation, proinsulin processing, and glucose-stimulated insulin secretion, ultimately resulting in reduced ISG numbers and impaired secretion. However, loss of a single ISG cargo protein can drive

compensatory behaviours in other ISG cargo proteins [106], suggesting ISG contents is a dynamic system.

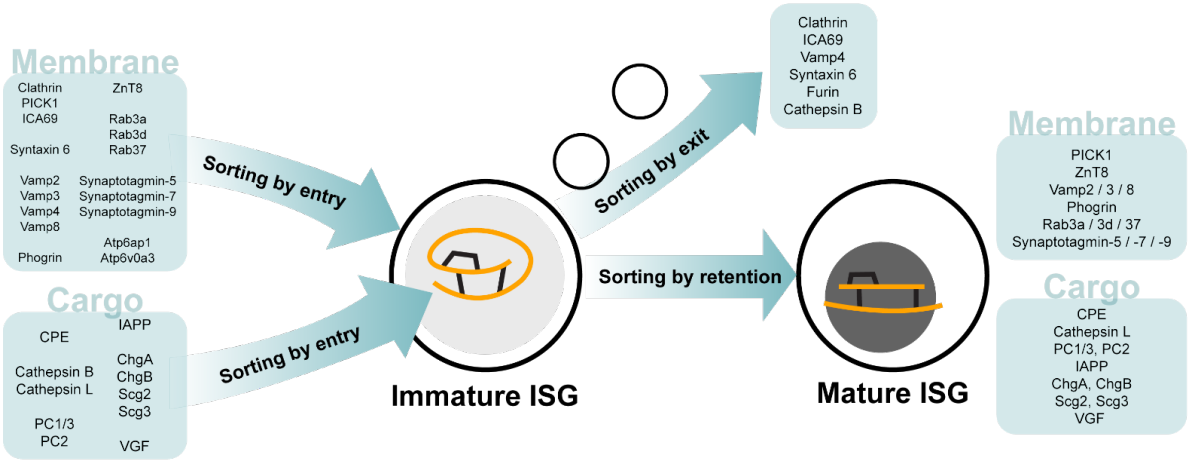

Figure 8: ISG membrane and cargo proteins of the immature and mature ISG. ISG proteins associated with the 'sorting by entry,' 'sorting by exit' and 'sorting be retention' steps of ISG biogenesis and maturation.

2. Isolating the Insulin Granule

ISG isolation has long been used in the beta-cell physiology research, though the prioritization of purity in the context of proteomic analyses is relatively new. Techniques used for the isolation of ISGs can essentially be separated into two categories, (a) differential subcellular fractionation using density gradients [109-111] and (b) immuno-based isolation [83, 112-114]. In subcellular fractionation protocols, commercially available high-viscosity mediums such as Ficoll, Percoll, Optiprep and Nycodenz, or laboratory-prepared glycerol, sucrose or mannitol solutions are used to separate intact ISGs from cell lysates. These centrifugation techniques exploit physical properties including the size, density and/or shape of each subcellular compartment to separate ISGs from other organelles in collected fractions of various volumes. As these fractions are crude and undoubtedly contain contaminants, most studies employ the use of two or more subcellular fractionation steps to improve the purification of ISGs [109]. The main advantage of centrifugation techniques are that they are inexpensive and efficient [115], allowing researchers to obtain reasonably enriched ISG fractions within a few hours.

The second most common approach are immuno-based methods to enrich for ISGs [113, 116], which exploit the tagging of proteins expressed in or on ISGs for isolation using immunoprecipitation. Often, this technique is used in conjunction with differential density gradients. For example, Hickey and colleagues employed the use of an Optiprep density gradient followed by Vamp2 immunoprecipitation to isolate ISGs from rat insulinoma INS-1 cells [112]. Immunoprecipitation offers the advantage of increased specificity to ISG compared to centrifugation techniques; however, these methods are often more expensive and laborious, and rely on prior ISG protein knowledge. Interestingly, some proteins may be differentially expressed on ISGs. For example, CgB has heterogenous localization with insulin-positive granules in the INS-1 cell line [117]. Most importantly, immunoprecipitation of specific

granule proteins that may be heterogeneously expressed would lead to the selective isolation of a specific ISG pool and the unknowing loss of information about the total ISG population.

On the other hand, immunoprecipitation could also selectively enrich for a non-ISG pool. In the same example, while Vamp2 immunoprecipitation may enrich for ISG, Vamp2 can also be expressed on Golgi recycling vesicles and endosomal membranes [118], and contamination of an ISG immunoprecipitation by these organelles cannot be disregarded. SG cargo proteins may also be present in pre-ISG compartments during the sorting process. Finally, immunoprecipitation methods also can be extended to protein pull-down studies which do not enrich ISG themselves, but instead immunoprecipitated interacting partners of known ISG proteins. Though these studies cannot offer a complete picture of the ISG proteome, they can offer an additional layer of insight into ISG protein functions and relationships [119-121].

It is likely that some combination of both immuno-based and centrifugation methods will be necessary to obtain the purest ISG fractions. Techniques used by the studies that have attempted proteomic analysis of ISG isolations are summarized in Figure 3. There is currently no consensus on the optimal strategy for intact ISG isolation from whole beta-cells. Insulin SGs are intrinsically dynamic and distribute in many compartments of the beta-cell as they traffic through their maturation, secretion and degradation pathways [116]. Isolation of a pure ISG fraction is most challenging due to the association of ISG with proteins in multiple subcellular compartments [122, 123], and previous proteomic analyses of ISGs notably include contaminating proteins from pre-granule compartments such as the ER and trans-Golgi network (TGN), as well as cytoskeletal and lysosomal proteins associated with the trafficking and degradation of ISGs respectively [122, 123]. Mitochondrial contamination present in ISG purification methods is a major problem [124] and attempts to isolate ISGs often identify different mitochondrial proteins in insulin enriched fractions [112, 114, 123, 125-129].

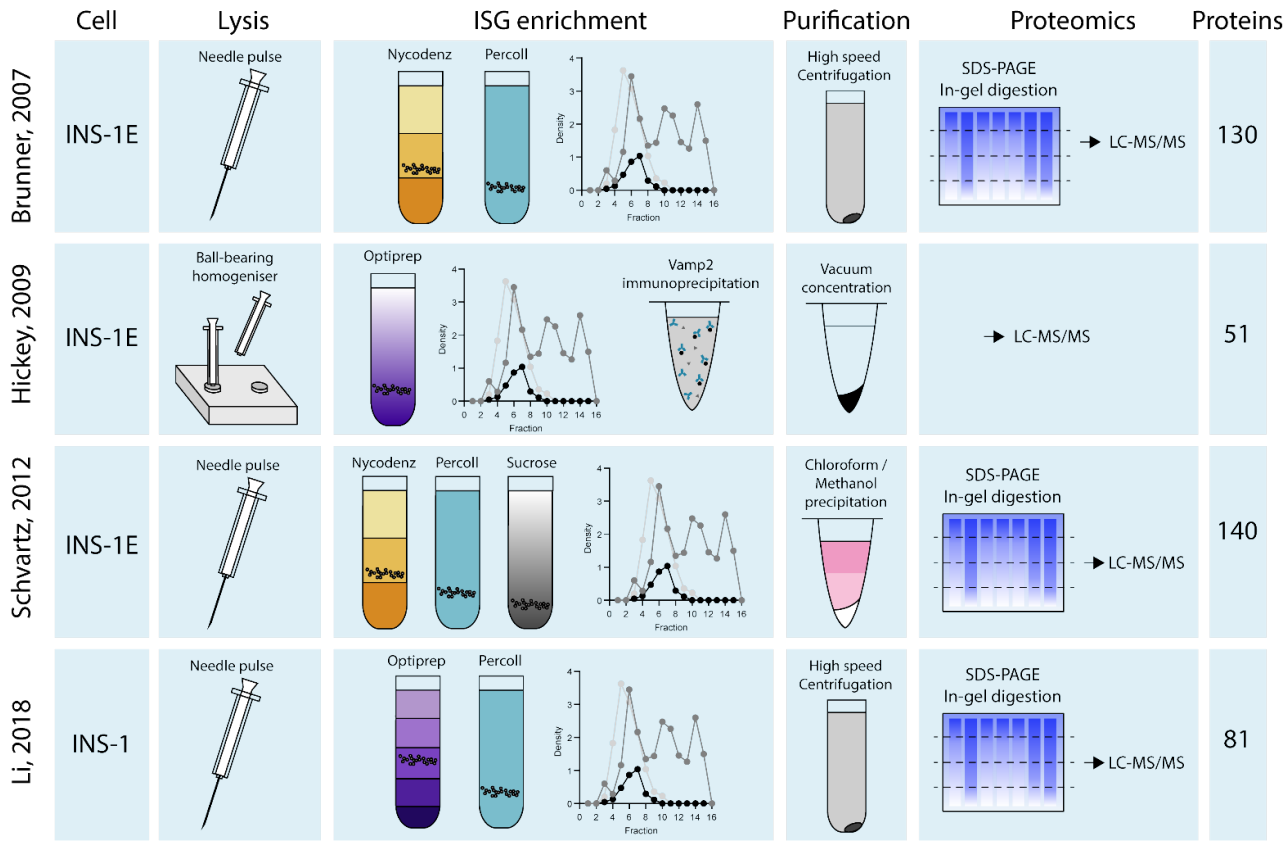

Figure 9: Schematic of insulin granule isolation and purification techniques across the 4 ISG proteomes.Rat insulinoma cells in all ISG proteomic studies are lysed before ISG enrichment through various density gradients or immunoprecipitations. ISG are then purified prior to proteomics analysis by LC-MS/MS to obtain list of ISG proteins. Data collated from Brunner *et al.*, 2007, Hickey *et al.,* 2009, Schvartz *et al.,* 2012 and Li *et al.,* 2018.

3. Identifying Insulin Granule Proteins

Only four studies have attempted to investigate ISG proteins by proteomic analysis to date [112, 123, 126, 129]. These studies employ various combinations of density gradient centrifugations, *in silico* analyses, and immunoprecipitation techniques (**Figure 9**). As a result, Li and colleagues identified 81 total ISG proteins from the INS-1 rat beta-cell line, while Schvartz *et al.* identified 140 ISG proteins, Hickey *et al.* identified 51 ISG proteins, and Brunner *et al.* identified 130 ISG proteins from the INS-1E rat beta-cell line (**Figure 10**). Proteomic data obtained from these four studies on ISG proteins from INS-1 or INS1-E cells produced a total of 5 proteins that were consistently identified. These were: Insulin-1 (Ins1), Insulin-2 (Ins2), Carboxypeptidase E (CPE), Chromogranin-A (CgA) and Prohormone convertase 2 (PC2). Rat beta-cells synthesize two different forms of insulin encoded by the *Ins*1 and *Ins*2 gene that share 90% homology [130, 131], hence two insulin forms found in these proteomes. Though different isolation techniques would influence the proteins identified, one would expect that using similar cell lines would result in more than a handful of proteins consistently identified across all four studies.

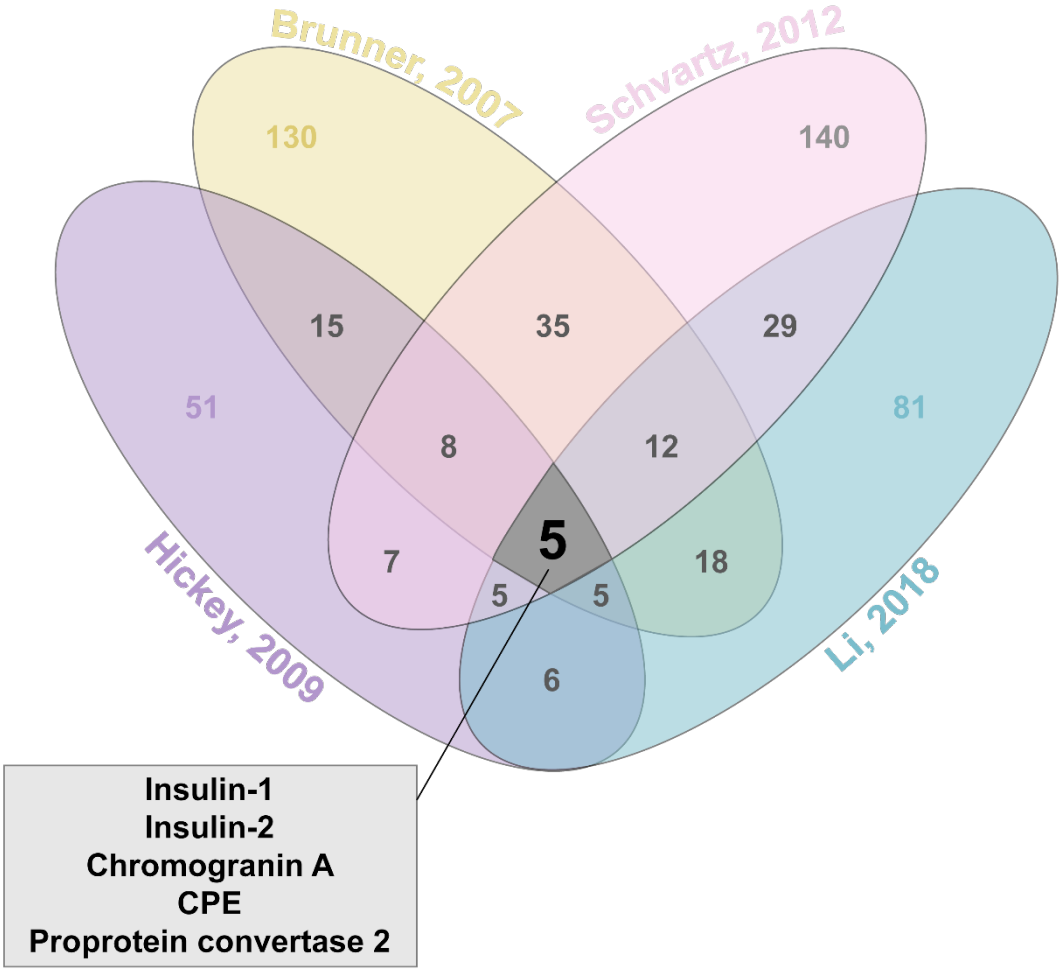

Figure 10: Venn diagram of overlapping proteins identified across the 4 ISG proteomes. Total of 5 proteins identified (box) in all proteomic analyses. Data collated from Brunner *et al.*, 2007, Hickey *et al.,* 2009, Schvartz *et al.,* 2012 and Li *et al.,* 2018.

Prior to ISG proteomics, Hutton *et al*. suggested ISGs may contain ~150 proteins using two-dimensional gel analysis of ISGs isolated from a rat islet tumour [110]. Approximately 30 specific proteins were described as ISG associated proteins before the first ISG proteome [126]. These proteins were individually classified primarily through cDNA screening and confocal microscopy. For example, the discovery of a well described ISG protein, the ZnT8 transporter was described as a pancreas-specific zinc transporter using RT-PCR on cDNA libraries with human tissue extracts [102]. Furthermore, ZnT8 was found to be localized specifically on ISGs through confocal microscopy of a fluorescent ZnT8 fusion protein expressed in INS-1 cells [102]. Similarly, phogrin was discovered as a membrane localized ISG protein through cDNA expression analysis and western blotting of phogrin with ISG enriched fractions [132]. These studies, among others were pivotal in uncovering different proteins that may modulate and affect insulin granule processes. Proteomics analysis of ISGs however provides an unbiased, comprehensive approach to the identification of multiple proteins simultaneously. Considering this however, all four studies lack the identification of these well-described ISG proteins such as ZnT8, any other zinc transporter and phogrin.

Here, we have classified the proteins identified in the ISG proteomes [112, 123, 126, 129] into three groups: i) intravesicular proteins, ii) membrane proteins and iii) other proteins:

3.1. Intravesicular Proteins

The most consistently identified intravesicular proteins in the proteomic studies were the previously well-characterised ISG proteins insulin (Ins1 and Ins2), CPE, PC2 and CgA [104, 106, 133-135]. Discovery of proinsulin processing of labelled insulin [136] and CgA [137] have allowed subsequent studies to identify localization of PC1/3 [138], PC2 [139] and CPE [140] as ISG localized enzymes. While all proteomes identified PC2 and CPE, PC1/3 was discovered only in two studies [123, 129]. Other intravesicular proteins identified were from

the chromogranin-secretogranin protein family. CgA in particular was identified in all four studies, with full-length CgA believed to be important for the biogenesis of granules in beta-cells [141]. Interestingly, CgA knockout mice display a reduced islet number, beta-cell to alpha-cell ratio and plasma insulin levels [142]; however, they exhibit normal blood glucose levels, as a result of compensation from other granin proteins [106]. CgB has been suggested to not be specifically involved in granule formation but instead is essential in the secretion of insulin and other islet hormones such as somatostatin and glucagon [93]. However, through pulse-chase labelling of CgB, Bearrows *et al*. show that in the absence of CgB, there is a delay in proinsulin trafficking from the TGN followed by a reduction in nascent ISGs at the plasma membrane [108]. CgB was identified in three of the four ISG proteomes (all but Li *et al*.). Significantly, aside from the full-length granins, PC1/3 and PC2 also cleave granins to form active peptides [133, 143]. Beta-granin is an example of a CgA derived peptide identified by Li *et al*. and is proposed to inhibit insulin secretion through unknown mechanisms [144]. This emphasises technical challenges in peptide identification in proteomics analysis, to differentiate the presence and eventual function of both granins and their derived peptides in future studies.

Hydrolases were found in two of the proteomics analyses [112, 126]. Cathepsins B and L were identified by Brunner *et al*. and are most intriguing as these proteins have been previously shown by electron microscopy to localise in immature ISGs, while cathepsin L alone remains in mature ISGs [100]. While some hydrolases have previously been described within ISGs [145, 146], other hydrolases present in proteomic analysis may be appearing due to crinophagy processes of ISGs with lysosomes [126, 147]. As such, further validation of hydrolase proteins will be essential to help elucidate their role in ISG biogenesis and processing. Particularly, the validation of cathepsins present in immature and mature ISGs demonstrates that these enzymes may follow sorting mechanisms out of immature ISGs via the

mannose 6-phosphate receptor [100, 148]. This adds weight to the '*sorting by retention*' and '*sorting by exit*' hypotheses in ISGs, in which immature ISGs may target proteins either for retention in maturing granules or exit towards the lysosome [100, 126, 149].

3.2. Membrane Proteins

A substantial proportion of ISG proteins identified by the proteomic analyses were membrane-bound or membrane-associated proteins. Of this group, the most commonly identified were synaptobrevin proteins (VAMPs), including Vamp3 [123, 126, 129], Vamp7 and Vamp8 [126]. VAMPs interact with their cognate t-SNAREs and other proteins that mediate the fusion of vesicles to the target membrane [150, 151], which in turn interact with a variety of presynaptic proteins and q-SNAREs to form the complete SNARE complex [152-154]. Vamp2 was first described as an ISG localised v-SNARE protein [155] by cDNA cloning and confocal microscopy. Brunner *et al*. then identified Vamp2 in their proteomics analysis and following this, Hickey *et al*. used Vamp2 antibodies to immuno-purify ISGs. Surprisingly, Hickey *et al*. and Li *et al*. do not identify Vamp2 in their proteomes, with Hickey *et al*. suggesting that it and many other docking proteins potentially remained on the immunoaffinity beads [112]. If these membranal proteins were left unidentified, this may explain why fewer proteins (51) were identified in comparison to other proteomes.

Rab proteins were also found to be enriched with ISG fractions. Rab proteins are a family of GTPases from the Ras superfamily [156] that modulate several stages of vesicle trafficking and fusion of ISGs with the plasma membrane [157, 158]. Through proteomic analysis and colocalisation imaging, Brunner's study illustrated that both VAMP8 and Rab37 are novel ISG associated proteins that colocalise with ISGs of INS1-E cells [126]. Previous to this, only 30 proteins were described as ISG associated proteins in beta-cells [126] and information surrounding the trafficking of ISGs was limited. Their proteomic analyses and validation of

novel proteins suggested a more complex trafficking process than previously established in beta-cells. Other SNARE complex proteins present in the proteomes include syntaxin-5 and 12, (Stx5, Stx12) [123] and granuphilin [126]. However, these proteins are believed to be localised to the plasma membrane [159] and not on ISG membranes, suggesting that they were present in contaminant co-purification with ISG fractions.

Many ATPase subunits were commonly identified in the four proteomic analyses, most notably the vacuolar-H^+ ATPases (V-type). These V-type ATPases have been previously shown to be localized to ISGs in beta-cells [160], and are important in producing and maintaining a proton gradient by acidifying the granule [160-162]. This facilitates the maturation of ISGs [36] as well as maintaining a suitable pH for intravesicular enzymes [76, 146]. Many other subunits of ATPases identified are lysosomal isoforms and should be validated as to whether they are genuine ISG proteins or proteins co-purified with ISGs.

3.3. Other Proteins

The remaining proteins identified with non-specific or unknown localization in ISGs are often grouped in these studies. These include cytoskeletal, cytoplasmic and organelle localized proteins. The cytoplasmic proteins identified range from mis-folding chaperones [112] and isomerases (PDIA3) [126] to N-ethylmaleimide sensitive fusion protein [123, 129]. Whether these proteins are genuinely ISG-associated, or technical contaminants, requires further validation. Different cytoskeleton-associated proteins are found across all four proteomes. Alpha-centractin [129], alpha and beta-actin [112] and kinesin subunits [129] are some examples of cytoskeletal associated proteins identified. ISGs are transported along microtubules by kinesins [163] and cytoskeleton remodelling is critical for ISG trafficking during glucose-stimulated insulin secretion [164]. The presence of these proteins is therefore unsurprising, though are likely present due to co-purification of these proteins through the

isolation of ISGs. Indeed, the presence of proteins localized to the ER, Golgi, mitochondria, and lysosomes are also commonly observed across all four studies. Examples include Erp44 (ER), Glg1 (Golgi), SHMT (mitochondria) and Lamp1 (lysosomes) [123, 129]. It is difficult to prevent the copurification of these proteins using present isolation techniques and their co-localisations with ISGs need further validation.

The presence of isomerases and proteins involved in protein folding is quite surprising. Hickey *et al*. in particular find a striking number of chaperone proteins (~20% of proteins identified) [112]. Recent studies have shown that ER chaperone proteins are vital in proinsulin handling and insulin-like growth factor folding [165]; however, none of these ER-resident proteins have been shown to be localized in ISGs. Interestingly, Stanniocalcin-1 (STC1) or its precursors were found in three of the four proteomes (Li, Schvartz, Brunner). STC1 is found in many tissue types such as muscle, kidney, adrenal and lung [166]. Human STC1 protein is described as an uncoupler of oxidative phosphorylation in mitochondria [167], and has been implicated in apoptotic mechanisms and carcinogenesis [168]. Its function in beta-cells is not well understood, however; immunocytochemistry, and *in situ* ligand binding and hybridization [169] show that STC1 colocalizes with insulin in mouse pancreatic beta-cells. The abundance of these chaperones, alongside identification of proteins such as STC1, illustrates the importance of ISG proteomics as a rich source of data to potentially identify novel ISG proteins that may modulate different processes of ISG biogenesis, trafficking, and secretion. Altogether, these studies highlight the importance of developing improved purification techniques that restrict isolation of ISGs to granules post-sorting and packaging from the TGN, and before degradation.

4. Understanding ISG Function through the Proteome

Many aspects of ISG biosynthesis, processing, trafficking and secretion have been well reported [170], with the majority of studies focusing on individual protein effects on beta-cell function. Fewer studies use a broad view approach of ISG proteins, and their interactions and localisations. Efforts to identify exclusive ISG proteins in beta-cells remains scarce, and it is obvious that experimental methodology is the primary challenge. Proteomic analysis is appealing because it provides an unbiased approach to uncovering new ISGs proteins, and validation of targets will help understand mechanisms underlying beta-cell function. Indeed, the proteomics-based discovery of VAMP8 and Rab37 as ISG proteins by Brunner and colleagues resulted in the detection of a novel set of proteins that regulate fusion of ISGs to the plasma membrane, and thus established the paradigm for ISG exocytosis [126]. In a similar fashion, the identification of hydrolases [100] within the ISG lumen suggests there are still many facets of ISG recycling and degradation that remain unappreciated.

Intrinsic ISG behaviour is an intriguing concept, and the evidence for functionally distinct populations of mature ISG is growing. For a long time, ISG have been believed to exist in either a ‘readily releasable pool (RRP)’ or ‘reserve pool (RP)’ of granules within the beta-cell cytoplasm [171-173]. The presence of Rab37a effector protein granuphilin on ISG appears to regulate granule docking at the plasma membrane, interacting with Syntaxin-1A-Munc18-1 complexes [55], and contributing to the RRP. However, ISG docking has been found to be a limiting step in ISG exocytosis and is not a requirement for granule fusion, as it restricts ISG motility and is dysregulated in T2D [174]. In contrast, newcomer granules from the RP have been identified to exhibit high mobility [175] and fusion competence irrelative of docking [176]. Newcomer granules abundantly express Syntaxin-3, which interacts with Munc-13-1 and Vamp8 to mediate their priming and fusion states [177]. Newcomer ISG also appear to have high calcium sensitivity, fusing away from Syntaxin-1A and L-type Ca^{2+} channels [178].

Whether these distinct subpopulations can be distinguished by their proteome will be critical to understanding the physiological relevance for granule pools in ISG function. Indeed, there is some evidence for the existence of distinct mature granule subpopulations differentiated by the expression of surface markers synaptotagmins-7 and -9 [179]. These ISG populations exhibit unique lipid compositions, calcium sensitivities, and even proprotein convertase protein distribution. Most significantly, relative proportions of these subpopulations are changed in diabetes, with the specific depletion of synaptotagmin-9 ISG observed in a model of T2D [179].

Recent studies have demonstrated that ISG age plays an important role in dictating secretion and degradation [63, 66, 82, 83, 180], with younger ISG preferentially secreted in first-phase glucose-stimulated insulin secretion. It is possible that changes in protein composition occur in aging ISG, controlling functional differences in these younger and older populations. Two unique strategies have since been used to identify age-distinct ISGs from beta-cells. The first is a fluorescent protein timer construct, syncollin-dsREDE5TIMER, that localises to the lumen of ISGs [83, 181] and changes its emission spectra over time. Integrating this construct into beta-cells and then applying a technique termed fluorescence-assisted organelle sorting (FAOS), submicron vesicles are thus fluorescently-labelled for sorting [182]. In the second, Neukam *et al.* and Ivanova *et al.* employ the use of pulse-chase labelling of ISGs using either a SNAP or CLIP tag fused to insulin or phogrin respectively, followed by immuno-purification using fluorescent dye TMR [63, 113]. The advantage of techniques that track syncollin or phogrin, as opposed to insulin, lie in the resulting exclusion of pre-sorting compartments within the beta-cell. Syncollin-dsREDE5TIMER is only red fluorescent in ISG from approximately 18 hours onwards, when ISG are distinctly mature, while phogrin-fused CLIP is immuno-precipitated by TMR only after its sorting in ISG. Neither technique has yet produced proteomic samples, potentially due to the challenge of separating old ISG from degradation pathways. Mature syncollin-dsREDE5TIMER is detectable within Lamp1-

positive vesicles (data not shown), while Hoboth and colleagues also visualise SNAP-tagged ISG within multigranular autophagic bodies [82]. Neukam *et al.* attempt to mitigate this issue with the addition of a second immunoprecipitation step with Lamp2 and Syp1 to deplete apparent lysosomal contamination [113]. The optimisation of these methodologies will help expand our current understanding of the underpinnings regulating insulin secretion and beta-cell function.

5. Moving Forward

The four proteomic analyses examined in this review used combinations of density gradients to isolate ISGs. The use of additional ISG markers by Hickey *et al.* to further purify ISG is desirable in theory, but practically results in additional challenges. Of note, their use of Vamp2 immuno-isolation of ISG did not result in the identification of Vamp2 (or any other Vamp proteins) within their proteome. Indeed, with only five proteins identified across all four ISG proteomes, many established ISG-exclusive proteins such as PC1/3 [138], phogrin [132] and the ZnT8 transporter (SLC30A8, [102]) were not identified consistently or at all, confirming major technical limitations. There have also been enormous leaps in mass spectrometry technology since Brunner and colleagues first established an ISG proteome in 2007, and the exceedingly increased sensitivities from mass spectrometers and improved peptide search databases currently available will allow deeper proteome depth and accuracy [183, 184]. Recent proteomics studies utilising library-based analyses techniques in mouse primary islets identified over 11,000 unique proteins using minimal starting material (unpublished data), suggesting similar database searches could generated and applied to the ISG proteomes to improve protein recognition. Li *et al.* additionally demonstrate the potential for novel protein discovery by utilising protein correlation profiling to match candidate proteins to known ISG markers based on Euclidean distance [123]. Recent development of different

protein sequencing, such as nanopore technology [185] and fluorescent "protein fingerprinting" [186] may also facilitate new ISG protein identification.

The majority of ISG isolation studies focus solely on the mature ISG. Immature ISG isolation is considerably more difficult since immature ISGs lack the dense zinc core, and more closely associate with pre-sorting compartments. Though Chen *et al.* demonstrate the use of fixed Percoll percentages to enrich immature ISG [109] using density, both ER and TGN membrane proteins were found to be contaminating in those fractions. There is potential that the use of immature ISG-specific proteins could be further exploited to isolate immature ISGs. For example, PICK1 and ICA69 form a protein complex on immature granules, but only PICK1 persists in mature granules [187]. Similarly, clathrin is '*sorted-by-exit*' from immature ISG, though is also present on non-ISG vesicles. Proteomic analyses of immature ISGs will improve our understanding of both sorting mechanisms at the TGN, and processing of the ISG itself during insulin maturation. Many beta-cell pathologies are intimately linked to ISG formation, despite the most common diabetes therapies targeting defective ISG secretion. Dysregulated ISG biogenesis leads to glucose intolerance *in vivo* [94, 97, 105, 188], while increased proinsulin / insulin ratios are archetypical of diabetic patients and indicative of impaired processing within immature ISG [189, 190].

Current ISG proteomes studies have only investigated rat insulinoma INS1 or INS1-E cell lines. This is most likely due to ease of culture and scaling to large starting material quantities, but it is important to consider how the ISG proteomes in mouse or human beta-cells may differ, potentially with the application of these methods to the MIN6 or EndoC-βH1 cell lines. Of the proteins with consensus across the ISG proteomes, all have human orthologs (INS, CHG, PCSK2, CPE), though humans only have a single insulin gene. Human beta-cell proteomics studies are also rare as they rely on precious and scarce material and are often

subject to contamination by other endocrine cell types. Up to 707 potential beta-cell proteins have been identified [191-193], though it is yet unknown how many of those are ISG-specific.

Moreover, it will be critical to translate those techniques established within cell lines to primary cells to provide a more accurate snapshot of ISG proteins *in vivo*. There is potential to incorporate flow cytometry sorting techniques to isolate primary beta-cells, separated by an insulin-tagged fluorophore [194], zinc dyes or probes [195, 196], or even NADPH autofluorescence [197, 198] prior to ISG enrichment. Following this, the application of immunoprecipitation of select ISG markers [112], or dynamic fluorophores such as dsRedE5TIMER [83], will further allow ISG population separation. Once optimised, these methodologies would provide a standard for ISG proteomics that could be applied to multiple models of insulin-associated pathologies, including T2D.

A clean proteomic analysis of ISGs will provide a resource for more complete understanding of ISG sorting, processing, and trafficking. Currently, ISG proteomes are scarce, limited to rat insulinoma cell lines, and contain significant contamination. With the continued development of improved ISG isolation techniques, purification strategies and advancements in proteomics, ISG proteomes should be revisited, applied to different cell lines and ISG subpopulations to investigate and uncover novel players in the ISG secretory pathway.

1.9 Summary

As reviewed in **Chapter 1**, only a few studies have attempted to obtain a comprehensive understanding of proteins on the ISG. Although these studies utilized different techniques and mass spectrometers, which may influence the proteins identified and make direct comparisons challenging. However, it is reasonable to expect that many of the highly abundant ISG proteins would be consistently identified across all 4 studies. While only a handful of proteins were found in consensus, many other canonical ISG proteins (e.g. ZnT8, IAPP, Vamp2) were not detected across all studies.

There is a strong understanding of ISG exocytotic defects in T2D, with current therapeutics primarily aimed at increasing insulin release from beta-cells [199]. Increasing evidence highlights the crucial role of the ISGs as signalling hubs, modulating normal beta-cell function [69, 200, 201]. Dysregulation of key ISG-associated proteins in concert with increased exocytosis of proinsulin may hint or suggest the potential loss of preferential ISG release in T2D development. Thus, therapies that focus solely on targeting the distal stages of ISG exocytosis may only delay further deterioration of beta-cell function in disease. Instead, more effort should be directed toward understanding the earlier stages of ISG biology, including biogenesis and ISG turnover to develop therapies aimed at restoring or improving ISG functionality in T2D that may help preserve or improve normal beta-cell function.

1.10 Aims and Hypotheses

There grows an increasing pool of evidence that ISG-resident proteins create an intrinsic mechanism that controls ISG processes and normal beta-cell function. However, we lack a complete understanding of ISG compositions that drive the existence of functionally distinct insulin granule populations. Moreso, with the identification of distinct populations driven by individual granule age, the mechanism by which younger granules are preferentially

selected for exocytosis is poorly defined. In this thesis, we aim to aimed to develop a transferrable protocol to characterise the insulin secretory granule holistically, implicating novel ISG-resident proteins (**Chapter 2**). Using this optimised protocol we then aimed to investigate potential changes in the composition of ISGs when beta-cells are perturbed with conditions of metabolic stress (**Chapter 3**). Lastly, we aimed to characterise the preferential release of young insulin granules from beta-cells (**Chapter 4**).

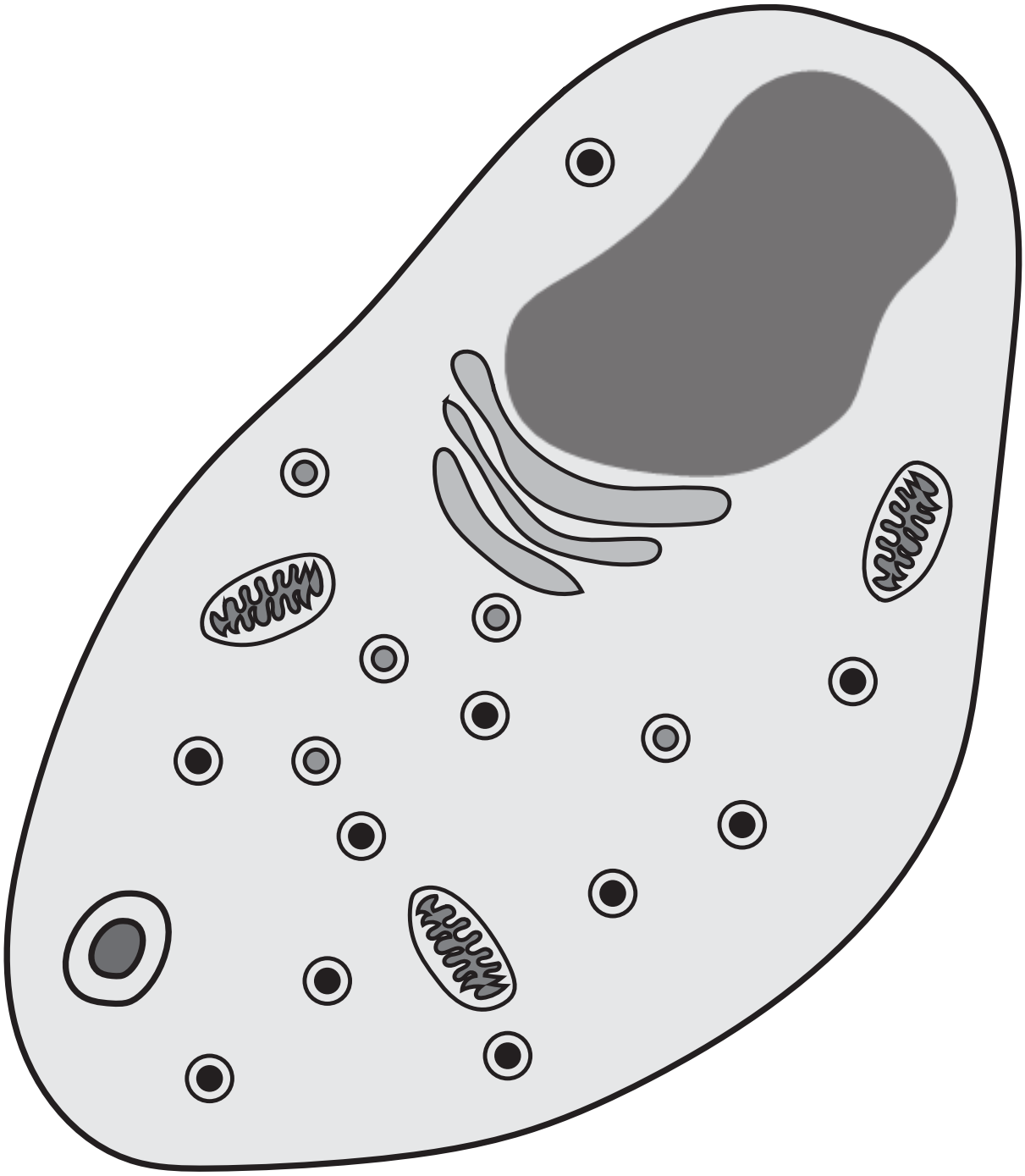

Chapter 2

Proteomics analysis of insulin secretory granules reveal novel regulators of insulin secretion

2.1 Introduction

Purification of ISGs remain a challenge within the field with a lack of a clear insulin granule proteome available, specifically the lack of a murine insulin granule proteome. The discovery of novel ISG proteins, lipids or other constituents that may intrinsically regulate insulin exocytosis is dependent on an efficient and effective purification protocol and subsequent analytical tools to piece a compositional map of ISGs that may function to postulate proteins vital for normal beta-cell function or perhaps a mechanism of ISG selection for secretion. The following section (**Chapter 2.2**) is a research article published in *Diabetes* (DOI: 10.2337/db24-0355) [202], with citation numbers updated to reflect current thesis structure. Figures were restructured to be readable in this current thesis. This research article summates the development of an efficient three-step purification method to isolate and purify ISGs from MIN6 beta-cells, using an unbiased and targeted machine learning proteomics analysis tool to resolve an ISG proteome and validate novel ISG-associated proteins that regulate insulin content and secretion from beta-cells.

2.2 Optimized proteomic analysis of insulin granules from MIN6 cells identifies Scamp3, a novel regulator of insulin secretion and content

Running Title: **Scamp3 is a novel regulator of insulin in β-cells.**

Nicholas Norris[1,2], Belinda Yau[1,2], Carlo Famularo[1,2], Hayley Webster[1,2], Thomas Loudovaris[3,4], Helen E. Thomas[3,4], Mark Larance[1,2], Alistair M. Senior[1,5], *Melkam A. Kebede[1,2]

1 Charles Perkins Centre, The University of Sydney, Camperdown, New South Wales, Australia

2 School of Medical Sciences, Faculty of Medicine and Health, The University of Sydney, New South Wales, Australia

3 St. Vincent's Institute, Fitzroy, Victoria, Australia

4 Department of Medicine, St. Vincent's Hospital, University of Melbourne, Fitzroy, Victoria, Australia

5 School of Life and Environmental Sciences, Faculty of Science, The University of Sydney, New South Wales, Australia

*Correspondence, melkam.kebede@sydney.edu.au, PHONE NUMBER - +61423508002

Word Count: 3998

Figures: 4 main figures, 2 supplemental figures

Tables: 1 main table, 6 supplemental excel files

Abstract

Pancreatic β-cells in the *Islets of Langerhans* are key to maintaining glucose homeostasis, by secreting the peptide hormone insulin. Insulin is packaged within vesicles named insulin secretory granules (ISGs), that have recently been considered to have intrinsic structures and proteins that regulate insulin granule maturation, trafficking, and secretion. Previously, studies have identified a handful of novel ISG-associated proteins using different separation techniques. Here, this study combines an optimized ISG isolation technique and mass spectrometry-based proteomics, with an unbiased protein correlation profiling and targeted machine learning approach to uncover 211 ISG-associated proteins with confidence. Four of these proteins: Syntaxin-7, Synaptophysin, Synaptotagmin-13 and Scamp3 have not been previously ISG-associated. Through colocalization analysis of confocal imaging we validate the association of these proteins to the ISG in MIN6 and human β-cells. We further validate the role for one (Scamp3) in regulating insulin content and secretion from β-cells for the first time. Scamp3 knock-down INS-1 cells show a reduction in insulin content and dysfunctional insulin secretion. These data provide the basis for future investigation of Scamp3 in β-cell biology and the regulation of insulin secretion.

Keywords: insulin secretory granule, beta-cell, pancreas, proteomics, syntaxin-7, synaptophysin, synaptotagmin-13, scamp3

Graphical Abstract

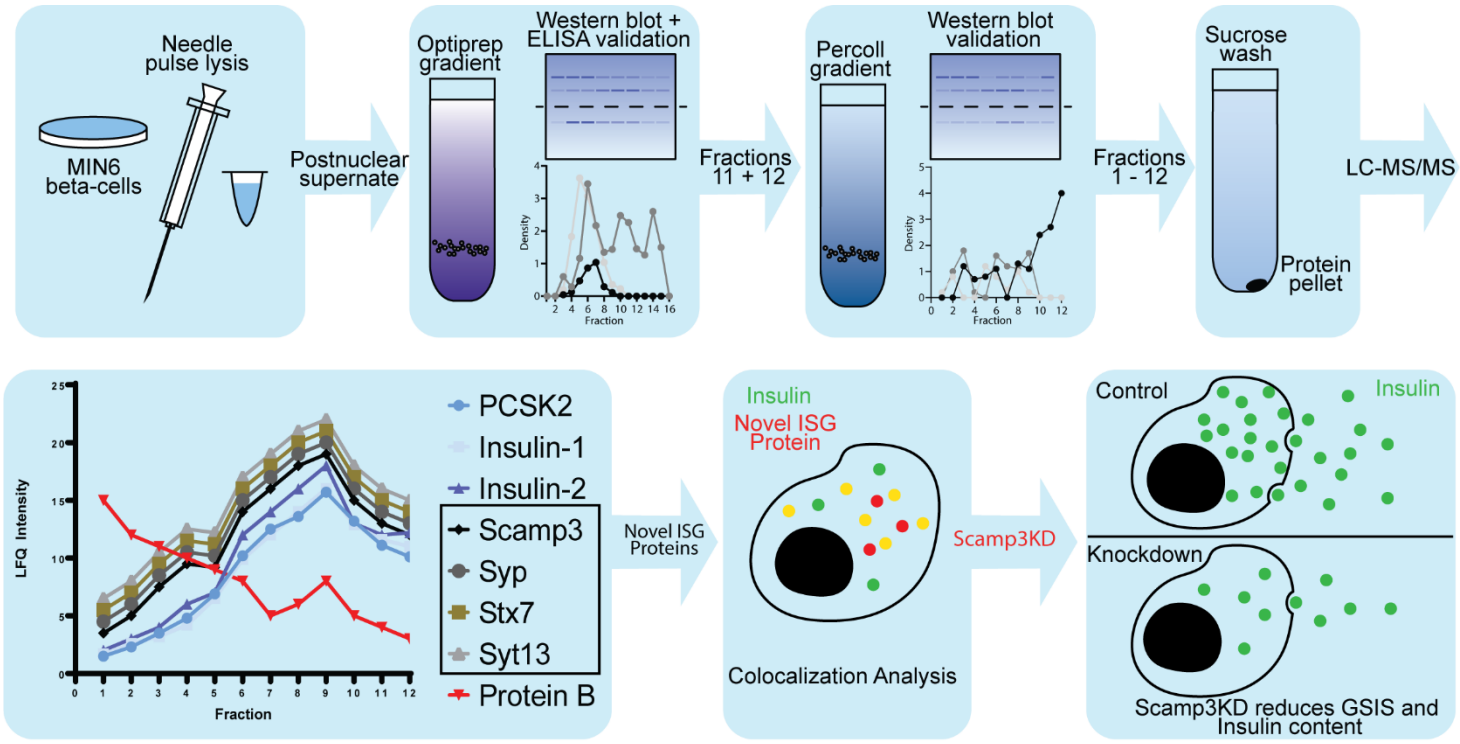

Article Highlights

- This study optimizes insulin granule isolation techniques alongside enhanced proteomics analyses to establish the first murine insulin secretory granule proteome.
- We investigated what proteins are present on insulin granules from MIN6 cells to further our understanding of insulin granule biogenesis, trafficking, and secretion.
- We found 211 insulin granule-associated proteins and validated 4 novel proteins.
- Through further functional studies, we implicated Scamp3 as a novel protein that regulates insulin content and secretion in β-cells.

INTRODUCTION

Pancreatic β-cells play a crucial role in maintaining blood glucose levels and their dysfunction is a hallmark of type 2 diabetes (T2D). Located within the *Islets of Langerhans,* these cells release insulin, which stimulates glucose uptake by adipose tissue, liver, and muscle [203]. In T2D, β-cells exhibit a reduction in glucose-stimulated insulin secretion (GSIS), and dysregulated insulin biogenesis and trafficking [42, 204].

In β-cells insulin is stored within the insulin secretory granules (ISGs), which are ~300 nm in diameter and contain a dense core [200]. In response to nutrient stimuli ISGs are triggered for exocytosis and transported to the plasma membrane where they fuse and release insulin.

ISG biogenesis begins at the trans-Golgi network (TGN), where proinsulin is sorted alongside prohormone convertases, co-secreted hormones, and carrier proteins [200] into immature ISGs (iISGs). Within iISGs, prohormones are cleaved into mature forms [205], granule lumen become acidified and undesired proteins are removed [206]. Mature insulin then crystallizes with zinc cations to form insulin hexamers, which constitute the dense core of the ISGs [207].

ISGs are dynamic structures, and numerous proteins residing within them play crucial roles in insulin biogenesis and secretion. For example, deficiencies in Chromogranin-B (ChgB) leads to impaired proinsulin processing, and reduction in GSIS *in vivo* [93] and *in vitro* [208]. Knock-out models of protein interacting with C Kinase-1 (PICK1) and islet cell autoantigen of 69 kDa (ICA1) also cause impaired insulin secretion and defective glucose metabolism [209]. As such, dysfunction of these ISG resident proteins contribute to metabolic disease and T2D. Thus, interrogating the ISG and discovering novel ISG-resident proteins will enhance our

understanding of insulin granule biogenesis, trafficking, and glucose-mediated secretion of ISGs.

Four previous studies have attempted to capture snapshot proteomes of ISG within β-cells [112, 123, 126, 129]. However, these studies assemble 5 proteins in consensus: Insulin-1 (Ins1), Insulin-2 (Ins2), Chromogranin-A (CgA), Prohormone convertase 2 (PCSK2) and Carboxypeptidase E (CPE). Given this, it is difficult to interpret the collective proteomic data due to the co-enrichment of contaminating proteins or fragments of subcellular organelles such as the Golgi network, lysosomes and most commonly, mitochondria [112, 123, 126, 129]. Our study addresses this caveat by employing an optimized protocol to enrich for ISGs and a dual unbiased and targeted proteomics approach to minimize contamination from other subcellular compartments.

Previous studies on ISG isolation methods and proteomics analyses have focused solely on rat insulinoma INS-1 or INS1-E cell lines [112, 123, 126, 129]. Here, we modify an ISG enrichment method described by Chen et al. 2015 [109], to enrich ISGs from the mouse insulinoma β-cell line MIN6. MIN6 cells are arguably a better model for human metabolism because they possess a larger pool of ISGs, respond similarly to human islets in response to lipotoxicity [210] and can form pseudo-islets in culture [211]. The modified three-step purification protocol involves sequential Optiprep and Percoll gradient enrichment followed by sucrose purification of mature ISGs (mISGs). LC-MS/MS analysis of fractionation samples identified 8021 unique peptides. Using protein correlation profiling (PCP) analysis, we identify 432 potential ISG proteins. Parallel analysis using proteomic-specific software allowed us to categorize proteins into defined subcellular organelles, assigning 211 proteins to the ISG with high confidence. To validate ISG targets, we conducted insulin colocalization analysis in immuno-stained MIN6 cells and human islets, confirming the ISG localization of Scamp3, Synaptophysin, Synaptotagmin-13 and Syntaxin-7. Finally, siRNA-mediated Scamp3

knockdown in INS-1 cells elicited a defect in insulin content, and GSIS, implicating the novel ISG protein in healthy β-cell insulin regulation for the first time.

Material and Methods

Human pancreata and ethics statement

Human pancreata tissue were obtained from deceased organ donors as part of the St Vincent's Institute islet isolation program, through Donatelife to obtain research consent and adhere to strict ethical guidelines developed by the National Health and Medical Research Council (NHMRC), Australia (Reference Number: E76, ISBN: 9781925129595). Donor information can be found in **Supplementary Table 1**. Male and female tissues were used, and sex was not considered a factor in statistical analyses of the data.

Cell Culture

MIN6 cells (male mouse derived) were purchased from AddexBio™ and cultured in standard culture media as stated previously [68]. INS-1 cells (male rat derived) were cultured in standard cultured media as previously described [68]. Culture media was changed every 2–3 days and cells were passaged every 4–5 days. MIN6 cells were used at passages between 15-26. INS-1 cell were used at passages between 19-33.

Optimized three-step purification of mature ISGs from MIN6 cells.

We optimized a two-step subcellular fractionation protocol described by Chen et al. 2015 [109]. MIN6 cells were grown on 15cm diameter petri dishes to 80 – 90% confluence. Plates were PBS washed, then cells scraped into 2mL of ice-cold PBS and centrifuged at 300xg for 3 min. The pellet was resuspended in 1mL of Buffer A (0.3 M sucrose, 1 mM EDTA, 1 mM $MgSO_4$, 10 mM MES-KOH, pH 6.5 containing EDTA-free protease inhibitors (Roche), then passed through a 21 G and 25 G gauge needle (10 times each). Homogenates were centrifuged

(1000 x g, 5 min) and the supernatant was loaded atop a discontinuous Optiprep gradient of five 3mL layers: (from top): 8.8, 13.2, 17.6, 23.4 and 30 %, diluted in Buffer B (2 mM EGTA, 20 mM MES-KOH, pH 6.5). Samples were centrifuged (100,000 x g, 80 mins) in a P50AT2 fixed angle rotor in a Hitachi 100NX ultracentrifuge set at half acceleration, and half deceleration. 1 mL fractions were removed from the top to obtain a total of 16 fractions. Percoll was used in the second step to further enrich and purify ISGs. mISG-enriched Fractions 11 and 12 were loaded on 10 mL of 27 % Percoll solution, diluted in Buffer A in a 16 mL polypropylene tube, then centrifuged (35,000 x g, 60 min) in a A22-24x16 (Thermo Fisher) fixed-angle rotor in a Sorvall Lynx 4000 Centrifuge (Thermo Fisher). 1 mL fractions were removed from the top to bottom to obtain 12 fractions. In the third step, twelve 1 mL fractions following Percoll enrichment were suspended in 9 mL each of sucrose wash buffer (0.3 M sucrose, 5 mM HEPES, 1 mM EGTA, pH 7) and centrifuged (23,700 x g, 15 min) to pellet ISGs and remove Percoll from solution. Supernatants were discarded and the pellet was resuspended in 4 % sodium deoxycholate (SDC) in H_2O and boiled (100 °C, 10 min) for mass spectrometry (MS) analysis.

LC-MS/MS

LC-MS/MS samples were prepared as previously described [212]. Peptides were reconstituted with 5 % formic acid in MS-grade H_2O, sealed and stored at 4 °C until LC-MS/MS acquisition. Using a ThermoFisher RSLCnano ultrahigh performance liquid chromatograph, peptides in 5 % (v/v) formic acid (3 µL injection volume) were injected onto a 50 cm x 75 µm C18Aq (Dr Maisch; 1.9 µm) fused analytical column with a ~10 µm pulled tip, coupled online to a nanospray electrospray ionization source. Peptides were resolved over gradient from 5 – 40% acetonitrile for 70 min, with a flow rate of 300 nL min^{-1} (Capillary flow). Electrospray ionization was done at 2.3 kV. Tandem MS analysis was carried out on a Q-Exactive HFX mass spectrometer (ThermoFisher) using data-independent acquisition

(DIA). DIA was performed as previously described using variable isolation widths for different m/z ranges [213]. Stepped normalized collision energy of 25±10% was used for all DIA spectral acquisitions.

Raw MS data were analyzed using quantitative DIA proteomics software DIA-NN (v. 1.8) [214]. Complete mouse proteome databased from UNIPROT was used for neural network generation, deep spectral prediction enabled. Protease digestion was set to trypsin (fully specific) allowing for two missed cleavages and one variable modification. Oxidation of Met and acetylation of the protein N-terminus were set as variable modifications. Carbamidomethyl on Cys was set as a fixed modification. Match between runs and remove likely interferences were enabled. Neural network classifier was set to double-pass mode. Protein interferences were based on genes. Quantification strategy was set to any liquid chromatography (LC, high accuracy). Cross-run normalization was set to RT-dependent. Library profiling was set to smart profiling.

SDS-PAGE

Protein concentrations of fractions or insulin granule pellets from fractionation methods were analysed using Pierce BCA Protein assay (ThermoFisher) and subjected to SDS-PAGE. All antibodies used are listed in **Table 1**. Protein signals were detected by chemiluminescence (Millipore) on a ChemiDoc MP Imaging System (Bio-Rad). Insulin SDS-PAGE was performed using modified SDS-PAGE protocol described previously [215].

Immunofluorescent Staining

Cells and human pancreata were prepared for immunofluorescent staining following standard procedure previously described [68, 216]. Cell cultures were fixed with 4 % PFA, fixed and sectioned human pancreata were provided by the St Vincent's Institute.

Microscopy

Microscope slides were imaged using the Leica LCS SP8 confocal microscope (Wetzlar, Germany). Slides were imaged using a 93X magnification glycerol lens (cells) or a 40 X oil lens (human pancreata), white & STED lasers. Leica LAS X software was used for image collection and colocalization analysis done with Fiji ImageJ [217].

Insulin and Proinsulin ELISA

Insulin concentrations for INS-1 content and subcellular fractionation (Optiprep) were measured using the Ultra-Sensitive Mouse Insulin ELISA Kit (Crystal Chem, USA), Proinsulin concentrations were measured by Rat/Mouse Proinsulin ELISA Kits (Mercodia).

siRNA Knockdown of Scamp3

Scamp3 knockdown (KD) cells was generated by transfecting INS-1 cells with siRNA mediated oligomers. INS-1 cells were cultured on glass microscope coverslips for immunofluorescent imaging or 6-well and 12-well plates for SDS-PAGE and GSIS respectively. Cells were transfected using two commercial rat Scamp3 siRNAs (TriFECTa DsiRNA, IDs: rn.Ri.Scamp3.13.2 #613664206 (si#1), rn.Ri.Scamp3.13.3 #613664207 (si#2), and a non-targeting siRNA (TriFECTa DsiRNA, Lot #0000865210) complexed with Lipofectamine 2000 (ThermoFisher) at a concentration of 10nM. Cells were fixed or harvested 48 hours post transfection to validate Scamp3 KD by SDS-PAGE and confocal imaging. GSIS assays were performed on INS-1 cells 48 hours post transfection.

Quantitative RT-PCR

RNeasy kit (Qiagen) was used to extract total RNA. cDNA synthesis was performed using 500ng of RNA with iScript Reverse Transcription Supermix (Biorad). RT-PCR was labelled using SYBR select master mix (ThermoFisher) and fluorescence quantified by LightCycler 480 II (Roche) normalized to rat GAPDH. The following primer sequences used were: Scamp3(rat), forward, 5’-CAGGAGAAGAGCCAGAGTGC-3’, and reverse,

5’AGAGACTGCAGGGATAGGGG-3’. Pdx1(rat), forward 5’AAATCCACCAAAGCTCACGC-3’, and reverse, 5’AAGTTGAGCATCACTGCCAGC-3’, GAPDH (rat), forward, 5’-CAAAATGGTGAAGGTCGGTGTG-3’ and reverse,5’-TGATGTTAGTGGGGTCTCGCTC-3’, Insulin-1(rat), forward, 5’-CCTTTGTGGTCCTCACCTGG-3’, and reverse, 5’TGCCAAGGTCTGAAGATCCC-3’, Insulin-2(rat), forward, 5’-GCAGGTGACCTTCAGACCTT-3’, and reverse, 5’-CAGAGGGGTGGACAGGGTAG-3’.

Glucose-stimulated insulin secretion (GSIS) & Insulin HTRF

GSIS in Scamp3KD and control cells were performed as previously described[68] and HTRF Insulin Ultra-sensitive Detection Kit (Cisbio) was used to measure secreted insulin.

Data analysis

All output raw MS data was analysed using Rstudio (v. 4.1.1.). Variance stabilization normalization (vsn) was performed on the data using the *vsn* package. PCP analysis was done using the functions: hclust, numClusters and cutree (Rstudio). To assign proteins to organelles and complexes within cells, we used support vector machine learning implemented with the ‘svmOptimisation’ and ‘svmClassication’ functions in the R package *pRoloc* [218, 219]. For intraclass correlation coefficients, our model fitted sample fraction IDs (Fraction 1-12) as a random effect, and normalized expression number for known ISG proteins as the outcome variable. ICC was calculated as the ratio of between fraction variance to the total variance. To assign proteins within our samples as markers for other organelles distinct from ISGs, we used the publicly available *Mus musculus* library, available through the package *pRolocdata* [220]. GraphPad Prism (v.8.0) was used for statistical analyses. Results were considered significant at P-value<0.05.

Data Source & Resource availability

Any data required to re-analyse the data reported in this paper is available upon request from the corresponding author. This paper does not produce original code. Resources including the mass spectrometry proteomics data have been deposited to the ProteomeXchange Consortium via the PRIDE partner repository with the dataset identifier PXD051136, Username: reviewer_pxd051136@ebi.ac.uk, Password: GnZTdMqQ". Resources available upon request.

RESULTS

Optimized three-step ISG enrichment method

Our subcellular fractionation protocol uses a three-step purification of MIN6 post-nuclear cell lysates on a discontinuous gradient (8.8 - 30%) (**Figure 11 - A & B**). Insulin concentrations were quantified in 16 Optiprep fractions, revealing two distinct peaks of insulin (**Figure 11C**) corresponding to iISGs (Fraction 5 – 7) and mISGs (Fractions 11 – 13). SDS-PAGE analyses of the fractions confirmed enrichment of mature insulin in the later fractions, and proinsulin in earlier fractions (**Figure 11D**). Furthermore, through SDS-PAGE analysis, there is a clear enrichment of mISGs lacking contaminants from the cytoskeleton (beta-actin) and endosomes (EEA1). Enrichment of PCSK2 (an ISG marker) was also present that matched the ISG enrichment. Fraction 13 exhibited maximal insulin enrichment but also contained contaminating mitochondria (**Figure 11D**). Fractions 11 and 12 were chosen for subsequent purification as these had less mitochondrial contamination but a high insulin enrichment (**Figure 11D**).

Optiprep Fractions 11 and 12 were loaded atop a 27% Percoll solution and ultra-centrifuged (**Figure 11E**), then washed in sucrose to enable SDS-PAGE analyses and tandem MS. SDS-PAGE analysis using antibodies against markers of subcellular compartments for ISG (insulin, PCSK2), cytoskeleton (beta-actin), autophagosomes (LC3A/B), mitochondria

(ATP5A) and lysosomes (Lamp1) (**Figure 11F**) confirmed insulin enrichment in later Percoll fractions, with minimal protein alignment from other organelles removed during the first-step fractionation.

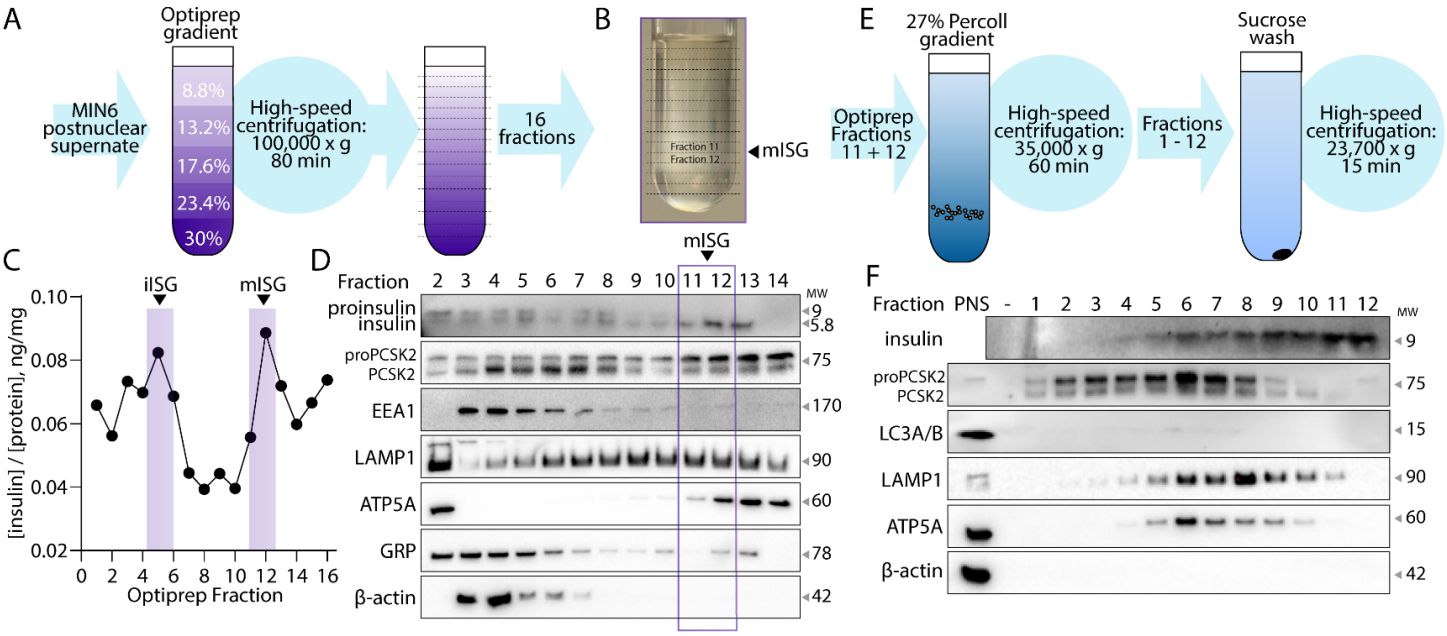

Figure 11*:* Analysis of isolation of immature and mature insulin secretory granules from MIN6 cells by Optiprep™ and Percoll. (**A**) *Optiprep workflow*: MIN6 post-nuclear supernatant is loaded atop 5 fixed concentrations of Optiprep and ultra-centrifuged for 80min at 100,000g. (**B**) Representative example of visible subcellular fractionation distribution after ultra-centrifugation. (**C**) Representative quantification of insulin enrichment from 16 fractions of Optiprep by insulin ELISA (**D**) Western blot analysis of pro- and insulin enrichment of Optiprep fractions, as well as marker proteins for subcellular components of β-cells, MW for molecular weights of proteins. (**E**) *Percoll workflow*: Fractions 11 and 12 from Optiprep gradients following insulin enrichment analysis are loaded on top of 27% Percoll and ultra-centrifuged for 60min at 35,000g. (**F**) SDS-PAGE analysis of insulin enrichment of Percoll fractionation, as well as marker proteins for subcellular components of MIN6 cells.

Unbiased proteomics analysis of fractions from three-step purification of ISGs (PCP)

All twelve sucrose-washed fractions from each experiment underwent MS-based proteomic analysis. Protein quantification was performed using label-free analysis in the MaxQuant package, and the protein-level data were subsequently analyzed by PCP and supervised machine learning using the R package *pRoloc* [219, 220]. Protein abundance across samples were normalized using variance stabilization normalization (VSN) using the *vsn* package [221]. Following this, the covariance of 5 known marker proteins (Ins1, Ins2, Cpe, Pcsk2, CgA) within each experiment (n=7) was quantified by intraclass correlation coefficient (ICC) to evaluate experiment reliability. ICCs were calculated based on random effects using a linear mixed model implemented in the package *lme4* [222]. Two out of seven replicate experiments exhibited low and outlying ICC values (<0.3) and were therefore excluded from downstream analysis (**Supplementary Table 2**).

Through PCP analysis, proteins with similar abundance patterns are clustered together based on their Euclidean distances that are measured iteratively between each protein. Hierarchical clustering of all proteins (**Supplementary Table 3**) resulted in identifications of 432 significant potential candidates of ISG proteins (**Supplementary Table 4**). Of interest, a single cluster contained well-established ISG marker proteins, including Insulin (Ins1 and Ins2), islet amyloid polypeptide (Iapp), prohormone convertases 1 and 2 (Pcsk1, Pcsk2), Chromogranin A (CgA), Secretogranin-2 and -3 (Scg2, Scg3), Carboxypeptidase E (Cpe), Zinc transporter 8 (Slc30a8), many proton ATP-ase subunits, syntaxins, synaptotagmins, vesicle associated membrane proteins (Vamp2, Vamp3 and Vamp7), and Rab-GTPases (Rab3a, Rab27a) (**Supplementary Table 4**), suggesting high efficiency of the three-step purification method and validity of the proteomics data. Representative protein profiles from a single replicate illustrated a high enrichment of this ISG-specific protein cluster (**Figure 12A**), further validating the purification method. Subsequent GO enrichment and STRING analysis of this

'ISG' cluster (**Figure 12B**) reveals a high strength index of proteins involved in insulin processing, secretory granule localization as well as granule trafficking (teal). However, some subsets of proteins within this cluster were identified as contaminants, including ribosomal subunits (yellow), lysosomal cathepsins (purple) and subunits of mitochondrial electron transport chain proteins (red). While *known* ISG proteins were identified through PCP analysis, many other proteins within this cluster may also be ISG-resident. For example, Synaptotagmin-5, and Synaptotagmin-like 4 are potential synaptotagmin isoforms present on ISGs in INS-1E cells[126]. Additionally, the identification of Synaptotagmin-13 (Syt13), Synaptophysin (Syp), and Syntaxin-7 (Stx7) suggest their potential residence on ISG membranes. Other proteins of interest are protein disulfide isomerases (e.g. Pdia6, Pdia3), which have been shown to facilitate insulin processing [223].

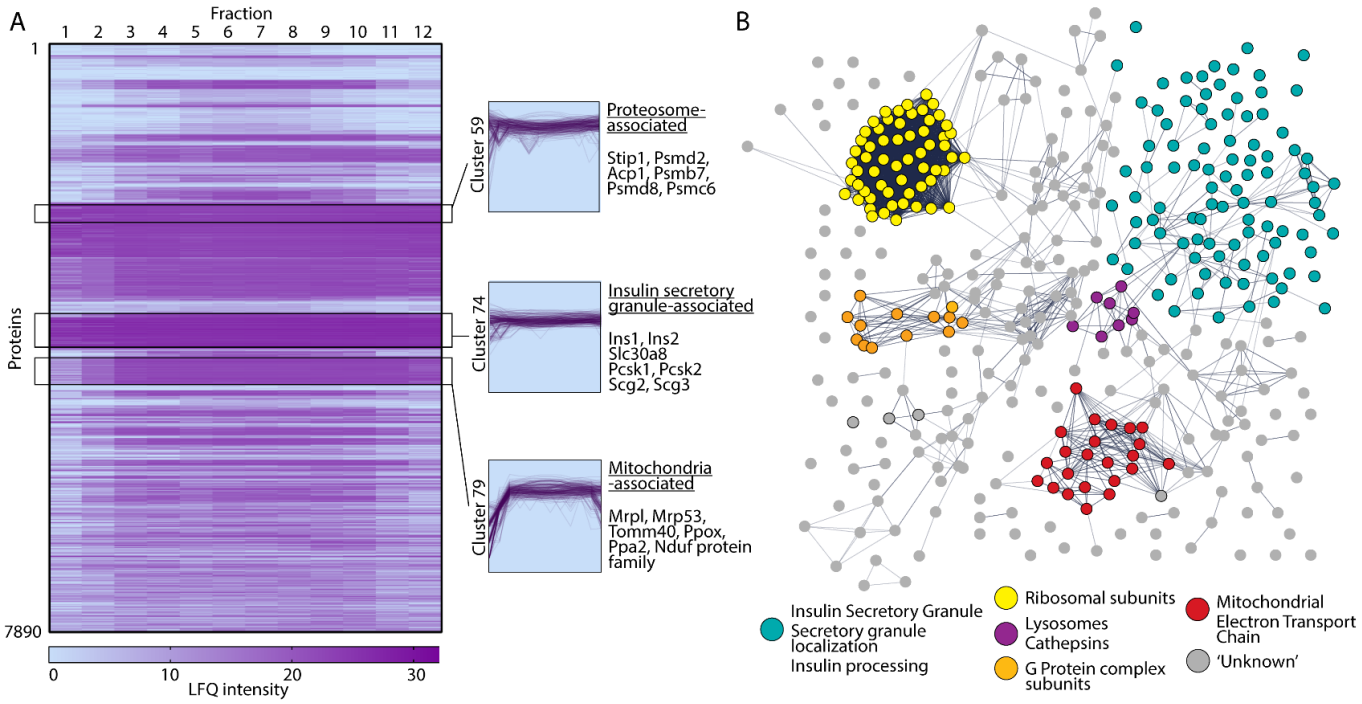

Figure 12: Heatmap of protein enrichment hierarchical clustering across 12 fractions after three-step purification of mISGs. *(A)* Representative heatmap of abundance levels of proteins across 12 fractions. All heatmaps for 5 experimental replicates (n = 5) available in **Supplementary Figure 1**. Boxes outlined indicates clusters enriched in proteasome, ISG and mitochondrial proteins. (**B**) Gene ontology enrichment analysis of Cluster 74 (ISG-associated proteins), with individual proteins coloured based on enriched biological processes.

Targeted proteomics analysis of fractions from three-step purification of ISGs (LOPIT-DC)

PCP analyses offer comprehensive insights beyond single snapshot proteomics of ISGs, enabling unbiased matching of co-abundant proteins across subcellular fractions. While previous ISG proteomes yielded only 5 consensus proteins [69], our PCP analysis identified these proteins along with other well-established ISG-resident proteins: ZnT8, ProSAAS, Iapp, Secretogranin-2 and Secretogranin-3 [133, 143, 208, 224, 225]. Subsequently, these 10 ISG proteins were selected as candidates for subcellular localization analyses. 'Marker' proteins were assigned for other non-ISG subcellular compartments of the β-cell using the *Mus musculus* library available in pRoloc. The 10 ISG proteins chosen were manually added as markers. Using a support vector machine learning (SVM; a form of supervised machine learning) within pRoloc [219, 220], unmarked protein profiles were correlated with marker protein profiles to generate a spatial proteome. Proteins assigned to the ISG exhibited high SVM score distributions (**Supplementary Figure 1)** across experimental replicates, indicating strong assignment accuracy. Notably, these proteins showed distinct profiles compared to proteins assigned to other subcellular localizations. With confidence, we identified a total of 211 ISG proteins across five experiment replicates (**Supplementary Table 5**). Notably, Syp, Syt13, and Stx7 were among the ISG-associated proteins identified. Additionally, Scamp3, initially missed in the PCP analysis, was found in all 5 replicates in our targeted LOPIT-DC analysis (**Supplementary Table 5**). Through both analyses, the remaining proteins unassigned to the ISGs clustered with other subcellular protein complexes (e.g. mitochondria, proteasomes) (**Figure 12A**). These proteins are non-contaminating, instead highlighting the potential for the identification of novel proteins in other subcellular localizations. Overlap of proteins identified in this study compared to previous ISG proteomes from INS-1 and INS-1E cell lines can be found in **Supplementary Table 6**.

Immunocytochemistry Validation of Candidate proteins

We further validated Syt13, Stx7, Syp and Scamp3 as ISG-resident proteins using immunocytochemistry. Colocalization analyses **(Figure 13A and B)** showed that all were present in MIN6 cells and had significant positive correlation with insulin. Chromogranin-A (ChgA), a well-established ISG cargo protein, exhibited high colocalization with insulin (**Figure 13A**), serving as a positive control, while ER (PDI) and cis-Golgi (GM130) markers were negative controls, and showed lower levels of colocalization with insulin. Syp was observed closer to the plasma membrane, while Scamp3 localized predominately in the peri-nuclear region with sparse cytosolic distribution. To validate the association of these proteins in human β-cells, we conducted immunostaining of pancreatic islets of non-diabetic human donors (**Figure 13C**). These proteins were found primarily in β-cells, demonstrating significant colocalization with insulin (**Figure 13D**), with additional staining present in other cell-types of the pancreatic islets for Syt13, Syp and Scamp3. We then selected Scamp3 as a candidate for further functional studies.

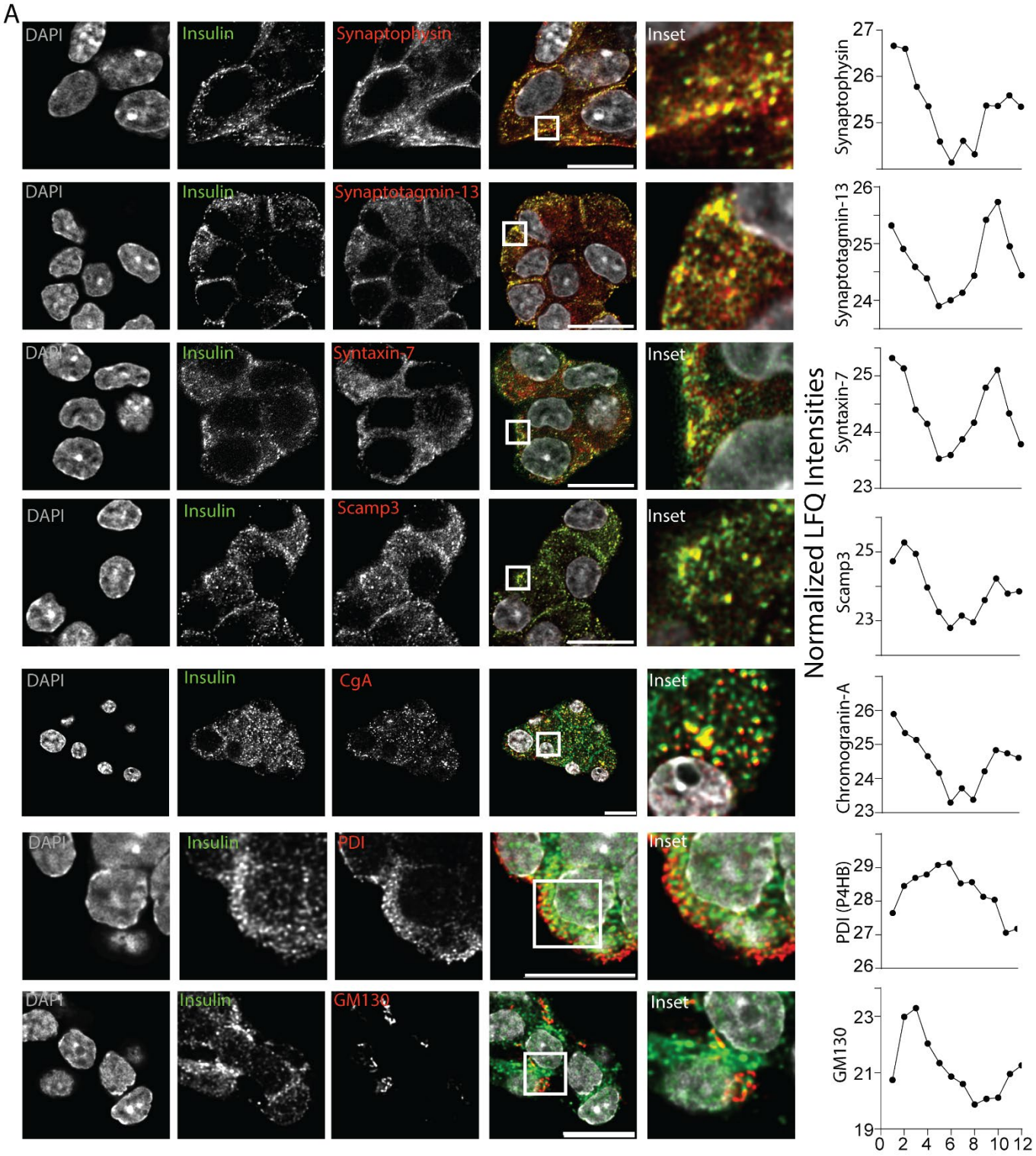
A
DAPI
Insulin
Synaptophysin
Inset
Synaptotagmin-13
Syntaxin-7
Scamp3
CgA
Chromogranin-A
PDI
PDI (P4HB)
GM130
Normalized LFQ Intensities
0 2 4 6 8 10 12

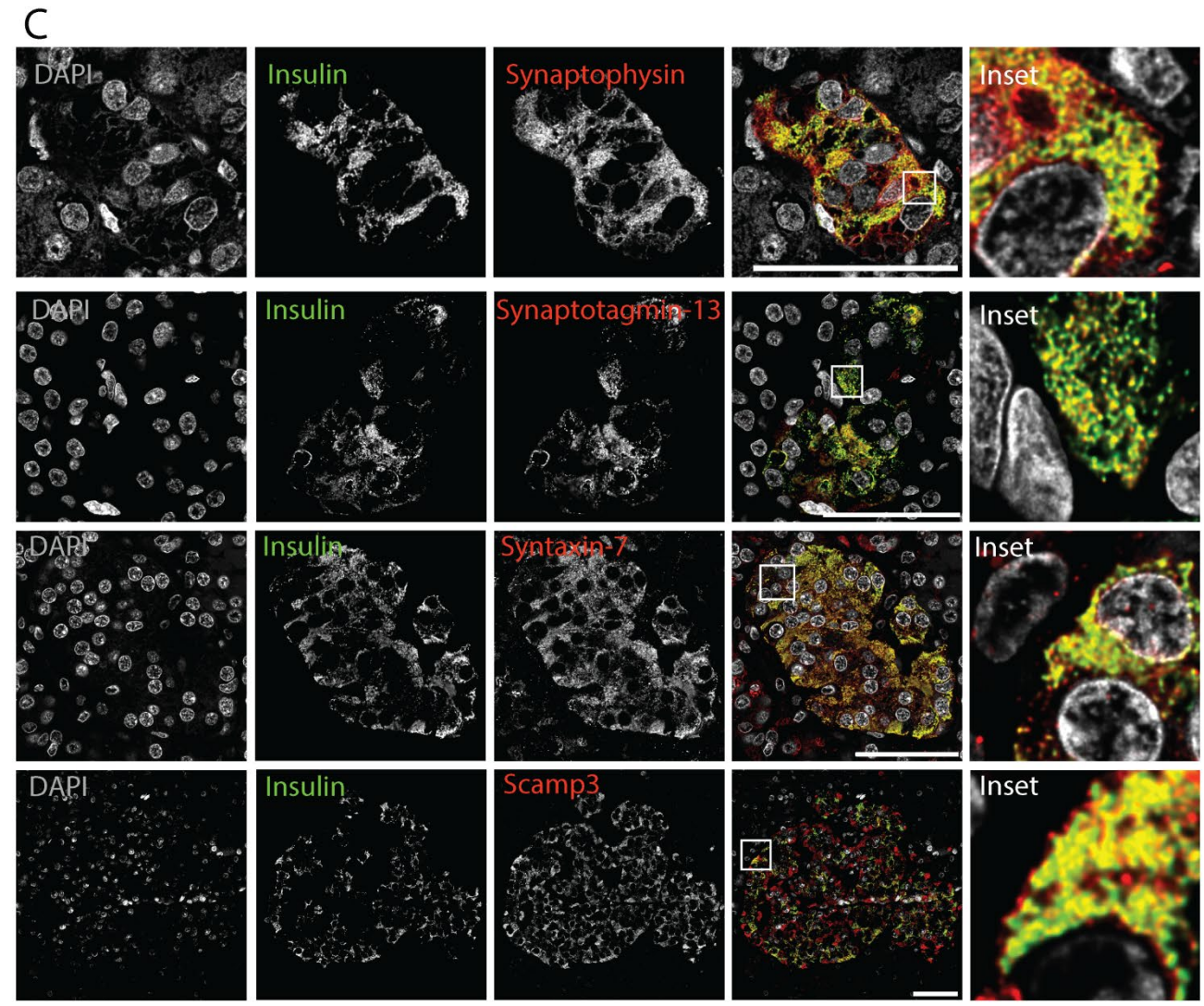
C
DAPI
Insulin
Synaptophysin
Inset
DAPI
Insulin
Synaptotagmin-13
Inset
DAPI
Insulin
Syntaxin-7
Inset
DAPI
Insulin
Scamp3
Inset

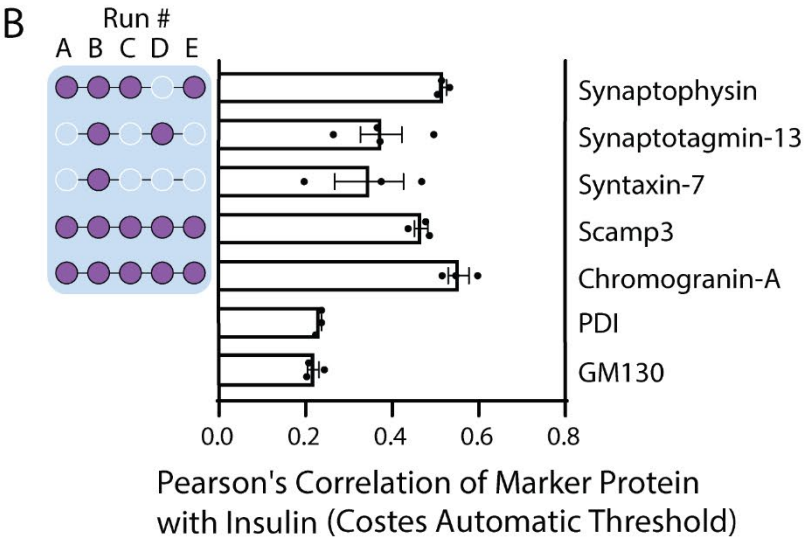
B
Run #
A B C D E
Synaptophysin
Synaptotagmin-13
Syntaxin-7
Scamp3
Chromogranin-A
PDI
GM130
0.0
0.2
0.4
0.6
0.8
Pearson's Correlation of Marker Protein
with Insulin (Costes Automatic Threshold)

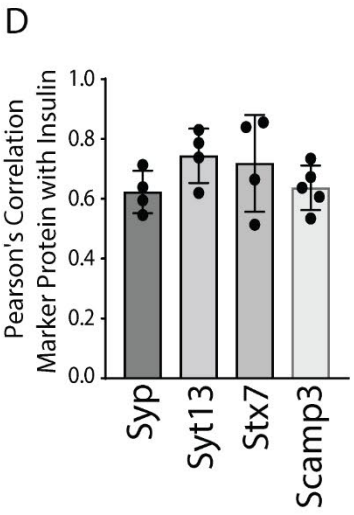
D
Pearson's Correlation
Marker Protein with Insulin
1.0
0.8
0.6
0.4
0.2
0.0
Syp
Syt13
Stx7
Scamp3

Figure 13: **Colocalization analysis on immunofluorescent stained MIN6 cells for candidate proteins from LC-MS/MS analysis (Figure across 2 pages for legibility).** (**A**) Confocal fluorescence imaging of MIN6 cells labelled with anti-insulin co-stained with anti-Synaptophysin (n = 3), anti-Synaptotagmin-13 (n = 4), anti-Syntaxin-7 (n = 3), anti-Scamp3 (n = 3), anti-Chromogranin A (n = 3), anti-PDI (n=3) and anti-GM130 (n=3), Scale bars = 10um. Enrichment profile of each candidate protein across 12 fractions from LC-MS/MS analysis to show protein abundance and co-enrichment. (**B**) Quantification of colocalization of candidate proteins with insulin using Pearson's correlation coefficient (with Costes' automatic thresholds). Filled dots in purple represent the number of experiments (Run #) these proteins appear within pRoloc analyses. (**C**) Confocal fluorescence imaging of human islets labelled with anti-insulin, co-stained with anti-synaptophysin (n = 4), anti-synaptotagmin-13 (n = 4), anti-syntaxin7 (n = 4) and anti-Scamp3 (n = 5), Scale bars = 50uM. (**D**) Quantification of colocalization of candidate proteins with insulin using Pearson's correlation coefficient (with automatic thresholds). All error bars represent standard error of the mean (± S.E.M.).

Investigation of SCAMP3 function in INS1 cells

First, we confirmed the expression and ISG co-localization of Scamp3 in INS1 cells (**Supplementary Figure 2A & B**). We then investigated the functional consequence of Scamp3 KD in INS1 cells by depleting endogenous Scamp3 with silencer RNAs targeting two unique sequences of rat Scamp3 mRNAs (TriFECTa, IDT). 48 hours post-transfection, INS-1 cells exhibited a significant reduction in Scamp3 mRNA levels (**Supplementary Figure 2C**) resulting in ~80% knock-down of Scamp3 protein in both siRNA conditions (**Figure 14A and B**) compared to cells transfected with non-targeting control siRNA. Scamp3 knockdown (Scamp3KD) INS1 cells display reduced cellular insulin content and GSIS, with no changes in proinsulin content (**Figure 14C-D and 14E-H**) or Ins-1, Ins-2 and Pdx1 mRNA levels (**Supplementary Figure 2D-F**). While control cells displayed a typical insulin secretory response with a 2-fold increase in insulin secretion under the stimulated (16.7mM) to basal (2.8mM) glucose condition, both Scamp3KD conditions did not exhibit significant differences between basal and stimulated conditions (**Figure 14G**). This resulted in a significant decrease in the fold changes of stimulated/basal conditions, indicating a blunted secretory response in Scamp3KD cells (**Figure 14H**).

Investigation of Scamp3 function in non-type 2 diabetic and Type 2 diabetic human pancreatic islets

We further analyzed the distribution and abundance of Scamp3 in human β-cells in non-T2D and T2D islets (**Figure 14I**). While a non-significant decrease in Scamp3 fluorescence intensity was noted in T2D islets compared to non-T2D islets (**Figure 14J**, n=5 per group), a slight reduction in Scamp3 and insulin localization was observed in T2D islets (**Figure 14K**). These findings offer initial insight into potential changes in Scamp3 expression and localization linked to T2D.

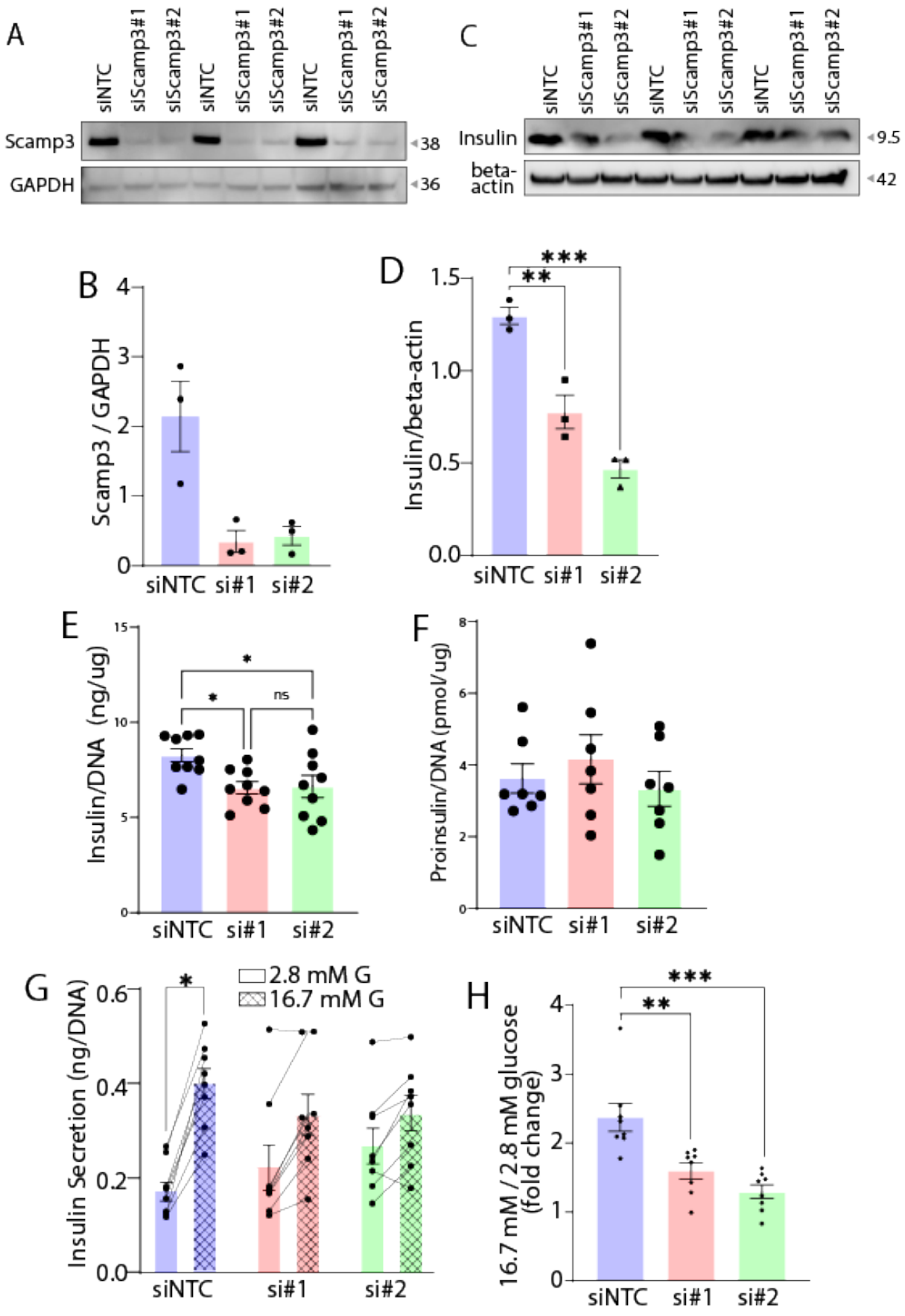
A
siNTC
siScamp3#1
siScamp3#2
Scamp3
GAPDH
38
36
C
Insulin
beta-actin
9.5
42
B
Scamp3 / GAPDH
siNTC si#1 si#2
D
Insulin/beta-actin
***
**
E
Insulin/DNA (ng/ug)
*
ns
F
Proinsulin/DNA (pmol/ug)
G
Insulin Secretion (ng/DNA)
2.8 mM G
16.7 mM G
H
16.7 mM / 2.8 mM glucose (fold change)

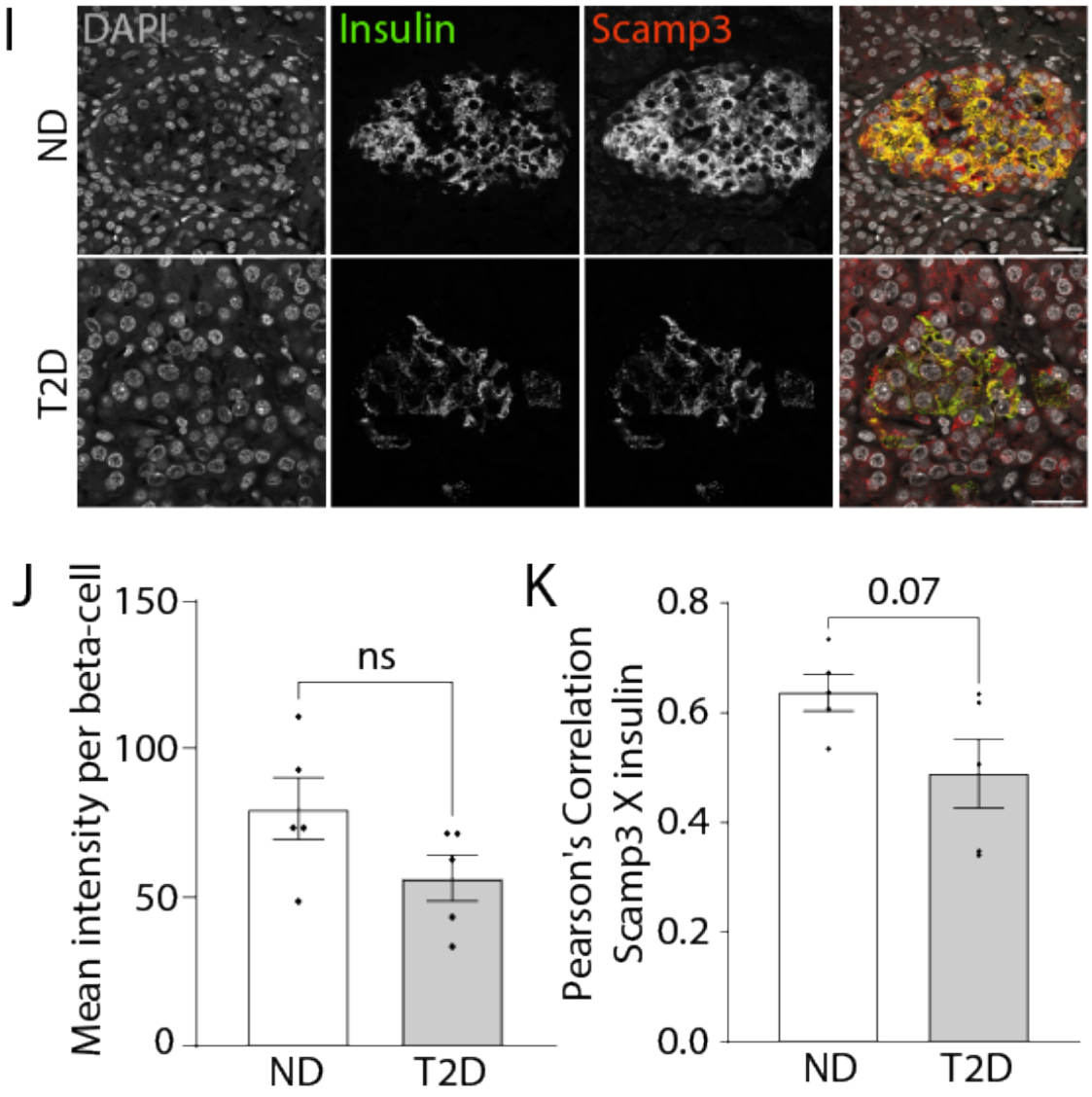

Figure 14: **Functional investigation of Scamp3 in INS-1 β-cells and human non-type 2 diabetic and type 2 diabetic pancreatic islets.** (**A**) SDS-PAGE analysis of INS-1 cell lysates 48 hours post transfection with a control non-targeting siRNA and two unique siRNAs specific to Scamp3 (siScamp3#1 and siScamp3#2) in 3 experimental replicates together (n = 3). (**B**) Densitometry quantification of knockdown efficiency of Scamp3 48 hours post transfection (n = 3) normalized to GAPDH. (**C**) Insulin SDS-PAGE analysis of INS-1 cell lysates 48 hours post transfection of control and siRNA KD INS-1 cells. (**D**) Densitometry quantification of insulin content in control and siRNA KD INS-1 cells (n = 3) normalized to beta-actin. (**E**)

Quantification of total insulin content 48 hours post transfection of control and siRNA KD INS-1 cells by Insulin ELISA (n=9) (Crystal Chem) (**F**) Quantification of total proinsulin content 48 hours post transfection of control and siRNA KD cells by Proinsulin ELISA (Mercodia) (**G**) Glucose-stimulated insulin secretion assay: insulin concentration after basal (2.8 mM) and stimulation (16.7 mM) glucose conditions from INS-1 control and siRNA KD cells measured by insulin HTRF (n = 8). (**H**) Fold-change of basal to stimulation glucose conditions from E (n = 8). (**I**) Representative confocal fluorescence imaging of human non-type 2 diabetic (n = 5) and type 2 diabetic (n = 5) islets labelled with anti-insulin and co-stained with Scamp3. (**J**) Mean fluorescence intensity of Scamp3 within β-cells of human non-type 2 diabetic and type 2 diabetic islets (**K**) Quantification of colocalization of Scamp3 with insulin using Pearson's correlation coefficient (with Costes' automatic thresholds) in human non-type 2 diabetic and type 2 diabetic islets. All error bars represent standard error of the mean (± S.E.M.). *P-value <0.05, ** P-value <0.01, *** P-value <0.001. *One- and two-way ANOVA, Sidak's multiple comparisons*.

Discussion

Our study presents an efficient approach to isolating insulin secretory granules, successfully enriching for them using a three-step subcellular fractionation procedure. This method is applicable to various cell lines or primary cells. Through unbiased quantitative PCP analysis, we establish the first MIN6 cell ISG proteome, identifying a total of 432 proteins associated with ISG. Additionally, machine learning analysis enhances the proteome, refining 211 proteins assigned with high confidence to ISGs. We validate the presence of 4 ISG-resident proteins of interest in MIN6 cells and human donor pancreatic islets. Through siRNA knockdown and functional analyses of Scamp3, we validate this novel ISG-associated protein's involvement in the glucose-regulated secretory pathway in β-cells. Scamp3 was not clustered with ISG proteins after PCP due to alignment with intracellular transport and cytoplasmic proteins. Inclusion of machine learning analysis bolster the data by elucidating other proteins that may be heterogeneously expressed that may be associated with ISGs at different points of the secretory pathway. Expanding the use of this framework may reveal alterations in ISG morphology or proteins, enhancing our understanding of changes in granule populations in β-cell dysfunction and development of T2D.

Previous proteomics analyses of ISGs in INS1 and INS-1E cell types have identified 50-140 candidate ISG proteins [112, 123, 126, 129], with one study using PCP. Here, we employ an unbiased PCP analysis to hierarchically cluster proteins with highly similar profiles, validating ISG separation techniques and identifying potential novel ISG resident proteins. Our approach identified many previously identified ISG proteins. GO enrichment analysis of these clusters further support our findings, indicating high strength indices for insulin processing, protein localization to secretory granules, and insulin metabolic processes.

PCP reveals the presence of many previously known ISG-associated integral membrane proteins, including members of the vSNARE family (Vamp2/3 and Vamp7), which are known contributors to insulin granule exocytosis [226, 227]. Additionally, our analysis identifies numerous Rab-GTPases including Rab3a, Rab27a, Rab8a, known small G-proteins that affect ISG movement [228].

Identified synaptic vesicle proteins such as membrane-localised synaptotagmins regulate ISGs exocytosis [229]; Syt13 in humans is abundantly expressed in the pancreas [230], regulates islet formation, and its knock-out affects α to β-cell ratios in islets [231]. Syt13 is downregulated in murine models of diabetes (*db/db*) and obesity (*ob/ob*) [232], demonstrating its clear involvement in β-cell development and GSIS.

Synaptotagmins interact with syntaxin proteins (e.g. Snap23, VAMPs) to form SNARE complexes that regulate granule fusion during insulin exocytosis in β-cells. Syntaxin-7 is identified as an ISG-associated protein and forms SNARE complexes with Vamp4, Stx8 and VTI1B, facilitating proinsulin degradation within the iISGs [233]. Additionally, Stx7 is involved in SNARE complex formation with Vamp7 and Stx8 during autophagosome formation [234].

Synaptophysin, typically associated with neurons and synaptic vesicle function, emerges as a novel ISG-associated protein (**Figure 13A & B**). While its roles in β-cells, possibly involving GABA secretion via synaptic-like microvesicles is debated [235], we have observed its upregulation in murine islets under conditions of high-fat diet and in mouse models of diabetes [232].

Identification of novel ISG protein Scamp3

One of the most intriguing ISG-associated proteins we uncovered is SCAMP3. While SCAMP protein family is widely expressed and found on post-Golgi vesicle membranes [236]

, SCAMP3's role in β-cells remained elusive. However, other SCAMP proteins have been implicated in GSIS [237]. Scamp3 is a ubiquitously expressed integral membrane protein found on post-Golgi trafficking pathways [238], involved in membrane budding with associations with other adaptor proteins to form coated vesicle carriers [239]. Other SCAMPs are linked to pore formation in later steps of secretory granule exocytosis, and Scamp3KD in PC12 cells reduces fusion pore opening and the number of docked granules [240]. Our study reveals clear association of Scamp3 within ISGs in rat, mouse, and human β-cells, and knocking down Scamp3 in INS1 cells significantly reduces GSIS (**Figure 14H**) and insulin content (**Figure 14D-E**). We observe no changes in mRNA transcript levels of both insulin isoforms and Pdx1 with Scamp3KD, indicating a role for Scamp3 in post-transcription pathways in β-cells (**Supplementary Figure 2D-F**). A single transcriptome-wide association study has shown the presence of splice sites in the SCAMP3 gene that associates with T2D susceptibility in human pancreatic islets [241]. In addition, previous proteomics studies have shown that mouse pancreatic islets exposed to high glucose result in a downregulation of Scamp3 compared to islets exposed to low glucose conditions [242]. In summary, we provide the first evidence of Scamp3's role in ISG biogenesis, trafficking, or secretory pathway. Further studies should focus on how Scamp3 regulates these processes in the β-cell.

Acknowledgments

We thank the core facilities at the Charles Perkins Centre at the University of Sydney. This study was made possible with access to the Sydney Mass Spectrometry and Sydney Microscopy & Microanalysis facilities. We thank the organ donors and their families for their generosity. We also thank the members of St Vincent's Institute in the islet isolation program and Donatelife for providing research consent and provision of human pancreata. St Vincent's Institute receives support from the Operational Infrastructure Support Scheme of the Government of Victoria. A. Prof. Melkam Kebede is the guarantor of this work and, as such,

has had full access to all the data in this study and takes responsibility for the integrity of data and accuracy of the data analysis. This work was supported by National Health and Medical Research Council (NHMRC) project grant GNT1139828 (to M.A.K.). N.N is supported by the University of Sydney Postgraduate Award (UPA).

Resource Availability

Corresponding author

Further information requests for reagents and resources used should be directed to lead contact, Melkam Kebede (melkam.kebede@sydney.edu.au).

Materials availability

This study did not generate any new unique reagents.

Author Contributions

Conceptualization, M.A.K. and B.Y.; Methodology, N.N. and B.Y.; Validation, M.A.K. and B.Y.; Formal Analysis, N.N., H.W., A.M.S. and M.L.; Investigation, N.N., B.Y., C.F., H.W. and M.L.; Resources, M.A.K., H.T. and T.L. Data Curation, N.N., B.Y., M.L and A.M.S; Writing – Original Draft, N.N.; Writing – Review & Editing, M.A.K., B.Y., M.A.S. and M.L.; Visualization, B.Y.; Supervision, M.A.K.; Project Administration, M.A.K. and B.Y.; Funding Acquisition, M.A.K.

Interest Declaration

The authors declare no potential conflicts of interest to this article.

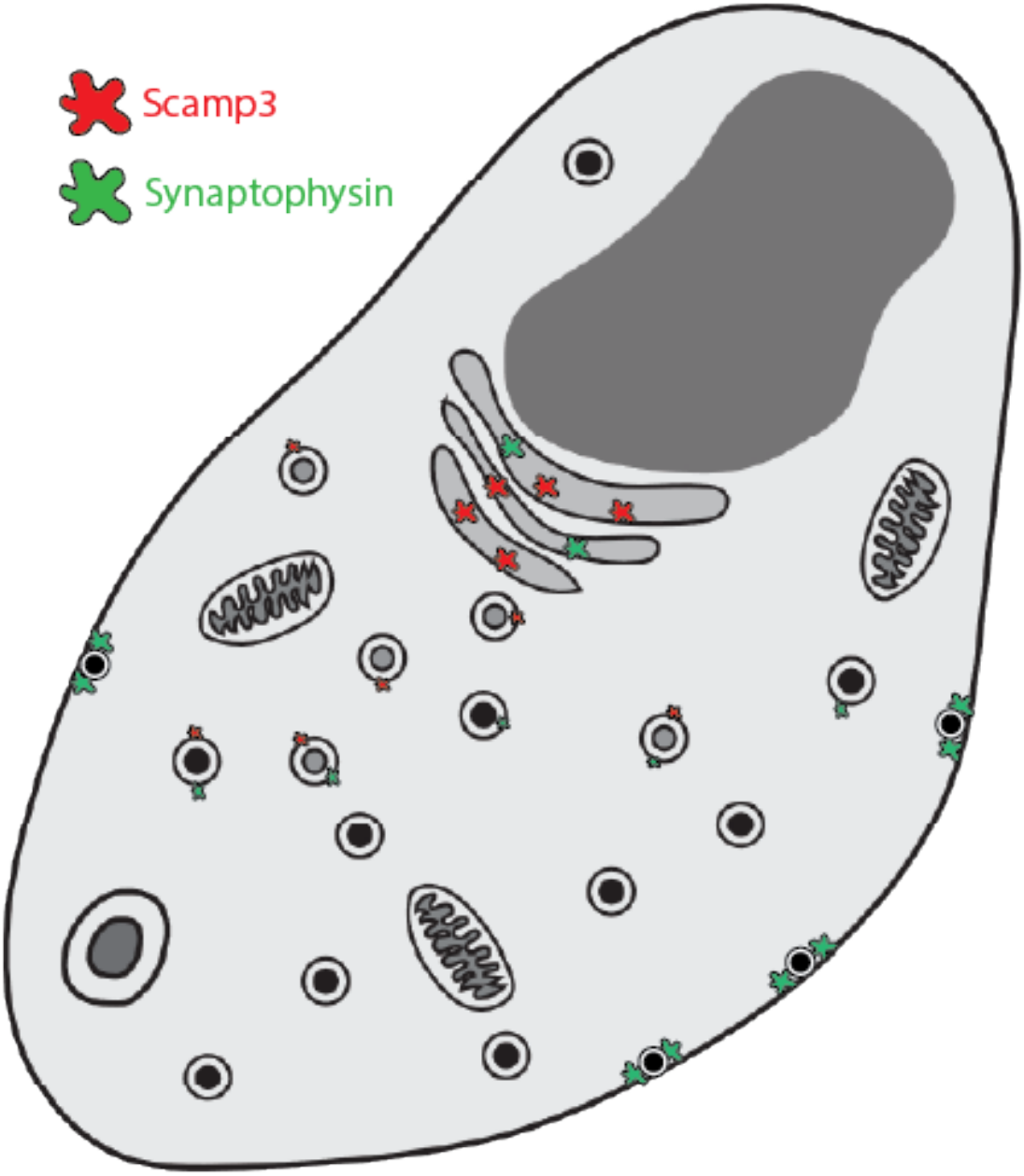

Chapter 2A

Investigating the role of synaptophysin in pancreatic beta-cells

2A.1 Introduction

After successfully purifying ISGs to obtain the first murine ISG proteome published to date, we turned to the discovery of novel ISG proteins. We performed follow-up analyses on two candidate proteins: Scamp3 and Synaptophysin, the former of which was published alongside the ISG proteome in *Diabetes*. To fit the journal's publication standards some data was omitted, and the methodology was concisely summarised. The following section (**Chapter 2A**) details the full description of methodology used within the published article and describes the characterisation and validation of a second candidate protein, Synaptophysin.

2A.2 Materials and methods

2A.2.1 Cell culture

Rat INS-1 insulinoma cell lines were cultured at 37° C and 5 % CO2 in Roswell Park Memorial Institute (RPMI) 1640 Medium (Gibco™) containing 11 mM glucose, 10 % FBS (Gibco™), 2 mM L-glutamine, 1 mM sodium pyruvate, 0.005% 2-beta-mercaptoethanol and 10 mM HEPES (Complete RPMI). INS-1 cells were passaged with TrypLE express enzyme (Gibco™) at 37 °C for 3 mins when ~90 % confluence. Culture medium was replaced every 2 – 3 days, passages used in **Chapter 2A** were between 16 – 29. All INS-1 cell cultures were mycoplasma negative.

2A.2.2 siRNA Knockdown optimisation of Synaptophysin & Scamp3

Synaptophysin knockdown (SypKD) INS1 cells were generated by transfecting the cells with commercially available siRNA oligomers. For SDS-PAGE and GSIS assays, cells were plated in 6 – or 12 – well plates respectively. Transfection was carried out using three unique rat Synaptophysin siRNAs (TriFECTa DsiRNA, IDs: rn.Ri.Syp.13.1 #109061930, #613664202 (si#1), rn.Ri.Syp.13.2 #109061933, #613664203 (si#2), rn.Ri.Syp.13.3 #109061936, #613664204 (si#3) or a non-targeting siRNA control (TriFECTa, DsiRNA, #0000865210 (NTC). All siRNAs were complexed with Lipofectamine 2000 (ThermoFisher), at concentrations of 5, 10 and 20 nM for 24 to 48 hours. GSIS assays were performed on INS-1 cells after 48 hours post transfection at 10 nM siRNA concentration.

Scamp3 knockdown (Scamp3KD) cells were generated using the same method described above, utilising two commercially available Scamp3 siRNAs with a non-targeting siRNA control. The unique Scamp3 siRNA used had the following IDs: rn.Ri.Scamp3.13.2 #613664206 (si#1), rn.Ri.Scamp3.13.3 #613664207 (si#2), and a non-targeting siRNA (TriFECTa DsiRNA, Lot #0000865210). The optimal conditions for both SypKD and

Scamp3KD cells were determined to be 10 nM siRNAs for 48 hours, achieving sufficient knockdown of the respective target proteins.

2A.2.3 Immunofluorescence Staining

All cell cultures, including non-targeting control INS-1, SypKD & Scamp3KD cells were prepared for immunofluorescence staining by culturing cells on glass coverslips. Following transfection with the appropriate siRNAs, cells were washed once with PBS, fixed with 4 % paraformaldehyde (PFA) (#15710, Electron Microscopy Sciences) for 20 minutes at RT. The coverslips were washed three times with PBS and cells permeabilised with 0.1 % SDS for 5 minutes at RT. After permeabilisation, cells were washed three times with IF wash buffer (0.1 % BSA, 0.01 % sodium azide in PBS) to remove residual SDS. Non-specific binding was blocked with Dako Protein serum-free buffer (#X0909) for 1 hour at RT. The coverslips were then incubated overnight at 4°C with anti-primary antibodies against Scamp3 or Syp, co-stained with anti-insulin (**Table 1**). After incubation, the coverslips were washed five times with IF buffer and subsequently incubated with secondary antibodies for 1 hour at RT (**Table 1**). Finally, the coverslips were dried for 5 min at RT, and mounted onto microscope slides with ProLong Antifade Diamond with DAPI mountant (P36962).

2A.2.4 Microscopy

Fixed microscope slides were imaged with the Leica LCS SP8 confocal microscope (Wetzlar, Germany). A 93X glycerol lens and a white laser were used for imaging. Image collection was conducted using Leica LAS X software and image analysis on FIJI ImageJ [217]. For the analyses performed in Chapter 2 using Pearson's correlation coefficients, values closer to 1 indicate a strong positive linear relationship between the protein of interest and insulin, meaning they are highly colocalized. A value of 0 suggests no linear relationship or

colocalization between the two proteins, while a value of -1 indicates a perfect negative correlation, where the two proteins are completely not colocalized.

2A.2.5 Glucose-stimulated insulin secretion assay

At 36 hours post transfection, Scamp3KD, SypKD and control cells were pre-incubated overnight in low glucose RPMI (2.8 mM glucose) prior to performing GSIS assays. The following day, cells were incubated in Krebs Ringer buffer with 10 mM HEPES (KRBH) containing 2.8 mM glucose for 1 hour at 37°C, in a 5% CO2 incubator. After incubation, supernatant was collected for insulin analysis. The same cells were then exposed to 16.7 mM glucose KRBH for 1 hour under the same conditions, after which a second supernatant was collected. Following the GSIS assay, cells were lysed using islet lysis buffer (100 mM Tris, 10 mM NaF, 2 mM sodium orthovanadate, 300 mM NaCl) to obtain total cellular content. Total DNA from cell lysates were quantified using the Quant-iT PicoGreen assay (ThermoFisher). Insulin content and supernatants collected during GSIS were measured by insulin HTRF (Cisbio). Insulin secretions were normalised to total DNA content of the cells to account for differences in cell density.

2A.2.6 SDS-PAGE

Post-transfection, cell cultures were harvested in SDS lysis buffer (75 mM Tris-HCl, pH 6.8, 1 % SDS, 2.5 % sucrose, 10 % glycerol) and boiled at 95 °C for 5 minutes. Lysates were homogenised by sonication and protein concentrations were quantified using the Pierce BCA protein assay (ThermoFisher) according to the manufacturer's protocol. Protein concentrations and loading volumes were standardised using SDS lysis buffer and Laemmli sample buffer (62.5 mM Tris, pH 6.7, 10 % glycerol, 1.25 % SDS, 0.00125 % bromophenol blue) with 1 % 2-beta-mercaptoethanol then heated for 5 minutes at 95 °C.

Proteins were separated by SDS-PAGE then transferred onto a PVDF membrane (Millipore) using a transfer buffer containing 20 % methanol and 0.05 % SDS at 100 V for 1 hour. Membranes were blocked using SuperBlock™ blocking buffer for 1 hour at RT and subsequently incubated with primary antibodies (**Table 1**) overnight at 4 °C. The membranes were then washed with TBST and incubated with secondary IgG conjugated to horseradish peroxidase (HRP) conjugated antibodies (**Table 1**) for 1 hour at RT, followed by three 10 minute washes in TBST. Protein signals were detected and visualised by chemiluminescence (Millipore) using the ChemiDoc MP Imaging System (Bio-Rad).

2A.2.7 Insulin SDS-PAGE

SDS-PAGE for insulin was performed using a similar protocol with a few key modifications. Samples were diluted with Laemmli buffer **without** 1 % 2-beta-mercaptoethanol and heated at 95 °C for 5 minutes. Proteins were separated by SDS-PAGE and transferred onto a PVDF membrane using a transfer buffer containing 20 % methanol and 0.05 % SDS at 100 V for 1 hour. Membranes were pre-blocked with 1 % skim milk and 0.1 % BSA in PBST (PBS with 0.1 % Tween 20) for 5 minutes. Following pre-blocking, membranes were washed and fixed with 0.2 % glutaraldehyde in PBST for 20 minutes at RT. The membranes were washed again and subjected to a second blocking step using 1 % skim milk, 0.1 % BSA in PBST for 1 hour at RT. Primary antibodies (**Table 1**) were applied to the membranes and incubated overnight at 4 °C. The following day, the membranes were washed with TBST and incubated with a horseradish peroxidase conjugated secondary antibody (**Table 1**) for 1 hour at RT. The membranes were then washed three times for 10 minutes each with TBST. Insulin signal was detected as detailed in **Chapter 2A.2.6**.

2A.3 Results

2A.3.1 Optimisation of siRNA knockdown of Scamp3 in INS-1 cells

To investigate the role of Scamp3, a protein identified through proteomics analysis of ISGs (**Chapter 2**), Scamp3KD cells were generated through siRNA-mediated knockdown to transiently deplete Scamp3 expression. Firstly, INS-1 cells were transfected with varying concentrations of a Scamp3 targeting siRNA or with a non-targeting siRNA control (5 – 20 nM). Scamp3 protein concentrations were analysed at two different time points post-transfection to optimise the conditions of endogenous knock-down of Scamp3 efficiency. Western blot analysis of Scamp3 and insulin levels were normalised to GAPDH, revealing a dose- and time- dependent knockdown (**Figure 15A**). Optimal KD conditions were established using 10 nM of Scamp3-targeting siRNA (siScamp3#2) for 48 hours, which achieved approximately 70 % reduction in Scamp3 protein levels (**Figure 15A & B**) and a concurrent 40 % reduction in total insulin content (**Figure 15A & C**).

Notably, at 24 hours post-transfection with 5 and 10 nM siScamp3#2, there was a ~ 40 % reduction in total insulin content (**Figure 15B**), despite only a modest reduction in Scamp3 expression (**Figure 15A – C**). Immunofluorescence staining of Scamp3 and insulin (**Figure 15D**) further confirmed the depletion of Scamp3 in INS-1 cells, with ~ 40 % cells exhibiting little to no Scamp3 staining. Additionally, a reduction in insulin staining was observed, consistent with the Western blot findings.

These results demonstrate that a 48 hour transfection with 10 nM siRNA is optimal for efficient Scamp3KD, achieving significant depletion of Scamp3 and a reduction in total insulin content. This transfection condition was used for all subsequent KD experiments in **Chapter 2** and **Chapter 2A**.

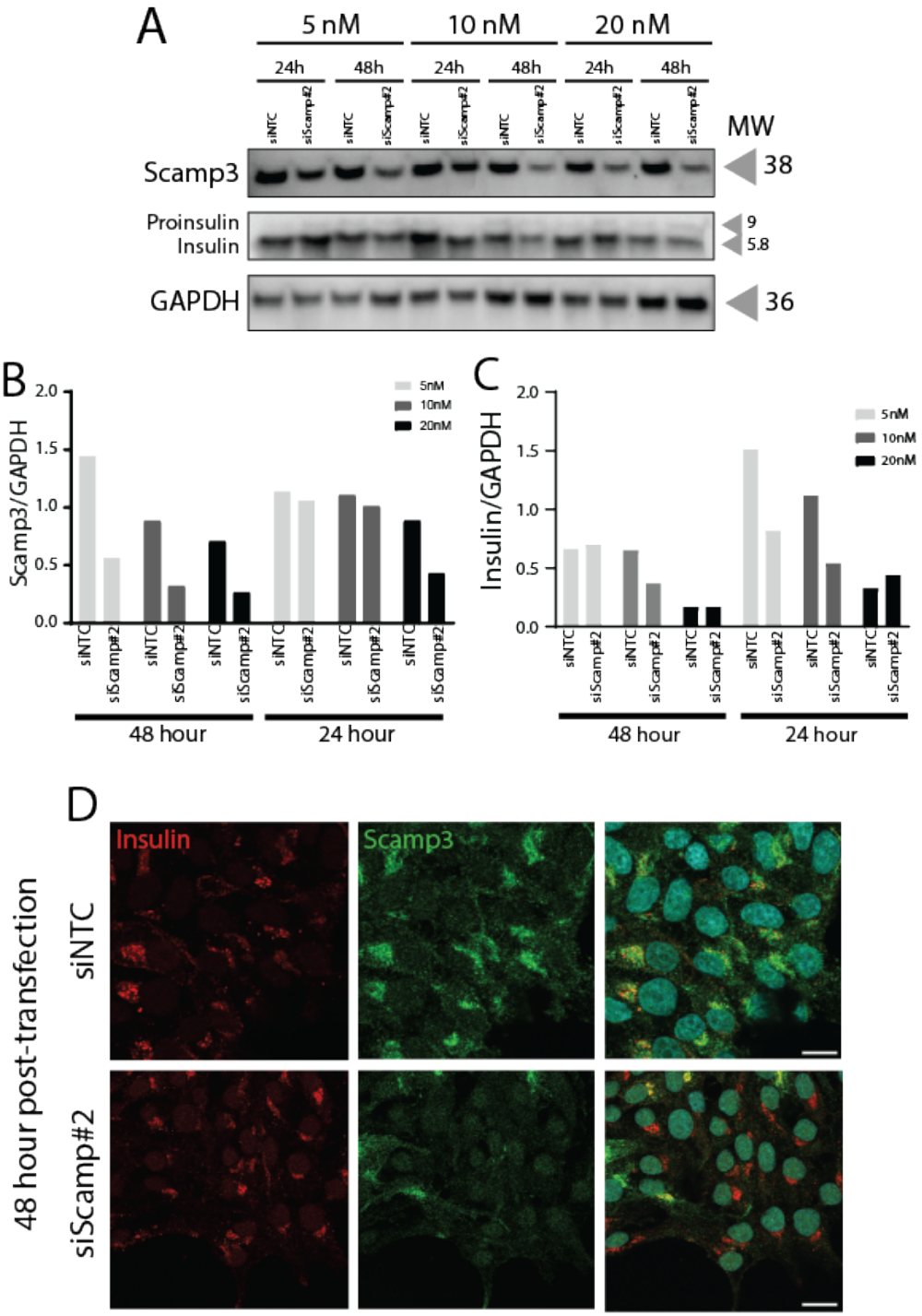

Figure 15: Scamp3 expression in INS-1 cells transfected with non-targeting (siNTC) or Scamp3 targeting (siScamp#2) siRNAs. (**A**) Western blot analysis of INS-1 cells transfected with 3 concentrations (5, 10 and 20 nM) of siScamp#2 or siNTC for 24 and 48 hours post-transfection. (**B-C**) Quantification of densitometry of Scamp3 and insulin normalised to GAPDH using FIJI software. (**D**) Confocal imaging of INS-1 cells transfected with 10 nM of

siScamp#2 or siNTC for 48 hours stained for anti-insulin and anti-Scamp3, scale bars represent 10 μm.

2A.3.2 Optimisation of siRNA knockdown of Synaptophysin in INS-1 cells

To investigate the role of Synaptophysin (Syp), a second protein confidently identified through proteomics analysis of ISGs (**Chapter 2**), SypKD cells were generated by transiently reducing Syp expression INS-1 cells using siRNAs. Briefly, INS-1 cells were transfected with varying concentrations (5 – 20 nM) of three Syp-targeting siRNAs at two different time points (24 and 48 hours) to determine optimal KD conditions.

Protein levels of Syp were assessed by SDS-PAGE and Western blot analysis (**Figure 16A**) with densitometric quantification normalised to beta-actin as a loading control. Dose- and time- dependent analysis revealed that a 48 hour transfection with 10 nM siRNA resulted in an approximately 50 % reduction in endogenous Syp expression (**Figure 16B**).

Immunofluorescence staining of Syp and insulin (**Figure 16C**) further confirmed the reduction of synaptophysin expression in INS-1 cells. Notably, the depletion was most prominent at the plasma membrane, while a perinuclear population of synaptophysin remained visible. Similarly to Scamp3KD, optimal KD of Syp was achieved with a 48 hour transfection at 10 nM of siRNAs, and these conditions were used for all subsequent SypKD analysis in **Chapter 2A**.

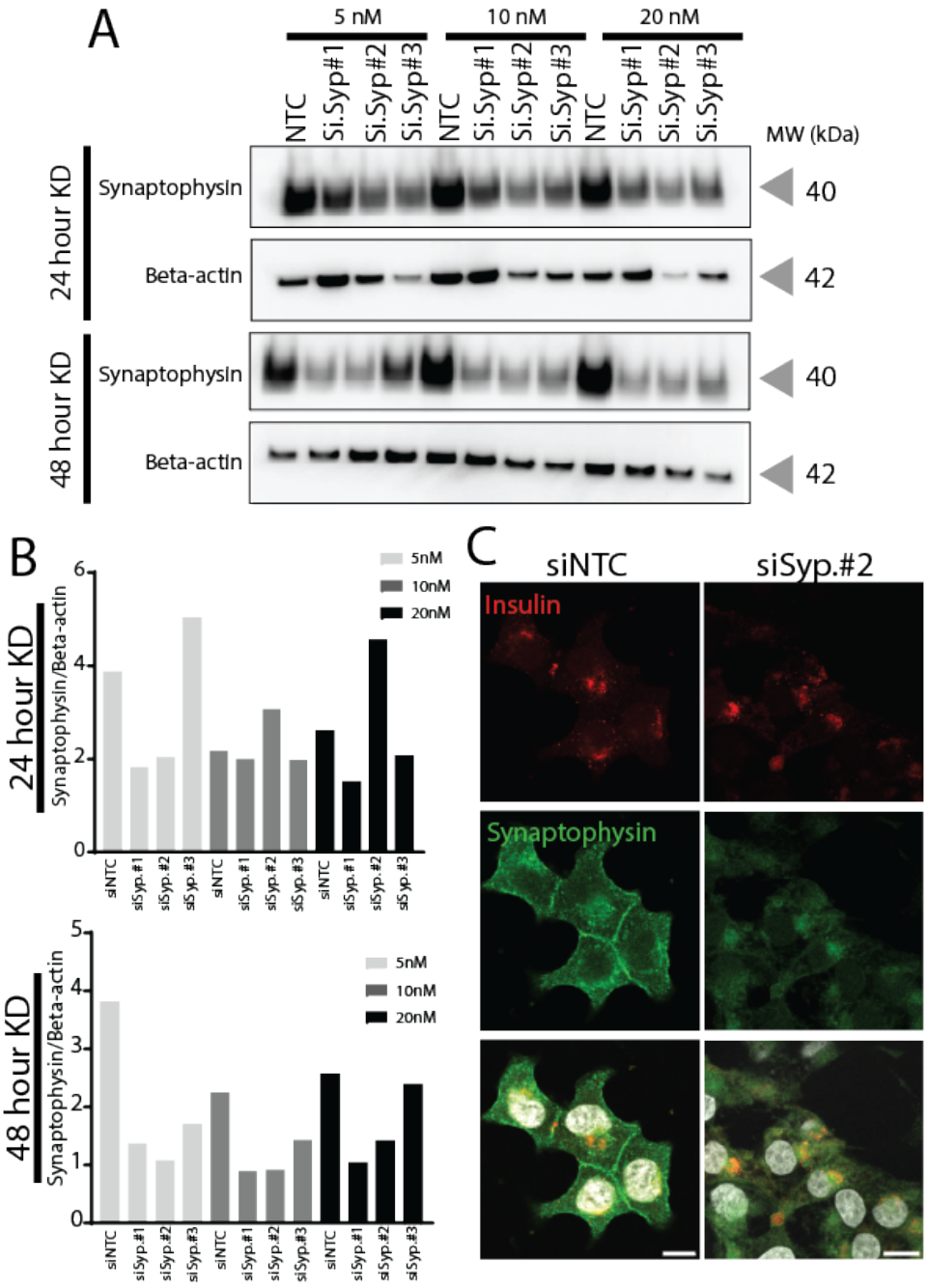

Figure 16: **Synaptophysin expression in INS-1 cells transfected with non-targeting (siNTC) or Syp targeting siRNAs**. (**A**) Western blot analysis of INS-1 cells transfected with 3 concentrations (5, 10 and 20 nM) of three Syp-targeting siRNAs (Si.Syp#1, Si.Syp#2, Si.Syp#3) or siNTC for 24 and 48 hours post-transfection. (**B**) Quantification of densitometry of Syp normalised to GAPDH using FIJI software. (**C**) Representative confocal imaging of INS-1 cells transfected with 10 nM of siSyp#2 or siNTC for 48 hours stained for anti-insulin and anti-Synaptophysin, scale bars represent 10 µm.

2A.3.3 Investigation of Synaptophysin function in INS-1 cells

Identification of Syp by proteomics analysis and further validation through colocalisation analysis of Syp with insulin in MIN6 beta-cells (**Chapter 2**) identified Syp as a strong candidate for association with ISGs and a potential role in regulating ISG turnover. Thus, Syp was selected as the second candidate for knockdown to investigate its role in regulating insulin content and GSIS.

Endogenous Syp was depleted in INS-1 rat insulinoma cells using three commercially available siRNAs, targeting three unique sequences of rat Syp (TriFECTa, IDT). 48 hours post transfection, INS-1 cells exhibited ~50 % knockdown of Syp in all siRNA conditions compared to cells transfected with a non-targeting control siRNA (**Figure 17A & B**). Functional characterisation of Syp was performed to assess its impact on GSIS. siNTC INS-1 cells show a typical insulin secretory response with a 2 - 3-fold increase in insulin secretion under stimulated (16.7 mM) glucose conditions, compared to the basal (2.8 mM) glucose conditions. Strikingly, in all three SypKD conditions, there was a marked reduction in insulin secretion under high glucose stimulation compared to siNTC cells, while basal insulin secretion remained unchanged (**Figure 17C**). This was further reflected in a significant reduction in the fold-change of stimulated/basal conditions, which resulted in a clear blunted secretory response from SypKD cells (**Figure 17D**).

Interestingly, quantification of total insulin content, normalised to total DNA following GSIS revealed no significant changes of insulin content between SypKD and siNTC cells (**Figure 17E**). These findings suggest that while SypKD impairs the dynamic secretory response to glucose stimulation, it does not alter total insulin content within the cells.

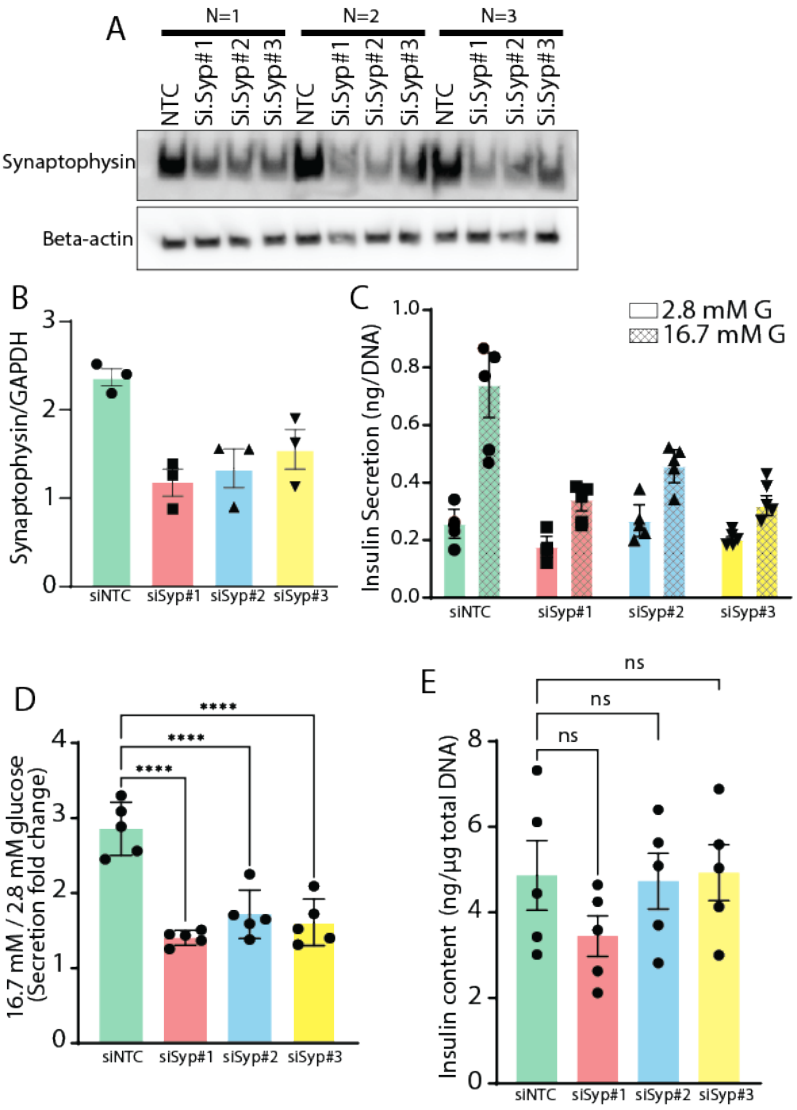

Figure 17: **Functional investigation of Synaptophysin in INS-1 beta-cells**. (**A**) SDS-PAGE analysis of INS-1 cell lysates 48 hours post transfection with a control non-targeting siRNA (green) and three unique siRNAs specific to Syp (Si.Syp#1 (red), Si.Syp#2 (blue) and Si.Syp#3 (yellow)) in 3 experimental replicates (n = 3). (**B**) Densitometry quantification of knockdown efficiency of Syp 48 hours post transfection normalised to GAPDH (n = 3). (**C**) Glucose-stimulated insulin secretion assay; insulin concentration after basal (2.8 mM glucose) and stimulation (16.7 mM) glucose conditions from INS-1 control and SypKD cells, measured by insulin HTRF (Cisbio) (n = 5). (**D**) Fold-change of basal to stimulated glucose conditions from C (n = 5). (**E**) Insulin content of INS-1 control and SypKD cells normalised to DNA content

measured by insulin HTRF and Quant-IT PicoGreen respectively. All error bars represent standard error of the mean (±S.E.M.). ****P-value < 0.0001. *One-way ANOVA*.

2A.4 Discussion

The application of machine learning analytical tools has proven to be instrumental in deciphering the complex proteomics data derived from our subcellular fractionation of ISGs. By developing and integrating this approach (**Chapter 2**), we identified 211 proteins and further validated four high confidence candidate proteins that colocalise with insulin in MIN6 cells. This comprehensive protein list also serves as a valuable resource for investigating the molecular mechanisms that regulate ISG processes in future. Scamp3 was then knocked-down and functional analyses performed. Further analysis included cross-referencing with the Type 2 diabetes knowledge portal (T2DKP, type2diabetesgenetics.org), and a single Scamp3 variant is interestingly associated with Type 1 diabetes as well [243]. However, further validation and functional studies are required for many of these proteins before their roles in beta-cell function can be firmly established.

Chapter 2A focuses on the functional analysis of synaptophysin, a candidate protein consistently identified through 4 out of 5 experimental replicates using the pRoloc machine learning approach. Given the known similarities in protein expression and exocytotic machinery between beta-cells and neuroendocrine cells [244, 245], the identification of synaptophysin as an ISG-associated protein was notable, though not entirely unexpected. Previous studies have postulated that synaptophysin is involved in forming synaptic-like microvesicles for GABA secretion in beta-cells [246, 247], though this is still debated [235]. We previously reported that synaptophysin expression is upregulated in murine islets under high-fat diet (HFD), as well as in islets from the diabetic *db/db* and obese *ob/ob* mouse models

[232]. Beta-cells may compensate in these models by increasing ISG production, and thus an upregulation of Syp protein productions would likely follow in parallel.

In **Chapter 2** & **2A,** we validated the localisation of Syp within ISGs in multiple beta-cell models including rat, mouse and human. Knockdown of Syp using siRNAs in INS-1 cells resulted in a significant reduction in fold-change GSIS (**Figure 17D**), while total insulin content remained unchanged compared to control cells (**Figure 17E**). These results implicate the involvement of Syp in the glucose-regulated secretory pathway within pancreatic beta-cells. This directly contrasts with previous studies indicating that Syp is absent on insulin-containing large dense core vesicles (LDCVs) [64, 248].

The established role of synaptophysin in neuronal cells provides further insight into its potential role in beta-cells. In neurons, Syp is known to participate in neurotransmitter exocytosis by reversibly binding to v-SNARE proteins and stabilising VAMP2 [249, 250]. Co-transfection studies of Syp and VAMP2 demonstrate a clear interaction between these two proteins [251]. This interaction is remarkably interesting, as VAMP2 has been shown to localise to the ISG and interact with other SNARE complex proteins and calcium-sensing synaptotagmins to drive the fusion of ISGs with the plasma membrane [252, 253]. These findings support the hypothesis that Syp may similarly interact with SNARE complex proteins at the site of exocytosis in beta-cells, stabilising the fusion of ISGs with the PM. Further studies should explore the specific molecular mechanisms through which Syp contributes to ISG exocytosis and how this may be altered in conditions of metabolic stress or diabetes.

2A.5 Conclusion

Taken together, these Chapters (**2 & 2A**) present an optimised, efficient and transferrable approach to isolating ISGs from beta-cells. Using both unbiased and machine learning tools to identify novel ISG associated proteins, Scamp3 and synaptophysin were

validated in mouse and rat beta-cell lines, and human donor pancreatic islets, alongside additional proteins Syntaxin-7 and Synaptotagmin-13. Through siRNA mediated knockdown and functional analysis of Scamp3 and Syp, we provide evidence for their roles in regulating the GSIS pathway in pancreatic beta-cells. Our findings underscore the functional significance of these novel ISG-associated proteins and open future studies to further investigate their roles in beta-cell physiology and their involvement in metabolic diseases like T2D.

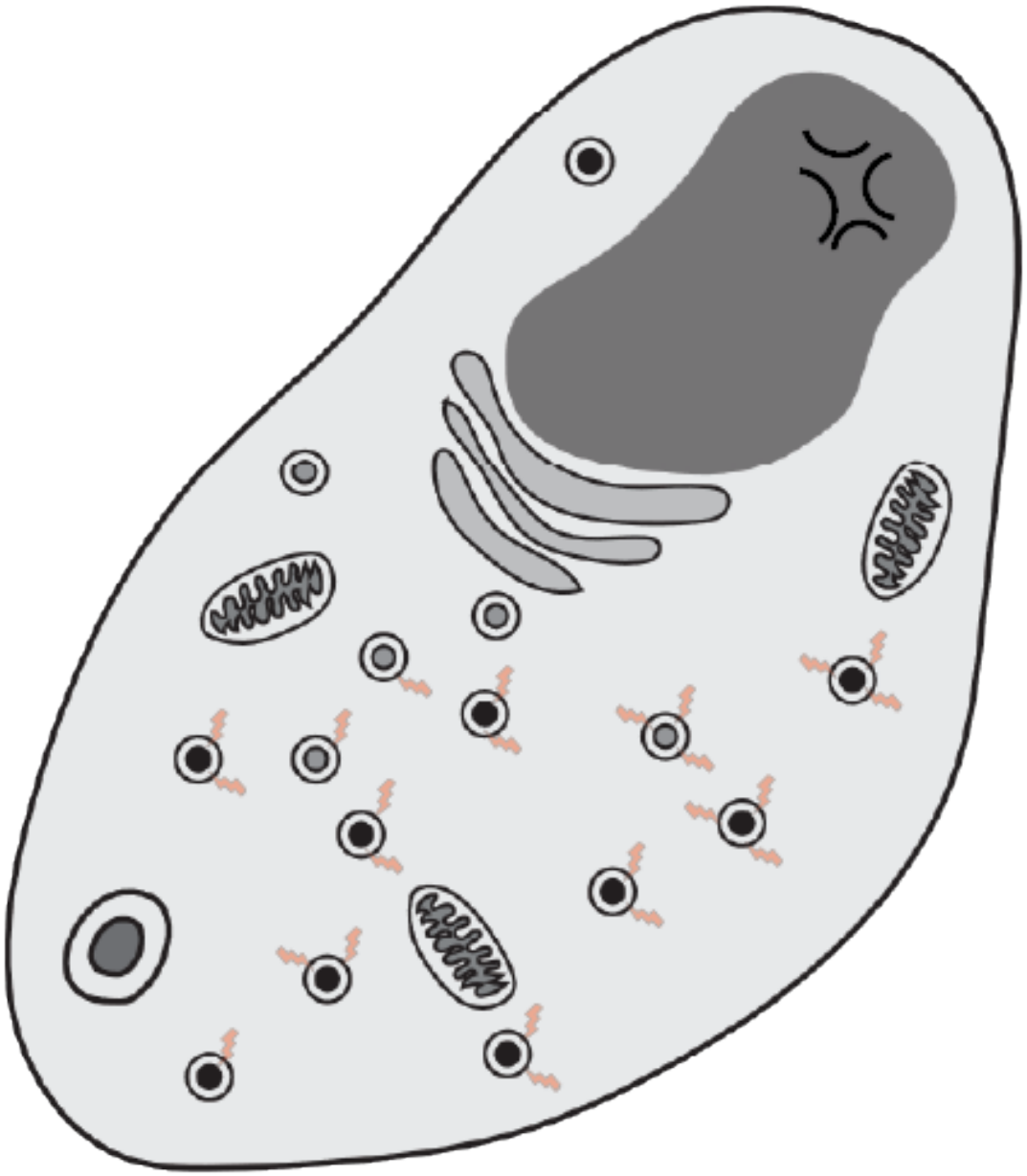

Chapter 3

Investigating the effects of glucolipotoxicity on the proteome of the insulin secretory granule

3.1 Introduction

3.1.1 Acute effects of free fatty acids on beta-cell function

Insulin secretion is mainly controlled by elevated blood glucose levels; however, many coupling factors have been shown to contribute to an amplification of glucose-stimulated insulin secretion (GSIS) including circulating free fatty acids (FFAs) [254, 255]. In fact, when pancreatic islets are starved of FFAs, GSIS is diminished [256, 257]. While fatty acids alone do not trigger insulin secretion, they have been shown to potentiate and augment GSIS [258, 259] (**Figure 18**). This process occurs via the activation of free fatty acid receptor 1 (FFAR1) signaling by FFAs, or metabolically active lipids such as long-chain acyl-CoA (LC-CoA), diacylglycerol (DAG) and monoacylglycerol (MAG) [254, 260].

Within the cytoplasm, fatty acids undergo oxidation, a process facilitated by carnitine palmitoyl transferase-1 (CPT-1) which transports LC-CoAs across the mitochondrial membrane [261]. This process is primarily inhibited by the metabolism of glucose in beta-cells [260, 262]. Consequently, elevated glucose levels lead to an accumulation of cytosolic LC-CoA, which directly influences GSIS by modulating K_{ATP}-channels and enhancing protein kinase C activity [263, 264]. In parallel, accumulation of cytosolic LC-CoAs may enter the non-esterified fatty acid (NEFA) cycle, promoting the formation of di- and mono-acylglycerols, which further modulate ISG exocytosis [264-266].

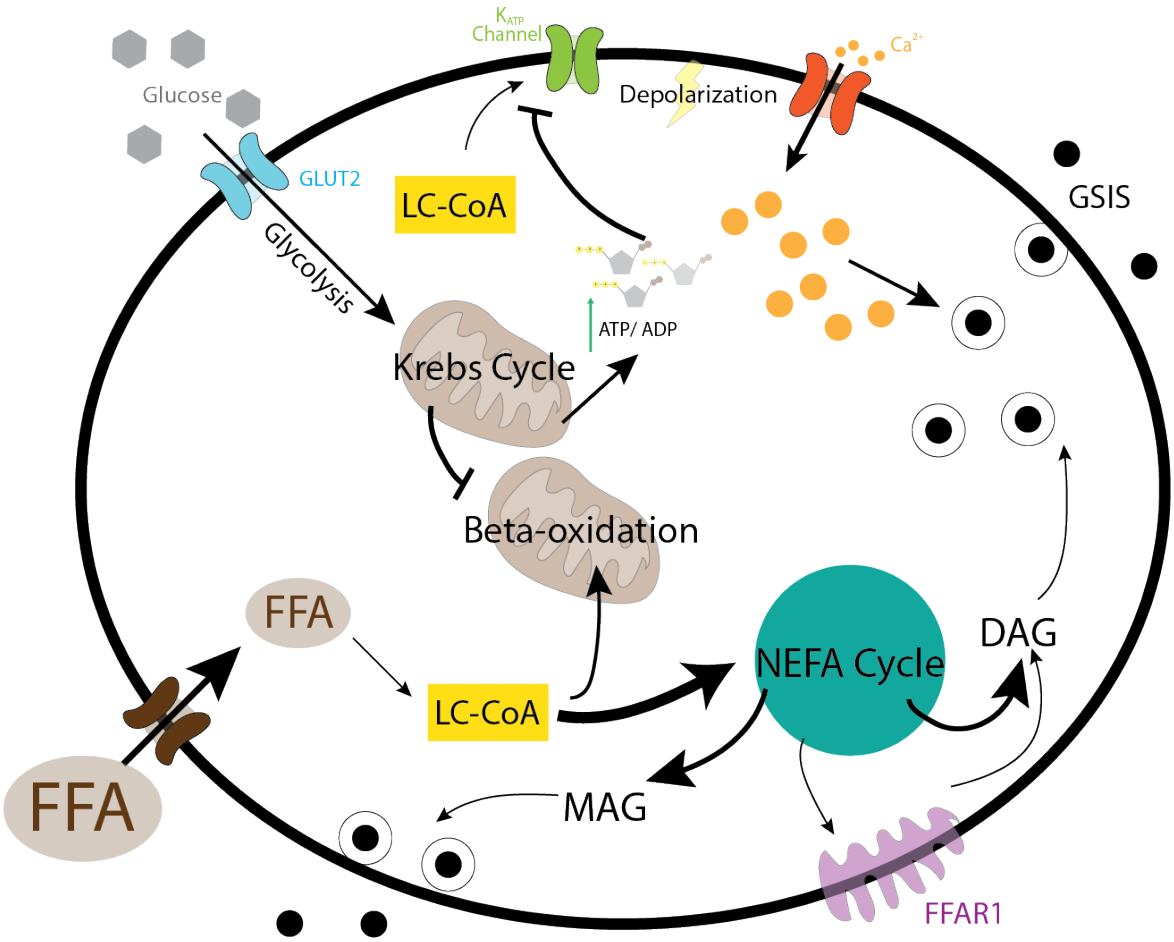

Figure 18: **Mechanisms of free fatty acid-mediated augmentation of Glucose-Stimulated Insulin Secretion in the Pancreatic Beta-cell**. The glycolysis and oxidation of glucose through the Krebs cycle inhibits beta-oxidation, thereby redirecting LC-CoAs into the NEFA cycle (teal). This process generates DAGs and MAGs, which promote the exocytosis of ISGs. Additionally, cytoplasmic FFAs activate FFAR1 (purple). Activation of FFAR1 triggers the production of DAGs through phospholipase C, further amplifying GSIS. *Adapted from Oberhauser, L. and Maechler, P. (2021)* [267].

3.1.2 Glucotoxicity and lipotoxicity in Type 2 Diabetes and Obesity

In obesity and the development of T2D, beta-cell dysfunction and death are driven by two key factors: glucotoxicity and lipotoxicity; collectively referred to as glucolipotoxicity.

Glucotoxicity is defined by the chronic exposure of beta-cells to elevated glucose levels that directly impacts beta-cell function, reducing insulin synthesis and GSIS through changes in insulin gene expression that drives beta-cell dedifferentiation [268]. Glucotoxicity contributes to the failure of beta-cells to compensate for insulin resistance in peripheral tissues, causing prolonged hyperglycaemia. This occurs in T2D and results in the loss of beta-cell secretory capacity [269] and up to 60 % reduction in total beta-cell mass [270, 271]. Additionally, there is a strong correlation between increased plasma glucose and the loss of first-phase GSIS [272].

The correlation between lipotoxicity and beta-cell dysfunction, however, is less established [273]. *In vivo* studies have experimentally elevated FFAs in circulation in humans using intravenous lipid emulsions and show that acute FFA elevation enhances GSIS [274, 275], but chronic 24 – 48 hour exposure to increased FFAs induce beta-cell dysfunction and reductions in GSIS [276, 277]. These are consistent *in vitro* and *ex-vivo*, with cell lines [278, 279], isolated rodent islets [280, 281] and isolated human islets [282, 283] acutely treated with FFAs stimulating insulin secretion. Importantly, however, chronic FFA treatment causes diminished GSIS and basal hypersecretion [282, 283].

Obesity is associated with elevated levels of circulating FFAs, a consequence of impaired FFA clearance and the expansion of adipose tissue [284]. Studies have sought to establish a connection between obesity and the pathophysiology of T2D by investigating the role of increased FFAs in the development of insulin resistance and exacerbation of beta-cell dysfunction [285]. However, epidemiological studies suggest that the concentration of FFAs

alone has less influence on glucose homeostasis and instead, FFA compositions have stronger effects on glucose homeostasis [286-288]. In humans, measurements of basal plasma lipids indicate that individuals with T2D have a higher proportion of palmitate [286-288] – the most abundant saturated FFA in humans, which is associated with an increased risk of developing T2D [288]. Consequently, a significant proportion of research on beta-cell lipotoxicity utilises palmitate *in vitro* to investigate its effects on beta-cell function and survival.

3.1.3 Effects of elevated FFAs in vitro and ex vivo

The effects of chronically elevated FFA levels on beta-cells has been widely studied, revealing several molecular mechanisms that implicate lipotoxicity and glucolipotoxicity in beta-cell dysfunction and death. These mechanisms include mitochondrial impairment, ER stress, autophagy dysfunction and oxidative stress within beta-cells. Studies have shown that exposure to elevated FFAs induces significant changes in the expression of genes associated with GSIS, including a reduction in preproinsulin mRNA levels [289]. Another study shows a reduction in insulin mRNA levels in islets treated with oleate and palmitate, though interestingly the number of granules per beta-cell remain unchanged [290]. Additionally, exposure to palmitate has been shown to significantly reduce mRNA levels of several critical genes involved in beta-cell function including *Ins1*, *Ins2*, *Pdx1*, *MafA*, *Glut2* and *Gck* [291].

Elevated FFAs have also been linked to mitochondrial and ER dysfunction through multiple mechanisms. One key pathway involves the binding of FFAs to CD36, an abundantly expressed fatty acid transporter in pancreatic beta-cells [292, 293]. This interaction triggers a pro-inflammatory response, leading to increased oxidative stress and cellular damage within the beta-cells.

Calcium signaling pathways play a crucial role in ISG exocytosis, with Ca^{2+} released from both the mitochondria and the ER during GSIS [294]. However, chronic exposure to FFAs

disrupts the replenishment of Ca^{2+} stores in these organelles, resulting in diminished GSIS [295].

In addition to mitochondrial and ER dysfunction, FFAs have been shown to reduce lysosomal activity [296, 297] leading to the accumulation of autophagosomes [298]. Autophagy, a process essential for protein turnover and cellular homeostasis is significantly disrupted in beta-cells treated with palmitate. This impairment in autophagic flux contributes to decreased protein turnover and often results in palmitate-induced cell death [299].

3.1.4 Linking FFAs to the ISGs

Alterations in ISG protein mRNA levels, despite the preservation of granule numbers suggests an uncoupling between insulin biosynthesis and secretion. This indicates that while the structural integrity of the ISG is maintained, their functionality or exocytotic capacity may be impaired. Further, dysregulation of autophagy directly impedes ISG turnover, affecting the recycling of ISG proteins. Given that ISGs function as intrinsically regulated signaling hubs, the ISGs themselves may respond to elevated FFAs through alterations in their compositions, ultimately contributing to the observed loss of GSIS. Additionally, FFAs within the cytosol may directly modify the lipid composition of ISG membranes, altering their fluidity and fusion capacity with the PM. These changes may compromise the ability of ISGs to effectively undergo exocytosis, thereby impairing insulin release.

3.1.5 Aims and Hypotheses

A substantial body of research has explored the impact of glucolipotoxicity on beta-cell function, establishing clear links to mitochondrial and ER stress, impaired autophagy, inflammation and altered gene and protein expression. However, the specific effect of these perturbations on ISGs remain poorly understood. Increased levels of FFAs have been shown to induce significant changes in ISG protein expression, granule dynamics and ISG turnover

within the beta-cells. These changes may alter the composition of the ISGs, potentially affecting their synthesis, packaging, or exocytosis in response to its nutritional environment. Such alterations could have profound implications for insulin secretion and beta-cell function during metabolic stress.

In this chapter, we aim to investigate the role of FFA-induced metabolic stress on the protein composition of ISGs within pancreatic beta-cells. We hypothesise that beta-cells alter their ISG compositions in response to their nutritional environment and that may explain how ISGs are differentially regulated in conditions of metabolic stress.

3.2 Materials and Methods

3.2.1 MIN6 insulinoma cell culture

Mouse MIN6 insulinoma cell lines were obtained from AddexBio™ and cultured at 37° C and 5 % CO_2 in Dulbecco's Modified Eagle Medium (DMEM) (Gibco™) containing 10 % foetal bovine serum (FBS) (Gibco™), 25 mM glucose, 44 mM NaHCO3, 4 mM L-glutamine, 1 mM sodium pyruvate, 0.005 % 2-beta-mercaptoethanol and 1 % penicillin-streptomycin (Complete DMEM). Cultures were passaged with TrypLE express enzyme (Gibco™) at 37 °C for 3 minutes upon reaching 80 - 90 % confluence. Culture media was changed every 2 – 3 days, and passages used in **Chapter 3** were between 3 – 20. All cell cultures were tested mycoplasma negative.

3.2.2 Palmitate complexing for the acute and chronic treatments in MIN6 cells

Palmitate treatment of MIN6 cells first requires complexing palmitate with BSA. A 150 mM Palmitate stock solution was prepared by dissolving palmitic acid in 50 % ethanol at 65°C, followed by vortexing until fully dissolved. This stock solution was then complexed with 10 % BSA (prepared in Milli-Q Water) at a 1:21 ratio (PA stock: 10 % BSA) for 1 hour in a 37°C water bath. The resulting palmitate/BSA complex solution were then diluted in Complete DMEM to achieve a final concentration of 0.5 mM palmitate. Control solutions were made (Vehicle/BSA) by adding 50 % ethanol complexed with 10 % BSA at 1:21 ratio for 1 hour in a 37 °C water bath, diluted again in Complete DMEM. Cells were treated with either vehicle control or 0.5 mM Palmitate for 24 - 48 hours.

For acute palmitate treatment in GSIS assays, the same protocol was used to prepare the PA/BSA or Vehicle/BSA controls. However, these solutions were diluted in Krebs buffer (KRBH) supplemented with 16.7 mM glucose.

3.2.3 SDS-PAGE and Western Immunoblotting

Protein concentrations from all fractions from subcellular fractionation or resuspended insulin granule pellets were measured using the Pierce BCA Protein Assay (ThermoFisher). Proteins were separated under denatured conditions using Bolt™ Bis-Tris Plus 4 – 12 % gels for non-insulin Western blot analysis. Electrophoresis was performed at 100 V for 75 minutes. The separated proteins were transferred to a methanol activated PVDF membrane (Immobilon, Millipore) at 100 V for 1 hour.

The membranes were blocked with SuperBlock™ Blocking Buffer for 20 min at RT, followed by a single wash with TBST (TBS with 0.1 % Tween 20). They were then incubated overnight at 4 °C with primary antibodies (**Table 1**) diluted in TBST containing 5 % BSA and 0.1 % sodium azide. After incubation, membranes were washed three times for 10 minutes each with TBST and then incubated for 1 hour at RT with secondary antibodies diluted in TBST containing 5 % skim milk. Finally, membranes were washed three times for 10 minutes each with TBST, and protein signals were detected using Immobilon Western Chemiluminescent HRP substrates (Merck) on a ChemiDoc MP imaging system.

3.2.4 Insulin Western Immunoblotting

For Western immunoblotting with insulin antibodies, the same procedures described in as **Chapter 3.2.3** were followed, with the exception of using non-denaturing conditions. After transfer, membranes were pre-blocked for 5 min in a solution containing 1 % BSA and 1 % skim milk in PBST (PBS with 0.1 % Tween 20), followed by fixation with 0.2 % glutaraldehyde in PBST for 20 min. After fixation, membranes were blocked for 1 hour with 1 % BSA and 1 % skim milk in PBST.

3.2.5 Three-Step Subcellular Fractionation

Three-step subcellular fractionation was performed on MIN6 control and 0.5 mM Palmitate-treated cells.

MIN6 cells were cultured on 15 cm diameter petri dishes to ~90 % confluence. Cells were washed once with PBS, scraped into 2 mL ice-cold PBS, centrifuged at 300 x g for 5 min. MIN6 cell pellets were resuspended in 1 mL of Buffer A (0.3 M sucrose, 1 mM $MgSO_4$, 1 mM EDTA, 10 mM MES-KOH, pH 6.5 with 1X EDTA-free protease inhibitors (Roche™). Resuspensions were passed through 21 and 25 G needles 10 times each respectively. Cell homogenates were then centrifuged for 5 minutes at 1000 x g to remove unbroken cells and nuclear debris. Optiprep 30 % was diluted in Buffer B (2 mM EGTA, 20 mM MES-KOH, pH 6.5). This 30 % solution was further diluted into 8.8, 13.2, 17.6 and 23.4 % with Buffer A. Cell supernatants were loaded onto a discontinuous Optiprep gradient with these five Optiprep solutions, 3 mL each. Samples were centrifuged at 100,000 x g for 80 min in a P50AT2 fixed angle rotor in a Hitachi 100NX ultrafuge at 4 °C, 50 % acceleration and deceleration to ensure no disturbance of Optiprep layers. Sixteen fractions were removed from the top to bottom to obtain a total of sixteen 1mL fractions.

Fractions were analysed for insulin content using insulin ELISA (Crystal Chem) according to the manufacturer's instructions with normalisation to total protein determined by Pierce BCA Protein Assay (ThermoFisher) and SDS-PAGE. The two fractions most enriched in mature ISGs (Between Fractions 10 - 14) were layered onto 10 mL of 27 % Percoll solution prepared in Buffer A within a polypropylene tube. This mixture was centrifuged at 35,000 x g for 60 mins using a fixed-angle a A22-24x16 rotor (Thermo Fisher) in a Sorvall Lynx 4000 Centrifuge (Thermo Fisher) set to 4 °C. Twelve 1 mL fractions were removed from top to bottom.

For the third step of separation, each 1 mL fraction from Percoll was diluted in 9 mL of sucrose wash buffer (0.3 M sucrose, 5 mM HEPES, 1 mM EGTA, pH 7) and centrifuged for 15 mins at 23,700 x g to pellet mISGs and remove Percoll. The supernatants were carefully discarded, and mISG pellets were resuspended in 4 % sodium deoxycholate (SDC) in Milli-Q water. The resuspended pellets were boiled at 95 °C for 5 minutes followed by tryptic digest.

3.2.6 LC-MS/MS Tryptic Digest and Peptide Clean-up

Equal volumes (50 µL) of each gradient fraction were adjusted to a final volume of a 100 µL with a solution containing 4% SDC, 0.1 M Tris-HCl, pH 9.0, 10 mM TCEP and 40 mM chloroacetamide in Milli-Q water. The samples were incubated on an Eppendorf Thermomixer-C at 1000 rpm at 95 °C for 10 minutes. Following incubation, samples were diluted with water to achieve a final concentration of 1 % SDC. Digestion was carried out overnight at 37 °C using 200 ng of MS-grade trypsin (Sigma) in 50 mM acetic acid with continuous mixing at 1000 rpm on an Eppendorf Thermomixer-C. Ethyl acetate was then added to a final concentration of 50 % (v/v), and the samples were vortexed until the precipitated SDC was fully dissolved. Sample purification was performed using SDB-RPS StageTips as previously described [212]. The resulting peptides were reconstituted in 5 % formic acid in MS-grade water, sealed and stored at 4 °C until LC-MS/MS acquisition.

3.2.7 LC-MS/MS Acquisition

Peptides in 5 % (v/v) formic acid (injection volume: 3 µL) were directly injected onto a 50 cm x 75 µm C18Aq (Dr Maisch; 1.9 µm) fused silica analytical column with a ~ 10 µm pulled tip, using a ThermoFisher RSLCnano ultrahigh performance liquid chromatograph system. The column was coupled online to a nanospray electrospray ionisation source. Peptides were resolved over a gradient from 5 % - 40 % acetonitrile over 70 mins with a flow rate of 300 nL min-1 (capillary flow). Peptides were then ionised by electrospray ionisation at 2.3 kV.

Tandem mass spectrometry analysis was performed on a Q-Exactive HFX mass spectrometer (ThermoFisher) using data-independent acquisition (DIA). DIA was conducted as previously described using variable isolation widths for different m/z ranges [213]. Spectral acquisitions were performed using a stepped normalised collision energy of 25 ± 10%.

3.2.8 LC-MS/MS Analysis

Raw data were processed using the quantitative DIA proteomics software DIA-NN (version 1.8) [214]. All label-free quantitation within this thesis (**Chapter 3** and **Chapter 2**) was performed using the MaxLFQ algorithm from MaxQuant that is integrated to the DIA-NN environment. The complete mouse proteome from Uniprot was used to generate a neural network with deep spectral prediction enabled. Protease digestion was performed with trypsin (fully specific), allowing for up to two missed cleavages and one variable modification. Oxidation of methylation and acetylation of protein N-terminus were set as variable modifications. Carbamidomethylation of cysteine residues was set as a fixed modification.

The 'match between runs' and 'remove likely interferences' were enabled. The neural network classifier was configured to double-pass mode with protein interference based on gene-level identification. The quantification strategy was set to accommodate any liquid chromatography (LC) with high accuracy. Cross-run normalisation was performed using retention time (RT)-dependent normalisation and library profiling was set to smart profiling.

3.2.9 LC-MS/MS Raw data processing

All raw MS data outputted was analysed using Rstudio (v 4.2.1). A variance stabilisation normalisation (vsn) was first performed using the *vsn* package [221].

3.2.10 Machine Learning

Assigning proteins to different organelles and complexes within MIN6 beta-cells was performed in Rstudio using the support vector machine (SVM) learning. This is implemented

within the 'svmOptimisation' and 'svmClassification' functions within the R package pRoloc [219]. Protein markers present within the vsn normalised MS outputs were assigned using the publicly available *Mus musculus* library that is provided through the *pRolocdata* package [219, 220]. SVM scores were calculated, and proteins with scores above the global median were assigned to the corresponding marker proteins, facilitating accurate classification of subcellular localisation.

3.2.11 Immunofluorescent staining

MIN6 cells were cultured on glass coverslips in complete DMEM under standard culture conditions. Cells were washed once with PBS and fixed with 4 % paraformaldehyde (PFA) (#15710, Electron Microscopy Sciences) for 20 mins at RT. After fixation, coverslips were then washed with PBS three times to remove remaining PFA, and permeabilised with 0.1 % SDS for 5 min at RT. Coverslips were then washed with IF wash buffer (0.1 % BSA, 0.01 % Sodium azide in 1X PBS). To prevent non-specific binding, cells were blocked with Dako Protein serum-free Ready-to-use buffer (#X0909) for 1 hour at RT. Following blocking, coverslips were incubated overnight at 4 °C with appropriate primary antibodies (**Table 1**) diluted in Dako Antibody Diluent (#S0809). The next day, coverslips were washed five times with IF wash buffer before incubation with secondary antibodies (**Table 1**) for 1 hour at RT. Afterwards, coverslips were washed three times with IF wash buffer and mounted onto glass microscope slides with ProLong Antifade Diamond with DAPI mountant (P36962). Mounted slides were allowed to cure overnight before imaging.

3.2.12 MIN6 glucose stimulated insulin secretion (GSIS)

MIN6 cells were cultured in complete DMEM in 6-well plates. 18 hours before GSIS assays, cells were starved in low glucose complete DMEM (5.5 mM glucose containing 10 %

foetal bovine serum (FBS) (Gibco™), 25 mM glucose, 44 mM NaHCO3, 4 mM L-glutamine, 1 mM sodium pyruvate, 0.005 % 2-beta-mercaptoethanol and 1 % penicillin-streptomycin.

On the day of the assay, cells were pre-incubated in basal Krebs buffer (KRBH) 10 mM HEPES, 0.1 % fatty-acid free BSA, pH 7.4) containing 2.8 mM glucose for an hour. The assay was performed under standard culture conditions at 37 °C and 5 % CO_2. Cells were first incubated with 1 mL of 2.8 mM glucose KRBH for 1 hour, followed by 1 mL of 16.7 mM glucose KRBH for an additional hour. After each hour, supernatants were collected and centrifuged for 3 min at 300 x g to remove any aspirated cells. Insulin concentrations in the supernatant were measured by HTRF assay (Cisbio, #62IN2PEH).

Following stimulation, cells were lysed in islet lysis buffer (100 mM Tris, 300 mM NaCl, 10 mM NaF, 2 mM Na_3VO_4 and Roche EDTA-free protease inhibitors (cOmplete, Sigma) and sonicated. Total cellular insulin content again was quantified by insulin HTRF assay, following manufacturer's instructions, with samples diluted with Milli-Q water to fit within the standard curves of the HTRF assay. DNA content of cell lysates was measured using Quant-iT™ PicoGreen ™ dsDNA assay kits (Invitrogen™) according to manufacturer's instructions. Total protein content of cell lysates was measured using the Pierce BCA Protein Assay (ThermoFisher). Insulin HTRF readings were obtained using the Infinite F200 PRO Tecan Microplate reader and data was analysed with Magellan software at 620 nm and 665 nm.

3.2.14 General statistics

All proteomics data analysis was performed on RStudio (v. 4.2.1). Statistical significance testing was assessed by a one- or two-way ANOVA using Prism Version 10 Software (GraphPad, San Diego, CA). Significance was considered $P < 0.05$.

3.3 Results

3.3.1 Effect of chronic palmitate exposure in MIN6 beta-cell GSIS

To validate the effects of palmitate exposure on GSIS, MIN6 beta-cells were incubated for 24 or 48 hours with 0.5 mM palmitate-BSA or a vehicle control. After 24 hours of treatment, there were no significant differences in insulin secretion under basal (2.8 mM glucose) or stimulated (16.7 mM glucose) conditions between vehicle- and palmitate-treated cells (**Figure 19A**). Similarly, the fold-change in insulin secretion between basal and stimulated glucose conditions remained unchanged after 24 hours (**Figure 19B**). These results indicate that a 24 hour exposure to palmitate was insufficient to induce significant changes in GSIS.

In contrast, a 48 hour exposure to 0.5 mM palmitate resulted in a significant reduction in insulin secretion under stimulated glucose conditions (16.7 mM) compared to both control groups (**Figure 19C**). This reduction was further reflected in a significant decrease in the fold-change of GSIS compared to controls (**Figure 19D**). Importantly, the addition of the BSA vehicle alone had no significant effect on GSIS relative to untreated controls (**Figure 19C & D**). These findings establish that a 48 hour exposure to 0.5 mM palmitate reliably induces a significant reduction in GSIS. These conditions were used in the subsequent experiments to investigate the effects of glucolipotoxicity on ISG composition in MIN6 cells.

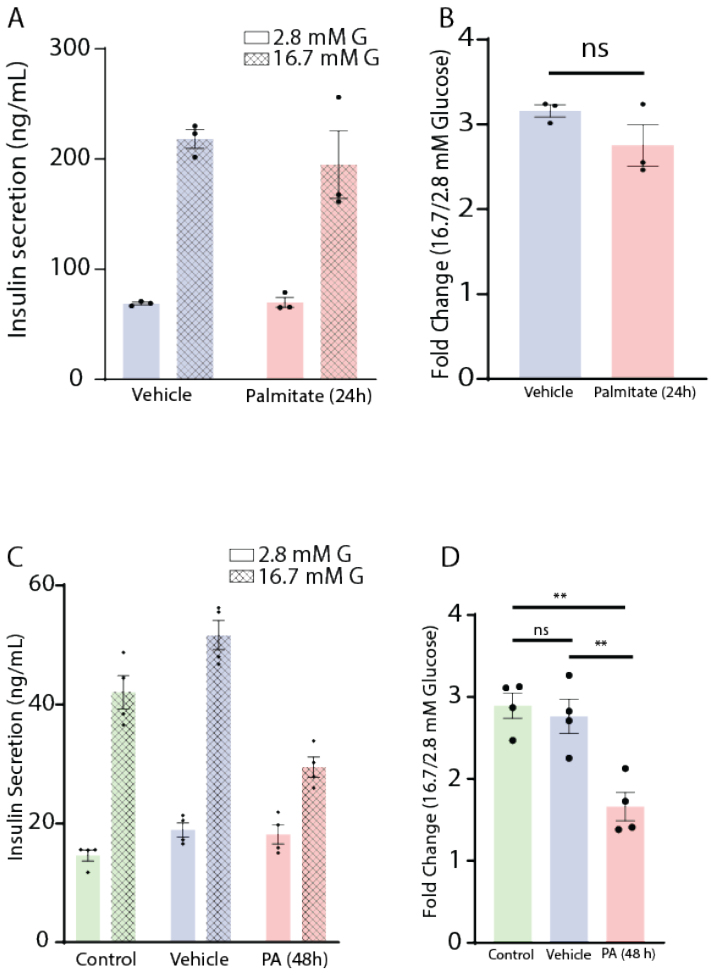

Figure 19: **Effect of chronic palmitate on glucose-stimulated insulin secretion in MIN6 cells**. (**A**) Glucose-stimulated insulin secretion assay; insulin concentration (measured by insulin HTRF (Cisbio) after basal (2.8 mM) and stimulated (16.7 mM) glucose conditions from MIN6 beta-cells incubated in complete DMEM without (Vehicle) or with 0.5 mM palmitate for 24 hours (n = 3). (**B**) Fold-change of basal to stimulated glucose conditions from **A** (n = 3). (**C**) Glucose-stimulated insulin secretion assay, insulin concentrations after basal and stimulated glucose conditions from MIN6 beta-cells incubated in complete DMEM without BSA/EtOh supplement (control), with BSA/EtOh complexing vehicle (Vehicle) and 0.5 mM palmitate (PA 48h) for 48 hours prior (n = 4). (**D**) Fold-change of basal to stimulated glucose conditions from **C** (n = 4). Stimulated and basal conditions were performed in the same well. Error bars represent ± S.E.M. * $P < 0.05$, ** $P < 0.01$, *** $P < 0.001$, **** $P < 0.0001$. *One way ANOVA*.

3.3.2 Subcellular fractionation of MIN6 cells by Optiprep

To investigate the effect of palmitate on ISGs, MIN6 post-nuclear cell lysates from control and 0.5 mM palmitate-treated cells were subjected to a three-step purification process using a discontinuous Optiprep gradient (8.8 – 30 %) as previously described in **Chapter 2**. The analysis focused on the later Optiprep fractions (Fractions 6-14) to prioritise the quantification of mature insulin using an insulin ELISA (**Figure 20A and B**). The distribution of insulin concentrations across these fractions was consistent between control and palmitate-treated cells, with peak mISG enrichment in fractions 11 & 12 (outlined in red**, Figure 20A & B**). SDS-page analyses of the Optiprep fractions further confirmed the enrichment of mature insulin within later fractions and proinsulin bands present in the earlier fractions, aligning with iISGs (**Figure 21A & B**). Notably, this pattern was consistent across both control and palmitate-treated conditions, indicating that chronic exposure to 0.5 mM palmitate did not alter the density or distribution of ISGs.

Enrichment of mISGs was evident in both conditions, with minimal contamination from the cytoskeleton, as evidenced by the absence of beta-actin in these fractions. However, due to density similarities between mISGs and the mitochondria, co-enrichment of mISGs and the mitochondrial marker ATP5A was observed. Therefore, the selection of fractions for subsequent purification step using Percoll was guided by maximising insulin enrichment while minimising mitochondrial contamination. For the representative experiment shown in **Figure 21A and B**, Fractions 11 & 12 were selected for further purification in both control and palmitate-treated conditions. Taken together, insulin ELISA and SDS-PAGE analysis revealed no significant differences in insulin distribution or ISG density between control and palmitate treated MIN6 cells. These findings suggest that chronic exposure to elevated FFAs does not significantly alter the overall density or enrichment of mISGs.

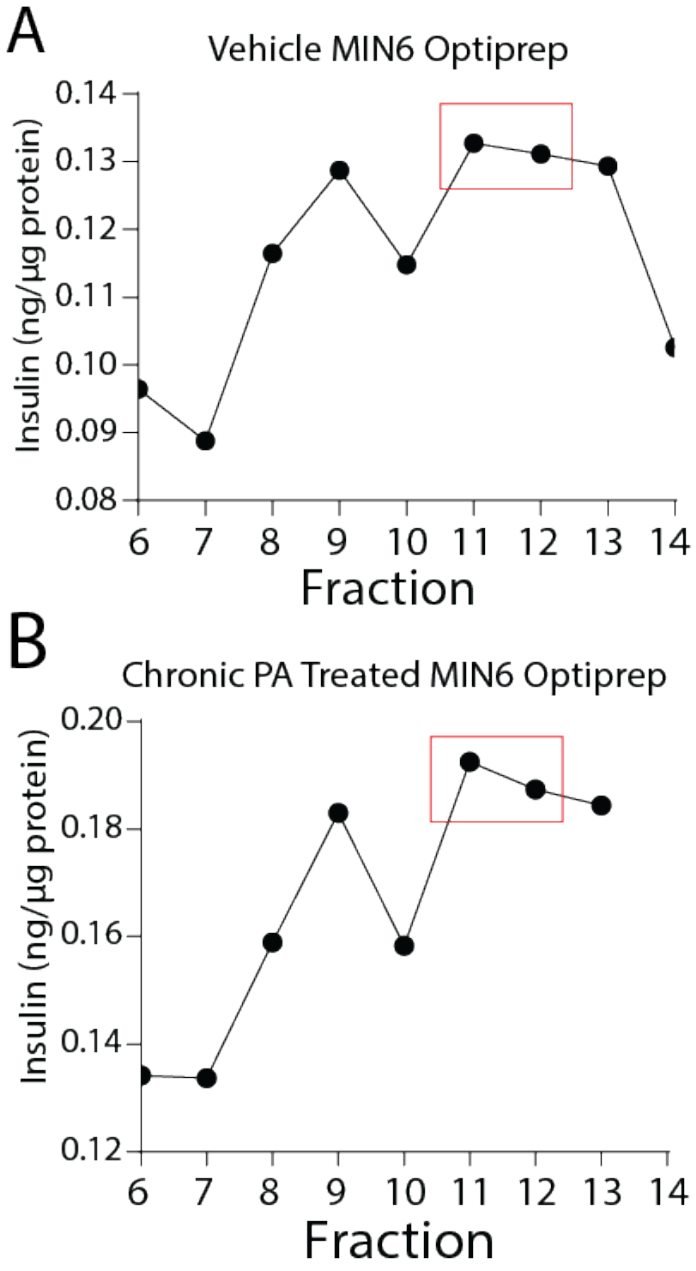

Figure 20: **Analysis of immature and mature insulin secretory granules from MIN6 cells by Optiprep™** (**A**) Representative quantification of insulin content enrichment from fractions 6 - 14 of Optiprep separation by insulin ELISA (Crystal Chem) from 48 hour vehicle DMEM treated MIN6 cells. (**B**) Representative quantification of insulin content enrichment from fractions 6 - 14 of Optiprep separation by insulin ELISA (Crystal Chem) from 48 hour 0.5 mM palmitate treated MIN6 cells.

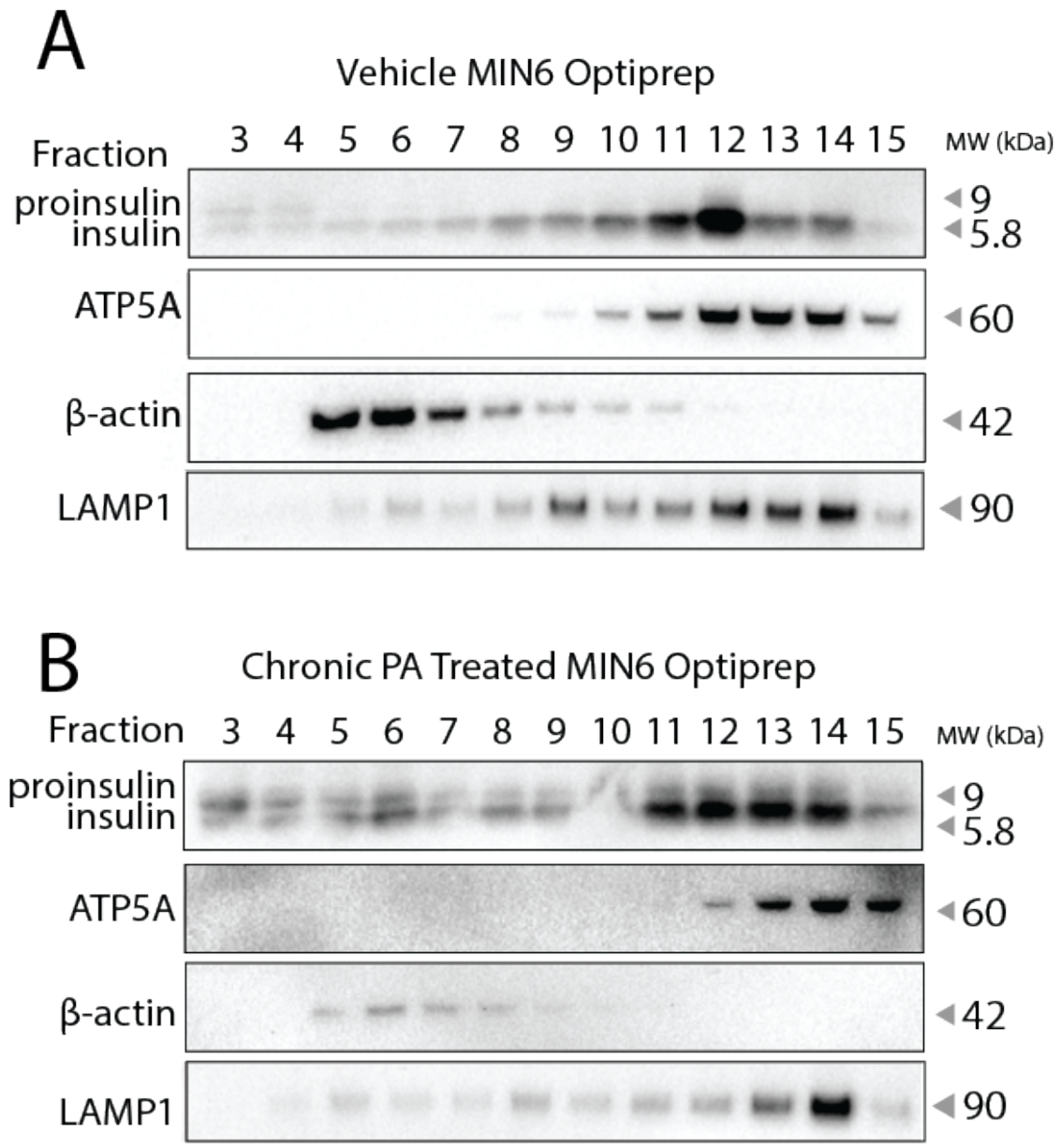

Figure 21: **SDS-PAGE analysis of mature and immature ISGs separated by Optiprep™ in vehicle and Palmitate treated MIN6 cells.** (**A**) SDS-PAGE analysis of proinsulin and insulin enrichment of Optiprep fractions from 48 hour vehicle DMEM treated MIN6 cells and (**B**) SDS-PAGE analysis of proinsulin and insulin enrichment of Optiprep fractions from 48 hour palmitate DMEM treated MIN6 cells with marker proteins for different subcellular components of beta-cells, MW for the kDa molecular weight of each protein.

3.3.3 Second-step enrichment of insulin from MIN6 cells with Percoll

The two Optiprep fractions with maximal insulin enrichment and minimal mitochondrial contamination were loaded atop of 27 % Percoll solutions and subjected to ultra centrifugation. Following centrifugation, the samples were washed in a sucrose buffer to pellet mISGs. The pelleted mISGs were resuspended in 4 % SDC for subsequent SDS-PAGE analysis and LC-MS/MS.

SDS-PAGE analysis was performed using antibodies against insulin, mitochondria (ATP5A) and lysosomes (LAMP1) to assess the purity and enrichment of mISGs within the Percoll fractions (**Figure 22A & B**). The results demonstrated maximal insulin enrichment in the later fractions of the Percoll gradients, while mitochondrial markers were predominately present in the earlier fractions. This indicates successful separation of mitochondria from the most enriched insulin fractions. The absence of lysosomal marker LAMP1 in these later fractions further confirmed the specificity and purity of the mISG preparations. These results validate the use of the Percoll gradient ultracentrifugation step in isolating mISGs with minimal mitochondrial and lysosomal contamination from the most enriched insulin fractions.

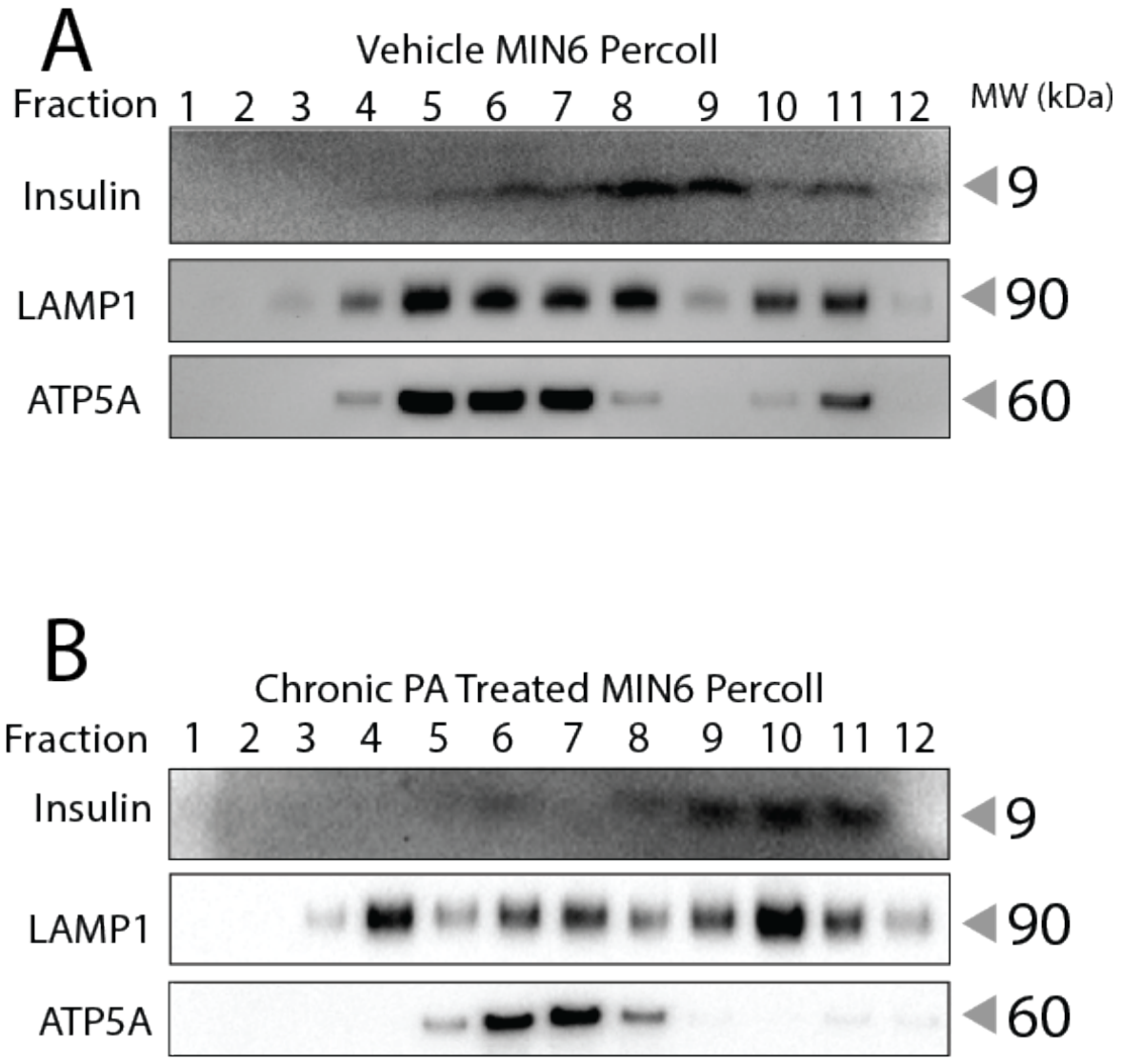

Figure 22: **SDS-PAGE of mature ISGs separated by Percoll in vehicle and Palmitate treated MIN6 cells.** (**A**) SDS-PAGE analysis of insulin enrichment of Optiprep fractions from 48 hour vehicle DMEM treated MIN6 cells and (**B**) SDS-PAGE analysis of insulin enrichment of Optiprep fractions from 48 hour palmitate DMEM treated MIN6 cells with marker proteins for common contaminants of ISG isolations, MW for the kDa molecular weight of each protein.

3.3.4 Targeted proteomics analysis of ISGs from palmitate and control treated MIN6 cells

We first performed machine learning proteomics analysis on fractions from the three-step purification in MIN6 cells treated with or without palmitate to obtain the ISG proteomes of each condition. All twelve sucrose-washed fractions from each experiment and condition were put through MS-based proteomics analysis. Protein quantification was done by label-free analysis in the MaxQuant package. Protein-level data was analysed by supervised machine learning and LIMMA using the R packages pRoloc and LIMMA respectively [219, 220, 300]. Protein abundances were normalised using variance stabilisation (VSN) with the vsn package [221, 301] in RStudio. Missing values were not imputed, and proteins with largely missing values were excluded per experiment.

For pRoloc machine learning analysis, we assigned the same 10 proteins named in **Chapter 2**: Zinc transporter 8, ProSAAS, Islet amyloid polypeptide, Secretogranin-2, Secretogranin-3, Insulin-1, Insulin-2, Carboxypeptidase E, Prohormone convertase 2 and Chromogranin-A as ISG marker proteins. 'Marker' proteins were also assigned for non-ISG subcellular compartments using the publicly available *Mus Musculus* library available in pRoloc on RStudio. The 10 proteins listed were added manually as ISG 'marker' proteins. Using the support vector machine learning within pRoloc [219, 220], remaining unmarked protein profiles were then correlated with all 'marker' proteins, generating a spatial proteome for each experimental replicate in control and palmitate treated MIN6 cells (n = 3). ISG proteins identified in each condition within each experimental replicate can be found in **Supplementary Table 7**.

3.3.5 Statistical analysis of individual ISG associated proteins by linear model ANOVAs

To first identify if there were any significant changes in protein abundance of well-established ISG proteins, we fitted a linear model to examine the relationship between individual protein abundance and the factors (treatment, fraction & experiment) using the lm function in Rstudio. The linear model includes an interaction term between treatment and fraction (Treatment*Fraction), that observes whether the effect of palmitate/control on protein abundance of each protein is fraction dependent. Additionally, we include an experimental factor as a co-variate to account for the variability across the experimental replicates. Example of the linear model below used in Rstudio:

lm (Abundance_X~ Treatment * Fraction + Experiment)

Where abundance_X is the abundance of an individual protein. Treatment corresponds to control/palmitate, Fractions 1-12 and Experiments 1-3. The proteins we chose to fit this model were the 10 established ISG-proteins used for pRoloc analysis (Ins1, Ins2, Pcsk1n, CPE, CgA, Iapp, PCSK2, PCSK1, Scg2, Scg3) as well as the novelly described ISG-associated proteins in **Chapter 2** (Scamp3, Stx7, Syp, and Syt13). An ANOVA was then performed on the linear model to assess the statistical significance of each factor on the 14 proteins listed. ANOVA summary statistics for each protein can be found in **Supplementary Table 8**. As expected, across all 14 proteins tested, fraction factors were statistically significant, which simply implies each protein had a distinct distribution pattern across 12 fractions (i.e. each protein was not uniformly distributed). Interestingly however, in only 8 of 14 proteins did treatment have a significant effect on the abundance (**Supplementary Table 8**): Ins1, Ins2, Pcsk1n, CPE, Scg2, Syp, Syt13 & ZnT8). This implies an increased, selective sensitivity of these proteins to the

effects of palmitate. We then looked at the coefficient values of the linear model, which showed that palmitate had a negative effect on these 8 proteins, which indicates a down-regulation of abundance (**Supplementary Table 8**). These results coincide with *in vitro* models of elevated FFA treatment, showing that ISG proteins may be negatively regulated by FFA [172, 282, 289, 293, 302]. Lastly, in all proteins except Ins1, there was no interaction between the treatment and fraction, suggesting that these two factors are acting independently on the abundance in all proteins except Ins1. Additionally, coefficients of the linear model for Ins1 show a significant interaction between palmitate treatment only in fractions 11-12 (Palmitate: Fraction11, $\mathbf{p < 0.0163}$ & Palmitate: Fraction11, $\mathbf{p < 0.007}$), which often correspond to the fractions most enriched in ISGs.

3.3.6 Targeted analysis on the compositional changes to the ISG in response to palmitate treatment

To explore potential changes in the ISG proteome in response to elevated FFA levels, we compared the ISG proteomes of control and palmitate-treated MIN6 cells across three experimental replicates. This comparison enabled us to compile a list of proteins that were unique to each condition in each experimental replicate, highlighting the differences in ISG protein presence or absence between the two conditions (**Supplementary Table 7**). Most notably, subsequent STRING and GO enrichment analysis identified key biological processes with proteins unique to control cells (**Figure 23**), that include proteins involved in vesicle docking, vesicle exocytosis and V-type ATPase complex assembly as well as the regulation of the constitutive secretory pathway. In contrast, analysis of proteins unique to palmitate-treated cells (**Figure 24**) revealed proteins involved in phagolysosome assembly, ER membrane organisation and most interestingly mirroring the control condition, SNARE complex disassembly.

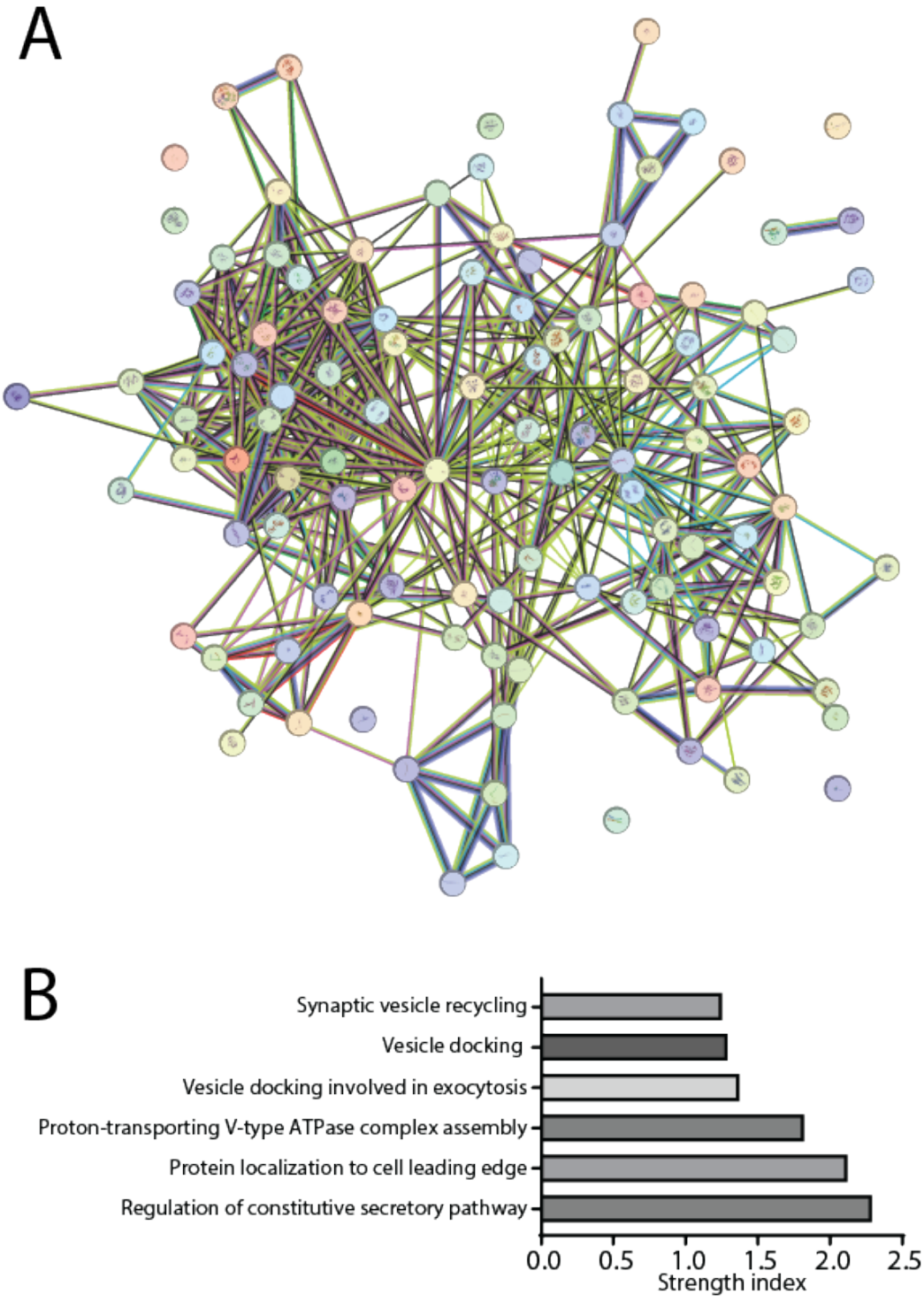

Figure 23: **String and GO enrichment analysis of proteins unique to control ISGs** (A) String analysis of ISG proteins unique to control (n = 3) compared to palmitate-treated cells (n

= 3), generated from the string database [303]. (B) Gene ontology enrichment analysis of proteins listed in A with biological process strength indices.

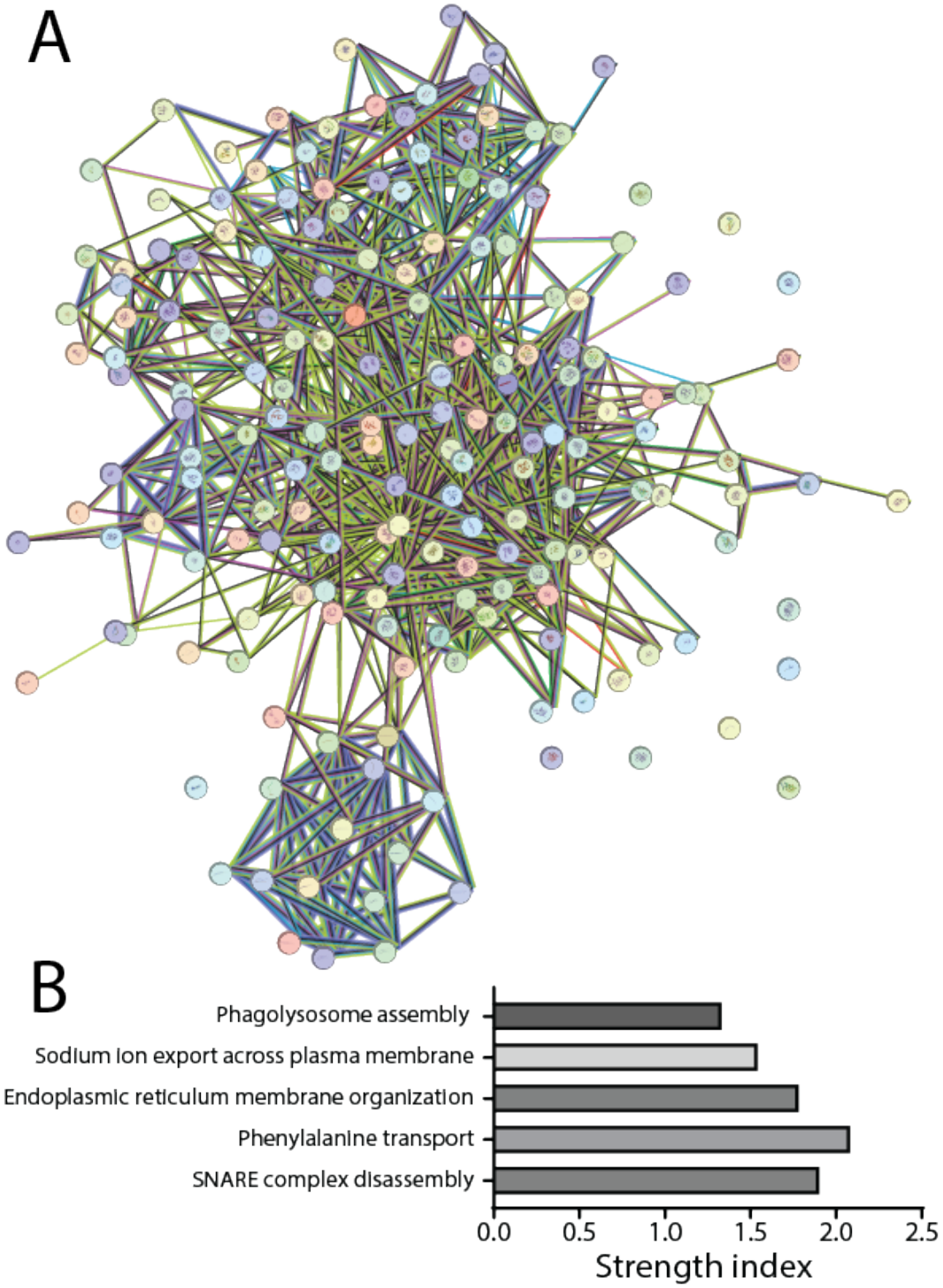

Figure 24: **String and GO enrichment analysis of proteins unique to ISGs isolated from palmitate treated cells.** (**A**) String analysis of ISG proteins unique to palmitate-treated cells

(n = 3) compared to control (n = 3), generated from the string database [303]. (**B**) Gene ontology enrichment analysis of proteins listed in A with biological process strength indices.

3.3.7 General proteomics analysis of ISG enrichment by Percoll

We further investigated the expression of all proteins between control and palmitate-treated cells from Percoll fractionation. Overall, a total of 604 proteins were identified as significantly up- or downregulated in response to palmitate (**Figure 25A**) (Full protein list available in **Supplementary Table 9**). Isolating the top 100 differentially expressed proteins (**Figure 25B, Supplementary Table 10**), canonical ISG proteins Vamp2 and Rab3a were significantly reduced in response to palmitate. Rho GTPase activating protein 17 (Arhgap17) is a cytosolic protein that may be involved in the exocytosis of ISGs in beta-cells that was also downregulated in response to palmitate. Another protein, Syntaxin binding protein 2 (Stxbp2, also known as Munc-18-2) is a SNARE complex protein shown to coordinate insulin exocytosis by modulating Ca^{2+} sensitivity [304]. Another SNARE complex protein, VTI1A, which interacts with Vamp4 (a canonical ISG protein) also showed a significant reduction in expression in palmitate conditions. Of the 604 proteins identified, only 96 proteins were significantly upregulated in response to palmitate (**Supplementary Table 9**). Rab32 was among these highlighted, as it is involved in lysosomal mTOR trafficking in HeLa cells [305], and may have a similar role in beta-cells. Principal-components analysis, however, showed clustering between fractions of both conditions, with a distinct shift from one another (**Figure 25C**). Subsequent GO enrichment analysis on the 604 proteins revealed a high strength index of proteins involved in vesicle trafficking to the PM, exocytic processes, vesicle tethering, vesicle docking, membrane docking and lysosome localisation (**Figure 25D**).

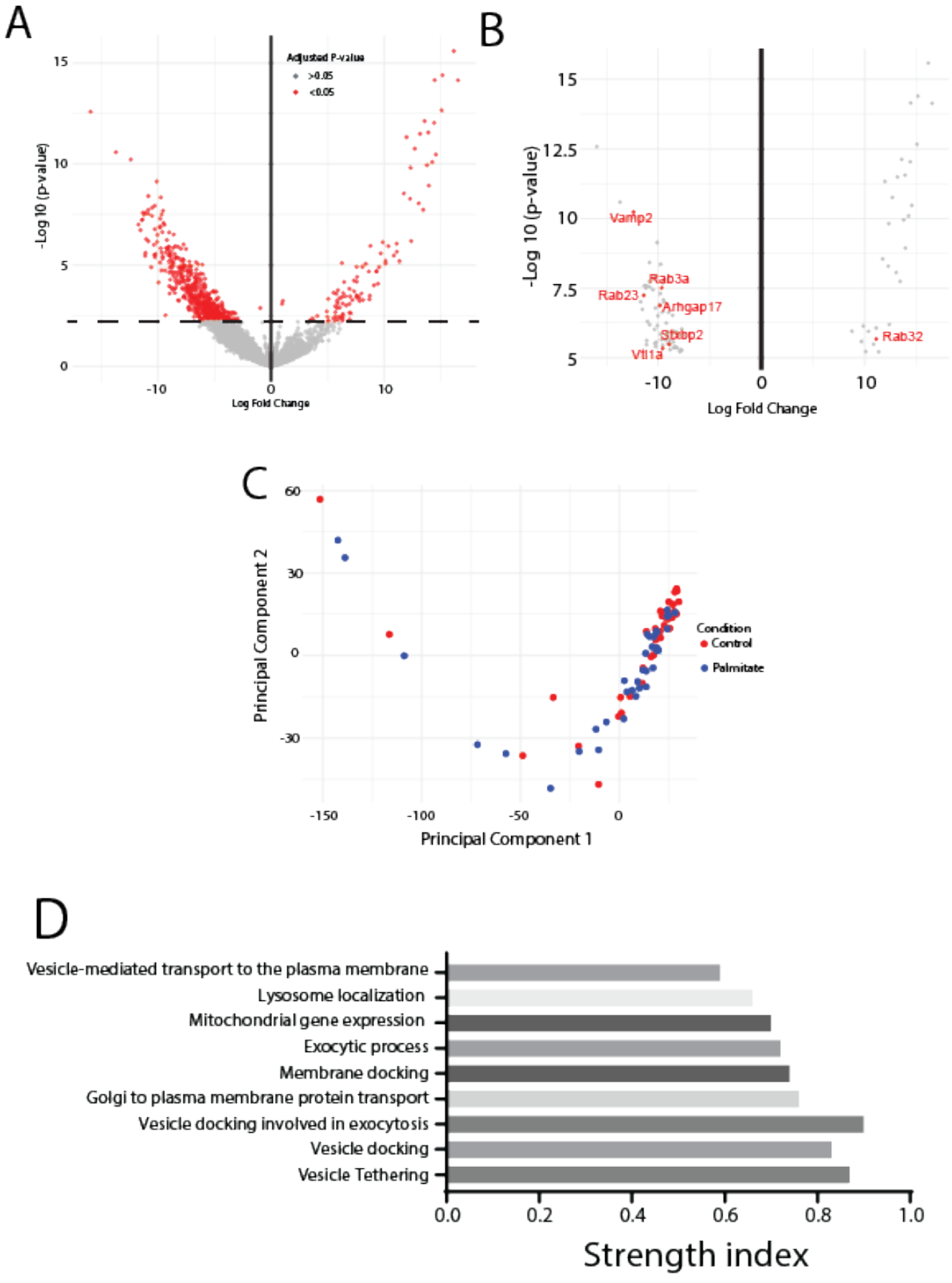
A
Adjusted P-value
>0.05
<0.05
-Log 10 (p-value)
Log Fold Change
B
-Log 10 (p-value)
Vamp2
Rab3a
Rab23
Arhgap17
Stxbp2
Vti1a
Rab32
Log Fold Change
C
Principal Component 2
Principal Component 1
Condition
Control
Palmitate
D
Vesicle-mediated transport to the plasma membrane
Lysosome localization
Mitochondrial gene expression
Exocytic process
Membrane docking
Golgi to plasma membrane protein transport
Vesicle docking involved in exocytosis
Vesicle docking
Vesicle Tethering
Strength index

Figure 25: **Differential protein expression with palmitate treatment**. Volcano plot displaying differential protein expressions across all 12 fractions in three experimental replicates in 48 hour palmitate-treated compared to control MIN6 cells of (**A**) all proteins and (**B**) top 100 up- or down-regulated proteins. Specific proteins of interest highlighted in red. (**C**) PCA plot showing distribution on first two principal components, each point represents a single fraction from each condition, control in red and palmitate in blue. (**D**) Gene ontology (GO) enrichment analysis on the biological processes of all up- and down-regulated proteins, generated from the STRING database [303] (**604 proteins**).

3.4 Discussion

While previous studies have explored the effects of FFAs on pancreatic beta-cells, they often focus on metabolic outcomes such as insulin secretion, apoptosis and metabolic stress responses [172, 279, 280, 282, 289, 291, 302] without considering the impact on the composition of the insulin-containing vesicles. This chapter adds a novel facet by investigating the effects of palmitate treatment on the protein expression within ISGs, which may provide insights into the mechanisms that underpin beta-cell dysfunction in metabolic disorders.

3.4.1 Physical ISG properties

We first assessed the effects of chronic palmitate exposure to identify a treatment duration that would effectively induce reduced GSIS in MIN6 beta-cells. We validate that the chronic exposure (48 hours) with palmitate was sufficient for inducing typical changes in GSIS reduction in response to elevated FFAs (**Figure 19**). However, no significant changes were observed in GSIS from a 24 hour chronic treatment with palmitate. We utilised the methods optimised in **Chapter 2** to isolate and purify mISGs from MIN6 cells treated with or without 48 hours of palmitate. Through insulin ELISA, we validate the enrichment of mature insulin in the later fractions of Optiprep (**Figure 20**). By Western blot analysis on Optiprep fractionation, we demonstrate the distribution of both immature and mature ISGs which remained consistent between the control and palmitate treated conditions, suggesting that the ISG density itself may not be altered (**Figure 21 & Figure 22**). This may be explained by the decoupling of proinsulin synthesis and ISG degradation, as studies have shown that granule numbers are unchanged despite alterations in ISG protein mRNA levels [290, 306, 307], suggesting that the overall ISG structure is maintained in elevated FFA conditions. Interestingly, there was a small increase in the overall insulin/protein concentration levels in palmitate compared to control cells,

potentially indicating an accumulation of ISGs due to the impaired ISG exocytosis, exacerbated by the dysregulated autophagy that is often observed in response to chronic FFA exposure.

3.4.2 Proteomics analysis of ISGs in response to palmitate

ANOVA results interestingly showed a subset of ISG proteins that had significant reduction in protein abundance (Ins1, Ins2, Pcsk1n, CPE, Scg2, Syp, Syt13 and ZnT8). These proteins are involved in key ISG processes, insulin biosynthesis (Ins1, Ins2), ISG maturation (CPE, Pcsk1n, ZnT8) and potentially vesicular trafficking and exocytosis (Syt13, Syp), which coincide with previous studies showing elevation of FFAs directly affect proteins related to ISG function [179, 308, 309]. These results show that the density or overall physical properties of the ISG are unchanged, but the proteins expressed within them may be downregulated.

ISG density is primarily driven by Zn^{2+} crystallisation with insulin [310], thus, no observable changes in density are unsurprising. We then investigated potential protein-level changes of the ISG, using the targeted machine learning approach outlined in **Chapter 2**. We first obtained ISG proteomes of control and palmitate treated MIN6 cells and using GO enrichment analysis by DAVID [303], we isolated proteins unique to each condition in each experiment, identifying a potential destabilisation of the insulin granule docking machinery at the PM in response to palmitate (**Figure 23 & Figure 24**). In particular, the proteins Napa (also known as Snap-α) and Nsf (N-ethylmaleimide-sensitive factor) were identified in palmitate treated ISG proteomes. Snap-α is an adaptor protein that helps Nsf bind to SNARE complexes that leads to the stimulation of Nsf ATP-ase activity and the disassembly of SNARE complexes [311]. The presence of Rab7, a small GTPase involved in lysosomal trafficking in beta-cells [312] may also indicate the accumulation of ISGs within the phagolysosomes. In striking contrast, control ISGs almost mirrored the result of palmitate conditions and GO enrichment showed proteins involved in vesicle trafficking, docking, and exocytosis, including canonical

ISG proteins Vamp2, Rab3a and Stxbp1 (Munc-18-1), all of which contribute to insulin granule secretory dynamics [118, 155, 313, 314].

We then further investigated the global expression of all proteins identified by LC-MS/MS in twelve sucrose-washed fractions, identifying 604 proteins that were significantly up- or downregulated in response to palmitate (**Figure 25**, **Supplementary Table 9**). The downregulation of the canonical ISG proteins Vamp2 and Rab3a present in the top 100 proteins further bolsters the ISG proteome differences, indicating that elevated FFAs can disrupt the insulin secretion pathways, potentially impairing SNARE complexes and vesicle trafficking. The presence of other syntaxin binding proteins Munc-18-2 further suggests a potential alteration in the regulation of exocytosis, while the upregulation of Rab32 may hint to the beta-cell's compensatory mechanism to degrade ISGs in response to the elevated FFAs. VTI1A is a q-SNARE protein shown to interact with Vamp4, a v-SNARE protein involved in targeting ISGs to the lysosome, and its downregulation may suggest mistargeting of ISGs to lysosomal degradation.

Through the addition of GO enrichment analyses, a significant involvement of proteins related to vesicle trafficking, docking and exocytosis and lysosomal localisation were identified. Taken altogether, these results provide first evidence of ISG compositional changes in response to chronic FFA exposure, which affects molecular mechanisms critical for insulin granule trafficking and release, potentially contributing to the impairment observed in insulin secretion, as granules lose their docking and fusing capabilities.

FFA exposure has been established to contribute to beta-cell dysfunction, impairing insulin secretion and promoting apoptosis through increased oxidative stress, mitochondrial dysfunction and inflammatory signaling [189, 274, 279]. **Chapter 3** provides additional context to the known effects of FFAs on beta-cell function. Specifically, FFAs can disrupt the

proteins involved in ISG formation, trafficking and exocytosis which may contribute to the diminished ability for beta-cells to release insulin in response to glucose [279, 280, 289, 293]. For example, ISGs have been shown to contain fatty acid translocases that have been shown to affect uptake of FFAs and directly modulate insulin secretion [315]. Therefore, changes in ISG proteins such as FA translocases may directly impair secretory capacity of individual ISGs and contribute to diminished GSIS.

Previous studies have focused primarily on the functional effects of FFAs on beta-cell function without considering ISG composition that may directly influence signaling within the beta-cell. Alterations to the ISG proteome provide an additional layer of complexity that complements the well-established mechanisms of FFA-induced beta-cell dysfunction. While these changes are likely interconnected with other cellular responses (oxidative stress, apoptosis), the disruption of ISG proteins offers a unique insight into how FFAs directly affect secretion machinery, contributing independently to beta-cell dysfunction. Though, these changes may also contribute synergistically with other known stress responses. Whether these protein-level changes are outcomes or triggers for metabolic stress responses, however, remains unknown.

3.4.3 Limitations and future directions

This study presents some limitations that should be acknowledged. Firstly, the half-life of insulin is ~3 - 5 days [316, 317], thus, while 48 hour palmitate treatment durations may elicit effects on GSIS in MIN6 cells, it may not necessarily fully capture turnover, so proteome differences may not be comprehensive. Subcellular fractionation methods may introduce variability between experiments and, in an ideal scenario, a larger sample size to perform intraclass correlation analysis (as outlined in **Chapter 2**) would be useful in bolstering the evidence presented. Lastly, FFA treatments in this regard present a potential paradox: while ISGs are diminished in beta-cells exposed to palmitate, indicating a reduction in turnover, these

ISGs may also be sequestered within phagolysosomes [312]. This ISG entrapment and granule turnover changes may affect the potential for granule populations to change over the 48 hour period. Future studies should aim to characterise changes in the ISG proteome through other methods to further strengthen this study, potentially through *ex vivo* analysis of pancreatic beta-cells after a high-fat diet.

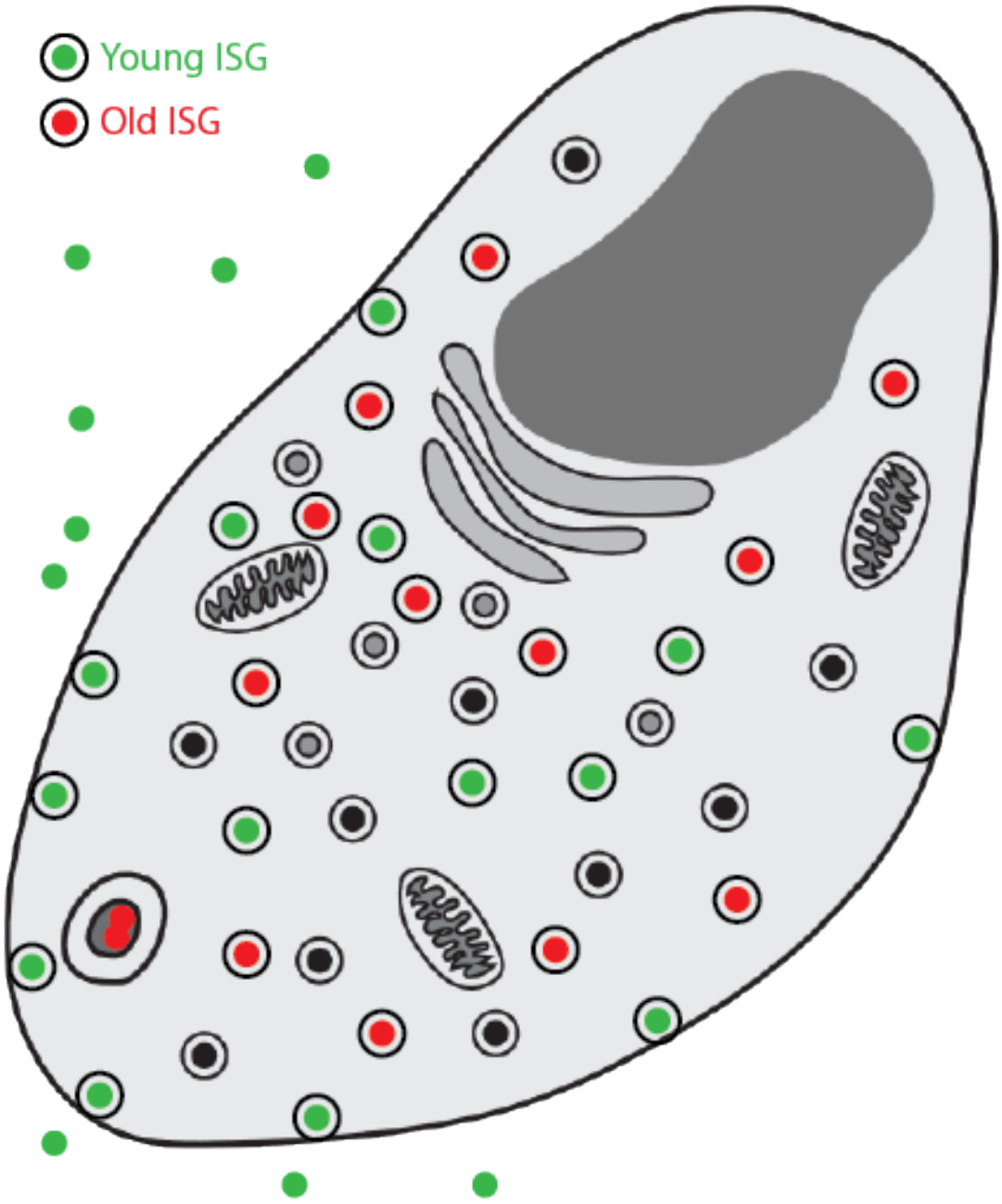

Chapter 4

Characterising the preferential release of young insulin secretory granules

4.1 Introduction

4.1.1 Insulin granule life cycle

The life cycle of an ISG in pancreatic beta-cells are well studied, involving the key stages outlined in **Chapter 1**, including: (1) biogenesis and formation, where the hormone and other ISG proteins are first synthesised and packaged into immature ISGs in the cytoplasm, (2) maturation, which involves processing enzymes and membrane bound transporters, (3) storage, in which mature granules are then stored within the cytoplasm, forming their spatiotemporally distinct populations within the cell, (4) exocytosis, in which ISGs undergo exocytosis upon stimulation and (5) recycling and degradation, the disposal of non-secreted ISGs or recycling of ISG granule membranes post-exocytosis. Furthermore, the facet of ISG age has added further complexity to understanding ISG storage, exocytosis, and degradation in pancreatic beta-cells.

4.1.2 Labelling ISGs to determine age

Many groups have explored the use of different labelling techniques to visualise age-distinct populations of ISGs [63, 64, 68, 82, 180]. A pivotal study by Duncan et al. use a fluorescent timer protein dsRED-E5 [67] conjugated to a secretory vesicle cargo protein, ANF (Atrial natriuretic peptide) in bovine adrenal chromaffin cells. This allowed the identification of secretory granules that were functionally and spatially segregated in these cells [65], and found that younger granules were preferentially secreted upon stimulation. dsRED-E5 is an interesting timer protein; a mutant of dsRED with staggered folding mechanics, resulting in a protein with emission spectra that change as the protein fully matures [67]. When first synthesised, this protein emits a green spectrum (~500 nm), and over the span of ~18 hours dsRED-E5 when fully mature emits a red spectrum (~560-580 nm). The use of these fluorophore-conjugated proteins has since been used to label insulin containing SGs within the

pancreatic beta-cells, however, targeting it specifically to ISGs was initially challenging. Hays et al. explored the use of Syncollin, a 13 kDa soluble protein expressed in the pancreatic exocrine tissue that is packaged into vesicles for exocytosis [181]. Pancreatic beta-cells do not express syncollin, however, when syncollin and a syncollin-GFP chimera were transduced into beta-cells with an adenovirus, it was shown to be targeted and sorted into ISGs [181]. Interestingly, syncollin expressing beta-cells had dysfunctional insulin secretion, however syncollin-GFP expressing beta-cells maintained normal GSIS [181].

The development of dsREDE5 and the discovery of syncollin-fluorophore chimera ISG localisation, were then used in tandem to develop a protein construct, syncollin-dsREDE5, which was capable of labelling ISGs with a timer protein. Syncollin-dsREDE5 has since been used to examine and distinguish distinct ISG pools based on the age of the granules [68, 97]. Identical to dsREDE5 alone, syncollin-dsREDE5 fluoresces green when first synthesised, and around ~18 hours of maturation begin to fluoresce red. ISGs under confocal microscopy primarily fluorescing green are considered young (~8 hours), while those around ~24 hours are considered aged/old ISGs. Granules with overlapping emission spectra appear yellow/orange and are considered middle-aged ISGs. The age range of insulin granules can vary depending on labelling techniques used, but generally, young granules are between 1 to 6-8 hours old, while older granules are typically those older than 16-18 hours [63, 64, 68, 82].

This construct has now been used to characterise young and old ISGs [83]. Firstly, younger granules were seen to be spatially segregated from older granules in multiple beta-cell models. Young granules localised closer to the PM, in contrast to older granules localised further within the perinuclear regions. Furthermore, upon glucose stimulation, younger granules displayed increased motility compared to older granules and were preferentially released. This study utilised the pancreatic islets isolated from diabetic (db/db) mice, a mouse strain with a mutation in the leptin receptor that results in leptin deficiency and the development

of diabetes. Islets transfected with the syncollin-dsREDE5 construct had a distinct increase in the ratio of older granules secreted compared to healthy mouse islets in response to glucose, indicating a potential loss of preferential young ISG release in a disease state.

Initially, young ISGs exhibit their maximal exocytic potential and as they age move from the readily releasable pool of ISGs to a reserve pool of granules [82, 172]. There is a clear link between the age of mature granules and their potential for secretion or degradation. This suggests that aging may affect the physical and/or functional properties of granules as they age, consequently changing their insulin secretion efficacy. Understanding these changes has been at the crux of this field, as isolating distinct populations of granules to investigate changes because of aging remains technically difficult. A very recent study, however, has employed the use of fluorescently labelled ISGs using a canonical ISG protein (phogrin) tagged to a cleavable CLIP protein [64]. Lipid compositions were shown to change over time, with older granules exhibiting higher membrane fluidity compared to younger granules. Proteomics analysis further identified a positive association of Rab3a and kinesin-1 heavy chain (KIF5b) with the younger granules, postulating that changes in the association of these proteins during ISG aging negatively impacts granule exocytic properties [64]. In addition, ISG proteins such as GTPases or SNARE proteins have been shown to be modulated by post-translational modifications (PTMs) that affect insulin secretion [318, 319]. Taken together, older ISGs may accumulate PTMs or have partially degraded ISG proteins that impact the bioactivity of insulin within these ISGs and reduce their secretion capacity. Difficulty in ISG age-discrimination and isolation is due to the heterogeneity of ISGs both younger and older as they remain similar in appearance, size and densities. Furthermore, ISG isolation as covered in Chapter 1 without age discrimination is already difficult, though the implementation of our improved methods covered in **Chapter 2**, **2A** and **3** in tandem with fluorescent labelling is an attractive strategy,

though, scaling these techniques to obtain adequate material for downstream omics analysis has been a large hurdle to overcome in the ISG biology field.

4.1.3 Insulin granule populations in the context of disease

The interplay between peripheral insulin resistance and beta-cell dysfunction is a well-established pathway leading to the development of T2D. There are clear insulin secretory dysfunctions observed in human diabetic pancreatic beta-cells in response to prolonged hyperglycaemia [320]. First-phase insulin secretion, essential for regulating postprandial glucose levels is notably impaired in T2D [44, 50, 61]. However, the mechanisms that dictate the loss of first-phase secretion remains unknown. Currently, it is unclear how populations of insulin granules are altered throughout T2D progression. One study hints at a shift in granule populations to older ISGs under diabetic conditions [232].

The development of T2D has been associated with the dysfunction of autophagy in pancreatic beta-cells, resulting in an increase in the degradation of cellular content [321, 322]. ISG aging is tightly linked to degradation in beta-cells, with aged granules targeted for lysosomal degradation [82]. Thus, ISG aging shifts in disease may potentially accelerate ISG degradation, or delay ISG maturation that may explain the increase in immature insulin secretion observed in T2D [323]. In direct contrast, dysfunction of aged ISGs targeted for degradation may result in ISG accumulation that leads to the impairment of newly synthesised ISGs. Furthermore, anti-diabetic drugs do not consider these functionally distinct populations. Thus, this warrants investigation to understand the process of preferential ISG release in beta-cells and whether anti-diabetic treatments in fact mimic healthy secretion patterns.

4.1.4 Management of Type 2 Diabetes with insulin secretagogues

Individuals with pre-diabetes or early stages T2D will often be prescribed lifestyle changes that include dietary and/or physical activity interventions to manage disease and

improve glycaemic control [324], often reducing the need or reliance on glucose-lowering medications [325]. However, those in later stages of T2D disease development often require the use of pharmacological medicines to maintain glycaemic control [324]. There exist a wide range of drug classes used to treat T2D [326] that act on different tissues to maintain euglycaemia. These may be prescribed individually, or in a combination with others. This chapter (**Chapter 4**) focuses on the use of anti-diabetic drugs that directly target the pancreatic beta-cells to stimulate insulin secretion, which include: 1) sulfonylureas, 2) meglitinides, 3) dipeptidyl peptidase IV (DPP-4) inhibitors and 4) glucagon like peptide 1 (GLP-1) receptor agonists. Sulfonylureas (e.g. tolbutamide and glibenclamide) are a class of first and second-generation anti-diabetic drugs that act on the ATP-sensitive K^+ channels (K_{ATP} channel), closing them to stimulate insulin secretion from beta-cells [327] (**Figure 26**). Meglitinides are structurally distinct drugs from sulfonylureas but work similarly by binding to and closing K_{ATP} channels, stimulating the release of insulin from beta-cells [328] (**Figure 26**).

Besides GSIS (**Figure 26**), insulin secretion can be stimulated through the GLP-1 receptor in beta-cells. GLP-1 is a type of incretin hormone, recognised by GLP-1 receptors on the beta-cell PM, and through signal cascades ultimately leads to the increase in cellular cAMP, consequently increasing insulin secretion from beta-cells [329] (**Figure 26**). DPP-4 is an enzyme that works to catalyse and degrade incretins (GLP-1 and GIP) [330]. Therefore, GLP-1 receptor agonists (e.g. Exendin-4) work to stimulate beta-cells to secrete insulin (**Figure 26**) [331], while DPP-4 inhibitors (e.g. Vildagliptin) are used to inhibit the degradation of GLP-1, therefore increasing GLP-1R binding and sustained insulin secretion from pancreatic beta-cells [332].

4.1.5 Aims and hypotheses

In this chapter, we aim to investigate the preferential release of young ISGs in pancreatic beta-cells and if this preference is maintained in response to different insulin

secretagogues. We also aim to investigate potential functional differences in aging granules. Furthermore, we aim to evaluate the efficacy (bioactivity) of insulin by stimulating glucose uptake in 3T3-L1 adipocytes using insulin extracted from young or old ISGs.

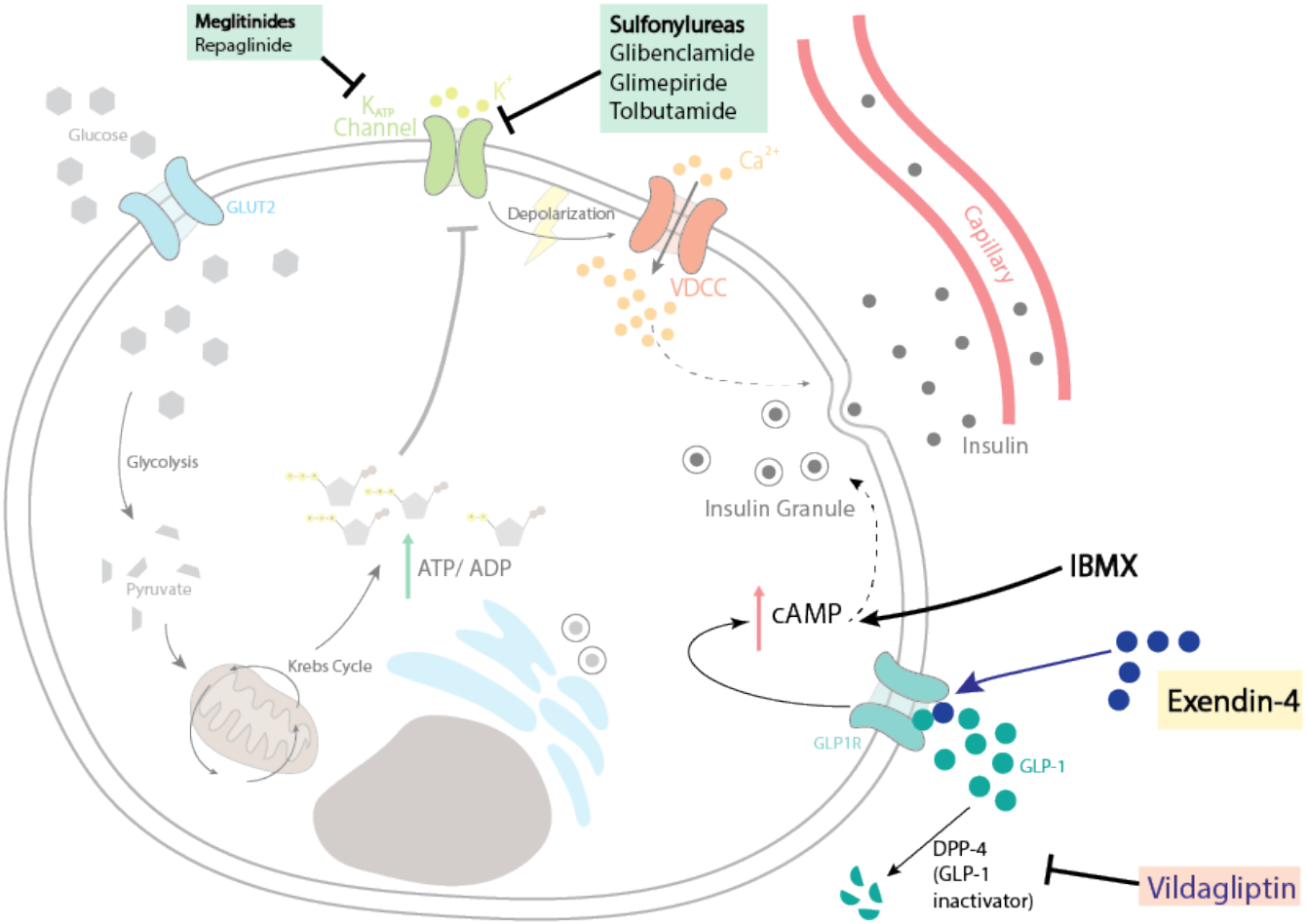

Figure 26: **Mechanism of action of anti-diabetic drugs and insulinotropic secretagogues in pancreatic beta-cells**. Sulfonylureas and Meglitinides bind to different sites on the sulfonylurea receptor (SUR1), a subunit of K_{ATP} channels. 3-Isobutyl-1-methylxanthine (IBMX) is a phosphodiesterase (PDE) inhibitor, an enzyme that is responsible for catalysing the breakdown of cAMP to cGMP, thus increasing intracellular cAMP levels, activating PKA further stimulating insulin secretion. Exendin-4, a GLP-1 receptor agonist, activating adenylate

cyclase, increasing intracellular cAMP levels. Vildagliptin is a dipeptidyl peptidase-4 (DPP-4) inhibitor, an enzyme responsible for breaking down GLP-1, thus maintaining elevated GLP-1 levels extracellularly.

4.2 Materials and Methods

4.2.1 MIN6 cell culture

MIN6 insulinoma cell lines were obtained from AddexBio™, cultured in complete 25 mM glucose DMEM (Gibco™) supplemented with 10 % FBS (Gibco™), 4 mM L-glutamine, 1 mM sodium pyruvate, 44 mM NaHCO3 and 0.005 % 2-beta-mercaptoethanol and 1 % penicillin-streptomycin. Cultures were passaged with TrypLE express enzyme (Gibco™) at 37 °C for 3 – 5 minutes upon reaching ~80 % confluence. Culture media changed every 2 – 3 days, passages used for MIN6 cells in **Chapter 4** were 4 – 25. All cultures were tested mycoplasma negative.

4.2.2 Human pancreatic islets

Human islets used in this chapter were sourced from the Westmead Islet Transplant Program. Human islet research approval was obtained from the University of Sydney Human Research Ethics Committees (Approval 2022/HE000137). Human pancreata were obtained from heart-beating, brain-dead donors, with informed consent from the next of kin. Human islets were isolated through intraductal perfusion and pancreatic digestion using collagenase and purified via Ficoll density gradients. The purified islets were cultured in Connaught Medical Research Laboratories (CMRL) 1066 medium (Invitrogen), which was supplemented with 4 % human serum albumin, 2 mM L-glutamine and 100 units/mL penicillin, 100 µg/mL streptomycin. Cultures were maintained at standard conditions (37 °C, 5 % CO_2). For transduction with Adsyncollin-dsREDE5, human islets were dispersed using TrypLE express enzyme (Gibco™) for 3 minutes and seeded onto glass coverslips in 24-well plates with 11

mM glucose RPMI supplemented with 100 units/mL penicillin and 100 µg/mL streptomycin containing 10 % FBS.

4.2.3 Adenoviral construct

Syncollin-dsREDE5 construct was amplified and characterised by ViraQuest, Inc. (Iowa, USA). MIN6 cells were infected with Adsyncollin-dsREDE5 (Adsync) at multiplicity of infection (MOI) of 100 in complete DMEM. Dispersed human islets were infected at 100 MOI in RPMI supplemented with 100 units/mL penicillin and 100 µg/mL streptomycin containing 10 % FBS. 24 hours post Adsync addition, cells and dispersed islets were washed thrice with fresh DMEM and RPMI respectively, incubated at 37 °C with 5 % CO_2.

4.2.4 Glucose stimulated insulin secretion (GSIS) assay

For the characterisation of insulin secretion from Adsync-transduced MIN6 cells: MIN6 cells were seeded in 6 – well plates in complete DMEM in standard culture conditions (37 °C at 5 % CO_2). 18 hours prior to GSIS assay, media was replaced with 5.5 mM glucose complete DMEM. Cells were put in pre-basal 2.8 mM glucose Krebs Buffer (KRBH) for 1 hour prior to the assay. KRBH was replaced with fresh 2.8 mM glucose KRBH for an additional hour, and then in stimulation KRBH mediums: (1) Low glucose KRBH (2.8 mM glucose), (2) High glucose (16.7 mM) KRBH, (3) Tolbutamide 100 µM in low glucose KRBH and (4) High glucose KRBH with 0.5 mM palmitate-BSA complexed as described in **Chapter 3**. Supernatant from basal and stimulation KRBH was then collected after each hour, spun down at 300 x g for 5 minutes to pellet aspirated cells or debris. Insulin concentrations from supernatants were quantified by insulin HTRF (Cisbio, #62IN2PEH).

MIN6 cells for immunofluorescent imaging: MIN6 cells were seeded onto coverslips in 6 - well plates. MIN6 cells were put into 5 mM glucose complete DMEM 18 hours prior to GSIS. Cells were then put in low glucose KRBH for 1 hour to pre-basal, followed by an

additional hour in low glucose KRBH. The following stimulation mediums were then used for 20 minutes: (1) Low glucose (2.8 mM) KRBH , (2) High glucose (16.7 mM) KRBH, (3) Tolbutamide 100 µM in Low glucose KRBH, (4) Glibenclamide 10 mM in Low glucose KRBH, (5) Glimepiride 100 nM in Low glucose KRBH, (6) 80 nM Exendin-4 (7) 50 nM Repaglinide (8) 0.5 mM palmitate-BSA in high glucose KRBH (9) Stimulatory cocktail (CT) containing 25 mM glucose, 1 mM IBMX, 40 mM KCl, 10 µM tolbutamide in KRBH. Concentrations were determined by dose-curve assays for the use of anti-diabetic drugs. Supernatant was collected after 20 minutes (to observe first-phase GSIS) and then fixed with 4 % PFA immediately after for 20 minutes at RT. Coverslips were washed thrice with IF wash buffer, mounted onto glass microscope slides for confocal imaging using ProLong Antifade Diamond with DAPI mountant (P36962) and cured overnight. Secreted insulin was analysed by HTRF assay (Cisbio, #62IN2PEH).

Dispersed human islets seeded onto coverslips on 24-well plates, 72 hours post transduction with Adsync, were placed in pre-basal KRBH for 1 hour. After the hour, KRBH was discarded and replaced with fresh 2.8 mM glucose KRBH for 1 hour. Dispersed islets were then stimulated with low glucose KRBH, high glucose KRBH, 100 µM tolbutamide in low glucose KRBH or the stimulatory cocktail for 20 minutes. Coverslips were then immediately fixed with 4 % PFA for 20 minutes at RT, washed three times and mounted onto glass cover slides for confocal imaging using ProLong Antifade Diamond with DAPI mountant (P36962), cured overnight. Secreted insulin was analysed by HTRF assay (Cisbio, #62IN2PEH).

4.2.5 Augmentation of ISG populations with Brefeldin-A and cocktail stimulation and acid-ethanol extraction of insulin

For confocal imaging, MIN6 cells were cultured onto glass coverslips in 6 – well plates in complete DMEM and standard culture conditions (37 °C and 5 % CO_2). Cells were then

transduced with Adsyncollin-dsREDE5 for 48 hours. Medium was then replaced with either normal complete DMEM for 3 hours (control), complete DMEM supplemented with 10 µg/mL Brefeldin-A (diluted in DMSO) for 3 hours (Bref-A), or a stimulatory cocktail in DMEM (25 mM glucose supplemented with 1mM IBMX, 40 mM KCl and 10 µM tolbutamide, cocktail) for 1 hour. After each condition timing, cells were washed three times with PBS and fixed with 4 % PFA for 20 minutes at RT. Coverslips were then mounted with ProLong Antifade Diamond with DAPI mountant (P36962) and cured overnight before confocal imaging. For augmentation of ISG populations for insulin extraction, MIN6 cells were grown on 10 cm petri dishes until 80 – 90 % confluence. Medium was replaced as the conditions above (Bref-A, cocktail and control). Cells were then washed two times with ice-cold PBS and scraped into 2 mL of PBS. This solution was then centrifuged at 500 x g for 5 minutes to pellet cells. Supernatant was discarded and cells were resuspended in MQ water, sonicated for 15 seconds at 90 % power. Sonicated solutions were then mixed with an acid-ethanol solution (0.18 M HCl in 96 % ethanol (vol/vol)) at a 1:3 ratio of sonicate to acid-ethanol. The mixed acid-ethanol sonicate solution was then incubated at 4 °C overnight to extract insulin, proinsulin and C-peptide. Insulin concentrations were measured by mouse insulin ELISA (Crystal Chem) to prepare insulin stocks for glucose-uptake assays (see section ***4.2.10***).

4.2.6 Immunofluorescence Staining

MIN6 cells were cultured onto glass coverslips in complete DMEM, standard culture conditions. 72 hours post transduction with Adsyncollin-dsREDE5, cells were washed once with PBS, followed by fixation with 4 % PFA (#15710, Electron Microscopy Sciences) for 20 minutes at RT. Cells were then washed three times with IF wash buffer followed by permeabilisation in a solution with 0.1 % SDS for 5 minutes at RT. Coverslips were washed with IF wash buffer three times. Non-specific binding was blocked using DAKO Protein serum-free buffer (#X0909) for 1 hour at RT. Blocked coverslips were then incubated with

primary antibodies (**Table 1**) overnight at 4 °C, diluted in Dako Antibody Diluent (#S0809). Coverslips were then washed five times with IF wash buffer, followed by incubation with secondary antibodies (**Table 1**) for 1 hour at RT. Coverslips were then mounted onto glass microscope slides with ProLong Antifade Diamond with DAPI mountant (P36962) and cured overnight before imaging.

4.2.7 Microscopy

All fixed and mounted slides were imaged using a white light laser, with a 93 X magnification glycerol lens on the Leica LCS SP8 confocal microscope (Wetzlar, Germany). Image acquisition performed using the Leica LAS X software, exported and then subsequently analysed on FIJI ImageJ [217].

4.2.8 Colocalisation and fluorescence intensity analyses

Images obtained from confocal imaging were analysed using JACoP [333] plugin on FIJI software [217]. Thresholds were set on images to remove background before measuring Mander's Overlap Coefficients (MOC) of the channels within each image. For fluorescence intensity measures, images obtained from confocal imaging were again analysed in FIJI software [217]. ROIs were drawn around each beta-cell and measured the mean fluorescence intensity was measured in the young (green) channel and old (red) channel.

4.2.9 3T3-L1 fibroblast culture and adipocyte differentiation

3T3-L1 fibroblasts were from Howard Green (Harvard Medical School) cultured in 25 mM Glucose DMEM (Gibco™) supplemented with 10 % FBS (Gibco™) and 2 mM GlutaMax (Gibco™) (Fibroblast medium) in 10 % CO_2 at 37 °C. Fibroblasts were differentiated as described previously [334, 335]. Briefly, 100 % confluent 3T3-L1 fibroblasts were differentiated using fibroblast medium as above supplemented with 0.22 µM dexamethasone, 2 µg/mL insulin, 100 ng/mL biotin and 500 µM IBMX at Day 0. After 72 hours (Day 3), media

was replaced with fibroblast medium supplemented with 2 µg/mL insulin. A further 72 hours later (Day 6), media was replaced with fresh fibroblast medium and was replaced every 48 hours. Adipocytes used for subsequent glucose-uptake assays were used at Day 10 after the start of differentiation with a ~ 90 % of cells differentiated.

4.2.10 Adipocyte glucose uptake assays

Adipocytes at Day 10 post-differentiation were serum starved for 2 hours using 25 mM glucose DMEM (Gibco™) supplemented with 2 mM GlutaMax (Gibco™) at 10 % CO_2 and 37 °C. Adipocytes were then washed twice with PBS then washed once with KRP buffer (Krebs-ringer 0.2 % BSA, 0.6 mM Na_2PO_4, 0.4 mM NaH_2PO_4, 6 mM KCl, 1 mM $CaCl_2$, 120 mM NaCl, 1.2 mM $MgSO_4$ and 12.5 mM HEPES, pH 7.4) and left for 5 minutes to recover. Cells were then stimulated with 10 nM insulin for 15 minutes with either standard mouse insulin or 10 nM insulin isolated from Bref-A, Control or Cocktail treated MIN6 cells. Non-specific glucose uptake was determined with addition of 25 µM cytochalasin B (Sigma-Aldrich) before the addition of 2-[3H] deoxyglucose (2-DOG) (PerkinElmer/Revvity). After 15 minutes, 2-DOG was added to the adipocytes (0.25 µCi, 50 µM). Adipocytes were washed three times with ice-cold PBS and lysed with Triton X-100 (1 % in PBS). 2-DOG uptake was measured using liquid scintillation counting (PerkinElmer Tri-Carb 2810TR) after diluting lysed supernatant in scintillation fluid (Ultima Gold XR, Revvity) and normalised against protein concentration measured by Pierce Protein BCA (ThermoFisher). Data for each condition was also normalised to the basal control condition.

4.3 Results

4.3.1 Colocalisation of syncollin-dsREDE5 with subcellular compartments of MIN6 cells

To validate the localisation of the syncollin-dsREDE5 construct to ISGs, Adsync transduced MIN6 cells were stained with different markers for compartments within the beta-cell (**Figure 27A**). Colocalisation analysis (**M1** values, young or old with co-stains) showed a strong level of overlap between both young and old fluorescence with insulin (**Figure 27A & B**). Positive markers for ISGs, including Vamp8 and Chromogranin-A (CgA) exhibited high degrees of colocalisation with both young and old vesicles. These results confirm the specificity of syncollin-dsREDE5 to insulin-containing vesicles, as M1 values of young and old granules with insulin, Vamp8 and CgA were significantly higher than those observed with markers for other subcellular compartments. These compartments included the early endosomes (EEA1), endosomes (Rab5A), autophagosomes (LC3A/B), cis-Golgi (GM130), mitochondria (ATP5A) and the nucleus (KDM1/LSD1).

Interestingly, colocalisation analysis of syncollin-dsREDE5 with the lysosomal marker Lamp1 demonstrated overlap with both young and old granules. However, the degree of colocalisation was significantly higher for older granules compared to younger granules (**Figure 27A**).

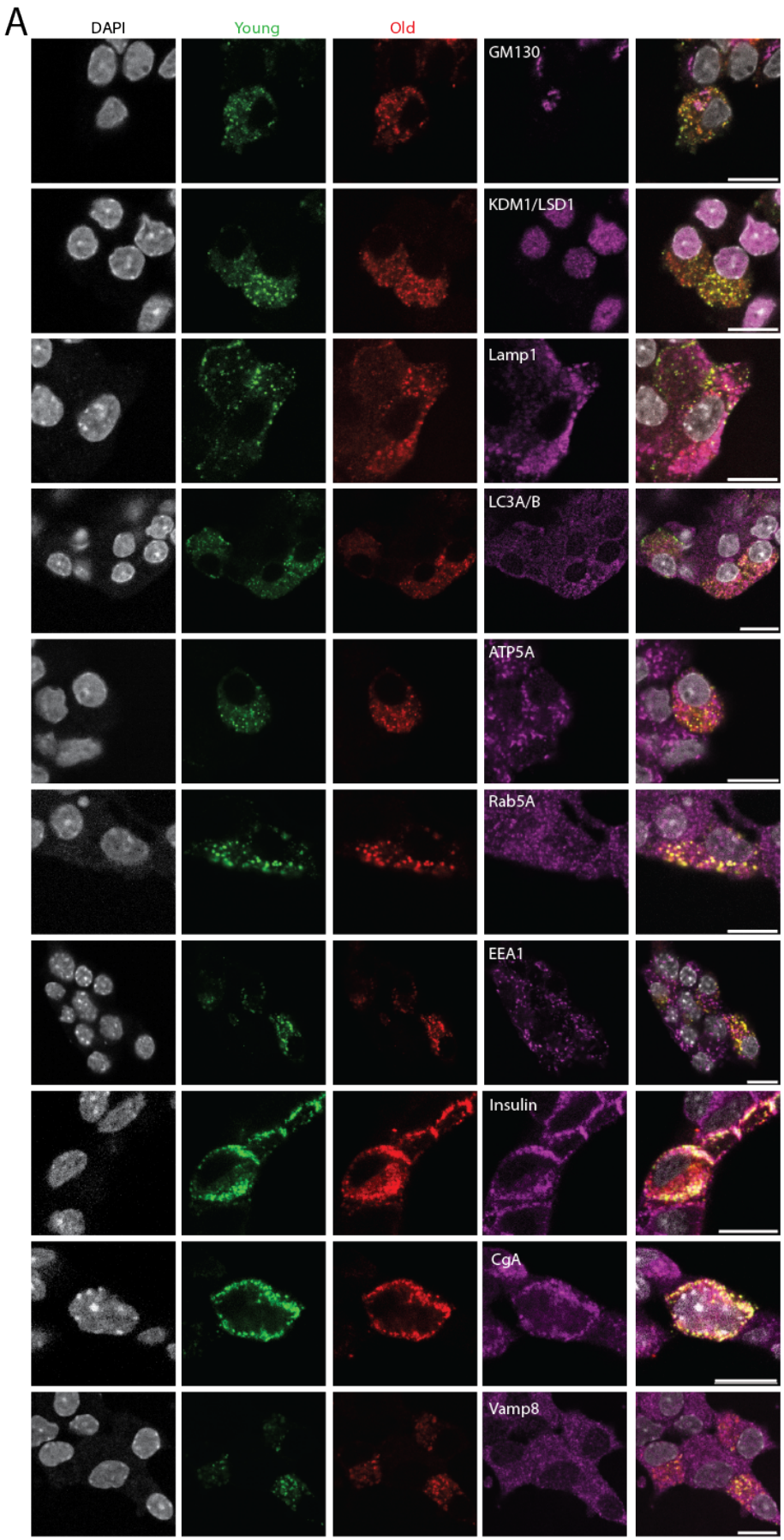
A
DAPI
Young
Old
GM130
KDM1/LSD1
Lamp1
LC3A/B
ATP5A
Rab5A
EEA1
Insulin
CgA
Vamp8

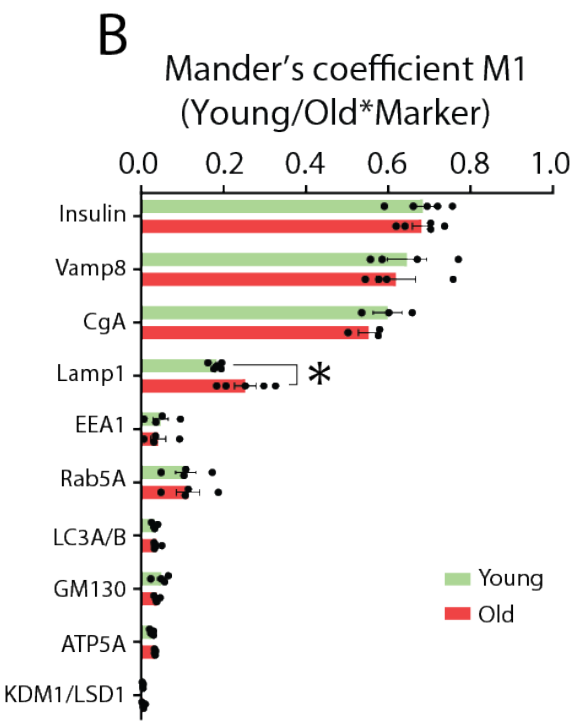
B
Mander's coefficient M1
(Young/Old*Marker)
0.0
0.2
0.4
0.6
0.8
1.0
Insulin
Vamp8
CgA
Lamp1
EEA1
Rab5A
LC3A/B
GM130
ATP5A
KDM1/LSD1
*
Young
Old

Figure 27: **Localisation analysis of syncollin-dsREDE5 with markers of subcellular localisations in MIN6 cells.** MIN6 cells were transduced with Adsync for 72 hours, fixed and stained with anti-GM130 (cis-golgi) (n = 4), anti-KDM1/LSD1 (nucleus) (n = 4), anti-Lamp1 (lysosomes) (n = 5), anti-LC3A/B (autophagosomes) (n = 4), anti-ATP5A (mitochondria) (n = 4), anti-Rab5A (endosomes) (n = 4), anti-EEA1 (early endosomes) (n = 4), anti-insulin (n = 5) and anti-chromogranin-A (ISGs) (n = 3). * $p < 0.05$. Error bars represent ± S.E.M. Scale bars represent 10 μM. *Two-way ANOVA*, *Sidak's multiple comparisons*.

4.3.2 Characterisation of insulin secretion from Adsync-transduced MIN6 beta-cells

Syncollin-dsREDE5 has been previously shown to be compatible with beta-cell function, with 48 hour Adsync-transduced MIN6 cells secreting syncollin, PCSK2, and insulin upon stimulation with 16.7 mM glucose, compared to non-transduced controls [68]. The aim of this chapter was to characterise the preferential secretion of insulin granules in response to different insulin secretagogues. To begin, we characterised the insulin secretion responses of Adsync-transduced MIN6 cells under various stimulation conditions.

72 hour post transduction, MIN6 cells were challenged with low glucose (2.8 mM), high glucose (16.7 mM), tolbutamide (100 µM) in low glucose, palmitate (0.5 µM) in high glucose and KCl (40mM) in low glucose (**Figure 28A & B**). As expected, Adsync-transduced MIN6 cells had a significant increase in insulin secretion in response to elevated glucose levels alone (**Figure 28A**), with a doubling of the fold-change of basal to stimulated insulin secretion (**Figure 28B**). Additionally, in response to common insulin secretagogues such as tolbutamide and KCl, which depolarise the PM even in low glucose conditions, similar secretory responses were observed (**Figure 28A & B**). Finally, GSIS at 16.7 mM glucose could be further augmented with the introduction of palmitate (**Figure 28A & B**).

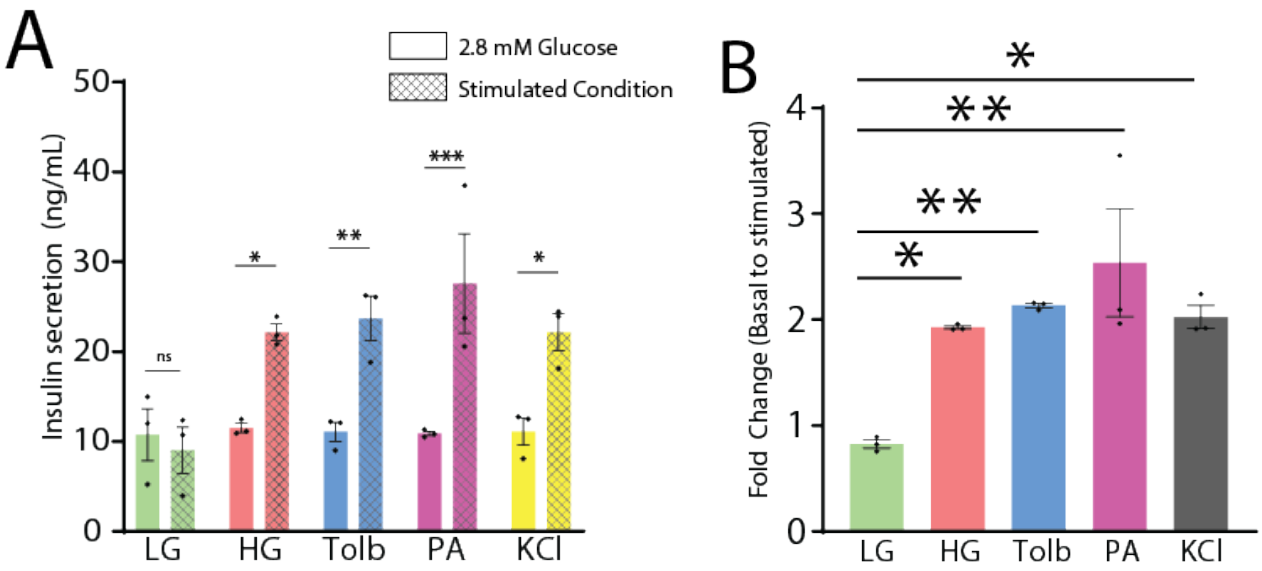

Figure 28: **Characterisation of syncollin-dsREDE5 transduced MIN6 beta-cells**. *(A)* Insulin secretion measurements by insulin HTRF (Cisbio) of MIN6 cells 72 hours post transduction with Adsync at 1 hour basal glucose (2.8 mM) KRBH (clear bars) followed by 1 hour stimulated conditions in the same well (hashed bars): LG (2.8 mM glucose), HG (16.7 mM glucose), Tolb (100µM tolbutamide) in 2.8 mM glucose, PA (0.5 mM palmitate in 16.7 mM glucose) and KCl (40 mM KCl) in 2.8 mM glucose (n = 3 per condition). (**B**) Fold change (stimulated over basal) of insulin concentration from **A** of each stimulation condition. * $P < 0.05$, ** $P < 0.01$, *** $P < 0.001$. **LG**, Low glucose. **HG**, High glucose. **PA**, Palmitate. **Tolb**, tolbutamide. Error bars represent ± S.E.M. Basal and stimulated conditions were performed sequentially in the same well. *One-way ANOVA (B) and two-way ANOVA (B) with Sidak's multiple comparisons*.

4.3.3 Characterisation of preferential secretion of young insulin granules in MIN6 cells

To further investigate the preferential secretion of ISGs in mouse beta-cells, immunofluorescent imaging of Adsync-transduced MIN6 cells was performed post-stimulation with different insulin-stimulating secretagogues. Briefly, 72 hours post-transduction, MIN6 cells were incubated overnight in low glucose DMEM (5.5 mM glucose), followed by a 1 hour incubation with basal KRBH (2.8 mM glucose) at 37°C, 5% CO_2. Cells were then stimulated for 20 minutes to induce first-phase insulin secretion with various stimulation media and anti-diabetic drugs. After stimulation, cells were fixed, and confocal images were captured to observe the granule populations that remained in the cytoplasm after secretion (**Figure 29A**).

Visually, in the low glucose condition, there was an approximately equal ratio of young-to-old ISGs, with merged images showing a yellow-green hue across the cell (**Figure 29A**, low glucose) which was reflected in a quantified young/old fluorescence intensity ratio of ~1 (**Figure 29B**). In contrast, under high glucose conditions, there was a depletion of younger granules, observable by a predominance of the orange-red ISG population remaining (**Figure 29A**, high glucose), and a significantly lower young/old fluorescence ratio (**Figure 29B**). This indicates the preferential secretion of younger granules upon high glucose stimulation, with only more mature granules remaining in the cytoplasm after first-phase insulin secretion.

Notably, in response to all anti-diabetic drugs, MIN6 cells showed an increase in secretion (**Figure 29C**); however, immunofluorescent imaging revealed the retention of younger SGs, with common sulfonylureas (tolbutamide, glibenclamide, and glimepiride) showing no significant changes in the ratio of young-to-old granules (**Figure 29A & B**). In contrast, in response to the meglitinide, repaglinide and the GLP-1 receptor agonist, Exendin-4, Adsync-transduced MIN6 cells exhibited a significant increase in the ratio of young to old

ISGs (**Figure 29B**), and representative imaging showed a depletion of red fluorescence (**Figure 29A**).

Interestingly, in two other conditions (high glucose with the addition of a stimulation cocktail and palmitate), a depletion of younger ISGs was still observed, with a significant reduction in the young-to-old insulin SG ratio (**Figure 29A & B**). Finally, insulin secretion in all conditions was confirmed via insulin HTRF assays (**Figure 29C**), to ensure that fluorescence imaging was only conducted on cells that responded to the different stimulation conditions.

Interestingly, in certain conditions, younger SGs localised close to the PM were retained at low glucose and anti-diabetic drug conditions (**Figure 29D**), but this was not observed under high glucose conditions.

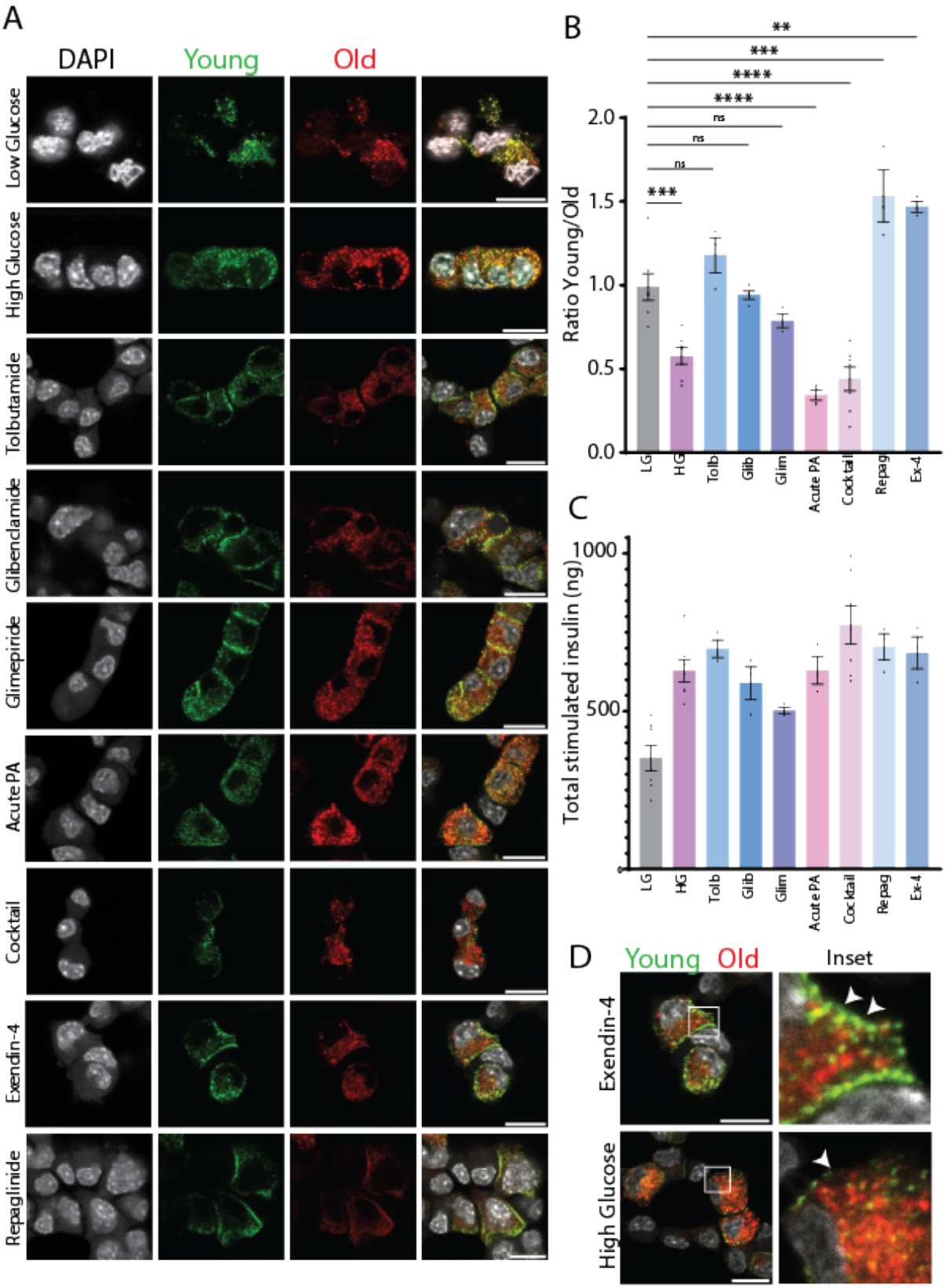

Figure 29: Glucose-dependent preferential release of young insulin granules from MIN6 cells. **(A)** Representative confocal imaging of MIN6 cells, 72 hours post transduction with

Adsyncollin-dsREDE5, after 20 minutes of stimulation conditions in low glucose (2.8 mM), high glucose (16.7 mM), tolbutamide, glibenclamide, glimepiride, acute palmitate, cocktail, exendin-4 and repaglinide, DAPI in grey. Green and red for young and old granules respectively. **(B)** Average young-to-old fluorescence ratios per beta-cell across ~20-30 cells per condition per experiment (n = 3 for tolbutamide, glimepiride, repaglinide and exendin-4, n = 7 for low glucose, high glucose and cocktail, n = 4 for glibenclamide and n = 5 for acute palmitate). (**C**) Total stimulated insulin concentrations (1^{st} phase) after 20 minutes of stimulation conditions. (**D**) Representative confocal imaging of MIN6 cells to highlight retained localisation of young granules at the PM in Exendin-4 compared to high glucose (Young, green and Old, red). **LG**, low glucose. **HG**, High glucose. **CT**, cocktail. **Tolb,** tolbutamide. **Glib**, Glibenclamide. **Glim**, Glimepiride. **Repag**, Repaglinide. **Ex-4**, Exendin-4. **Acute PA**, acute palmitate. Scale bars represent 10 μM. Error bars are ± S.E.M, *One-way ANOVA.*

4.3.4 Characterisation of preferential secretion of young insulin granules in human pancreatic islets

We then characterised the preferential secretion of young ISGs from human beta-cells isolated from a non-diabetic human donor (**Figure 30**). Pancreatic islets were isolated from a single donor and dispersed onto coverslips. These islets were transduced with Adsync for 72 hours and then stimulated with four conditions that were used in MIN6 cells before fixation for confocal imaging: (1) low glucose, (2) high glucose, (3) cocktail, and (4) 100 µM tolbutamide. Although the experiment was performed with only a single donor, a similar trend was observed post-stimulation.

In the low glucose condition, the ratio of green to red fluorescence intensity was nearly 1:1 (**Figure 30B & C**). In contrast, both high glucose and cocktail stimulation conditions showed a markedly reduced population of green fluorescence (**Figure 30A, B & C**) reflecting a decrease in young fluorescence intensity and a lower young/old fluorescence ratio. Consistent with observations in MIN6 cells, human beta-cells stimulated with tolbutamide did secrete insulin (**Figure 30D**), but did not lose young fluorescence (**Figure 30B**), maintaining an almost 2:1 ratio of young to old fluorescence (**Figure 30C**) due to the concurrent loss of old fluorescence within the beta-cell.

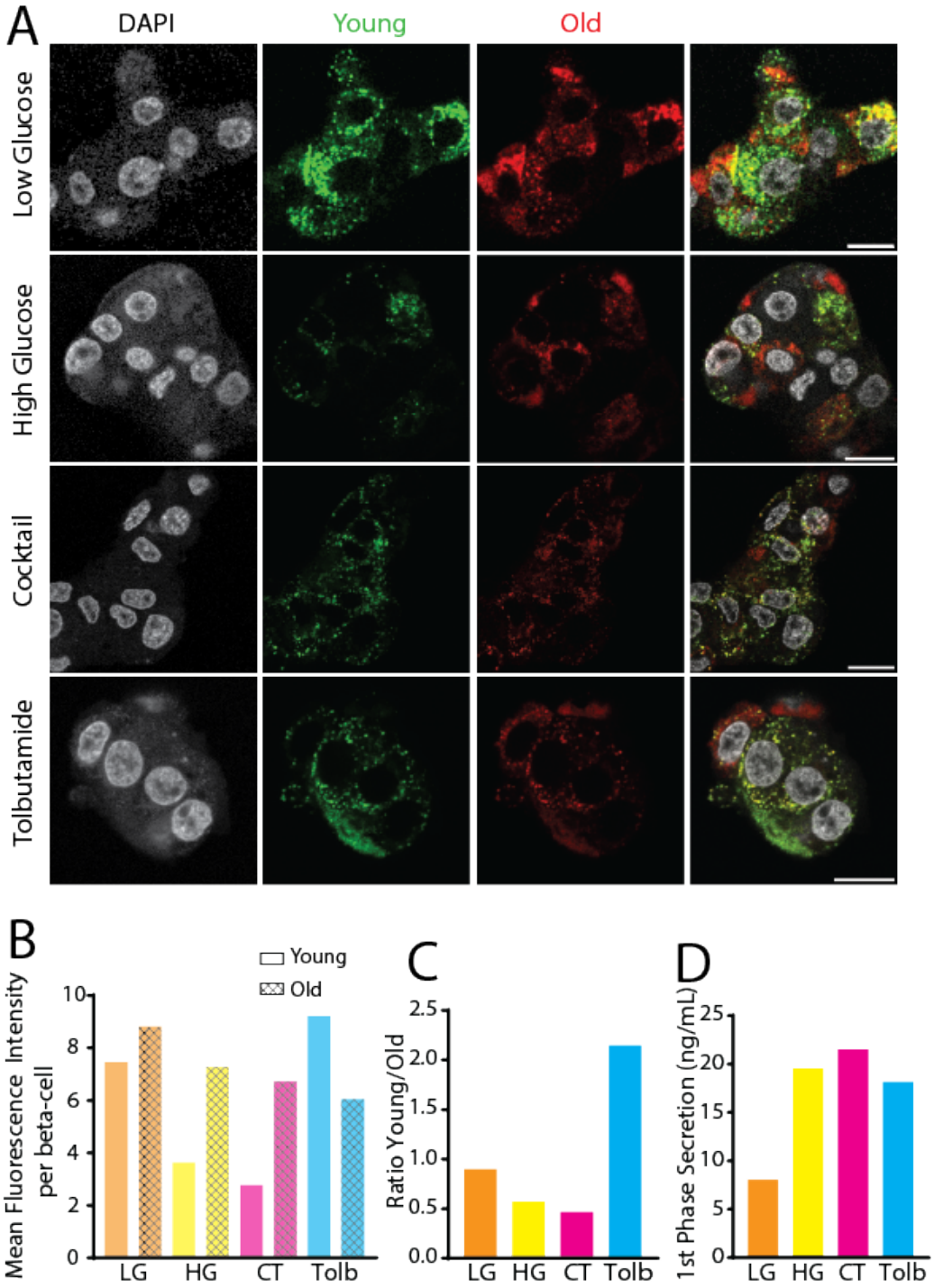

Figure 30*:* Glucose-dependent preferential release of young insulin granules from dispersed human pancreatic islets. (**A**) Representative confocal imaging of dispersed human islets, 72 hours post transduction with Adsyncollin-dsREDE5, after 20 minutes of stimulation conditions in low glucose (2.8 mM), high glucose (16.7 mM), cocktail and tolbutamide. Green and red for young and old granules respectively. (**B**) Average of the mean fluorescence intensities per beta-cell of young and old granules across ~20-30 cells per condition from one

donor (**n = 1**). (**C**) Average young to old fluorescence ratios per beta-cell across ~20-30 cells per condition from one donor (**n = 1**). (**D**) Insulin concentrations of stimulated insulin (1st phase) after 20 minutes of stimulation conditions. **LG**, Low glucose. **HG**, High glucose. **CT**, cocktail. **Tolb**, tolbutamide. Scale bars represent 10 μM. Basal and stimulation conditions were performed in the same well.

4.3.5 Investigation of degradation of young and old insulin granules in conditions of metabolic stress

We then aimed to investigate the preferential degradation of older ISGs from MIN6 beta-cells under control and palmitate-induced metabolic stress conditions (**Figure 31**). Adsync-transduced MIN6 beta-cells were treated with control conditions or 0.5 mM palmitate for 24 hours in complete DMEM. Confocal microscopy and quantification of colocalisation with Lamp1 (MOC) revealed a clear statistical difference between the young and old ISGs in control cells (**Figure 31A & B**), with an increase in the colocalisation of older ISGs with Lamp1.

When cells were exposed to palmitate, there was an increase in colocalisation of both young and old ISGs with Lamp1 (**Figure 31**). However, the preferential targeting of older granules to the lysosomes was not observed (**Figure 31**).

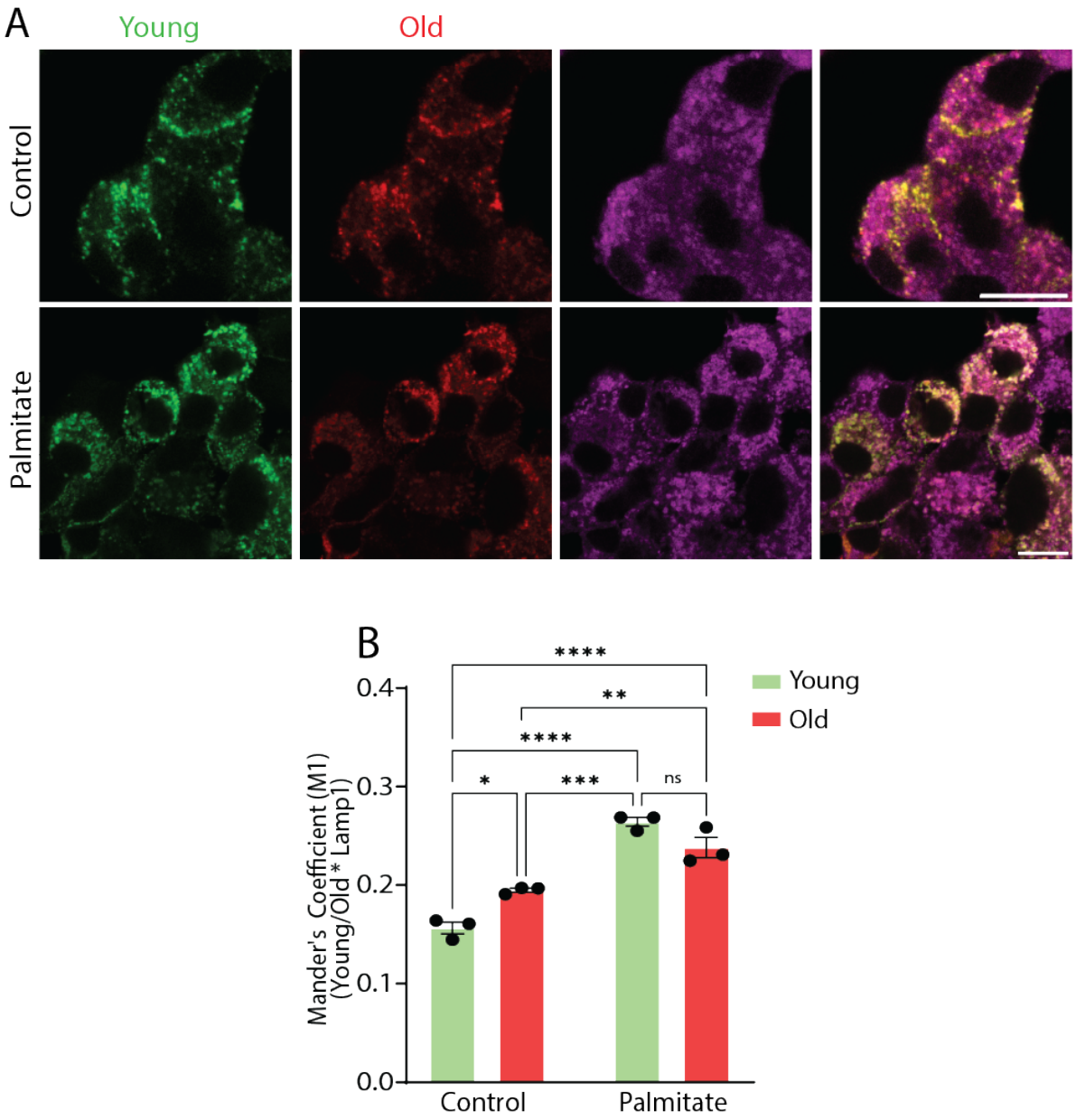

Figure 31: **Preferential degradation of old granules under glucolipotoxicity. (A)** Representative confocal imaging of dispersed human islets, 72 hours post transduction with Adsyncollin-dsREDE5 under control and palmitate (24 hour chronic exposure). Green and red for young and old granules respectively, co-stained with lysosomal marker (Lamp1). **(B)** Quantification of Mander's overlap coefficient (M1) of young or old granules with Lamp1 in both control (n = 3) and 24 hour palmitate (n = 3) conditions. * $P < 0.05$, ** $P < 0.01$, *** $P < 0.001$, **** $P < 0.0001$. Scale bars represent 10 µM. Error bars represent ± S.E.M. *Two-way ANOVA, Sidak's multiple comparisons*.

4.3.6 Augmentation of insulin granule populations in MIN6 cells to investigate functional differences in aged ISG populations

To evaluate functional differences between young and aged ISG populations in beta-cells, we first introduced Brefeldin-A to MIN6 cells to stall post-Golgi vesicle trafficking for 3 hours. This resulted in a noticeable increase in red fluorescence compared to DMSO-treated control cells (**Figure 32A**). Fluorescence intensity quantification showed a statistically significant increase in red fluorescence (**Figure 32B**) in Brefeldin-A treated cells compared to DMSO, which was reflected in a significant increase in the ratio of old-to-young fluorescence intensity (DMSO in complete DMEM, 25 mM glucose) (**Figure 32C**). This shift in the granule populations and the increase in the old-to-young fluorescence ratio are attributed to the depletion of ISG biogenesis from the trans-Golgi network.

In contrast, the addition of a stimulatory cocktail for 1 hour was used to induce exocytosis of older ISGs and stimulate insulin biosynthesis and ISG biogenesis (**Figure 32A**). The cocktail stimulation resulted in a noticeable increase in green fluorescence (**Figure 32A**), which was significantly higher compared to DMSO controls (**Figure 32B, clear bars**). However, there were no significant changes in red fluorescence between the cocktail and control cells (**Figure 32B, hashed bars**). Nevertheless, the 1 hour cocktail stimulation was sufficient to significantly reduce the old-to-young fluorescence intensity ratio (**Figure 32C**), leading to a visible shift in yellow-green granule populations within the cell (**Figure 32A**).

Using this assay, we aimed to characterise the functional differences between young and aged ISG populations in beta-cells by altering the overall age of the granule populations in MIN6 cells. Insulin was then extracted from the same three conditions (Bref-A, cocktail, control) using an acidified ethanol buffer overnight (12 hours) to extract both insulin and C-peptide. Insulin concentrations were measured by ELISA and diluted to 10 nM for glucose

uptake assays on differentiated 3T3-L1 adipocytes. Interestingly, although not statistically significant, the average glucose uptake from insulin isolated from Bref-A conditions were trended lower compared to the cocktail and control conditions (**Figure 32D**).

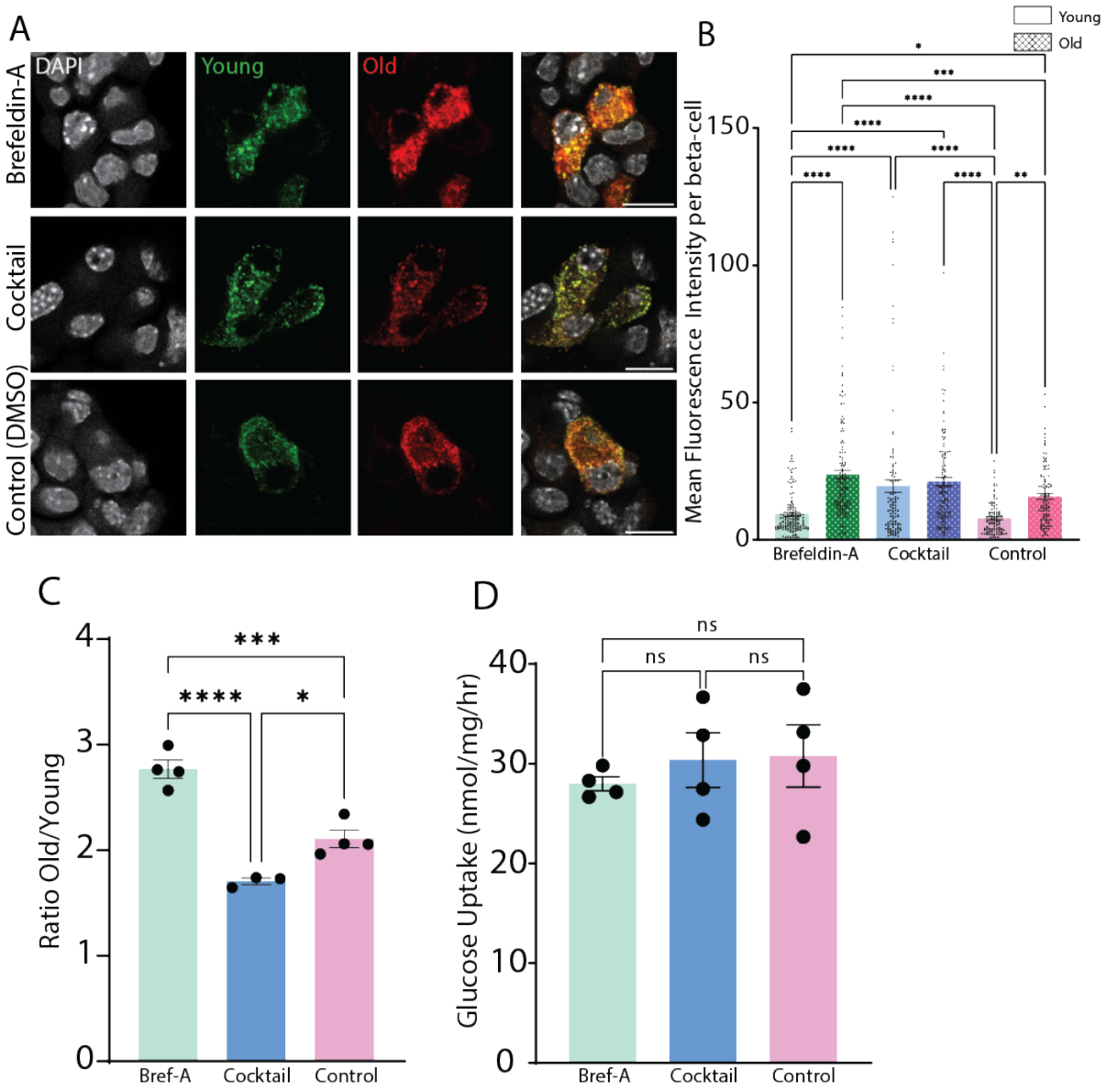

Figure 32: **Effect of brefeldin-A and insulin secretion stimulus on syncollin-dsREDE5 granule populations in MIN6 cells**. (**A**) Confocal imaging of MIN6 cells 48 hours post transduction with syncollin-dsREDE5 after treatment with 10µg/mL of brefeldin-A in complete DMEM for 3 hours, cocktail stimulation in complete DMEM for 1 hour or 25 mM glucose control complete DMEM. (**B**) Quantification of mean fluorescence intensity of green and red fluorescence per beta-cell across 30 - 50 cells per experiment in 3 - 4 separate experiments (Bref-A and Control: n = 4, Cocktail n = 3). (**C**) Average of the ratio of old to young granule intensity from **B** (n = 3/4). (**D**) Glucose uptake assay in 3T3-L1 adipocytes using insulin isolated after MIN6 cell treatment with Bref-A, cocktail or control DMEM with acid-ethanol

extraction at 10 nM of insulin. (n = 4 per condition). * P < 0.05, ** P < 0.01, *** P < 0.001, **** P < 0.0001. **Bref-A**, Brefeldin-A. Error bars represent ± S.E.M. *One-way and Two-way ANOVA with Sidak's multiple comparisons*.

4.4 Discussion

4.4.1 Characterising the localisation and compatibility of syncollin-dsREDE5 in MIN6 beta-cells

In this chapter, we first validated the specificity of the syncollin-dsREDE5 construct for localisation to ISGs in MIN6 cells (**Figure 27**). We demonstrated its utility for identifying and characterising ISG age, showing that it highly colocalised with insulin, Vamp8, and Chromogranin-A—well-established markers for ISGs. The high overlap in MOC confirms that syncollin-dsREDE5 effectively labels insulin-containing secretory granules. The lower MOC values for other subcellular compartments (including early endosomes (EEA1), late endosomes (Rab5A), autophagosomes (LC3A/B), cis-Golgi (GM130), mitochondria (ATP5A), and nuclei (KDM1/LSD1)) further highlight the specificity of syncollin-dsREDE5 for ISGs rather than other vesicular compartments in the beta-cell. Notably, syncollin-dsREDE5 exhibits significant colocalisation with lysosomes (Lamp1), particularly in the 'older' granule population, which aligns with previous studies showing that older granules are targeted for lysosomal degradation and can be visualised within multi-granular autophagic bodies [82].

Next, we characterised insulin secretion from Adsync-transduced MIN6 cells in response to different insulin secretagogues. 72 hours post-transduction, the transduced cells exhibited a robust insulin secretion response to elevated glucose alone (**Figure 28**), with a two-fold increase in (GSIS) (**Figure 28B)**. This further confirms that syncollin-dsREDE5 expression does not impair the ability of MIN6 cells to respond to elevated glucose. Additionally, transduced cells responded similarly to insulin secretagogues such as tolbutamide and KCl under low-glucose conditions. The addition of palmitate to high glucose further enhanced GSIS, highlighting a synergistic mechanism that augments insulin release and is maintained after Adsync transduction. Collectively, these results support the use of syncollin-

dsREDE5-transduced MIN6 cells as a model for understanding and dissecting insulin granule dynamics, providing a foundation for more detailed studies investigating the role of aging in insulin granule processes.

4.4.2 Preferential release of young insulin is glucose-dependent

With the established use of syncollin-dsREDE5 in MIN6 cells, we next investigated the secretion of young or old ISGs in response to different anti-diabetic drugs and insulin secretagogues. In these assays, cells were stimulated for 20 minutes to induce first-phase insulin secretion and observe the remaining ISG populations in the cytosol post-stimulation. Notably, we observed a markedly reduced population of younger ISGs when cells were stimulated with high glucose compared to low glucose controls (**Figure 29**). This is consistent with previous models showing that younger, newly synthesised ISGs are preferentially released in response to elevated glucose levels [65, 82, 83, 180].

In striking contrast, when treated with anti-diabetic drugs, MIN6 cells retained younger ISGs even post-stimulation (**Figure 29**) indicating that while the drugs effectively triggered insulin release under low-glucose conditions (**Figure 29C**), they did not induce the same preferential secretion of younger granules. This retention of younger ISGs was consistent across all anti-diabetic drugs tested, raising an important question about whether insulin secreted under these treatments is functionally distinct and whether this affects its action.

Furthermore, we investigated whether the preferential secretion of young ISGs is present in human islets under similar secretagogues. The secretion profiles of young ISGs from dispersed human donor islets aligned with those observed in MIN6 cells, reinforcing that selective granule secretion is stimulus dependent. Under low glucose conditions, human beta-cells maintained a relatively equal young-to-old ISG ratio, preserving their intracellular ISG stores. However, high glucose and stimulatory cocktail conditions (**Figure 30**), led to a

significant depletion of younger ISGs, suggesting a preferential release in response to glucose. In contrast, tolbutamide treatment retained young ISGs in human beta-cells while triggering insulin release, altogether supporting a glucose-regulated, pathway-specific role in preferential granule release (**Figure 30**).

These results highlight a potential limitation in the mechanisms of action of common anti-diabetic drugs. All the anti-diabetic drugs tested in **Chapter 4** increase insulin secretion by targeting the distal stages of insulin exocytosis—either through membrane depolarisation (e.g., sulfonylureas and meglitinides) or by increasing cytosolic cAMP levels (e.g., GLP-1 receptor agonists). However, these drugs bypass glycolysis and mitochondrial glucose metabolism (**Figure 26**). As a result, they do not mimic the increase in Krebs cycle products (ATP, glutamate, citrate, NAD(P)H) that couple glucose metabolism to ISG exocytosis [336, 337].

The effects of glucose and ATP on ISG mobility are mediated by kinesins, which require ATP hydrolysis to transport ISGs to the site of exocytosis [338-340]. One study shows that younger ISGs have a specific heavy-chain kinesin (KIF5b) which is absent on older granules [64]. Another study showed that mutant forms of kinesins reduce ISG mobility and exocytosis [341]. Taken together, these findings suggest that younger ISGs may be more glucose-responsive due to the presence of different motor proteins on their membranes—motor proteins that are not activated by anti-diabetic drugs. Despite the ability of these insulin secretagogues to stimulate insulin release, they appear to bypass the beta-cell's natural preference for releasing younger ISGs.

Surprisingly, the effect of high glucose paired with additional stimuli through palmitate or stimulatory cocktails still drive the release of younger ISGs from beta-cells (**Figure 29**, **Figure 30**, **Figure 32**). Additionally, the retention of younger ISGs at the PM in response to

anti-diabetic drugs may indicate the lack of signaling the release of the readily releasable pool of granules (RRP) (**Figure 29D**). Taken together, these results indicate a clear selective secretion of young insulin granules in both MIN6 and human pancreatic beta-cells [82, 83, 180]. Furthermore, these results indicate that the preference for young ISG secretion is strictly glucose dependent. These findings underscore the complexity of ISG populations and beta-cell granule release in response to varied stimuli. The selective retention of young ISGs in the presence of anti-diabetic drugs might suggest that these drugs alter the natural granule dynamics or interfere with docking and fusion machinery that is preferentially engaged by younger ISGs. This could potentially impact overall beta-cell adaptation over time, as beta-cells may fail to respond with optimally functional insulin granules during prolonged treatment. We suggest that while anti-diabetic drugs may enhance insulin secretion, they bypass the natural selection of ISGs for biphasic release dynamics, enhancing both first- and second-phase insulin [342, 343], in an indiscriminate manner, further impacting beta-cell health and functionality over time.

4.4.3 Investigating the functional differences between young and old ISGs

While anti-diabetic drugs increase insulin secretion without selectively promoting the release of younger ISGs, it raises the question of whether younger granules are more effective than older ones at glucose-lowering. To investigate potential functional differences, we aimed to augment ISG populations in MIN6 beta-cells. Treatment with Brefeldin-A for 3 hours effectively stalls post-Golgi trafficking, leading to a notable accumulation of aged (red) granules at high glucose. This was reflected in a significant increase in the ratio of old-to-young fluorescence (**Figure 32A – C**) as Brefeldin-A impedes the formation of younger ISGs, resulting in a predominance of cytosolic older granules. In contrast, exposure to a stimulatory cocktail not only triggered exocytosis of older granules but also induced new insulin biosynthesis and ISG formation, leading to a remarkable increase in younger (green) granules.

(**Figure 32A & B)**. This was accompanied by a significant reduction in the old-to-young fluorescence ratio, compared to Brefeldin-A and control conditions (**Figure 32C**).

Autophagy is the primary mechanism employed by all cells to target unused or damaged organelles to the lysosomes, thereby maintaining cellular homeostasis and recycling nutrients [84, 344, 345]. Consistent with previous findings we show that beta-cells preferentially target older ISGs to the lysosome (**Figure 31**) under normal conditions. In conditions of metabolic stress, there is a marked increase in the degradation of younger ISGs [84] (**Figure 31**). Glucose metabolism in beta-cells produces many reactive oxygen species (ROS) [346] which may damage ISGs as they accumulate in the cytosol over time. Aged ISGs may, therefore, accumulate ROS-induced damage, PTMs, or partial degradation of ISG proteins, potentially affecting the bioactivity of insulin within these granules. Retention of younger ISGs could suggest that anti-diabetic drugs primarily mobilise older, possibly more 'damaged' ISGs that are less functionally optimal. This may compromise the amount or quality of insulin released during drug treatments aimed at maintaining glucose homeostasis in T2D. However, this was not observed when adipocytes were stimulated with insulin from aged ISG populations compared to younger ISGs (**Figure 32D**). Notably, using a radioactive tracer to measure glucose uptake, no significant differences were observed across the three treatments.

A trend towards lower glucose uptake with insulin from Brefeldin-A treated cells may suggest reduced insulin potency or altered composition due to the absence of younger ISGs. However, future experiments are needed to isolate distinctly young and old ISGs to investigate potential changes in insulin hormone activity and bioactivity. A limitation of this study is that the assays do not exclusively separate young and old ISGs but only shift the proportions of these age-distinct granules. Therefore, any changes in glucose uptake may be marginal. Overall, the findings of this chapter emphasise the dynamic role of ISG age in determining granule composition and secretory responses, highlighting how stimuli-specific modulation of

ISG populations meets metabolic demands. Current studies have characterised molecular differences in aging granules [64], while others have shown an increase in older ISGs in diabetic mouse models (db/db) [68]. Future studies should focus on characterising the functional properties of these age-distinct ISG populations and how they shift during the progression of T2D. Understanding these differences could help refine current therapeutic strategies by targeting the proximal stages of insulin granule maturation and release. Such an approach could optimise the secretion of younger, more functionally effective granules, preserving or even restoring the natural selectivity of ISG release and glucose responsiveness, particularly under conditions of metabolic stress. By focusing therapeutic strategies on enhancing or restoring the production of younger ISGs, rather than simply stimulating an increase in insulin granule release, future treatments could improve glucose homeostasis and beta-cell function more sustainably.

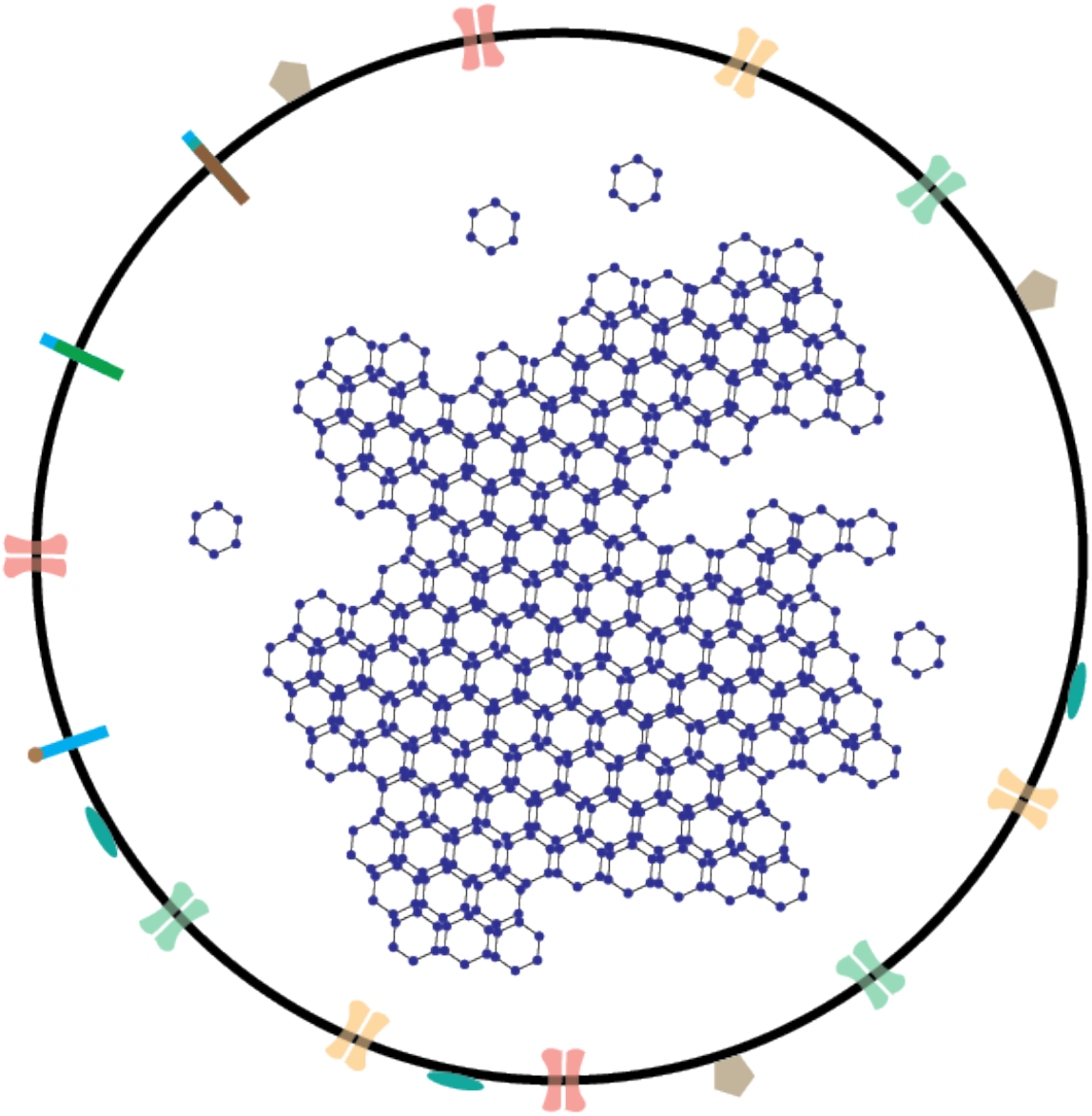

Chapter 5

Final Discussion

5.1 Understanding beta-cell function through ISG composition

Many studies have extensively investigated the role of pancreatic beta-cells in the pathogenesis of T2D, with a growing focus on the proximal stages of ISG biogenesis, trafficking, and maturation [94, 97, 146, 347]. Dysfunction in the molecular mechanisms that underpin proper ISG production, storage, and secretion is tightly linked to the decline in beta-cell function in T2D [47, 149, 338, 348]. Current therapeutic strategies, however, focus solely on increasing overall ISG exocytosis without considering the existence of functionally heterogeneous populations of ISGs within the beta-cell [199, 338]. Few studies have attempted to investigate the composition of ISGs, leaving much to be understood about how various ISG proteins may drive key processes [64, 112, 114, 123, 126, 129, 349]. Other research into ISG proteins focuses on individual proteins in isolation, providing limited insight into the broader mechanisms governing ISG function [94, 133, 224]. These studies are important as many ISG-associated SNPs are implicated in diabetes [94, 158, 350-352] and may play a role in the genetic susceptibility to the disease, linked to dysregulated function of the proximal stages of insulin exocytosis. To gain a more comprehensive understanding, we shift toward investigating the protein composition of the ISG in a mouse model to reveal novel ISG proteins that may drive normal ISG and beta-cell function.

In **Chapter 2**, this thesis developed an efficient and effective method for purifying ISGs from beta-cells using a range of subcellular fractionation techniques. This purification process yields ISGs suitable for various functional analyses. Here, we employ LC-MS/MS, unbiased protein correlation profiling, and targeted machine learning tools to successfully generate and publish the first proteome of murine ISGs from the MIN6 cell line [202]. Using this framework, we identify 211 ISG-associated proteins (**Supplementary Table 5**) and validate four novel ISG-associated proteins: Synaptotagmin-13, Syntaxin-7, Synaptophysin, and Scamp3 (**Chapter 2**). Through functional analyses and knockdown of Scamp3, we also implicate its

role as a novel regulator of insulin content and secretion in pancreatic beta-cells (**Chapter 2**). Scamp3 knockdown cells show a reduction in mature insulin content, with no changes in proinsulin or insulin mRNA transcription (**Figure 14**, **Supplementary Figure 2**). This suggests that Scamp3 is likely involved in post-Golgi trafficking in beta-cells. However, further studies should aim to elucidate the specific mechanisms by which Scamp3 regulates insulin content and exocytosis.

We also investigated the role of a second novel ISG-associated protein, synaptophysin (**Chapter 2A**). Through siRNA-mediated knockdown and GSIS analysis, we implicate its role in insulin secretion. In contrast to Scamp3, however, synaptophysin showed no reduction in total insulin content (**Figure 17**). Immunofluorescent staining of synaptophysin show a strong localisation to ISGs (**Figure 13**) and to the PM in INS-1 cells (**Figure 16**). Based on these data and previous studies on the role of synaptophysin in vesicular exocytosis [251, 353], we hypothesise that synaptophysin is involved in late-stage exocytosis by interacting with Vamp2 and other SNARE complex proteins to dock ISGs to the PM, facilitating fusion pore opening and the release of ISG cargo. Future studies should aim to investigate the role of synaptophysin in beta-cells to further elucidate its interactions with the ISG and other SNARE proteins.

By examining how the proteomic or lipidomic composition of ISGs changes in response to metabolic stressors or disease states, we can identify key regulatory proteins and pathways involved in beta-cell function and insulin exocytosis. This enhances the potential of this newly optimised method to provide deeper insights into beta-cell biology and pathophysiology, as well as identify potential novel therapeutic targets for T2D. In **Chapter 3**, we applied this approach to investigate how lipotoxic conditions affect the composition and function of ISGs in diabetic contexts.

5.2 Compositional changes to the ISG under glucolipotoxicity

Previous studies have largely focused on FFA effects on pancreatic beta-cells, primarily examining metabolic outcomes including insulin secretion, apoptosis and stress responses [255, 257, 258, 299]. In **Chapter 3**, we offer a new perspective by investigating how FFA exposure, specifically chronic palmitate treatment, impacts the protein composition within the ISGs to potentially uncover mechanisms that drive beta-cell dysfunction in metabolic disease. We confirmed reductions in GSIS following 48 hour chronic palmitate exposure in MIN6 beta-cells (**Figure 19**), though physical ISG density seem largely unaffected. The stability of ISG structure despite compositional changes suggests that specific proteins may underlie the impairment of ISG exocytosis. Using label free quantification proteomics on ISGs revealed reductions in abundance of essential ISG proteins such as Ins1, Ins2, CPE, Pcsk1n, ZnT8 in response to elevated FFAs. These proteins are integral to insulin biosynthesis and ISG maturation and disruption in these ISG proteins suggests that FFAs compromise ISG functionality at different stages, from synthesis to maturation. Through GO enrichment analysis, we detected alterations to the ISG docking machinery, suggesting that elevated FFAs also impair docking capacity of the ISGs.

Broader proteomics analysis revealed downregulations in classical ISG proteins Vamp2 and Rab3a as well as other regulatory proteins involved in trafficking, docking and exocytosis. Reductions in proteins like VTI1A and canonical ISG SNAREs and small GTPases may imply a potential mistargeting of ISGs, potentially toward the lysosome, a feature seen in other studies with the retention of ISGs within phagolysosomes in response to elevated FFAs [84, 302, 354]. Together, these findings demonstrate that FFAs impaired insulin exocytosis and overall beta-cell function. This provides a new perspective on the impacts of chronic FFA exposure, implicating changes in the molecular machinery essential for insulin granule stability, docking and exocytosis. Further, these data underscore the importance of considering the ISG

composition in understanding beta-cell dysfunction, highlighting the need for further studies on the mechanisms by which glucolipotoxicity drive these changes.

5.3 Preferential release of young insulin is glucose-dependent

Chapter 2 and **3** analyses primarily centered on the global proteome of the entire ISG population in beta-cells. In **Chapter 4** we introduce and address the functional diversity within the ISGs, through age-distinct subpopulations of ISGs. We validate the use of an adenoviral construct, Adsyncollin-dsREDE5, to specifically target insulin-containing vesicles in MIN6 beta-cells and show that it is detectable within Lamp1-positive vesicles (**Figure 27**). Through this construct, consistent with previous studies, we show that beta-cells preferentially secrete younger, more newly synthesised insulin granules [82, 83, 180] . Furthermore, we show that while anti-diabetic drugs including sulfonylureas, meglitinides and GLP1R agonists are effective at stimulating insulin secretion, they by-pass the natural selectivity of younger ISG exocytosis observed in beta-cells, indicating a glucose-regulated mechanism that drives young ISG exocytosis. These differences amongst ISG subpopulations could provide novel insights to how insulin secretion is regulated at a proximal, granular level, as opposed to considering ISGs as a homogeneous group. There is a clear complex interplay between granule composition, age and beta-cell function, suggesting that therapeutic strategies focused on solely stimulating insulin release may be insufficient if they fail to target the release of optimally functional ISGs.

5.4 Future directions for ISG biology

With the development of a more efficient methodology for studying ISG composition, future research could focus on coupling these techniques with age-labelling approaches, further optimizing them to overcome challenges associated with performing downstream analysis using purified ISGs. Additionally, future studies should explore other perturbations to beta-cells that could uncover how ISG composition directly impacts beta-cell function under

different states. For instance, using immune cytokines to induce a Type 1 diabetic phenotype in beta-cells and investigating the resulting changes in ISG composition, or analysing how ISGs respond to anti-diabetic drug treatments. Investigating the specific molecular pathways involved in granule aging and how these pathways are influenced by metabolic conditions could deepen our understanding of beta-cell dysfunction in disease. Lastly, scaling these methods to ex vivo models present a promising approach for more targeted studies of mouse and/or human pancreatic beta-cells. This would include the implementation of FACS sorting to isolate beta-cells from ex vivo pancreatic islets, followed by a single subcellular fractionation coupled with targeted machine learning analysis, enabling the study of ISG composition from fewer beta-cells.

5.5 Targeting the ISG to improve diabetes treatments

In summary, this thesis explores the dynamic nature of ISGs in beta-cells, starting with a comprehensive analysis of the entire ISG proteome in MIN6 cells to identify novel and key proteins involved in insulin granule turnover. Using this optimised ISG analysis method, it then examines how this composition may change in response to elevated FFAs, and its implications on insulin secretion under metabolic stress. Furthermore, it explores the preferential secretion of young insulin granules, which may play a more active role than their aged counterparts. Notably there exists a plethora of T2D associated polymorphisms in insulin granule genes [49, 97, 355-359] highlighting the relevance of these granule proteins to diabetes pathogenesis. Collectively, these findings underline the complexity of ISG function and highlight the absolute importance of considering subpopulations of ISGs with distinct functionality when studying insulin secretion and beta-cell function, especially under conditions of metabolic dysregulation. Linking altered ISG composition and functionality to impaired beta-cell function opens potential avenues for identifying potential therapeutic targets aimed at restoring and preserving ISG functionality to improve beta-cell health in metabolic diseases. Tailoring these therapies

to selectively activate the secretion of younger granules could offer a more targeted method to improve beta-cell function, addressing the underlying dysfunctional beta-cells seen in T2D without overburdening the beta-cells with non-selective stimulation.

References/Bibliography

1. Da Silva Xavier, G., *The cells of the islets of Langerhans.* Journal of clinical medicine, 2018. **7**(3): p. 54.
2. Steiner, D.J., et al., *Pancreatic islet plasticity: interspecies comparison of islet architecture and composition.* Islets, 2010. **2**(3): p. 135-145.
3. Brissova, M., et al., *Assessment of human pancreatic islet architecture and composition by laser scanning confocal microscopy.* Journal of Histochemistry & Cytochemistry, 2005. **53**(9): p. 1087-1097.
4. Orci, L., *The microanatomy of the islets of Langerhans.* Metabolism, 1976. **25**(11): p. 1303-1313.
5. Orci, L. and R. Unger, *Functional subdivision of islets of Langerhans and possible role of D cells.* The Lancet, 1975. **306**(7947): p. 1243-1244.
6. Bonner-Weir, S., B.A. Sullivan, and G.C. Weir, *Human islet morphology revisited: human and rodent islets are not so different after all.* Journal of Histochemistry & Cytochemistry, 2015. **63**(8): p. 604-612.
7. Erlandsen, S.L., et al., *Pancreatic islet cell hormones distribution of cell types in the islet and evidence for the presence of somatostatin and gastrin within the D cell.* Journal of Histochemistry & Cytochemistry, 1976. **24**(7): p. 883-897.
8. Bosco, D., et al., *Unique arrangement of α-and β-cells in human islets of Langerhans.* Diabetes, 2010. **59**(5): p. 1202-1210.
9. Lammert, E. and P. Thorn, *The role of the islet niche on beta cell structure and function.* Journal of molecular biology, 2020. **432**(5): p. 1407-1418.
10. Freckmann, G., et al., *Continuous glucose profiles in healthy subjects under everyday life conditions and after different meals.* Journal of diabetes science and technology, 2007. **1**(5): p. 695-703.
11. Persaud, S.J., A.C. Hauge-Evans, and P.M. Jones, *Insulin-secreting cell lines: Potential for research and diabetes therapy*, in *Cellular Endocrinology in Health and Disease*. 2014, Elsevier. p. 239-256.
12. Bouwens, L. and I. Rooman, *Regulation of pancreatic beta-cell mass.* Physiological reviews, 2005. **85**(4): p. 1255-1270.
13. Plum, L., B.F. Belgardt, and J.C. Brüning, *Central insulin action in energy and glucose homeostasis.* The Journal of clinical investigation, 2006. **116**(7): p. 1761-1766.
14. Cerasi, E. and R. Luft, *The plasma insulin response to glucose infusion in healthy subjects and in diabetes mellitus.* European Journal of Endocrinology, 1967. **55**(2): p. 278-304.

15. Curry, D.L., L.L. Bennett, and G.M. Grodsky, *Dynamics of insulin secretion by the perfused rat pancreas.* Endocrinology, 1968. **83**(3): p. 572-584.
16. Henquin, J.-C., et al., *Signals and pools underlying biphasic insulin secretion.* Diabetes, 2002. **51**(suppl_1): p. S60-S67.
17. Lacy, P.E., M.M. Walker, and C. Joan Fink, *Perifusion of isolated rat islets in vitro: participation of the microtubular system in the biphasic release of insulin.* Diabetes, 1972. **21**(10): p. 987-998.
18. Ferrannini, E., et al., *Effect of insulin on the distribution and disposition of glucose in man.* The Journal of clinical investigation, 1985. **76**(1): p. 357-364.
19. Edgerton, D.S., et al., *Insulin's direct hepatic effect explains the inhibition of glucose production caused by insulin secretion.* JCI insight, 2017. **2**(6).
20. Muretta, J.M. and C.C. Mastick, *How insulin regulates glucose transport in adipocytes.* Vitamins & Hormones, 2009. **80**: p. 245-286.
21. Barnett, A., et al., *Metabolic studies in unaffected co-twins of non-insulin-dependent diabetics.* Br Med J (Clin Res Ed), 1981. **282**(6277): p. 1656-1658.
22. Vauhkonen, I., et al., *Defects in insulin secretion and insulin action in non-insulin-dependent diabetes mellitus are inherited. Metabolic studies on offspring of diabetic probands.* The Journal of clinical investigation, 1998. **101**(1): p. 86-96.
23. Gautier, J.-F., et al., *Low acute insulin secretory responses in adult offspring of people with early onset type 2 diabetes.* Diabetes, 2001. **50**(8): p. 1828-1833.
24. Gastaldelli, A., et al., *Metabolic effects of visceral fat accumulation in type 2 diabetes.* The Journal of Clinical Endocrinology & Metabolism, 2002. **87**(11): p. 5098-5103.
25. DeFronzo, R.A., *Pathogenesis of type 2 diabetes mellitus.* Medical clinics, 2004. **88**(4): p. 787-835.
26. Dooley, J., et al., *Genetic predisposition for beta cell fragility underlies type 1 and type 2 diabetes.* Nature genetics, 2016. **48**(5): p. 519-527.
27. Weir, G.C., et al., *Beta-cell adaptation and decompensation during the progression of diabetes.* Diabetes, 2001. **50**(suppl_1): p. S154.
28. Liston, A., J.A. Todd, and V. Lagou, *Beta-cell fragility as a common underlying risk factor in type 1 and type 2 diabetes.* Trends in molecular medicine, 2017. **23**(2): p. 181-194.
29. Weir, G.C. and S. Bonner-Weir, *Five stages of evolving beta-cell dysfunction during progression to diabetes.* Diabetes, 2004. **53**(suppl_3): p. S16-S21.
30. Westermeier, F., et al., *Gluconeogenic enzymes in β-Cells: Pharmacological targets for improving insulin secretion.* Trends in Endocrinology & Metabolism, 2019. **30**(8): p. 520-531.
31. Evans-Molina, C., et al., *Glucose regulation of insulin gene transcription and pre-mRNA processing in human islets.* Diabetes, 2007. **56**(3): p. 827-835.

32. Liu, M., et al., *Proinsulin entry and transit through the endoplasmic reticulum in pancreatic beta cells.* Vitamins & Hormones, 2014. **95**: p. 35-62.
33. Orci, L., et al., *Coatomer-rich endoplasmic reticulum.* Proceedings of the National Academy of Sciences, 1994. **91**(25): p. 11924-11928.
34. Orci, L., M. Ravazzola, and A. Perrelet, *(Pro) insulin associates with Golgi membranes of pancreatic B cells.* Proceedings of the National Academy of Sciences, 1984. **81**(21): p. 6743-6746.
35. Davidson, H.W., C.J. Rhodes, and J.C. Hutton, *Intraorganellar calcium and pH control proinsulin cleavage in the pancreatic beta cell via two distinct site-specific endopeptidases.* Nature, 1988. **333**(6168): p. 93-6.
36. Orci, L., et al., *Proteolytic maturation of insulin is a post-Golgi event which occurs in acidifying clathrin-coated secretory vesicles.* Cell, 1987. **49**(6): p. 865-868.
37. Orci, L., et al., *Direct identification of prohormone conversion site in insulin-secreting cells.* Cell, 1985. **42**(2): p. 671-81.
38. Davidson, H.W., J.M. Wenzlau, and R.M. O'Brien, *Zinc transporter 8 (ZnT8) and β cell function.* Trends in Endocrinology & Metabolism, 2014. **25**(8): p. 415-424.
39. Thorens, B., *GLUT2, glucose sensing and glucose homeostasis.* Diabetologia, 2015. **58**(2): p. 221-232.
40. Cui, X., et al., *Akt signals upstream of L-type calcium channels to optimize insulin secretion.* Pancreas, 2012. **41**(1): p. 15-21.
41. Straub, S.G. and G.W. Sharp, *Glucose‐stimulated signaling pathways in biphasic insulin secretion.* Diabetes/metabolism research and reviews, 2002. **18**(6): p. 451-463.
42. Thurmond, D.C. and H.Y. Gaisano, *Recent Insights into Beta-cell Exocytosis in Type 2 Diabetes.* J Mol Biol, 2020. **432**(5): p. 1310-1325.
43. Lacy, P.E., *Beta cell secretion—from the standpoint of a pathobiologist.* Diabetes, 1970. **19**(12): p. 895-905.
44. Daniel, S., et al., *Identification of the docked granule pool responsible for the first phase of glucose-stimulated insulin secretion.* Diabetes, 1999. **48**(9): p. 1686-1690.
45. Izumi, T., K. Kasai, and H. Gomi, *Secretory vesicle docking to the plasma membrane: molecular mechanism and functional significance.* Diabetes, Obesity and Metabolism, 2007. **9**: p. 109-117.
46. Sheng, Z.-H., R.E. Westenbroek, and W.A. Catterall, *Physical link and functional coupling of presynaptic calcium channels and the synaptic vesicle docking/fusion machinery.* Journal of bioenergetics and biomembranes, 1998. **30**: p. 335-345.
47. Seino, S., T. Shibasaki, and K. Minami, *Dynamics of insulin secretion and the clinical implications for obesity and diabetes.* J Clin Invest, 2011. **121**(6): p. 2118-25.

48. Hou, J.C., L. Min, and J.E. Pessin, *Insulin granule biogenesis, trafficking and exocytosis.* Vitam Horm, 2009. **80**: p. 473-506.
49. Barg, S., et al., *A subset of 50 secretory granules in close contact with L-type Ca2+ channels accounts for first-phase insulin secretion in mouse beta-cells.* Diabetes, 2002. **51 Suppl 1**: p. S74-82.
50. Hosker, J.P., et al., *Similar reduction of first-and second-phase B-cell responses at three different glucose levels in type II diabetes and the effect of gliclazide therapy.* Metabolism, 1989. **38**(8): p. 767-772.
51. Ohara-Imaizumi, M., et al., *TIRF imaging of docking and fusion of single insulin granule motion in primary rat pancreatic β-cells: different behaviour of granule motion between normal and Goto–Kakizaki diabetic rat β-cells.* Biochemical Journal, 2004. **381**(1): p. 13-18.
52. Shibasaki, T., et al., *Essential role of Epac2/Rap1 signaling in regulation of insulin granule dynamics by cAMP.* Proceedings of the National Academy of Sciences, 2007. **104**(49): p. 19333-19338.
53. Seino, S., et al., *Roles of cAMP signalling in insulin granule exocytosis.* Diabetes, Obesity and Metabolism, 2009. **11**: p. 180-188.
54. Kasai, K., et al., *Docking is not a prerequisite but a temporal constraint for fusion of secretory granules.* Traffic, 2008. **9**(7): p. 1191-1203.
55. Gomi, H., et al., *Granuphilin molecularly docks insulin granules to the fusion machinery.* The Journal of cell biology, 2005. **171**(1): p. 99-109.
56. Orci, L. and W. Malaisse, *Hypothesis: single and chain release of insulin secretory granules is related to anionic transport at exocytotic sites.* Diabetes, 1980. **29**(11): p. 943-944.
57. Nemoto, T., et al., *Sequential-replenishment mechanism of exocytosis in pancreatic acini.* Nature cell biology, 2001. **3**(3): p. 253-258.
58. Takahashi, N., et al., *Sequential exocytosis of insulin granules is associated with redistribution of SNAP25.* The Journal of cell biology, 2004. **165**(2): p. 255-262.
59. Hanna, S.T., et al., *Kiss-and-run exocytosis and fusion pores of secretory vesicles in human beta-cells.* Pflugers Arch, 2009. **457**(6): p. 1343-50.
60. Tsuboi, T., H.T. McMahon, and G.A. Rutter, *Mechanisms of dense core vesicle recapture following "kiss and run"("cavicapture") exocytosis in insulin-secreting cells.* Journal of Biological Chemistry, 2004. **279**(45): p. 47115-47124.
61. Luzi, L. and R.A. DeFronzo, *Effect of loss of first-phase insulin secretion on hepatic glucose production and tissue glucose disposal in humans.* American Journal of Physiology-Endocrinology and Metabolism, 1989. **257**(2): p. E241-E246.
62. Rhodes, C.J. and P.A. Halban, *Newly synthesized proinsulin/insulin and stored insulin are released from pancreatic B cells predominantly via a regulated, rather than a constitutive, pathway.* The Journal of cell biology, 1987. **105**(1): p. 145-153.

63. Ivanova, A., et al., *Age-dependent labeling and imaging of insulin secretory granules.* Diabetes, 2013. **62**(11): p. 3687-96.
64. Neukam, M., et al., *Purification of time-resolved insulin granules reveals proteomic and lipidomic changes during granule aging.* Cell Reports, 2024. **43**(3).
65. Duncan, R.R., et al., *Functional and spatial segregation of secretory vesicle pools according to vesicle age.* Nature, 2003. **422**(6928): p. 176-180.
66. Tsuboi, T., et al., *Age-dependent preferential dense-core vesicle exocytosis in neuroendocrine cells revealed by newly developed monomeric fluorescent timer protein.* Mol Biol Cell, 2010. **21**(1): p. 87-94.
67. Terskikh, A., et al., *" Fluorescent timer": protein that changes color with time.* Science, 2000. **290**(5496): p. 1585-1588.
68. Yau, B., et al., *A fluorescent timer reporter enables sorting of insulin secretory granules by age.* Journal of Biological Chemistry, 2020. **295**(27): p. 8901-8911.
69. Norris, N., B. Yau, and M.A. Kebede, *Isolation and Proteomics of the Insulin Secretory Granule.* Metabolites, 2021. **11**(5).
70. Rorsman, P. and F.M. Ashcroft, *Pancreatic β-cell electrical activity and insulin secretion: of mice and men.* Physiological reviews, 2018. **98**(1): p. 117-214.
71. Weiss, M., D.F. Steiner, and L.H. Philipson, *Insulin Biosynthesis, Secretion, Structure, and Structure-Activity Relationships*, in *Endotext*, K.R. Feingold, et al., Editors. 2000: South Dartmouth (MA).
72. Gehart, H. and R. Ricci, *Saving the neck from scission.* Commun Integr Biol, 2013. **6**(2): p. e23098.
73. Arvan, P. and P.A. Halban, *Sorting ourselves out: seeking consensus on trafficking in the beta-cell.* Traffic, 2004. **5**(1): p. 53-61.
74. Sun, J., et al., *Proinsulin misfolding and endoplasmic reticulum stress during the development and progression of diabetes.* Mol Aspects Med, 2015. **42**: p. 105-18.
75. Chang, S.-G., et al., *Role of disulfide bonds in the structure and activity of human insulin.* Molecules & Cells (Springer Science & Business Media BV), 2003. **16**(3).
76. Orci, L., et al., *Conversion of proinsulin to insulin occurs coordinately with acidification of maturing secretory vesicles.* J Cell Biol, 1986. **103**(6 Pt 1): p. 2273-81.
77. Dunn, M.F., *Zinc-ligand interactions modulate assembly and stability of the insulin hexamer -- a review.* Biometals, 2005. **18**(4): p. 295-303.
78. Marsh, B.J., et al., *Regulated autophagy controls hormone content in secretory-deficient pancreatic endocrine β-cells.* Molecular Endocrinology, 2007. **21**(9): p. 2255-2269.
79. Rorsman, P. and E. Renstrom, *Insulin granule dynamics in pancreatic beta cells.* Diabetologia, 2003. **46**(8): p. 1029-1045.
80. Kasai, H., et al., *Exocytosis in islet beta-cells.* Adv Exp Med Biol, 2010. **654**: p. 305-38.

81. Yin, P., et al., *Syntaxin clusters at secretory granules in a munc18-bound conformation.* Molecular biology of the cell, 2018. **29**(22): p. 2700-2708.
82. Hoboth, P., et al., *Aged insulin granules display reduced microtubule-dependent mobility and are disposed within actin-positive multigranular bodies.* Proc Natl Acad Sci U S A, 2015. **112**(7): p. E667-76.
83. Yau, B., et al., *A fluorescent timer reporter enables sorting of insulin secretory granules by age.* J Biol Chem, 2020. **295**(27): p. 8901-8911.
84. Pasquier, A., et al., *Lysosomal degradation of newly formed insulin granules contributes to β cell failure in diabetes.* Nature communications, 2019. **10**(1): p. 1-14.
85. Schuit, F., P. In't Veld, and D. Pipeleers, *Glucose stimulates proinsulin biosynthesis by a dose-dependent recruitment of pancreatic beta cells.* Proceedings of the National Academy of Sciences, 1988. **85**(11): p. 3865-3869.
86. Riahi, Y., et al., *Autophagy is a major regulator of beta cell insulin homeostasis.* Diabetologia, 2016. **59**(7): p. 1480-1491.
87. Müller, A., et al., *A 4D view on insulin secretory granule turnover in the β‐cell.* Diabetes, Obesity and Metabolism, 2017. **19**: p. 107-114.
88. Orci, L., et al., *Insulin, not C-peptide (proinsulin), is present in crinophagic bodies of the pancreatic B-cell.* The Journal of cell biology, 1984. **98**(1): p. 222-228.
89. Fernández-Díaz, C.M., et al., *Pancreatic β-cell-specific deletion of insulin-degrading enzyme leads to dysregulated insulin secretion and β-cell functional immaturity.* American Journal of Physiology-Endocrinology and Metabolism, 2019. **317**(5): p. E805-E819.
90. Steneberg, P., et al., *The type 2 diabetes–associated gene Ide is required for insulin secretion and suppression of α-synuclein levels in β-cells.* Diabetes, 2013. **62**(6): p. 2004-2014.
91. Marselli, L., et al., *Are we overestimating the loss of beta cells in type 2 diabetes?* Diabetologia, 2014. **57**(2): p. 362-5.
92. Cinti, F., et al., *Evidence of β-cell dedifferentiation in human type 2 diabetes.* The Journal of Clinical Endocrinology & Metabolism, 2016. **101**(3): p. 1044-1054.
93. Obermüller, S., et al., *Defective secretion of islet hormones in chromogranin-B deficient mice.* PloS one, 2010. **5**(1): p. e8936.
94. Burns, C.H., et al., *Pancreatic β-Cell–Specific Deletion of VPS41 Causes Diabetes Due to Defects in Insulin Secretion.* Diabetes, 2021. **70**(2): p. 436-448.
95. White, M.G., J.A. Shaw, and R. Taylor, *Type 2 Diabetes: The Pathologic Basis of Reversible beta-Cell Dysfunction.* Diabetes Care, 2016. **39**(11): p. 2080-2088.
96. Nichols, C.G. and M.S. Remedi, *The diabetic beta-cell: hyperstimulated vs. hyperexcited.* Diabetes Obes Metab, 2012. **14 Suppl 3**: p. 129-35.

97. Kebede, M.A., et al., *SORCS1 is necessary for normal insulin secretory granule biogenesis in metabolically stressed beta cells.* J Clin Invest, 2014. **124**(10): p. 4240-56.
98. Liu, M., et al., *Normal and defective pathways in biogenesis and maintenance of the insulin storage pool.* Journal of Clinical Investigation, 2021. **131**(2): p. e142240.
99. Docherty, K., J. Hutton, and D. Steiner, *Cathepsin B-related proteases in the insulin secretory granule.* Journal of Biological Chemistry, 1984. **259**(10): p. 6041-6044.
100. Kuliawat, R., et al., *Differential sorting of lysosomal enzymes out of the regulated secretory pathway in pancreatic beta-cells.* J Cell Biol, 1997. **137**(3): p. 595-608.
101. Naik, A.R., et al., *vH+-ATPase-induced intracellular acidification is critical to glucose-stimulated insulin secretion in beta cells.* Histochemistry and cell biology, 2020. **153**(4): p. 279-285.
102. Chimienti, F., et al., *Identification and cloning of a β-cell–specific zinc transporter, ZnT-8, localized into insulin secretory granules.* Diabetes, 2004. **53**(9): p. 2330-2337.
103. Wang, Y.-S., et al., *VAMP8, a vesicle-SNARE required for RAB37-mediated exocytosis, possesses a tumor metastasis suppressor function.* Cancer letters, 2018. **437**: p. 79-88.
104. Rindler, M.J., *Carboxypeptidase E, a peripheral membrane protein implicated in the targeting of hormones to secretory granules, co-aggregates with granule content proteins at acidic pH.* Journal of Biological Chemistry, 1998. **273**(47): p. 31180-31185.
105. Stephens, S.B., et al., *The prohormone VGF regulates β cell function via insulin secretory granule biogenesis.* Cell reports, 2017. **20**(10): p. 2480-2489.
106. Hendy, G.N., et al., *Targeted ablation of the chromogranin a (Chga) gene: normal neuroendocrine dense-core secretory granules and increased expression of other granins.* Molecular Endocrinology, 2006. **20**(8): p. 1935-1947.
107. Yoshie, S., et al., *Immunological characterization of chromogranins A and B and secretogranin II in the bovine pancreatic islet.* Histochemistry, 1987. **87**(2): p. 99-106.
108. Bearrows, S.C., et al., *Chromogranin B regulates early-stage insulin granule trafficking from the Golgi in pancreatic islet beta-cells.* J Cell Sci, 2019. **132**(13).
109. Chen, Y., et al., *An efficient two-step subcellular fractionation method for the enrichment of insulin granules from INS-1 cells.* Biophys Rep, 2015. **1**: p. 34-40.
110. Hutton, J., E. Penn, and M. Peshavaria, *Isolation and characterisation of insulin secretory granules from a rat islet cell tumour.* Diabetologia, 1982. **23**(4): p. 365-373.
111. Jones, P.M., T. Saermark, and S.L. Howell, *A small-scale method for the isolation of insulin-containing secretory granules from islets of Langerhans.* Analytical biochemistry, 1987. **166**(1): p. 142-149.
112. Hickey, A.J., et al., *Proteins associated with immunopurified granules from a model pancreatic islet beta-cell system: proteomic snapshot of an endocrine secretory granule.* J Proteome Res, 2009. **8**(1): p. 178-86.

113. Neukam, M., et al., *Purification of age-distinct insulin secretory granules through antigen restriction using the CLIP-tag.* bioRxiv, 2020.
114. Guest, P.C., *Multiplex Sequential Immunoprecipitation of Insulin Secretory Granule Proteins from Radiolabeled Pancreatic Islets.* Methods Mol Biol, 2017. **1546**: p. 177-185.
115. Lee, Y.H., H.T. Tan, and M.C. Chung, *Subcellular fractionation methods and strategies for proteomics.* Proteomics, 2010. **10**(22): p. 3935-56.
116. Ferri, G., et al., *Insulin secretory granules labelled with phogrin-fluorescent proteins show alterations in size, mobility and responsiveness to glucose stimulation in living beta-cells.* Sci Rep, 2019. **9**(1): p. 2890.
117. Giordano, T., et al., *Beta cell chromogranin B is partially segregated in distinct granules and can be released separately from insulin in response to stimulation.* Diabetologia, 2008. **51**(6): p. 997-1007.
118. Ramm, G., et al., *Insulin recruits GLUT4 from specialized VAMP2-carrying vesicles as well as from the dynamic endosomal/trans-Golgi network in rat adipocytes.* Mol Biol Cell, 2000. **11**(12): p. 4079-91.
119. Yasuda, T., et al., *Rim2α determines docking and priming states in insulin granule exocytosis.* Cell metabolism, 2010. **12**(2): p. 117-129.
120. Fan, F., et al., *Exophilin-8 assembles secretory granules for exocytosis in the actin cortex via interaction with RIM-BP2 and myosin-VIIa.* Elife, 2017. **6**: p. e26174.
121. Zhang, K., et al., *CASK, APBA1, and STXBP1 collaborate during insulin secretion.* Molecular and Cellular Endocrinology, 2021. **520**: p. 111076.
122. Tooze, S.A., et al., *Characterization of the immature secretory granule, an intermediate in granule biogenesis.* J Cell Biol, 1991. **115**(6): p. 1491-503.
123. Li, M., et al., *Proteomic analysis of insulin secretory granules in INS-1 cells by protein correlation profiling.* Biophys Rep, 2018. **4**(6): p. 329-338.
124. MacDonald, M.J., et al., *Characterization of phospholipids in insulin secretory granules and mitochondria in pancreatic beta cells and their changes with glucose stimulation.* Journal of Biological Chemistry, 2015. **290**(17): p. 11075-11092.
125. Albrethsen, J., J.P. Goetze, and A.H. Johnsen, *Mining the granule proteome: a potential source of endocrine biomarkers.* Biomark Med, 2015. **9**(3): p. 259-65.
126. Brunner, Y., et al., *Proteomics analysis of insulin secretory granules.* Mol Cell Proteomics, 2007. **6**(6): p. 1007-17.
127. Chandramouli, K. and P.Y. Qian, *Proteomics: challenges, techniques and possibilities to overcome biological sample complexity.* Hum Genomics Proteomics, 2009. **2009**.
128. Rindler, M.J., et al., *Proteomic analysis of pancreatic zymogen granules: identification of new granule proteins.* J Proteome Res, 2007. **6**(8): p. 2978-92.

129. Schvartz, D., et al., *Improved characterization of the insulin secretory granule proteomes.* J Proteomics, 2012. **75**(15): p. 4620-31.
130. Lomedico, P., et al., *The structure and evolution of the two nonallelic rat preproinsulin genes.* Cell, 1979. **18**(2): p. 545-558.
131. Ullrich, A., et al., *Rat insulin genes: construction of plasmids containing the coding sequences.* Science, 1977. **196**(4296): p. 1313-1319.
132. Wasmeier, C. and J.C. Hutton, *Molecular cloning of phogrin, a protein-tyrosine phosphatase homologue localized to insulin secretory granule membranes.* Journal of Biological Chemistry, 1996. **271**(30): p. 18161-18170.
133. Hoflehner, J., et al., *Processing of secretogranin II by prohormone convertases: Importance ofPC1 in generation of secretoneurin.* FEBS letters, 1995. **360**(3): p. 294-298.
134. Laslop, A., et al., *Proteolytic processing of chromogranin B and secretogranin II by prohormone convertases.* Journal of neurochemistry, 1998. **70**(1): p. 374-383.
135. Orci, L., et al., *Direct identification of prohormone conversion site in insulin-secreting cells.* Cell, 1985. **42**(2): p. 671-681.
136. Davidson, H.W., M. Peshavaria, and J.C. Hutton, *Proteolytic conversion of proinsulin into insulin. Identification of a Ca2+-dependent acidic endopeptidase in isolated insulin-secretory granules.* Biochemical Journal, 1987. **246**(2): p. 279-286.
137. Hutton, J.C., H.W. Davidson, and M. Peshavaria, *Proteolytic processing of chromogranin A in purified insulin granules. Formation of a 20 kDa N-terminal fragment (betagranin) by the concerted action of a Ca2+-dependent endopeptidase and carboxypeptidase H (EC 3.4. 17.10).* Biochemical journal, 1987. **244**(2): p. 457-464.
138. Muller, L. and I. Lindberg, *The cell biology of the prohormone convertases PCI and PC2.* Progress in nucleic acid research and molecular biology, 1999. **63**: p. 69-108.
139. Bennett, D.L., et al., *Identification of the type 2 proinsulin processing endopeptidase as PC2, a member of the eukaryote subtilisin family.* Journal of Biological Chemistry, 1992. **267**(21): p. 15229-15236.
140. Guest, P.C., et al., *Molecular heterogeneity and cellular localization of carboxypeptidase H in the islets of Langerhans.* Endocrinology, 1991. **129**(2): p. 734-740.
141. Kim, T., et al., *Chromogranin A, an "on/off" switch controlling dense-core secretory granule biogenesis.* Cell, 2001. **106**(4): p. 499-509.
142. Portela-Gomes, G., et al., *The importance of chromogranin A in the development and function of endocrine pancreas.* Regulatory peptides, 2008. **151**(1-3): p. 19-25.
143. Udupi, V., et al., *Prohormone convertase-1 is essential for conversion of chromogranin A to pancreastatin.* Regulatory peptides, 1999. **83**(2-3): p. 123-127.
144. Schmid, G.M., et al., *Inhibition of insulin secretion by betagranin, an N-terminal chromogranin A fragment.* Journal of Biological Chemistry, 2007. **282**(17): p. 12717-12724.

145. Hutton, J.C., *Insulin secretory granule biogenesis and the proinsulin-processing endopeptidases.* Diabetologia, 1994. **37**(2): p. S48-S56.
146. Davidson, H.W. and J.C. Hutton, *The insulin-secretory-granule carboxypeptidase H. Purification and demonstration of involvement in proinsulin processing.* Biochemical journal, 1987. **245**(2): p. 575-582.
147. Sandberg, M. and L.H. Borg, *Intracellular degradation of insulin and crinophagy are maintained by nitric oxide and cyclo‐oxygenase 2 activity in isolated pancreatic islets.* Biology of the Cell, 2006. **98**(5): p. 307-315.
148. Klumperman, J., et al., *Mannose 6–phosphate receptors are sorted from immature secretory granules via adaptor protein AP-1, clathrin, and syntaxin 6–positive vesicles.* The Journal of cell biology, 1998. **141**(2): p. 359-371.
149. Arvan, P. and D. Castle, *Sorting and storage during secretory granule biogenesis: looking backward and looking forward.* Biochemical Journal, 1998. **332**(3): p. 593-610.
150. Lin, R.C. and R.H. Scheller, *Mechanisms of synaptic vesicle exocytosis.* Annual review of cell and developmental biology, 2000. **16**(1): p. 19-49.
151. Lam, P.P., et al., *Munc18b is a major mediator of insulin exocytosis in rat pancreatic β-cells.* Diabetes, 2013. **62**(7): p. 2416-2428.
152. Iorio, V., et al., *BAG3 regulates formation of the SNARE complex and insulin secretion.* Cell death & disease, 2015. **6**(3): p. e1684-e1684.
153. Gaisano, H.Y., *Recent new insights into the role of SNARE and associated proteins in insulin granule exocytosis.* Diabetes Obes Metab, 2017. **19 Suppl 1**: p. 115-123.
154. Qin, T., et al., *Munc18b increases insulin granule fusion, restoring deficient insulin secretion in type-2 diabetes human and Goto-Kakizaki rat islets with improvement in glucose homeostasis.* EBioMedicine, 2017. **16**: p. 262-274.
155. Regazzi, R., et al., *VAMP‐2 and cellubrevin are expressed in pancreatic beta‐cells and are essential for Ca (2+)‐but not for GTP gamma S‐induced insulin secretion.* The EMBO journal, 1995. **14**(12): p. 2723-2730.
156. Martinez, O. and B. Goud, *Rab proteins.* Biochimica et Biophysica Acta (BBA)-Molecular Cell Research, 1998. **1404**(1-2): p. 101-112.
157. Cheviet, S.v., et al., *The Rab-binding protein Noc2 is associated with insulin-containing secretory granules and is essential for pancreatic β-cell exocytosis.* Molecular Endocrinology, 2004. **18**(1): p. 117-126.
158. Wang, Z. and D.C. Thurmond, *Mechanisms of biphasic insulin-granule exocytosis–roles of the cytoskeleton, small GTPases and SNARE proteins.* Journal of cell science, 2009. **122**(7): p. 893-903.

159. Mizuno, K., et al., *Granuphilin exclusively mediates functional granule docking to the plasma membrane.* Scientific reports, 2016. **6**(1): p. 1-12.
160. Hatanaka, M., et al., *Wolfram syndrome 1 gene (WFS1) product localizes to secretory granules and determines granule acidification in pancreatic β-cells.* Human molecular genetics, 2011. **20**(7): p. 1274-1284.
161. Barg, S., et al., *Priming of insulin granules for exocytosis by granular Cl− uptake and acidification.* Journal of cell science, 2001. **114**(11): p. 2145-2154.
162. Gharanei, S., et al., *Vacuolar-type H+-ATPase V1A subunit is a molecular partner of Wolfram syndrome 1 (WFS1) protein, which regulates its expression and stability.* Human molecular genetics, 2013. **22**(2): p. 203-217.
163. Heaslip, A.T., et al., *Cytoskeletal dependence of insulin granule movement dynamics in INS-1 beta-cells in response to glucose.* PloS one, 2014. **9**(10): p. e109082.
164. Wang, B., et al., *The adaptor protein APPL2 controls glucose-stimulated insulin secretion via F-actin remodeling in pancreatic β-cells.* Proceedings of the National Academy of Sciences, 2020. **117**(45): p. 28307-28315.
165. Ghiasi, S.M., et al., *Endoplasmic reticulum chaperone glucose-regulated protein 94 is essential for proinsulin handling.* Diabetes, 2019. **68**(4): p. 747-760.
166. Varghese, R., et al., *Comparative analysis of mammalian stanniocalcin genes.* Endocrinology, 1998. **139**(11): p. 4714-4725.
167. Ellard, J.P., et al., *The respiratory effects of stanniocalcin-1 (STC-1) on intact mitochondria and cells: STC-1 uncouples oxidative phosphorylation and its actions are modulated by nucleotide triphosphates.* Molecular and cellular endocrinology, 2007. **264**(1-2): p. 90-101.
168. Iversen, P., D. Sorensen, and H. Benestad, *Inhibitors of angiogenesis selectively reduce the malignant cell load in rodent models of human myeloid leukemias.* Leukemia, 2002. **16**(3): p. 376-381.
169. Zaidi, D., et al., *Stanniocalcin-1 co-localizes with insulin in the pancreatic islets.* International Scholarly Research Notices, 2012. **2012**.
170. Vakilian, M., Y. Tahamtani, and K. Ghaedi, *A review on insulin trafficking and exocytosis.* Gene, 2019. **706**: p. 52-61.
171. Olofsson, C.S., et al., *Fast insulin secretion reflects exocytosis of docked granules in mouse pancreatic B-cells.* Pflugers Arch, 2002. **444**(1-2): p. 43-51.
172. Olofsson, C.S., et al., *Palmitate increases L‐type Ca2+ currents and the size of the readily releasable granule pool in mouse pancreatic β‐cells.* The Journal of physiology, 2004. **557**(3): p. 935-948.
173. Pottekat, A., et al., *Insulin biosynthetic interaction network component, TMEM24, facilitates insulin reserve pool release.* Cell reports, 2013. **4**(5): p. 921-930.

174. Gandasi, N.R., et al., *Glucose-dependent granule docking limits insulin secretion and is decreased in human type 2 diabetes.* Cell metabolism, 2018. **27**(2): p. 470-478. e4.
175. Hao, M., et al., *Regulation of two insulin granule populations within the reserve pool by distinct calcium sources.* Journal of cell science, 2005. **118**(24): p. 5873-5884.
176. Gaisano, H.Y., *Here come the newcomer granules, better late than never.* Trends Endocrinol Metab, 2014. **25**(8): p. 381-8.
177. Zhu, D., et al., *Syntaxin-3 regulates newcomer insulin granule exocytosis and compound fusion in pancreatic beta cells.* Diabetologia, 2013. **56**(2): p. 359-369.
178. Pedersen, M.G. and A. Sherman, *Newcomer insulin secretory granules as a highly calcium-sensitive pool.* Proceedings of the National Academy of Sciences, 2009. **106**(18): p. 7432-7436.
179. Kreutzberger, A.J., et al., *Distinct insulin granule subpopulations implicated in the secretory pathology of diabetes types 1 and 2.* Elife, 2020. **9**: p. e62506.
180. Hou, N., et al., *Preferential release of newly synthesized insulin assessed by a multi-label reporter system using pancreatic beta-cell line MIN6.* PLoS One, 2012. **7**(10): p. e47921.
181. Hays, L.B., et al., *Intragranular targeting of syncollin, but not a syncollinGFP chimera, inhibits regulated insulin exocytosis in pancreatic beta-cells.* J Endocrinol, 2005. **185**(1): p. 57-67.
182. Gauthier, D.J., et al., *Flow cytometry‐assisted purification and proteomic analysis of the corticotropes dense‐core secretory granules.* Proteomics, 2008. **8**(18): p. 3848-3861.
183. Macklin, A., S. Khan, and T. Kislinger, *Recent advances in mass spectrometry based clinical proteomics: applications to cancer research.* Clinical Proteomics, 2020. **17**: p. 1-25.
184. Yates, J.R., C.I. Ruse, and A. Nakorchevsky, *Proteomics by mass spectrometry: approaches, advances, and applications.* Annual review of biomedical engineering, 2009. **11**: p. 49-79.
185. Timp, W. and G. Timp, *Beyond mass spectrometry, the next step in proteomics.* Science advances, 2020. **6**(2): p. eaax8978.
186. Swaminathan, J., et al., *Highly parallel single-molecule identification of proteins in zeptomole-scale mixtures.* Nature biotechnology, 2018. **36**(11): p. 1076-1082.
187. Cao, M., et al., *PICK1 and ICA69 control insulin granule trafficking and their deficiencies lead to impaired glucose tolerance.* PLoS Biol, 2013. **11**(4): p. e1001541.
188. Li, H., et al., *BIG3 inhibits insulin granule biogenesis and insulin secretion.* EMBO Rep, 2014. **15**(6): p. 714-22.
189. Mezza, T., et al., *Increased beta-Cell Workload Modulates Proinsulin-to-Insulin Ratio in Humans.* Diabetes, 2018. **67**(11): p. 2389-2396.
190. Pradhan, A.D., et al., *Insulin, proinsulin, proinsulin:insulin ratio, and the risk of developing type 2 diabetes mellitus in women.* Am J Med, 2003. **114**(6): p. 438-44.

191. Brackeva, B., et al., *Potential of UCHL1 as biomarker for destruction of pancreatic beta cells.* Journal of proteomics, 2015. **117**: p. 156-167.
192. Martens, G., *Species-related differences in the proteome of rat and human pancreatic beta cells.* Journal of diabetes research, 2015. **2015**.
193. Brackeva, B., et al., *Quantitative proteomics of rat and human pancreatic beta cells.* Data in brief, 2015. **3**: p. 234-239.
194. Clardy, S.M., et al., *Rapid, high efficiency isolation of pancreatic ss-cells.* Sci Rep, 2015. **5**: p. 13681.
195. Jayaraman, S., *A novel method for the detection of viable human pancreatic beta cells by flow cytometry using fluorophores that selectively detect labile zinc, mitochondrial membrane potential and protein thiols.* Cytometry A, 2008. **73**(7): p. 615-25.
196. Lukowiak, B., et al., *Identification and purification of functional human beta-cells by a new specific zinc-fluorescent probe.* J Histochem Cytochem, 2001. **49**(4): p. 519-28.
197. Smelt, M.J., et al., *Pancreatic beta-cell purification by altering FAD and NAD(P)H metabolism.* Exp Diabetes Res, 2008. **2008**: p. 165360.
198. Van De Winkel, M. and D. Pipeleers, *Autofluorescence-activated cell sorting of pancreatic islet cells: purification of insulin-containing B-cells according to glucose-induced changes in cellular redox state.* Biochem Biophys Res Commun, 1983. **114**(2): p. 835-42.
199. Seino, S., et al., *β‐Cell signalling and insulin secretagogues: A path for improved diabetes therapy.* Diabetes, Obesity and Metabolism, 2017. **19**: p. 22-29.
200. Germanos, M., et al., *Inside the Insulin Secretory Granule.* Metabolites, 2021. **11**(8).
201. Suckale, J. and M. Solimena, *The insulin secretory granule as a signaling hub.* Trends Endocrinol Metab, 2010. **21**(10): p. 599-609.
202. Norris, N., et al., *Optimised proteomic analysis of insulin granules from MIN6 cells identifies Scamp3, a novel regulator of insulin secretion and content.* Diabetes, 2024: p. db240355.
203. Honka, M.-J., et al., *Insulin-stimulated glucose uptake in skeletal muscle, adipose tissue and liver: a positron emission tomography study.* European journal of endocrinology, 2018. **178**(5): p. 523-531.
204. Gandasi, N.R., et al., *Glucose-Dependent Granule Docking Limits Insulin Secretion and Is Decreased in Human Type 2 Diabetes.* Cell Metab, 2018. **27**(2): p. 470-478 e4.
205. Ramzy, A., A. Asadi, and T.J. Kieffer, *Revisiting Proinsulin Processing: Evidence That Human beta-Cells Process Proinsulin With Prohormone Convertase (PC) 1/3 but Not PC2.* Diabetes, 2020. **69**(7): p. 1451-1462.
206. Arvan, P. and D. Castle, *Protein sorting and secretion granule formation in regulated secretory cells.* Trends Cell Biol, 1992. **2**(11): p. 327-31.

207. Merriman, C. and D. Fu, *Down-regulation of the islet-specific zinc transporter-8 (ZnT8) protects human insulinoma cells against inflammatory stress.* J Biol Chem, 2019. **294**(45): p. 16992-17006.
208. Bearrows, S.C., et al., *Chromogranin B regulates early-stage insulin granule trafficking from the Golgi in pancreatic islet β-cells.* Journal of cell science, 2019. **132**(13): p. jcs231373.
209. Cao, M., et al., *PICK1 and ICA69 control insulin granule trafficking and their deficiencies lead to impaired glucose tolerance.* PLoS Biol, 2013. **11**(4): p. e1001541.
210. Sargsyan, E. and P. Bergsten, *Lipotoxicity is glucose-dependent in INS-1E cells but not in human islets and MIN6 cells.* Lipids in health and disease, 2011. **10**(1): p. 1-7.
211. Chowdhury, A., et al., *Functional differences between aggregated and dispersed insulin-producing cells.* Diabetologia, 2013. **56**: p. 1557-1568.
212. Harney, D.J., et al., *Small-protein Enrichment Assay Enables the Rapid, Unbiased Analysis of Over 100 Low Abundance Factors from Human Plasma.* Mol Cell Proteomics, 2019. **18**(9): p. 1899-1915.
213. Bruderer, R., et al., *Extending the limits of quantitative proteome profiling with data-independent acquisition and application to acetaminophen-treated three-dimensional liver microtissues.* Mol Cell Proteomics, 2015. **14**(5): p. 1400-10.
214. Demichev, V., et al., *DIA-NN: neural networks and interference correction enable deep proteome coverage in high throughput.* Nat Methods, 2020. **17**(1): p. 41-44.
215. Okita, N., et al., *Modified Western blotting for insulin and other diabetes-associated peptide hormones.* Scientific reports, 2017. **7**(1): p. 6949.
216. Cottle, L., et al., *Structural and functional polarisation of human pancreatic beta cells in islets from organ donors with and without type 2 diabetes.* Diabetologia, 2021. **64**: p. 618-629.
217. Schindelin, J., et al., *Fiji: an open-source platform for biological-image analysis.* Nature methods, 2012. **9**(7): p. 676-682.
218. Gatto, L. and K.S. Lilley, *MSnbase-an R/Bioconductor package for isobaric tagged mass spectrometry data visualization, processing and quantitation.* Bioinformatics, 2012. **28**(2): p. 288-9.
219. Gatto, L., et al., *Mass-spectrometry-based spatial proteomics data analysis using pRoloc and pRolocdata.* Bioinformatics, 2014. **30**(9): p. 1322-4.
220. Breckels, L.M., et al., *A Bioconductor workflow for processing and analysing spatial proteomics data.* F1000Res, 2016. **5**: p. 2926.
221. Huber, W., et al., *Variance stabilization applied to microarray data calibration and to the quantification of differential expression.* Bioinformatics, 2002. **18 Suppl 1**: p. S96-104.
222. Bates, D., et al., *Fitting Linear Mixed-Effects Models Using lme4.* Journal of Statistical Software, 2015. **67**(1): p. 1-48.

223. Rajpal, G., et al., *Action of protein disulfide isomerase on proinsulin exit from endoplasmic reticulum of pancreatic beta-cells.* J Biol Chem, 2012. **287**(1): p. 43-47.
224. Lawson, R., W. Maret, and C. Hogstrand, *ZnT8 haploinsufficiency impacts MIN6 cell zinc content and β-cell phenotype via ZIP-ZnT8 coregulation.* International journal of molecular sciences, 2019. **20**(21): p. 5485.
225. Lukinius, A., et al., *Co-localization of islet amyloid polypeptide and insulin in the B cell secretory granules of the human pancreatic islets.* Diabetologia, 1989. **32**: p. 240-244.
226. Xiong, Q.Y., et al., *Key proteins involved in insulin vesicle exocytosis and secretion.* Biomed Rep, 2017. **6**(2): p. 134-139.
227. Torrejon-Escribano, B., et al., *Glucose-dependent changes in SNARE protein levels in pancreatic beta-cells.* Endocrinology, 2011. **152**(4): p. 1290-9.
228. Waselle, L., et al., *Involvement of the Rab27 binding protein Slac2c/MyRIP in insulin exocytosis.* Mol Biol Cell, 2003. **14**(10): p. 4103-13.
229. Brown, H., et al., *Synaptotagmin III isoform is compartmentalized in pancreatic beta-cells and has a functional role in exocytosis.* Diabetes, 2000. **49**(3): p. 383-91.
230. Andersson, S.A., et al., *Reduced insulin secretion correlates with decreased expression of exocytotic genes in pancreatic islets from patients with type 2 diabetes.* Molecular and cellular endocrinology, 2012. **364**(1-2): p. 36-45.
231. Bakhti, M., et al., *Synaptotagmin-13 orchestrates pancreatic endocrine cell egression and islet morphogenesis.* Nature Communications, 2022. **13**(1): p. 4540.
232. Yau, B., et al., *Proteomic pathways to metabolic disease and type 2 diabetes in the pancreatic islet.* IScience, 2021. **24**(10).
233. Li, M., et al., *VAMP4 regulates insulin levels by targeting secretory granules to lysosomes.* Journal of Cell Biology, 2022. **221**(10): p. e202110164.
234. Moreau, K., M. Renna, and D.C. Rubinsztein, *Connections between SNAREs and autophagy.* Trends in biochemical sciences, 2013. **38**(2): p. 57-63.
235. Menegaz, D., et al., *Mechanism and effects of pulsatile GABA secretion from cytosolic pools in the human beta cell.* Nature metabolism, 2019. **1**(11): p. 1110-1126.
236. Wu, T.T. and J.D. Castle, *Tyrosine phosphorylation of selected secretory carrier membrane proteins, SCAMP1 and SCAMP3, and association with the EGF receptor.* Molecular biology of the cell, 1998. **9**(7): p. 1661-1674.
237. Dong, G., et al., *Palmitoylation couples insulin hypersecretion with β cell failure in diabetes.* Cell metabolism, 2023. **35**(2): p. 332-344. e7.
238. Castle, A. and D. Castle, *Ubiquitously expressed secretory carrier membrane proteins (SCAMPs) 1-4 mark different pathways and exhibit limited constitutive trafficking to and from the cell surface.* Journal of Cell Science, 2005. **118**(16): p. 3769-3780.

239. Fernandez-Chacon, R. and T.C. Südhof, *Novel SCAMPs lacking NPF repeats: ubiquitous and synaptic vesicle-specific forms implicate SCAMPs in multiple membrane-trafficking functions.* Journal of Neuroscience, 2000. **20**(21): p. 7941-7950.
240. Liao, H., et al., *Nonredundant function of secretory carrier membrane protein isoforms in dense core vesicle exocytosis.* American Journal of Physiology-Cell Physiology, 2008. **294**(3): p. C797-C809.
241. Atla, G., et al., *Genetic regulation of RNA splicing in human pancreatic islets.* bioRxiv, 2021: p. 2021.11. 11.468254.
242. Waanders, L.F., et al., *Quantitative proteomic analysis of single pancreatic islets.* Proceedings of the National Academy of Sciences, 2009. **106**(45): p. 18902-18907.
243. Costanzo, M.C., et al., *The Type 2 Diabetes Knowledge Portal: An open access genetic resource dedicated to type 2 diabetes and related traits.* Cell metabolism, 2023. **35**(4): p. 695-710. e6.
244. Zhang, W., et al., *Munc-18 associates with syntaxin and serves as a negative regulator of exocytosis in the pancreatic β-cell.* Journal of Biological Chemistry, 2000. **275**(52): p. 41521-41527.
245. Fujimoto, K., et al., *Piccolo, a Ca2+ sensor in pancreatic β-cells: involvement of cAMP-GEFII· Rim2· Piccolo complex in cAMP-dependent exocytosis.* Journal of Biological Chemistry, 2002. **277**(52): p. 50497-50502.
246. Thomas‐Reetz, A.C. and P. De Camilli, *A role for synaptic vesicles in non‐neuronal cells: clues from pancreatic β cells and from chromaffin cells.* The FASEB Journal, 1994. **8**(2): p. 209-216.
247. Chessler, S.D., et al., *Expression of the vesicular inhibitory amino acid transporter in pancreatic islet cells: distribution of the transporter within rat islets.* Diabetes, 2002. **51**(6): p. 1763-1771.
248. Wheeler, M.B., et al., *Characterization of SNARE protein expression in beta cell lines and pancreatic islets.* Endocrinology, 1996. **137**(4): p. 1340-1348.
249. Thiel, G., *Synapsin I, synapsin II, and synaptophysin: marker proteins of synaptic vesicles.* Brain Pathology, 1993. **3**(1): p. 87-95.
250. Alder, J., et al., *Overexpression of synaptophysin enhances neurotransmitter secretion at Xenopus neuromuscular synapses.* Journal of Neuroscience, 1995. **15**(1): p. 511-519.
251. Pennuto, M., et al., *Fluorescence resonance energy transfer detection of synaptophysin I and vesicle-associated membrane protein 2 interactions during exocytosis from single live synapses.* Molecular biology of the cell, 2002. **13**(8): p. 2706-2717.

252. Krishnakumar, S.S., et al., *A conformational switch in complexin is required for synaptotagmin to trigger synaptic fusion.* Nature structural & molecular biology, 2011. **18**(8): p. 934-940.
253. Gaisano, H.Y., *Recent new insights into the role of SNARE and associated proteins in insulin granule exocytosis.* Diabetes, Obesity and Metabolism, 2017. **19**: p. 115-123.
254. Oberhauser, L., et al., *Glucolipotoxicity promotes the capacity of the glycerolipid/NEFA cycle supporting the secretory response of pancreatic beta cells.* Diabetologia, 2022: p. 1-16.
255. Nolan, C.J., et al., *Fatty acid signaling in the β-cell and insulin secretion.* Diabetes, 2006. **55**(Supplement_2): p. S16-S23.
256. Dobbins, R.L., et al., *Circulating fatty acids are essential for efficient glucose-stimulated insulin secretion after prolonged fasting in humans.* Diabetes, 1998. **47**(10): p. 1613-1618.
257. Stein, D.T., et al., *Essentiality of circulating fatty acids for glucose-stimulated insulin secretion in the fasted rat.* The Journal of clinical investigation, 1996. **97**(12): p. 2728-2735.
258. Kebede, M., et al., *The fatty acid receptor GPR40 plays a role in insulin secretion in vivo after high-fat feeding.* Diabetes, 2008. **57**(9): p. 2432-2437.
259. Chalkley, S., et al., *NEFA elevation during a hyperglycaemic clamp enhances insulin secretion.* Diabetic medicine, 1998. **15**(4): p. 327-333.
260. Prentki, M., et al., *Nutrient-induced metabolic stress, adaptation, detoxification, and toxicity in the pancreatic β-cell.* Diabetes, 2020. **69**(3): p. 279-290.
261. Prentki, M., B.E. Corkey, and S.M. Madiraju, *Lipid-associated metabolic signalling networks in pancreatic beta cell function.* Diabetologia, 2020. **63**(1): p. 10-20.
262. Brun, T., et al., *Glucose regulates acetyl-CoA carboxylase gene expression in a pancreatic beta-cell line (INS-1).* Journal of Biological Chemistry, 1993. **268**(25): p. 18905-18911.
263. Larsson, O., et al., *Activation of the ATP-sensitive K+ Channel by Long Chain Acyl-CoA: A ROLE IN MODULATION OF PANCREATIC β-CELL GLUCOSE SENSITIVITY (∗).* Journal of Biological Chemistry, 1996. **271**(18): p. 10623-10626.
264. Yaney, G.C., H.M. Korchak, and B.E. Corkey, *Long-chain acyl coa regulation of protein kinase c and fatty acid potentiation of glucose-stimulated insulin secretion in clonalβ-cells.* Endocrinology, 2000. **141**(6): p. 1989-1998.
265. Poursharifi, P., S.R.M. Madiraju, and M. Prentki, *Monoacylglycerol signalling and ABHD6 in health and disease.* Diabetes, Obesity and Metabolism, 2017. **19**: p. 76-89.
266. Yaney, G.C., et al., *Potentiation of insulin secretion by phorbol esters is mediated by PKC-α and nPKC isoforms.* American Journal of Physiology-Endocrinology and Metabolism, 2002. **283**(5): p. E880-E888.
267. Oberhauser, L. and P. Maechler, *Lipid-induced adaptations of the pancreatic beta-cell to glucotoxic conditions sustain insulin secretion.* International Journal of Molecular Sciences, 2021. **23**(1): p. 324.

268. Jonas, J.-C., et al., *Chronic hyperglycemia triggers loss of pancreatic β cell differentiation in an animal model of diabetes.* Journal of Biological Chemistry, 1999. **274**(20): p. 14112-14121.

269. Garvey, W.T., et al., *The effect of insulin treatment on insulin secretion and insulin action in type II diabetes mellitus.* Diabetes, 1985. **34**(3): p. 222-234.

270. Butler, A.E., et al., *β-cell deficit and increased β-cell apoptosis in humans with type 2 diabetes.* Diabetes, 2003. **52**(1): p. 102-110.

271. Rahier, J., et al., *Pancreatic β-cell mass in European subjects with type 2 diabetes.* Diabetes, Obesity and Metabolism, 2008. **10**: p. 32-42.

272. Pratley, R. and C. Weyer, *The role of impaired early insulin secretion in the pathogenesis of type II diabetes mellitus.* Diabetologia, 2001. **44**: p. 929-945.

273. Weir, G.C., *Glucolipotoxicity, β-cells, and diabetes: the emperor has no clothes.* Diabetes, 2020. **69**(3): p. 273-278.

274. Carpentier, A., et al., *Acute enhancement of insulin secretion by FFA in humans is lost with prolonged FFA elevation.* American Journal of Physiology-Endocrinology and Metabolism, 1999. **276**(6): p. E1055-E1066.

275. Paolisso, G., et al., *Opposite effects of short-and long-term fatty acid infusion on insulin secretion in healthy subjects.* Diabetologia, 1995. **38**: p. 1295-1299.

276. Giacca, A., et al., *Lipid-induced pancreatic β-cell dysfunction: focus on in vivo studies.* American Journal of Physiology-Endocrinology and Metabolism, 2011. **300**(2): p. E255-E262.

277. Carpentier, A.C., et al., *Plasma nonesterified fatty acid intolerance and hyperglycemia are associated with intravenous lipid-induced impairment of insulin sensitivity and disposition index.* The Journal of Clinical Endocrinology & Metabolism, 2010. **95**(3): p. 1256-1264.

278. Watson, M.L., et al., *Chronic effects of palmitate overload on nutrient-induced insulin secretion and autocrine signalling in pancreatic MIN6 beta cells.* PloS one, 2011. **6**(10): p. e25975.

279. Kristinsson, H., et al., *FFAR1 is involved in both the acute and chronic effects of palmitate on insulin secretion.* Endocrinology, 2013. **154**(11): p. 4078-4088.

280. Kato, T., et al., *Palmitate impairs and eicosapentaenoate restores insulin secretion through regulation of SREBP-1c in pancreatic islets.* Diabetes, 2008. **57**(9): p. 2382-2392.

281. Thams, P. and K. Capito, *Differential mechanisms of glucose and palmitate in augmentation of insulin secretion in mouse pancreatic islets.* Diabetologia, 2001. **44**: p. 738-746.

282. Roomp, K., et al., *Combined lipidomic and proteomic analysis of isolated human islets exposed to palmitate reveals time-dependent changes in insulin secretion and lipid metabolism.* PloS one, 2017. **12**(4): p. e0176391.

283. Zhou, Y. and V. Grill, *Long term exposure to fatty acids and ketones inhibits B-cell functions in human pancreatic islets of Langerhans.* The Journal of Clinical Endocrinology & Metabolism, 1995. **80**(5): p. 1584-1590.
284. Boden, G., *Obesity and free fatty acids.* Endocrinology and metabolism clinics of North America, 2008. **37**(3): p. 635-646.
285. Lytrivi, M., et al., *Recent insights into mechanisms of β-cell lipo-and glucolipotoxicity in type 2 diabetes.* Journal of molecular biology, 2020. **432**(5): p. 1514-1534.
286. Vessby, B., et al., *The risk to develop NIDDM is related to the fatty acid composition of the serum cholesterol esters.* Diabetes, 1994. **43**(11): p. 1353-1357.
287. Wang, L., et al., *Plasma fatty acid composition and incidence of diabetes in middle-aged adults: the Atherosclerosis Risk in Communities (ARIC) Study.* The American journal of clinical nutrition, 2003. **78**(1): p. 91-98.
288. Forouhi, N.G., et al., *Differences in the prospective association between individual plasma phospholipid saturated fatty acids and incident type 2 diabetes: the EPIC-InterAct case-cohort study.* The lancet Diabetes & endocrinology, 2014. **2**(10): p. 810-818.
289. Kelpe, C.L., et al., *Palmitate inhibition of insulin gene expression is mediated at the transcriptional level via ceramide synthesis.* Journal of Biological Chemistry, 2003. **278**(32): p. 30015-30021.
290. Olofsson, C.S., et al., *Long-term exposure to glucose and lipids inhibits glucose-induced insulin secretion downstream of granule fusion with plasma membrane.* Diabetes, 2007. **56**(7): p. 1888-1897.
291. Nie, Y., et al., *Negative effects of cyclic palmitate treatment on glucose responsiveness and insulin production in mouse insulinoma Min6 cells Are Reversible.* DNA and Cell Biology, 2019. **38**(4): p. 395-403.
292. Okamura, D.M., et al., *CD36 regulates oxidative stress and inflammation in hypercholesterolemic CKD.* Journal of the American Society of Nephrology, 2009. **20**(3): p. 495-505.
293. Ly, L.D., et al., *Oxidative stress and calcium dysregulation by palmitate in type 2 diabetes.* Experimental & molecular medicine, 2017. **49**(2): p. e291-e291.
294. Zhao, Y., et al., *Linoleic acid stimulates [Ca2+] i increase in rat pancreatic beta-cells through both membrane receptor-and intracellular metabolite-mediated pathways.* PLoS One, 2013. **8**(4): p. e60255.
295. Biden, T.J., et al., *Lipotoxic endoplasmic reticulum stress, β cell failure, and type 2 diabetes mellitus.* Trends in Endocrinology & Metabolism, 2014. **25**(8): p. 389-398.
296. Petcherski, A., et al., *Elamipretide promotes mitophagosome formation and prevents its reduction induced by nutrient excess in INS1 β-cells.* Journal of molecular biology, 2018. **430**(24): p. 4823-4833.

297. Assali, E.A., et al., *Nanoparticle‐mediated lysosomal reacidification restores mitochondrial turnover and function in β cells under lipotoxicity.* The FASEB Journal, 2019. **33**(3): p. 4154.
298. Fujitani, Y., et al., *β-cell autophagy: A novel mechanism regulating β-cell function and mass-Lessons from β-cell-specific Atg7-deficient mice.* Islets, 2009. **1**(2): p. 151-153.
299. Mir, S.U., et al., *Inhibition of autophagic turnover in β-cells by fatty acids and glucose leads to apoptotic cell death.* Journal of biological chemistry, 2015. **290**(10): p. 6071-6085.
300. Ritchie, M.E., et al., *limma powers differential expression analyses for RNA-sequencing and microarray studies.* Nucleic acids research, 2015. **43**(7): p. e47-e47.
301. Valikangas, T., T. Suomi, and L.L. Elo, *A systematic evaluation of normalization methods in quantitative label-free proteomics.* Brief Bioinform, 2018. **19**(1): p. 1-11.
302. Martino, L., et al., *Palmitate activates autophagy in INS-1E β-cells and in isolated rat and human pancreatic islets.* PloS one, 2012. **7**(5): p. e36188.
303. Szklarczyk, D., et al., *STRING v11: protein-protein association networks with increased coverage, supporting functional discovery in genome-wide experimental datasets.* Nucleic Acids Res, 2019. **47**(D1): p. D607-D613.
304. Mandic, S.A., et al., *Munc18-1 and Munc18-2 proteins modulate β-cell Ca2+ sensitivity and kinetics of insulin exocytosis differently.* Journal of Biological Chemistry, 2011. **286**(32): p. 28026-28040.
305. Drizyte-Miller, K., et al., *The small GTPase Rab32 resides on lysosomes to regulate mTORC1 signaling.* Journal of cell science, 2020. **133**(11): p. jcs236661.
306. Horii, T., et al., *Lipid droplet accumulation in β cells in patients with type 2 diabetes is associated with insulin resistance, hyperglycemia and β cell dysfunction involving decreased insulin granules.* Frontiers in Endocrinology, 2022. **13**: p. 996716.
307. Liu, M., et al., *Normal and defective pathways in biogenesis and maintenance of the insulin storage pool.* The Journal of Clinical Investigation, 2021. **131**(2).
308. Rorsman, P. and F.M. Ashcroft, *Pancreatic beta-Cell Electrical Activity and Insulin Secretion: Of Mice and Men.* Physiol Rev, 2018. **98**(1): p. 117-214.
309. Tong, X., et al., *Lipid droplets' role in the regulation of β-Cell function and β-Cell demise in type 2 diabetes.* Endocrinology, 2022. **163**(3): p. bqac007.
310. Emdin, S., et al., *Role of zinc in insulin biosynthesis: some possible zinc-insulin interactions in the pancreatic B-cell.* Diabetologia, 1980. **19**: p. 174-182.
311. May, A.P., S.W. Whiteheart, and W.I. Weis, *Unraveling the mechanism of the vesicle transport ATPase NSF, the N-ethylmaleimide-sensitive factor.* Journal of Biological Chemistry, 2001. **276**(25): p. 21991-21994.

312. Zhou, Y., et al., *RILP restricts insulin secretion through mediating lysosomal degradation of proinsulin.* Diabetes, 2020. **69**(1): p. 67-82.
313. Regazzi, R., et al., *Expression, localization and functional role of small GTPases of the Rab3 family in insulin-secreting cells.* Journal of Cell Science, 1996. **109**(9): p. 2265-2273.
314. Tomas, A., et al., *Munc 18‐1 and granuphilin collaborate during insulin granule exocytosis.* Traffic, 2008. **9**(5): p. 813-832.
315. Noushmehr, H., et al., *Fatty acid translocase (FAT/CD36) is localized on insulin-containing granules in human pancreatic β-cells and mediates fatty acid effects on insulin secretion.* Diabetes, 2005. **54**(2): p. 472-481.
316. Matthews, D., et al., *The half‐life of endogenous insulin and C‐peptide in man assessed by somatostatin suppression.* Clinical endocrinology, 1985. **23**(1): p. 71-79.
317. Tomasi, T., et al., *Insulin half-life in normal and diabetic subjects.* Proceedings of the Society for Experimental Biology and Medicine, 1967. **126**(1): p. 315-317.
318. Metz, S., et al., *Modulation of insulin secretion from normal rat islets by inhibitors of the post-translational modifications of GTP-binding proteins.* Biochemical Journal, 1993. **295**(1): p. 31-40.
319. Yang, C., et al., *Regulation of insulin secretion by the post-translational modifications.* Frontiers in Cell and Developmental Biology, 2023. **11**: p. 1217189.
320. Guthrie, R.A. and D.W. Guthrie, *Pathophysiology of diabetes mellitus.* Critical care nursing quarterly, 2004. **27**(2): p. 113-125.
321. Lee, M.-S., *Role of islet β cell autophagy in the pathogenesis of diabetes.* Trends in Endocrinology & Metabolism, 2014. **25**(12): p. 620-627.
322. Jaisson, S. and P. Gillery, *Impaired proteostasis: role in the pathogenesis of diabetes mellitus.* Diabetologia, 2014. **57**: p. 1517-1527.
323. Kim, N.H., et al., *Serum insulin, proinsulin and proinsulin/insulin ratio in type 2 diabetic patients: as an index of β-cell function or insulin resistance.* The Korean journal of internal medicine, 2000. **15**(3): p. 195.
324. Care, D., *Standards of medical care in diabetes 2019.* Diabetes Care, 2019. **42**(Suppl 1): p. S124-38.
325. Pastors, J.G., et al., *The evidence for the effectiveness of medical nutrition therapy in diabetes management.* Diabetes care, 2002. **25**(3).
326. Feingold, K.R., *Oral and injectable (non-insulin) pharmacological agents for the treatment of type 2 diabetes.* Endotext [Internet], 2022.
327. Ashcroft, S.J. and F.M. Ashcroft, *The sulfonylurea receptor.* Biochimica et Biophysica Acta (BBA)-Molecular Cell Research, 1992. **1175**(1): p. 45-59.

328. Panten, U., et al., *Control of insulin secretion by sulfonylureas, meglitinide and diazoxide in relation to their binding to the sulfonylurea receptor in pancreatic islets.* Biochemical pharmacology, 1989. **38**(8): p. 1217-1229.
329. Sheikh, A., *Direct cardiovascular effects of glucagon like peptide-1.* Diabetology & Metabolic Syndrome, 2013. **5**: p. 1-13.
330. Andersen, E.S., C.F. Deacon, and J.J. Holst, *Do we know the true mechanism of action of the DPP‐4 inhibitors?* Diabetes, Obesity and Metabolism, 2018. **20**(1): p. 34-41.
331. Fonseca, V., et al., *Addition of vildagliptin to insulin improves glycaemic control in type 2 diabetes.* Diabetologia, 2007. **50**: p. 1148-1155.
332. Gallwitz, B., *Clinical use of DPP-4 inhibitors.* Frontiers in endocrinology, 2019. **10**: p. 389.
333. Cordelieres, F.P. and S. Bolte. *JACoP v2. 0: improving the user experience with co-localization studies*. in *ImageJ User & Developer Conference*. 2008.
334. Diaz-Vegas, A., et al., *A high-content endogenous GLUT4 trafficking assay reveals new aspects of adipocyte biology.* Life science alliance, 2023. **6**(1).
335. Norris, D.M., et al., *Glucose transport: Methods for interrogating GLUT4 trafficking in adipocytes.* Glucose Transport: Methods and Protocols, 2018: p. 193-215.
336. Rutter, G.A., et al., *Metabolic and functional specialisations of the pancreatic beta cell: gene disallowance, mitochondrial metabolism and intercellular connectivity.* Diabetologia, 2020. **63**(10): p. 1990-1998.
337. Jitrapakdee, S., et al., *Regulation of insulin secretion: role of mitochondrial signalling.* Diabetologia, 2010. **53**: p. 1019-1032.
338. Rorsman, P. and E. Renstrom, *Insulin granule dynamics in pancreatic beta cells.* Diabetologia, 2003. **46**(8): p. 1029-45.
339. POULI, A.E., et al., *Secretory-granule dynamics visualized in vivo with a phogrin–green fluorescent protein chimaera.* Biochemical Journal, 1998. **333**(1): p. 193-199.
340. Shimono, D., et al., *ATP enhances exocytosis of insulin secretory granules in pancreatic islets under Ca2+-depleted condition.* Diabetes research and clinical practice, 2005. **69**(3): p. 216-223.
341. Varadi, A., et al., *Involvement of conventional kinesin in glucose-stimulated secretory granule movements and exocytosis in clonal pancreatic β-cells.* Journal of cell science, 2002. **115**(21): p. 4177-4189.
342. Sola, D., et al., *State of the art paper Sulfonylureas and their use in clinical practice.* Archives of medical science, 2015. **11**(4): p. 840-848.
343. Donner, T. and S. Sarkar, *Insulin–pharmacology, therapeutic regimens, and principles of intensive insulin therapy.* 2015.

344. Efeyan, A., W.C. Comb, and D.M. Sabatini, *Nutrient-sensing mechanisms and pathways.* Nature, 2015. **517**(7534): p. 302-310.
345. Kaur, J. and J. Debnath, *Autophagy at the crossroads of catabolism and anabolism.* Nature reviews Molecular cell biology, 2015. **16**(8): p. 461-472.
346. Mukai, E., S. Fujimoto, and N. Inagaki, *Role of reactive oxygen species in glucose metabolism disorder in diabetic pancreatic β-cells.* Biomolecules, 2022. **12**(9): p. 1228.
347. Herold, Z., M. Doleschall, and A. Somogyi, *Role and function of granin proteins in diabetes mellitus.* World Journal of Diabetes, 2021. **12**(7): p. 1081.
348. Wijesekara, N., et al., *Beta cell-specific Znt8 deletion in mice causes marked defects in insulin processing, crystallisation and secretion.* Diabetologia, 2010. **53**(8): p. 1656-68.
349. Guest, P.C., *2D Gel Electrophoresis of Insulin Secretory Granule Proteins from Biosynthetically Labelled Pancreatic Islets.* Adv Exp Med Biol, 2017. **974**: p. 167-174.
350. Rosengren, A.H., et al., *Reduced insulin exocytosis in human pancreatic β-cells with gene variants linked to type 2 diabetes.* Diabetes, 2012. **61**(7): p. 1726-1733.
351. Andersen, R.C., et al., *Coding variants identified in patients with diabetes alter PICK1 BAR domain function in insulin granule biogenesis.* The Journal of Clinical Investigation, 2022. **132**(5).
352. Tanabe, A., et al., *Functional single-nucleotide polymorphisms in the secretogranin III (SCG3) gene that form secretory granules with appetite-related neuropeptides are associated with obesity.* The Journal of Clinical Endocrinology & Metabolism, 2007. **92**(3): p. 1145-1154.
353. Pennuto, M., et al., *Synaptophysin I controls the targeting of VAMP2/synaptobrevin II to synaptic vesicles.* Molecular biology of the cell, 2003. **14**(12): p. 4909-4919.
354. Ding, Y., et al., *Grape seed proanthocyanidins ameliorate pancreatic beta-cell dysfunction and death in low-dose streptozotocin-and high-carbohydrate/high-fat diet-induced diabetic rats partially by regulating endoplasmic reticulum stress.* Nutrition & metabolism, 2013. **10**: p. 1-12.
355. Nakamichi, Y. and S. Nagamatsu, *α-SNAP Functions in Insulin Exocytosis from Mature, but Not Immature Secretory Granules in Pancreatic β Cells.* Biochemical and biophysical research communications, 1999. **260**(1): p. 127-132.
356. Nagamatsu, S., et al., *Decreased expression of t-SNARE, syntaxin 1, and SNAP-25 in pancreatic beta-cells is involved in impaired insulin secretion from diabetic GK rat islets: restoration of decreased t-SNARE proteins improves impaired insulin secretion.* Diabetes, 1999. **48**(12): p. 2367-2373.
357. Tsunoda, K., et al., *Single nucleotide polymorphism (D68D, T to C) in the syntaxin 1A gene correlates to age at onset and insulin requirement in Type II diabetic patients.* Diabetologia, 2001. **44**: p. 2092-2097.

358. Yau, B., et al., *Type 2 diabetes-associated single nucleotide polymorphism in Sorcs1 gene results in alternative processing of the Sorcs1 protein in INS1 β-cells.* Scientific reports, 2019. **9**(1): p. 19466.
359. Atla, G., et al., *Genetic regulation of RNA splicing in human pancreatic islets.* Genome biology, 2022. **23**(1): p. 196.

(this page is intentionally blank)

Supplementary Figures

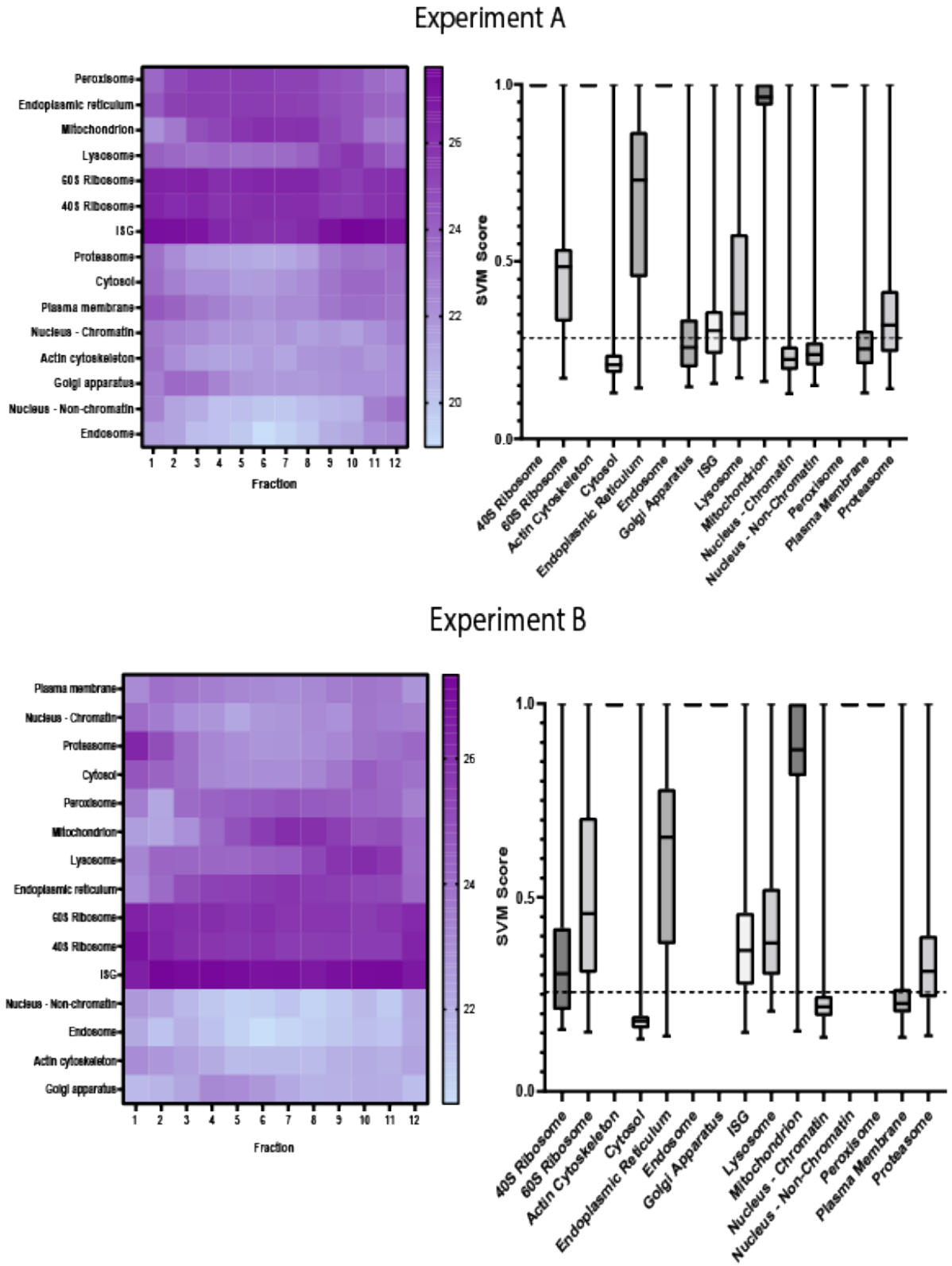

Experiment C

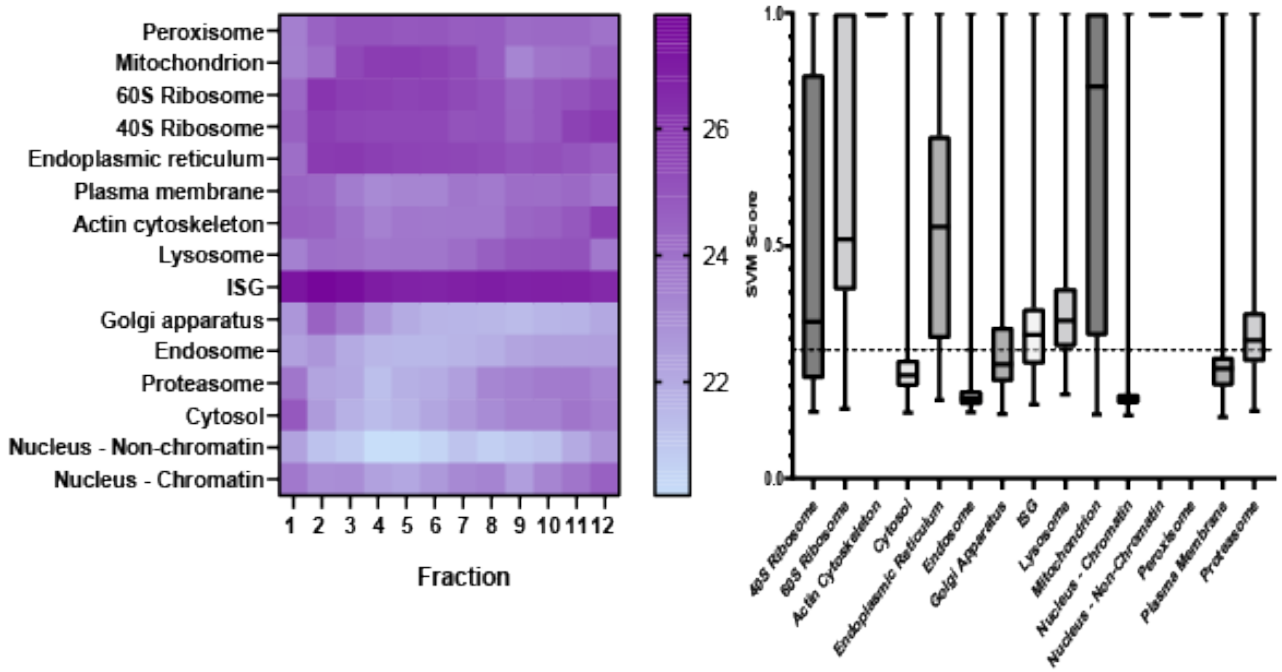

Experiment D

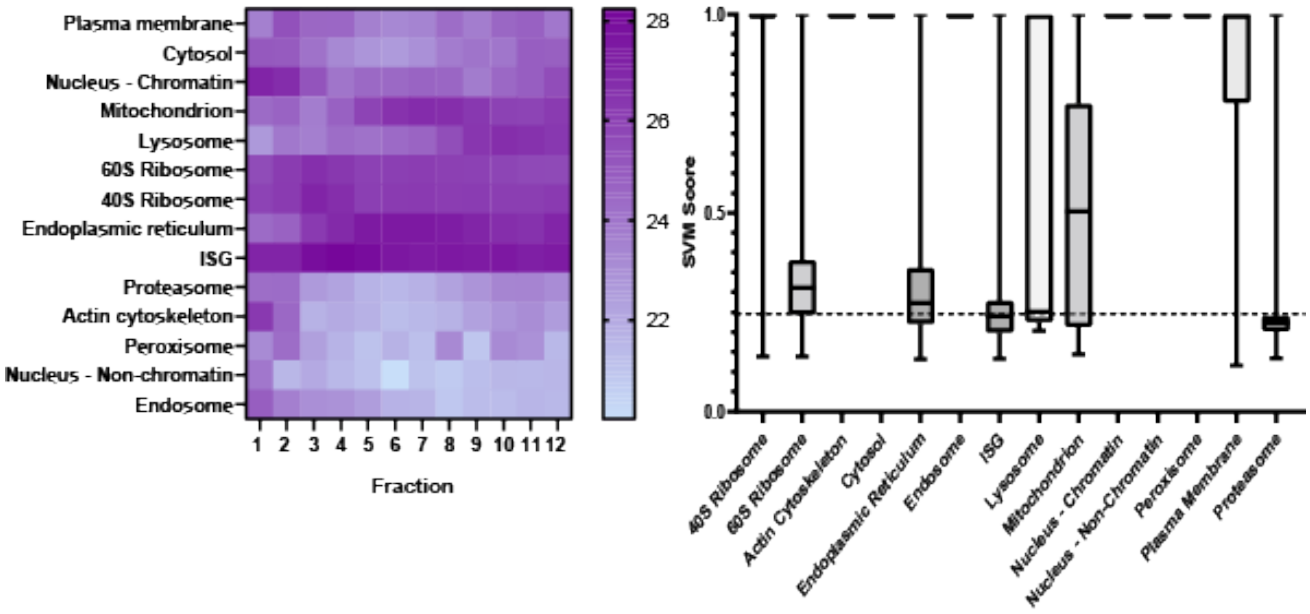

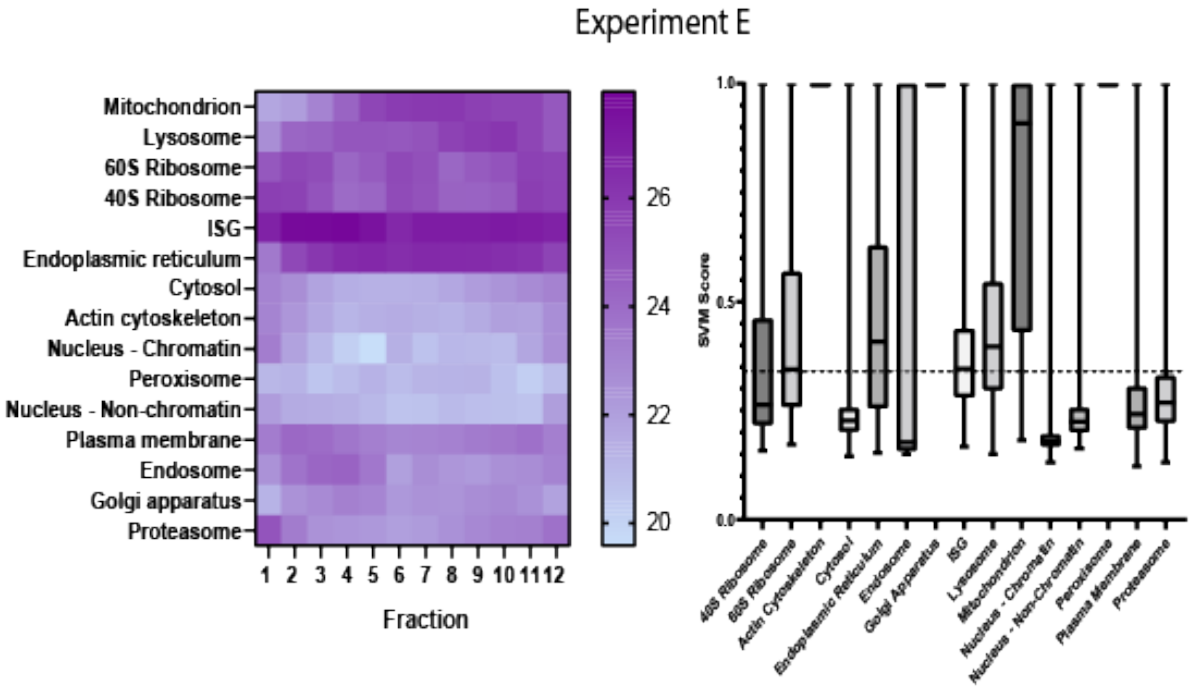

Supplementary Figure 1: Strength and enrichment of proteins assigned to different subcellular localizations of the MIN6 β-cell. Support Vector Machine (SVM) learning score distributions of subcellular organelles within the MIN6 β-cell of all experimental replicates (Experiment A-E). Heatmaps show the average LFQ intensity of proteins assigned to each subcellular localization in each experiment.

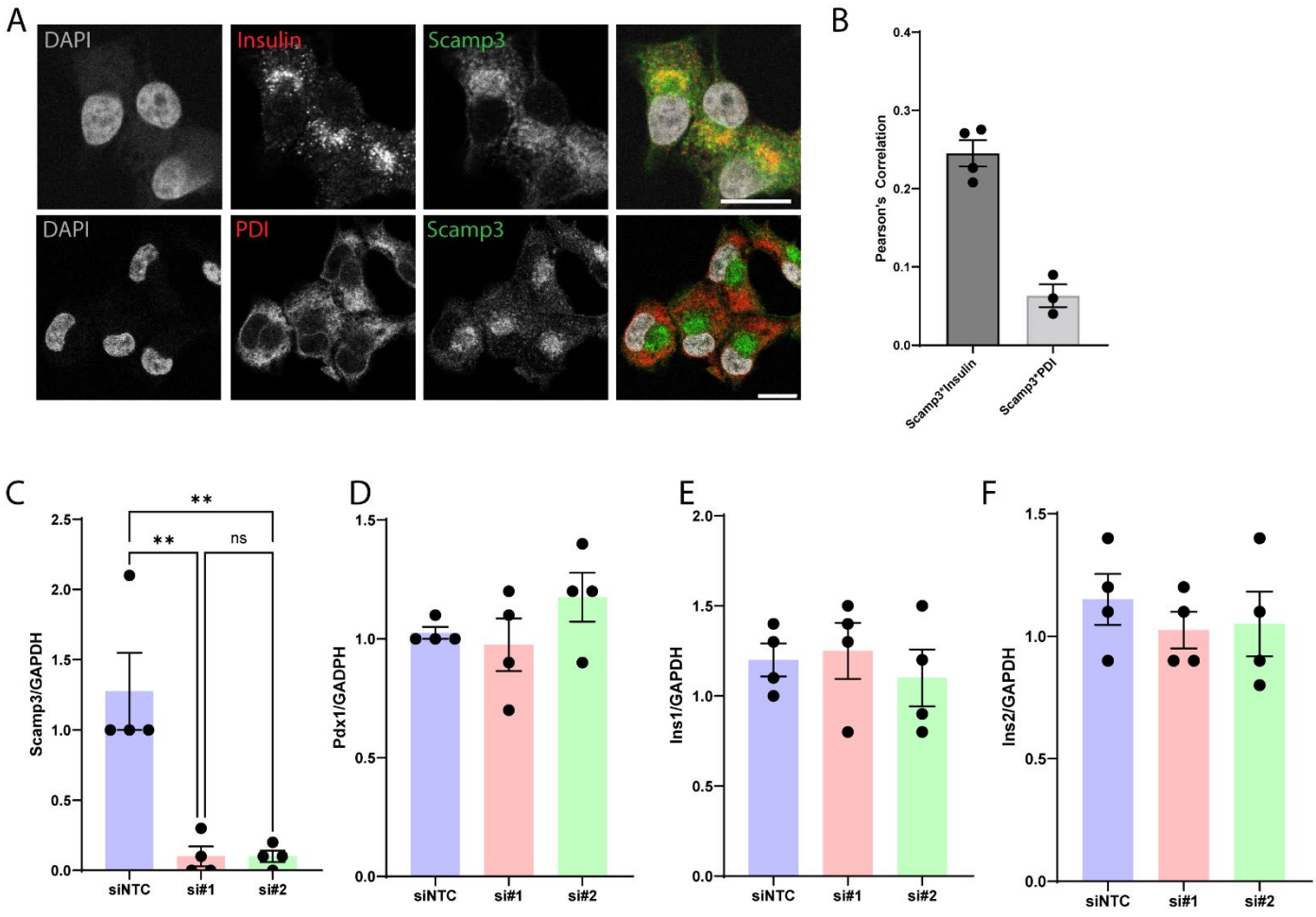

Supplementary Figure 2: **Validation of Scamp3 localization in INS-1 cells and mRNA transcription in Scamp3 KD INS-1 cells.** (**A**) Confocal fluorescence imaging of INS-1 cells labelled with Scamp3, co-stained with anti-insulin (n=4) and anti-PDI (n=3). Quantification of colocalization of Scamp3 with insulin and PDI with Pearson's correlation. (C) mRNA levels of Scamp3 normalized to GAPDH in control and siRNA KD INS-1 cells. (D) mRNA levels of Pdx1 normalized to GAPDH in control and siRNA KD INS-1 cells. (E) mRNA levels of Ins1 normalized to GAPDH in control and siRNA KD INS-1 cells. (F) mRNA levels of Ins2 normalized to GAPDH in control and siRNA KD INS-1 cells. All error bars represent standard error of the mean (± S.E.M.). Scale bars = 10uM. *P-value <0.05, ** P-value <0.01, *** P-value <0.001.

Supplementary Table 8:**Analysis of Variance (ANOVA) summary tables** evaluating the effects of treatment (0.5 mM Palmitate or Control), Fraction (1-12), and experimental replicate (1, 2 or 3) on the protein abundance of known ISG proteins and previously validated ISG-associated proteins (Chapter 2). Table shows the degrees of freedom (Df), sum of squares (Sum Sq), mean squares (Mean Sq), F-values and associated p-values (Pr(>F)) for each factor and their interaction. Significant effects observed are outlined by asterisks, Treatment:Fraction indicates the possible interaction between treatment and fractions. Significance codes: * p < 0.05, ** p < 0.01, *** p <0.001.

Protein		df	Sum sq	Mean Sq	F value	P value (>F)	Significance
Ins1	Treatment	1	3.1545	3.15447	33.2922	6.87E-07	***
	Fraction	11	21.1369	1.92154	20.2799	6.43E-14	***
	Experiment	2	2.1451	1.07254	11.3196	0.0001042	***
	Treatment*Fraction	11	2.7904	0.25367	2.6772	0.0098278	**
	Residuals	45	4.2638	0.09475			
Ins2	Treatment	1	10.175	10.1754	46.7754	1.77E-08	***
	Fraction	11	38.292	3.4811	16.0024	4.10E-12	***
	Experiment	2	7.279	3.6394	16.7303	3.70E-06	***
	Treatment*Fraction	11	2.046	0.186	0.8551	5.88E-01	
	Residuals	45	9.789	0.2175			
Pcsk1n	Treatment	1	2.4917	2.49174	13.0001	7.90E-04	***
	Fraction	11	5.3099	0.48272	2.5185	1.48E-02	*
	Experiment	2	3.2661	1.63306	8.5201	7.45E-04	***
	Treatment*Fraction	11	2.8294	0.25722	1.342	2.35E-01	
	Residuals	44	8.4335	0.19167			
CPE	Treatment	1	1.783	1.78299	26.6596	5.92E-06	***
	Fraction	11	9.5815	0.87105	13.024	2.16E-10	***
	Experiment	2	0.8851	0.44257	6.6174	3.12E-03	**
	Treatment*Fraction	11	0.2885	0.02622	0.3921	0.95182	
	Residuals	43	2.8758	0.06688			
ChgA	Treatment	1	0.5485	0.54846	3.7033	0.0604	
	Fraction	11	15.6774	1.42522	9.6234	1.30E-08	***
	Experiment	2	0.7482	0.37411	2.5261	0.09126	
	Treatment*Fraction	11	1.8453	0.16775	1.1327	0.35972	
	Residuals	45	6.6645	0.1481			
Iapp	Treatment	1	0.3486	0.3486	1.144	0.2903995	
	Fraction	11	20.9858	1.9078	6.2612	3.48E-06	***
	Experiment	2	6.4824	3.2412	10.6374	0.0001595	***
	Treatment*Fraction	11	5.7784	0.5253	1.724	0.0978269	
	Residuals	46	14.0163	0.3047			
PCSK2	Treatment	1	0.1761	0.17611	1.7703	0.190049	
	Fraction	11	2.1969	0.19972	2.0077	5.01E-02	
	Experiment	2	1.8013	0.90067	9.0538	0.000496	***
	Treatment*Fraction	11	0.1568	0.01425	0.1433	0.999303	
	Residuals	45	4.4766	0.09948			

Scamp3	Treatment	1	0.211	0.211	2.4369	0.1258	
	Fraction	11	25.5327	2.3212	26.8103	1.02E-15	***
	Experiment	2	6.6841	3.342	38.6018	2.52E-10	***
	Treatment*Fraction	11	1.316	0.1196	1.3818	0.2162	
	Residuals	43	3.7228	0.0866			
Scg2	Treatment	1	3.7097	3.7097	22.3991	2.14E-05	***
	Fraction	11	5.5184	0.5017	3.0291	4.07E-03	**
	Experiment	2	5.4114	2.7057	16.3371	4.36E-06	***
	Treatment*Fraction	11	2.5598	0.2327	1.4051	0.203069	
	Residuals	46	7.6184	0.1656			
Scg3	Treatment	1	0.2645	0.2645	3.039	8.84E-02	
	Fraction	11	10.2875	0.93523	10.7455	3.95E-09	***
	Experiment	2	2.387	1.19352	13.7133	2.47E-05	***
	Treatment*Fraction	11	0.5493	0.04994	0.5738	0.83916	
	Residuals	43	3.7425	0.08703			
Stx7	Treatment	1	0.585	0.5847	1.2887	2.62E-01	
	Fraction	11	24.055	2.1868	4.8194	7.15E-05	***
	Experiment	2	33.997	16.9985	37.4623	2.64E-10	***
	Treatment*Fraction	11	3.219	0.2927	0.645	0.7806	
	Residuals	45	20.419	0.4537			
Syp	Treatment	1	0.808	0.80783	5.7825	2.03E-02	*
	Fraction	11	31.854	2.89582	20.7284	2.88E-14	***
	Experiment	2	0.986	0.49291	3.5283	3.75E-02	*
	Treatment*Fraction	11	1.465	0.13318	0.9533	0.50055	
	Residuals	46	6.426	0.1397			
Syt13	Treatment	1	3.9658	3.9658	38.2024	2.39E-07	*
	Fraction	11	17.5783	1.598	15.3937	2.94E-11	***
	Experiment	2	6.5504	3.2752	31.5497	5.06E-09	*
	Treatment*Fraction	11	1.8848	0.1713	1.6506	0.1206	
	Residuals	41	4.2562	0.1038			
ZnT8	Treatment	1	0.1865	0.1865	1.6796	2.02E-01	*
	Fraction	11	13.4957	1.22688	11.0488	2.62E-09	***
	Experiment	2	3.4546	1.72732	15.5555	8.26E-06	*
	Treatment*Fraction	11	1.7303	0.1573	1.4165	0.2005	
	Residuals	43	4.7748	0.11104			

UNIPROT IDs: **Ins1** (P01325), **Ins2** (P01326), **Pcsk1n** (Q9QXV0), **CPE** (Q00493), **ChgA** (P26339), **Iapp** (P12968), **PCSK2** (P21661), **Scamp3** (O35609), **Scg2** (Q03517), **Scg3** (P47867), **Stx7** (Q8BH40), **Syp** (Q8CFI5), **Syt13** (Q9EQT6) and **ZnT8** (Q8BGG0).